Hydrogen as fuel for enteric bacteria: biochemistry of the membrane bound NiFe hydrogenase

Lindsey Anne Flanagan

Doctor of Philosophy

University of York

Biology

September 2016

Hydrogen as fuel for enteric bacteria: biochemistry of the membrane bound NiFe hydrogenase

Hydrogen is considered both a fuel for the future and an ancient fuel for life. Hydrogenases catalyse the interconversion of molecular hydrogen, H_2, and protons, H^+. A subgroup of hydrogenases, the membrane bound NiFe hydrogenases (MBH), have been the subject of much research interest. This is firstly due to their possible applications in biotechnology, but also because they have been implicated in the virulence of gut pathogens. The MBH are divided into O_2 tolerant and O_2 sensitive based on their ability to catalyse H_2 oxidation in the presence of O_2, and the two classes are both structurally and mechanistically distinct. Understanding these distinctions is important both for technology which aims to achieve more minimal models of enzymes, but also for relating the way different MBH are expressed at different stages of infection.

The properties of variants of two O_2 tolerant MBH, *Escherichia coli* Hyd-1 and *Salmonella enterica* Hyd-5 and one O_2 sensitive MBH, *E. coli* Hyd-2, have been examined with regards to how the properties of specific amino acids achieve control over catalysis and O_2 tolerance. Red®/ET® recombination methodology has been applied for the first time to hydrogenases. This methodology allows the rapid generation of hydrogenase knockouts and single site variants in *E. coli* in addition to the incorporation of polyhistidine tags to enable protein purification. Purified native and variant hydrogenases have been studied with protein film electrochemistry. Hyd-1 and Hyd-5 E73A and H229A variants were shown to have diminished O_2 tolerance whilst a Hyd-1 E73Q variant had an increased catalytic bias towards H_2 production. It was established that Hyd-1 was expressed during growth in glucose limited minimal media, although no change in growth rate or competitive ability was seen in a Hyd-1 knockout strain.

Contents

Chapter 1
Hydrogen and Hydrogenases

Chapter 2
Large subunit variants of *Salmonella enterica* membrane bound NiFe hydrogenase-5

Chapter 3
Development of a protocol to create NiFe hydrogenase variants in *E. coli*

Chapter 4

Role of large subunit residue 73 in H_2 production and catalytic bias of *E. coli* Hyd-1

Chapter 5

The role of the conserved histidine adjacent to the proximal cluster in O_2 tolerant and O_2 sensitive membrane bound NiFe hydrogenase of *Escherichia coli*

Chapter 6
The role of membrane bound NiFe hydrogenase Hyd-1 in the growth and competitive ability of *E. coli*

Chapter 7
Discussion and future perspectives

Chapter 8
Experimental materials and methods

List of Tables

List of Figures

Chapter 1

Chapter 2

Chapter 3

Chapter 4

Chapter 5

Acknowledgements

First and foremost, I would like to thank my supervisors Alison Parkin and James Moir for your guidance and support above and beyond the call of duty. Working with you has been amazing, and I have learnt more than I imagined possible. To my TAP members, Gavin Thomas and James Chong, thank you for your insight and advice that helped me turn my ideas into realities. To Frank Sargent, thank you for sharing your wealth of hydrogenase knowledge with me. To John Wright and Maxie Roessler, thank you for providing me with the vital EPR we needed so speedily.

I would like to thank the Wellcome Trust and the organisers of the CIDCATS program for funding me and for their backing both academically and in terms of outreach and engagement activities. Thanks to the Departments of Biology and Chemistry at the University of York for hosting me and for dealing with my slightly bizarre research needs. To the mechanical and electronics workshops and glassblowers at the University of York- this work wouldn't have been possible without you. To all the administrative staff at the Department of Biology, thank you for not drowning me in bureaucracy. To the infrastructure and stores staff, thank you for being helpful and cheerful always.

To Judith Hawkhead and Julia Walton, you are Queens of the labs, and I am grateful for you allowing me to enter your domains. To Hope, thank you for being more intelligent than I am, and for putting up with me when I get annoying. To all members of the Parkin, Fascione, Moir and Thomas groups (and various adoptees), thank you for making me smile. To my fellow CIDCATS, no tipi is complete without you.

Finally, thank you to my family for reading my papers even though you didn't understand them, and for not asking too often when I would get a proper job. And to Shaun, thank you for being beside me through it all.

Author's Declaration

This thesis is a presentation of original work and Lindsey Flanagan is the sole author. This work has not previously been presented for an award at this, or any other, University. All sources are acknowledged as references.

Chapter 1 is based on "Electrochemical insights into the mechanism of NiFe membrane-bound hydrogenases" by Lindsey Flanagan (the author) and Alison Parkin, published in 2016 in Biochemical Society Transactions, volume 44, issue 7, pages 315-326. Lindsey Flanagan was involved in creation of the figures, first draft and subsequent editing. Alison Parkin was involved in re-writing and editing of further drafts, guidance of figure production, and production of figures not included in this thesis.

Chapter 2 is based on "How the structure of the large subunit controls function in an oxygen-tolerant [NiFe]-hydrogenase" by Lisa Bowman, Lindsey Flanagan (the author), Paul Fyfe, Alison Parkin, William Hunter and Frank Sargent, published in 2014 in Biochemical Journal, volume 458, issue 3, pages 449-458. Lisa Bowman created the *Salmonella enterica* constructs and purified the proteins, Lindsey Flanagan performed the electrochemistry and Paul Fyfe performed the crystallography; Lisa Bowman, Lindsey Flanagan, Paul Fyfe, Alison Parkin, William Hunter and Frank Sargent designed the research, analysed the data and wrote the paper; and Alison Parkin, William Hunter and Frank Sargent supervised the research.

For the methylene blue assay described in Chapter 2, research technician Julia Walton purified the proteins from the constructs created by Lisa Bowman (above) and undergraduate student David Lloyd performed the assays.

The molecular biology work in Chapter 3 and the work in Chapter 4 has been described in "Re-engineering a NiFe hydrogenase to increase the H_2 production bias while maintaining native levels of O_2 tolerance" by Lindsey Flanagan (the

author), John Wright, Maxie Roessler, James Moir and Alison Parkin, published in 2016 in Chemical Communications, volume 52, pages 9133-9136. Lindsey Flanagan performed the molecular biology, protein purification, methylene blue assays and protein film electrochemistry. John Wright performed the EPR. Lindsey Flanagan, John Wright, Maxie Roessler, James Moir and Alison Parkin designed the research, analysed the data and wrote the paper. Maxie Roessler, James Moir and Alison Parkin supervised the research.

In Chapter 5, analysis of the surplus protein band in the SDS-PAGE gel was performed by Hope Adamson, PhD student at the University of York.

For Section 6.3.1 of Chapter 6, the growth curves described were performed by undergraduate summer student at the University of York, Hamid-Reza Danesh-Azari, under the supervision of Lindsey Flanagan (the author).

Chapter 1

Hydrogen and Hydrogenases

1.1 Introduction

1.1.1 Hydrogen as a future fuel for humankind

Molecular hydrogen, the simplest molecule, formed of just two protons and electrons, is a potential fuel of the future. H_2 has a high energy density of combustion of 142 kJ/g[1], nearly three times greater than that of the common household fossil fuel natural gas (methane, 55 kJ/g)[1]. In addition, the only product of H_2 combustion is water, while burning fossil fuels generates the greenhouse gas CO_2, identified as the major contributor to global warming[2]. In order to use H_2 as a fuel, large amounts will be needed. Many current routes of H_2 production still involve the use of fossil fuels, while others either require high temperatures or precious metals[1]. Much research has gone into finding a synthetic catalyst that produces H_2 without these requirements, but investigations in this field are still on-going.

1.1.2 H_2 as an ancient fuel for microbial life

Early earth had an atmosphere of up to 30% H_2 (equivalent to 0.234 M in aqueous solution), and this is considered to be an important factor in the origin of life[3]. Following the "great oxygenation event", i.e the biologically-induced appearance of atmospheric dioxygen, the amount of atmospheric H_2 diminished to the current level of 0.6 ppm[4] (equivalent to 0.47 nM in aqueous solution). Since then, H_2-utilising microorganisms have either evolved to use the low amounts of H_2 in the air[5], or to occupy pockets of the environment with higher H_2 concentrations, such as hydrothermal vents, which have H_2 concentrations of up to 19 mM[6].

1.1.3 The hydrogenases

The enzymes that microbes use to break apart molecular hydrogen are the hydrogenases. There are three major types of hydrogenases, the FeFe, NiFe and Fe only hydrogenases, which have been named after the metals present in the site at which H_2 binds[7]. Of these, NiFe hydrogenases have been the most studied as many of these enzymes are found in facultative aerobes[8-10] and are thus the most versatile with regards to their purification and manipulation. In contrast, the Fe-only hydrogenases are rare, and thus the least studied hydrogenases.

The FeFe and NiFe hydrogenases are further divided into subgroups, as most recently defined by Greening et al[11] and summarised in Table 1. This sub-characterisation considers both gene phylogeny and enzyme function, with a key consideration being whether the enzyme plays a role as a H_2-uptake catalyst ($H_2 \rightarrow 2H^+ + 2e^-$), or instead activates the reverse reaction of H_2 production ($2H^+ + 2e^- \rightarrow H_2$). Both reactions are useful in biology. H_2 production is often a by-product of formate metabolism[12-14] and also a potential solar fuel in some photosynthetic organisms[15]. By contrast, H_2 oxidation is important when H_2 is acting as an energy source[16]. Transfer of electrons from H_2 is used for the formation of cellular reducing equivalents such as NADH and reduced ferredoxin[17]. H_2 oxidation is also involved in H_2 recycling and H_2 oxidising hydrogenases are often coupled with H_2 producing hydrogenases[18].

Table 1.1 Groups and subgroups of the hydrogenases. Adapted from Greening et al[11].

Group/subgroup	Class/Function	Example
FeFe hydrogenases		
Group A1	Prototypical: couples oxidation of ferredoxin to evolution of H_2	*Desulfovibrio desulfuricans* DdHase
Group A2	Glutamate synthase linked (putative)	Uncharacterised
Group A3	Bifurcating: transfers electrons from H_2 to ferredoxin and NAD^+	*Acetobacterium woodii* HydABCD
Group A4	Formate dehydrogenase linked: formate oxidation is coupled to H_2 evolution	*Clostridium autoethanogenum* Hyt
Group B	Ancestral (putative): unknown function	Uncharacterised
Group C	Sensory (putative): predicted to induce cascades of kinases and phosphatases	*Ruminococcus albus* HydA2
NiFe hydrogenases		
Group 1	Membrane bound H_2 uptake NiFe hydrogenases	
1a	Ancestral: liberates electrons for respiration of sulfate, metals, organohalides and methanogenic heterodisulfide	*Desulfovibrio vulgaris* NiFeSe hydrogenase
1b	Prototypical: liberates electrons for respiration of sulfate, fumarate and nitrate	*Desulfovibrio gigas* HynAB
1c	Hyb type: liberates electrons for fumarate respiration	*Escherichia coli* Hyd-2
1d	Oxygen tolerant: provides electrons for aerobic and oxygen tolerant anaerobic respiration	*Escherichia coli* Hyd-1
1e	Isp type: liberates electrons for sulfur respiration	*Allochromatium vinosum* NiFe hydrogenase
1f	Oxygen protecting: unconfirmed, possible reduction of reactive oxygen species	*Geobacter sulfurreducens* Hya
1g	Crenarchaeota type: unconfirmed, possible sulfur respiration	*Acidianus ambivalens* Hyn
1h (Group 5)	Actinobacteria type: scavenging of atmospheric H_2 during starvation	*Ralstonia eutropha* AH
Group 2	Cytosolic H_2 uptake NiFe hydrogenases	
2a	Cyanobacteria type: H_2 recycling and provision of electrons for anaerobic respiration	*Mycobacterium smegmatis* Hyd1
2b	Regulatory: controls hydrogenase expression	*Ralstonia eutropha* RH
2c	Sensing (putative) predicted to induce cyclic di-GMP production in response to H_2	Uncharacterised
2d	Aquificae type: unconfirmed, may have role in carbon fixation or regulation	*Aquifex aeolicus*
Group 3	Cytosolic bidirectional NiFe hydrogenases	
3a	F_{420} coupled: H_2 oxidation coupled to F_{420} reduction in methanogenesis	*Methanothermobacter marburgensis* Frh
3b	$NADP^+$ coupled: couples oxidation of NADPH to H_2 production	*Mycobacterium smegmatis* Hyd3
3c	Heterodisulfide reductase linked: bifurcates electrons from H_2 to ferredoxin and heterodisulfide	*Methanothermobacter marburgensis* Mvh
3d	NAD^+ coupled: reduces NAD^+ with electrons from H_2	*Ralstonia eutropha* SH
Group 4	Membrane bound H_2 evolving NiFe hydrogenases	
4a	Formate hydrogenlyases: couples formate oxidation to H_2 production	*Escherichia coli* Hyd-3
4b	Mrp type antiporter linked: couples oxidation for formate or CO to H_2 production, generates Na^+ motive force	*Thermococcus kodakarensis* Mbh
4c	Carbon monoxide dehydrogenase linked: anaerobic respiration of CO	*Carboxydothermus hydrogenoformans* Coo
4d	Eha/Ehb type: H_2 oxidation coupled to ferredoxin reduction for anaplerotic and anabolic purposes	*Methanococcus maripaludis* Eha
4e	Ech type: couples ferredoxin oxidation to H_2 production	*Desulfovibrio gigas* Ech
4f	Ehf type (putative): unknown, possible coupling of H_2 production to oxidation of a one-carbon compound	Uncharacterised
[Fe]-hydrogenases		
Hmdl	Methenyl-H4MPT dehydrogenase: couples oxidation of hydrogen to 5,10-methenyltetrahydromethanopterin reduction during nickel limitation	*Methanocaldococcus jannaschii* Fe hydrogenase

This thesis will focus on NiFe hydrogenases. The majority of NiFe hydrogenases are classed as O_2 sensitive, meaning they do not sustain H_2 oxidation activity in the presence of O_2[7]. However, an "O_2 tolerant" sub-class of Group 1 enzymes exists that are capable of catalytic reaction with H_2 in the presence of O_2. Historically, hydrogenases of this special sub-set have been studied because they may be used in membrane-free H_2/O_2 fuel cells[19-21] and photocatalytic hydrogen

production[22]. It is to be noted that *Ralstonia eutropha* also expresses an oxygen tolerant group 3 NiFe hydrogenase which has been employed in cofactor-recycling systems[23], but this system will not be discussed further because of the large structural differences from the group 1 NiFe hydrogenases studied in this thesis.

1.2 Structure and function of the NiFe hydrogenases

1.2.1 Structural features of the NiFe hydrogenases
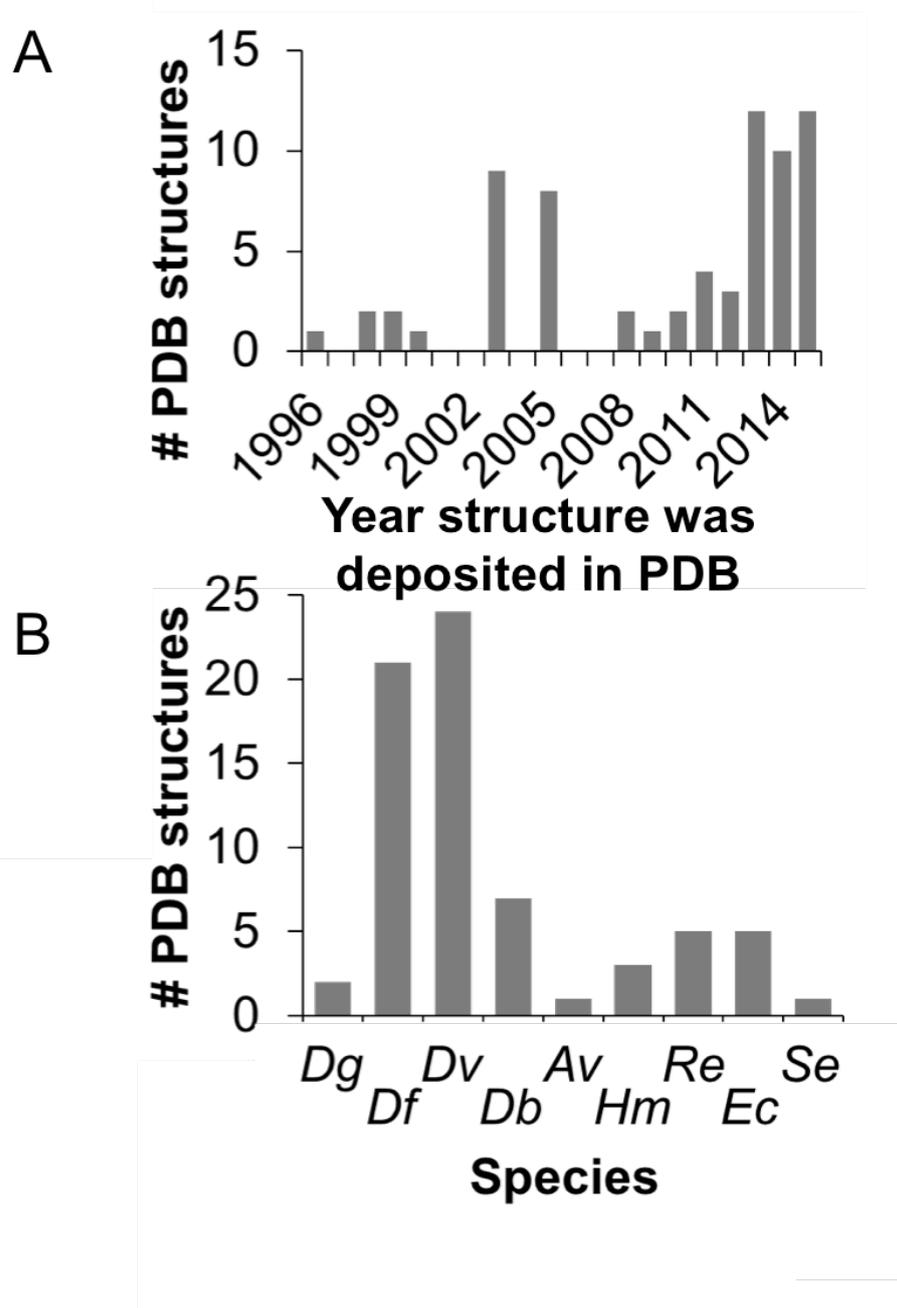
Figure 1.1 Structures of NiFe hydrogenase relating to A: year that the structure was deposited in the protein data bank and B: species from which the hydrogenase was isolated. Adapted from Flanagan and Parkin[24]. Abbreviations: Dg, *Desulfovibrio gigas*; Df, *Desulfovibrio fructosovorans*; Dv, *Desulfovibrio vulgaris*; Db, *Desulfomicrobium baculatum*; Av, *Allochromatium vinosum*; Hm, *Hydrogenovibrio marinus*; Re, *Ralstonia eutropha*; Ec, *Escherichia coli*; Se, *Salmonella enterica*.

The basic functional unit of a group 1 NiFe hydrogenase is a dimer of the large (or α) subunit, which contains the NiFe active site of H_2 catalysis, and the small (or β) subunit, which contains an electron transport chain of iron-sulfur clusters[25]. As shown in Figure 1.1, many crystal structures have been published over the last 20 years that show the large-small heterodimer. The first structure, solved by Volbeda et al at 2.85 Å[26], was of insufficient resolution to identify the species of metal in the active site, and it was in combination with spectroscopic studies that further details were revealed[27-30]. The structures in Figure 1.1 represent both O_2 tolerant[31-36] and O_2 sensitive[26, 37-46] NiFe hydrogenases from a diverse range of organisms. The majority of the structures are of the periplasmically orientated membrane bound NiFe hydrogenases. However, the soluble periplasmic hydrogenases of *Desulfovibrio gigas*[26, 37] and *Desulfovibrio fructosovorans*[38-40] and the soluble periplasmic NiFeSe hydrogenase of *Desulfomicrobio baculatum*[45-46] have been of vital importance in the characterisation of structural and mechanistic properties. Throughout the remainder of this chapter, "NiFe hydrogenase" will be used to refer to work where characterisation took place in soluble NiFe hydrogenases and both cytosolic and periplasmically orientated membrane bound NiFe hydrogenases, and "MBH" will be used to refer to work that characterises only the periplasmically orientated membrane bound NiFe hydrogenase.
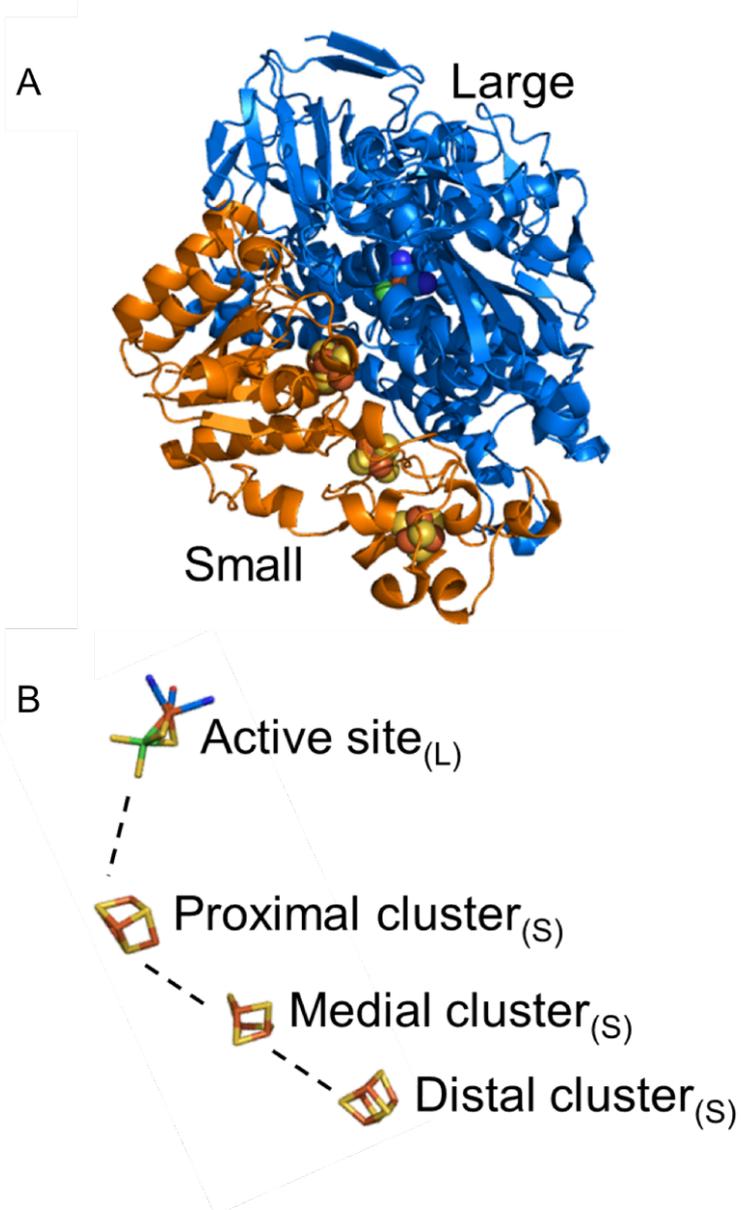
Figure 1.2 Crystal structure of the MBH from *Ralstonia eutropha* (PDB: 3RGW[47]). Adapted from Flanagan and Parkin[24]. A: Cartoon representation of the heterodimer that forms the basic functional unit, with the large subunit shown in blue and the small subunit shown in orange. The NiFe active site and iron sulfur clusters are shown as spheres. B: Stick representation of the special arrangement of the electron transport chain. Colours: green, nickel; orange, iron; yellow, sulfur; carbon, light blue; oxygen, red; dark blue, nitrogen.

The structure of the O_2 tolerant MBH of *Ralstonia eutropha* is shown in Figure 1.2. The heterodimer is bound at the periplasmic side of the bacterial inner membrane by a transmembrane helix that extends from the C-terminus of the small subunit[35] (not resolved in crystal structure). When the electrons that are the products of H_2 oxidation are produced at the NiFe active site they are transported down the chain of iron-sulfur clusters in the small subunit. From there they are transported into the *b*-type heme containing cytochrome subunit, the additional subunit found most MBH, and from there to the ubiquinone pool[35]. The *E. coli* MBH Hyd-2 also contains a ferredoxin type subunit that binds four iron-sulfur clusters, which has been shown to be essential for activity in the membrane, but beyond which little is known about its function[48]. This chapter, and this thesis, will largely focus on the characterisation of the catalytic heterodimer formed of the large and small subunits. This is because, firstly, as previously stated, this is the minimal functional unit essential to all catalytic hydrogenases[49]. Secondly, the large and small subunit are co-expressed and purified, whilst additional subunits commonly dissociate on purification[48], unless special care is taken to prevent this. For this reason, the vast majority of crystal structures, spectroscopic characterisations, experimental analyses and biotechnological applications have been performed using this minimal functional unit[50-53]. The implications of this will be discussed later in the chapter.

The NiFe hydrogenases possess several features that may be classed as unusual. The Fe of the NiFe active site is ligated by two molecules of CN and one of CO[27-30], which are uncommon species in nature[54]. In addition, the iron-sulfur clusters of the membrane bound hydrogenases have been shown as atypical through spectroscopic and crystallographic investigations. The distal (furthest from the active site) cluster is a 4Fe4S cluster with an unusual but highly conserved Cys_3His ligation[55]. The medial cluster is a 3Fe4S cluster[56]. And the proximal (closest to the active site) cluster differs depending on which group the hydrogenase is in, as shown in Figure 1.3. The majority of NiFe hydrogenases have a standard 4Fe4S proximal cluster ligated by 4 cysteines. However, for group 1d hydrogenases, the proximal cluster is a 4Fe3S cluster that is ligated by

6 cysteines (referred to as supernumerary)[57]. The properties of these clusters and their role in the hydrogenases are discussed later in this chapter.
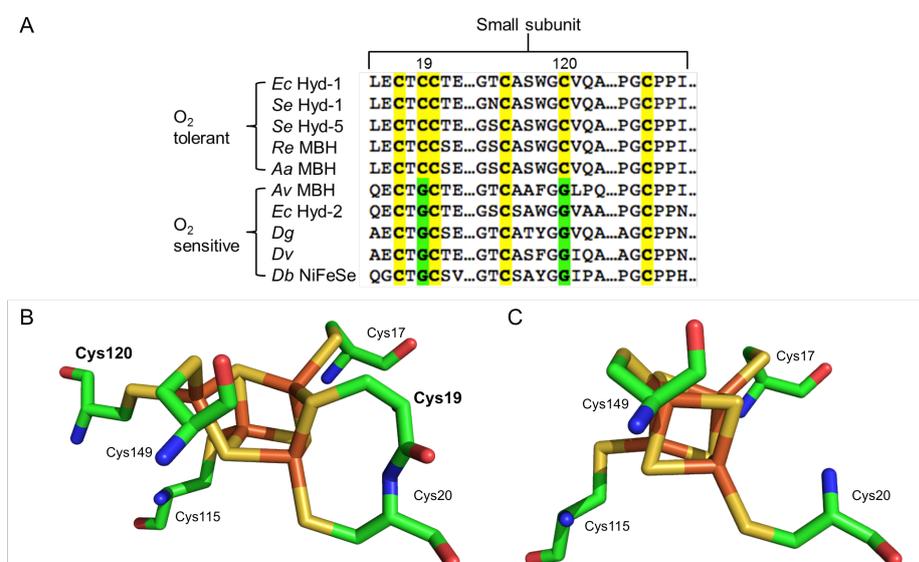
Figure 1.3 The supernumerary cysteines of the proximal cluster. Adapted from Flanagan and Parkin[24]. A: sequence alignment showing the cysteines ligating the proximal cluster, highlighting the conserved cysteines for the O_2 tolerant hydrogenases and conserved glycine for O_2 sensitive at positions 19 and 120 of the small subunit. Other abbreviations are: Se, *Salmonella enterica*; Re, *Ralstonia eutropha*; Aa, *Aquifex aeolicus*; Av, *Allochromatium vinosum*; Dg, *Desulfovibrio gigas*; Dv, *Desulfovibrio vulgaris*; Db, *Desulfomicrobium baculatum*. B: Crystal structure of the O_2 tolerant proximal cluster, with the supernumerary cysteines emboldened (PDB: 3RGW[47]). C: Crystal structure of the O_2 sensitive proximal cluster (PDB: 4UQY[39]). *E. coli* numbering is used throughout.

1.2.2 Mechanism of NiFe hydrogenase catalysis

The biochemical mechanisms by which the NiFe hydrogenases operate has been assessed using a combination of spectroscopic and crystallographic studies that have led to a basic understanding of the transitions involved in catalysis of H_2 oxidation in NiFe uptake hydrogenases[58-62]. This is shown in Figure 1.4. Much of the original nomenclature and labelling of various active site states originates in their initial characterisation by electron paramagnetic resonance (EPR), reflects this. For example, the active form of the hydrogenases is the $Ni^{II}Fe^{II}$ Ni-SI$_a$ state[63], where "SI" stands for EPR silent and "a" denotes active.
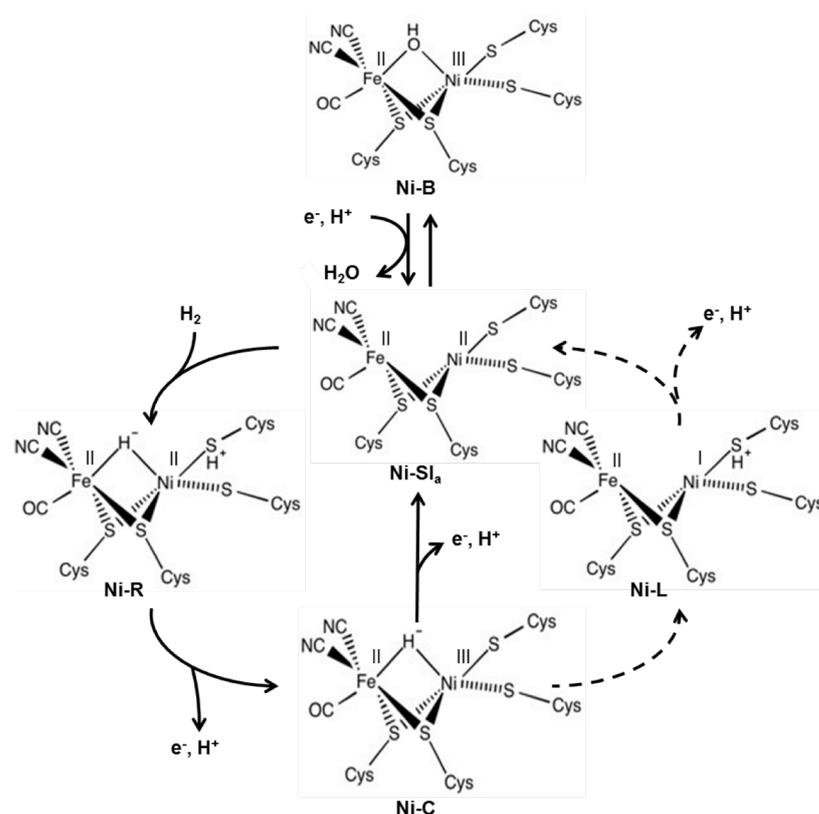
Figure 1.4 Transformations of the NiFe active site during catalysis. Adapted from Flanagan and Parkin[24]. Dotted arrows show the hypothesized additional transition in O_2 tolerant NiFe hydrogenases. Figure adapted as a combination of mechanisms from Ogata et al[64] and Hidalgo et al[65].

During H_2 binding to Ni-SI$_a$, one of the protons is abstracted by a base and the resultant hydride bridges the nickel and iron ions to form the Ni-R state (active, reduced). Ni-R is EPR silent but visible by fourier transform infrared spectroscopy (FTIR)[62], and a subatomic resolution structure has also been published, showing the bridging hydride[64]. The loss of an electron oxidises the nickel to a Ni^{III} state, giving Ni-C, which is EPR detectable[62]. Different routes are then hypothesized to occur for the O_2 sensitive and O_2 tolerant membrane bound hydrogenases[53, 65-66]. For O_2 sensitive hydrogenase, the loss of one electron and one proton allows the Ni^{III}Fe^{II} Ni-C state to return directly back to the Ni^{II}Fe^{II} Ni-SI$_a$ state. However, in O_2 tolerant MBH spectroscopic characterisations have found that an intermediate state appears, Ni-L, which is a Ni^{I}Fe^{II} state[53]. It is thought that the H$^-$ electrons of Ni-C are transferred to the Ni^{III}, oxidizing it to Ni^{I}, whilst the proton component of the hydride is abstracted by a base. Loss of

10

one electron then oxidises the Ni^IFe^{II} of Ni-L to $Ni^{II}Fe^{II}$ of Ni-SI$_a$, returning the enzyme to an active state ready to oxidise another molecule of hydrogen. O_2 sensitive hydrogenases also have spectroscopically detectable Ni^I states, but these have only been recorded at cryogenic temperatures, and under the application of light[66]. This is the origin of the name of the state, as Ni-L stands for light-induced. It is thought that H_2 production would originate by a simple reversal of the catalytic cycle.

1.2.3 Proton transfer pathways

The nature of the base that abstracts protons, first from the H_2 molecule and second from the bridging position of Ni-C, has been subject to some debate. Using a combination of Density Functional Theory (DFT), vibrational spectroscopy and high resolution crystallography, Ogata et al have suggested that the sulfur of cysteine 576 (*E. coli* numbering) is a strong candidate for the base[60, 64]. The protonated cysteine is shown in the crystal structure depicted in Figure 1.5, A. However, as small nickel complexes with thiolate ligands are not known for H_2 activation, this hypothesis is rejected by the Evans et al, who instead suggest that a deprotonated form of arginine 509 (*E. coli* numbering) may play the role of the base in catalysis[67]. The diminished turnover rate in a R509K mutant has been used to support this hypothesis. In their proposed mechanism of H_2 production, the hydride in Ni-R abstracts a proton from arginine to form molecular hydrogen and a deprotonated arginine (Figure 1.5 B (ii)). However, arginine has a pK_a of 12.48 and it is not known whether Ni-R would be a strong enough base to perform this reaction, particularly as H_2 production in the model protein only occurs at acidic pH values[68]. Furthermore, in order to perform H_2 oxidation, the deprotonated form of the arginine side chain must be present when H_2 binds to Ni-SI$_a$ (without Ni-R involvement). In the study by Evans et al[67], the nearby aspartate residues (Figure 1.5 A) which could act as bases were mutated into asparagine with only small consequence on the turnover. As the crystal structures in this work were not of high enough resolution (i.e. below ~0.9 Å) required to determine hydrogen position and thus

reveal the protonation state of relevant sites. Accordingly the effects of pH on activity were not explored, it is yet to be seen whether the rejection of Ogata's hypothesis is justified.
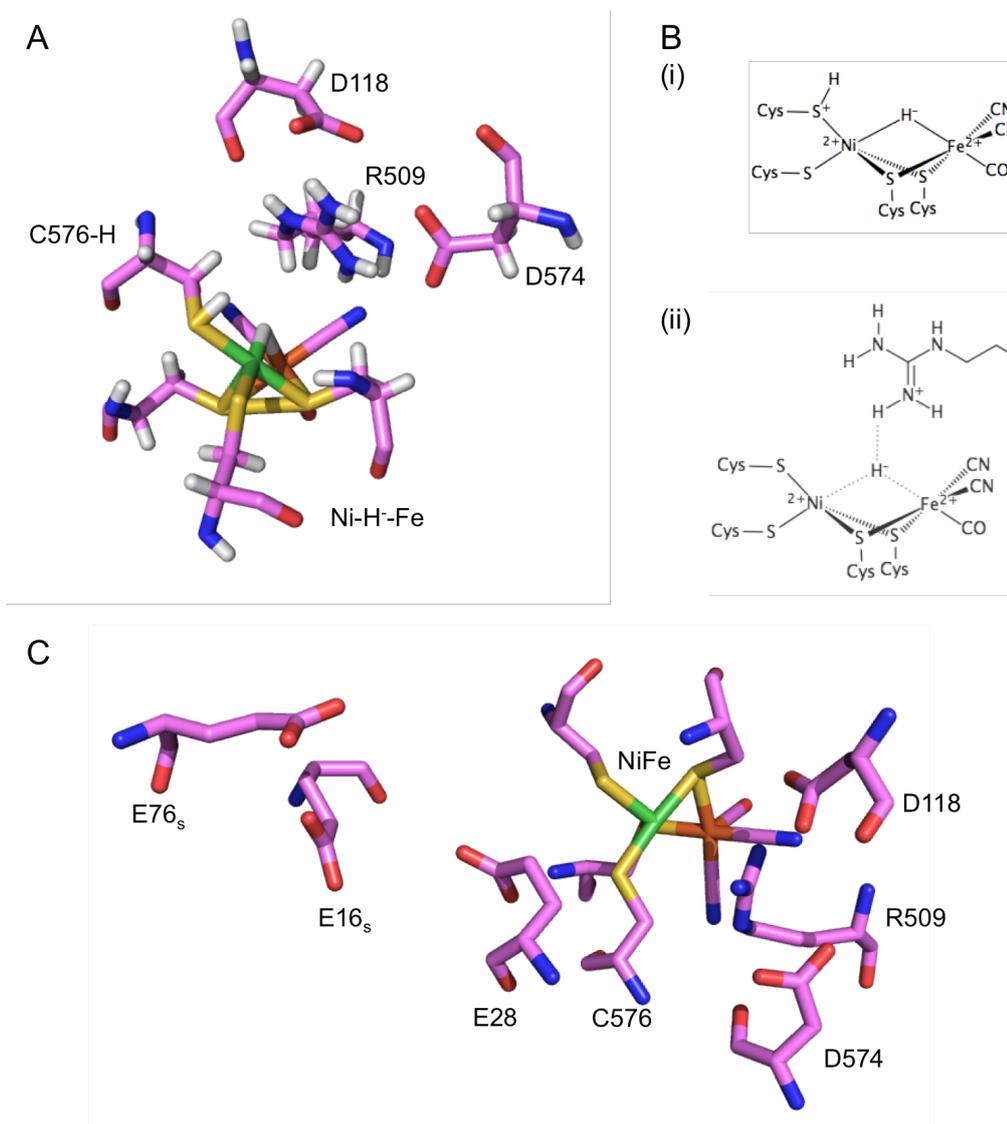
Figure 1.5 Proton transfer in catalysis. A: High resolution (0.89 Å) crystal structure of *D. vulgaris* NiFe hydrogenase (PDB: 4U9H[64]) showing the protonated cysteine adjacent to the hydride bridging the nickel and iron of the active site. B: Proposed mechanisms for the origin of the base in catalysis. (i) Hypothesis by Ogata et al[64], where the proton is abstracted by the active site cysteine. (ii) Hypothesis by Evans et al[67], where the proton is abstracted by a nearby deprotonated arginine. C: Possible proton transport pathways[69], as shown by the crystal structure of *E. coli* Hyd-1 (PBD: 3UQY[34]). *E. coli* Hyd-1 numbering used throughout. Colours: magenta, carbon; white, hydrogen; red, oxygen; blue, nitrogen; yellow, sulfur; orange, iron; green, nickel.

Figure 1.5 C depicts the two possible proton transport pathways described by Oteri et al[69]. One pathway involves transfer from a conserved glutamate of the large subunit (E28, *E. coli* numbering) to two small subunit glutamates (E16 and E76, *E. coli* numbering). The conserved large subunit glutamate has been named as an essential proton transfer gate[70], and a glutamate to glutamine amino acid substitution in *Desulfovibrio fructosovorans* resulted in a variant with less than 0.1% of the wild type activity. The proximity of this residue to cysteine 576 in the crystal structure (Figure 1.5 C) thus has important implications for the catalytic mechanism. However, Oteri et al[69] also suggested the Arg/Asp/Asp triad discussed above as a possible proton transfer pathway and suggested that the pathway involving the glutamate could be related to O_2 tolerance whilst the pathway involving the arginine may involve the transport of the products and substrates of catalysis. The exact nature of the proton transport pathways is thus not yet resolved and needs further evidence to be conclusively stated.

1.2.4 Hydrophobic substrate channels

Along with protons, the second substrate of a hydrogenase is, of course, molecular hydrogen. This is thought to travel from outside of the enzyme to the NiFe active site through hydrophobic substrate channels in the large subunit. Kalms et al[71] showed that in general O_2 sensitive MBH have double the number of hydrophobic channels as O_2 tolerant hydrogenases, and that the channels in O_2 tolerant hydrogenases are narrower, with fewer openings.

Figure 1.6 shows a recently released crystal structure of the *Ralstonia eutropha* membrane bound hydrogenase pressurized with krypton (black spheres), which shows a clear path of hydrophobicity from the exterior to the interior of the enzyme[71]. A conserved Val/Leu/Arg triad at the opening to a channel near the active site (yellow spheres, Figure 1.6) has been implicated in ligand migration[72]. The width of this channel is similar for O_2 tolerant and O_2 sensitive hydrogenases, suggesting that this property is not the defining feature of O_2 tolerance. However, in O_2 sensitive hydrogenases, replacing the valine with

larger residues which narrow the channel led to increased O_2 tolerance, although the sensitivity to H_2 was also decreased, as observable in the Michaelis constant[73].
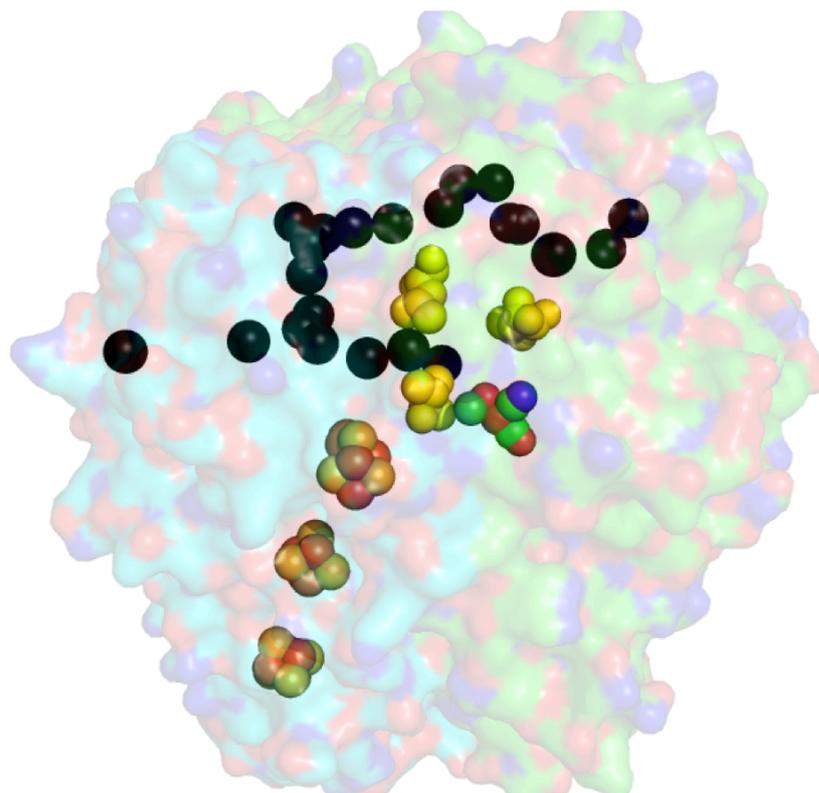
Figure 1.6 Hydrophobic channels in an O_2 tolerant NiFe hydrogenase from *R. eutropha* (PDB: 5D51[71]). Crystal structure of the catalytic heterodimer is shown as a translucent electrostatic surface with the neutral patches of the large subunit shown in green and the neutral surfaces of the small subunit shown in blue. NiFe active site and iron sulfur clusters shown as spheres. Hydrophobic tunnels marked by the position of docked krypton (black spheres). Residues shown as yellow spheres mark the position of the Val/Leu/Arg triplet.

1.2.5 States formed on inactivation with O_2

When NiFe hydrogenases react with O_2 the formation of two different states has been observed by EPR, the long lasting "unready" Ni-A state (proposed structures given in Figure 1.7), and the quickly reactivated "ready" Ni-B state[74] (structure given in Figures 1.6 and 1.8). O_2 tolerant hydrogenases are thought to only form the Ni-B state on inactivation with O_2 and thus quickly recover from O_2 exposure[75], although crystal structures showing additional bound oxygen at the NiFe centre have been published for one O_2 tolerant MBH[67]. In contrast, O_2 sensitive hydrogenases form a mixture of Ni-A and Ni-B states[74]. Prolonged exposure to O_2 traps greater and greater proportions of the enzyme in the Ni-A state, until the hydrogenase is fully inactivated.
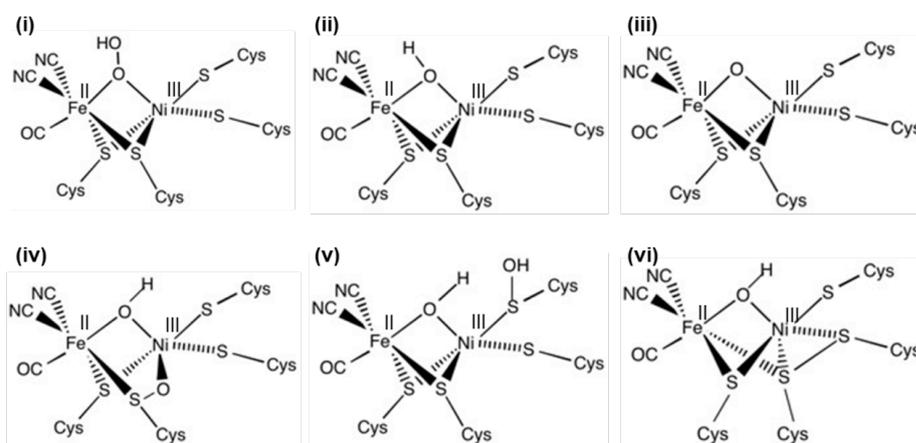
Figure 1.7 Hypothesised Ni-A structures. Adapted from Flanagan and Parkin[24]. (i) Bridging hydroperoxide[37]; (ii) hydroxide bridged stereoisomer of Ni-B[76]; (iii) bridging O^{2-} ligand[76]; (iv) Ni and S bridging oxo species[38]; (v) S–OH and bridging hydroxide form[58] and (vi) disulfide bond containing hydroxide-bridging structure[58].

The structure of Ni-B is well established as being a $Ni^{III}Fe^{II}$ state with a bridging hydroxide[75], although it has not been fully established whether this OH^- ligand is O_2 or solvent H_2O derived. In contrast, the structure of Ni-A has been strongly debated. Although there are many crystal structures of O_2-inactivated O_2 sensitive NiFe hydrogenases[38, 77-78], there has been difficulty assigning the electron density of Ni-A, a problem likely compounded by mixtures of Ni-A and Ni-B[59]. Some of the hypothesized Ni-A structures are shown in Figure 1.7.

Much of the debate has revolved around whether O_2 binds directly to the active site, or merely causes oxidation by the proximity of a strong electron acceptor. Initial assumption that the O_2 reacts directly with the NiFe active site and $^{17}O_2$ studies suggesting that O_2 is bound in close proximity to the nickel[79] led to the assignment of the extended electron density observed about the ligand bridging the nickel and iron as an O_2 derived peroxo group (Figure 1.7 (i)[78]). This model of reactivity has more recently been extended to include oxidation of the cysteine sulfurs (Figures 1.7 (iv-vi)) by work by Volbeda et al and Armstrong et al[38, 67, 77]. However, the involvement of O_2 binding to the active site has been disputed by the finding that Ni-A can be formed in the absence of oxygen[80].

The alternative hypothesis, that the O_2 acts as an electron acceptor and does not bind directly has been supported by studies performed using ^{17}O $H_2^{17}O$, which suggested that the bridging ligand was solvent derived[76]. This led to the suggestion that the bridging ligand of Ni-A could either be a hydroxide or an O^{2-} atom. Single crystal electron-nuclear double resonance (ENDOR) spectroscopy also suggested that the ligand is a bridging hydroxide, with the difference between Ni-B and Ni-A being rotation about one of the cysteines[81]. It is not known how two similar structures would have such different reactivation properties, although it is possible that this conformational change would prevent reactivation by turning the site away from the hydrophobic tunnel by which reactivating H_2 would enter.

1.2.6 The nature of O_2 tolerance

$$O_2 + 4H^+ + 3e^- + OH^- \; 2H_2O$$
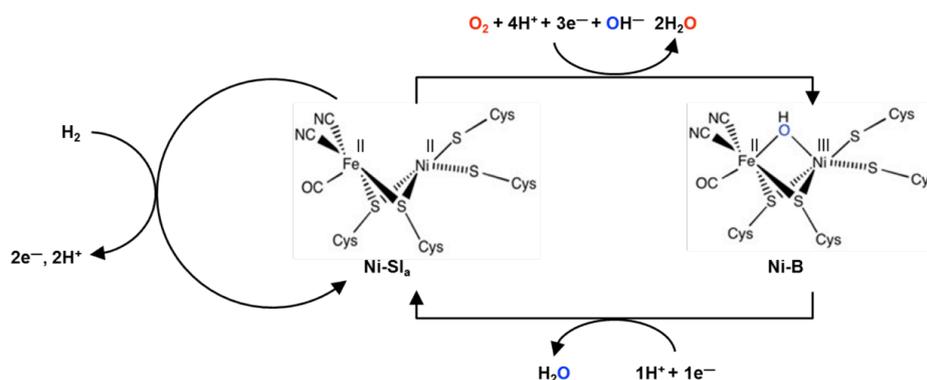
Figure 1.8 Hypothesised route of Ni-B formation and reactivation showing the need for four electrons. Adapted from Flanagan and Parkin[24]. Red shows O_2 derived oxygen and blue shows H_2O derived oxygen.

The property of O_2 tolerance depends on the ability of a hydrogenase to remove the slow pseudosubstrate molecular oxygen and reactivate the active site. A hypothetical reaction scheme for the formation of Ni-B from Ni-SI$_a$ is shown in Figure 1.8[75], using the solvent derived hydroxide ligand hypothesis. This reaction necessitates four electrons in total to completely reduce O_2 into H_2O. One of these electrons comes from the oxidation of the active site nickel from Ni^{II} to Ni^{III}. In O_2 tolerant MBH, the medial cluster is thought to be capable of contributing a second electron, based on a study by Evans et al, which found that when this 3Fe4S cluster was converted to a 4Fe4S cluster by a P242C mutation the *E. coli* O_2 tolerant MBH Hyd-1, the variant was no longer able to sustain activity under 1% O_2[56].

The proximal cluster of O_2 tolerant MBH has also been shown to be involved in the reduction of O_2. The supernumerary cysteines of this cluster support a structural transition as shown in Figure 1.9, in which the backbone nitrogen of cysteine 20 ligates Fe4 and the bond between S3 and Fe4 of the cluster is broken[33]. Formation of this "superoxidised" state from the reduced state allows the donation of two electrons for the reduction of oxygen[57]. This is hypothesized to allow the full reduction of O_2, and thus prompt formation of the readily reactivated Ni-B, in O_2 tolerant MBH[25].
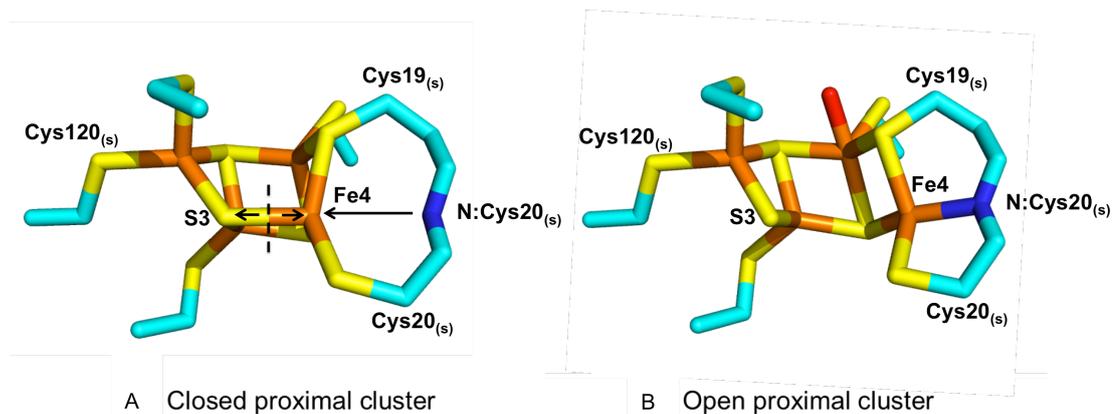
Figure 1.9 The structural transition of the O_2 tolerant proximal cluster on superoxidation. Adapted from Flanagan and Parkin[24]. Yellow: sulfur, orange: iron, blue: nitrogen, red: oxygen and cyan: carbon. A: Reduced, open proximal cluster (PDB: 3RGW[32]). B: Superoxidised, open proximal cluster (PDB: 4IUB[33]).

The limitation to this accepted mechanism of O_2 tolerance is that it fails to explain why O_2 sensitive hydrogenases form a mixture of both Ni-A and Ni-B after exposure to oxygen. To understand this it is necessary to consider that during catalysis the active site cycles through multiple states[82], with the most reduced being Ni-R, which can be considered as a protonated Ni^0 state or a hydride-bound Ni^{II}. When O_2 reacts with a hydrogenase in this state the additional electrons on the nickel could prevent formation of the more oxidized states, as shown in Figure 1.10, explaining why O_2 sensitive NiFe hydrogenases form Ni-B with O_2 and why O_2 tolerant MBH can cycle between active states, acting as an O_2 reductase.
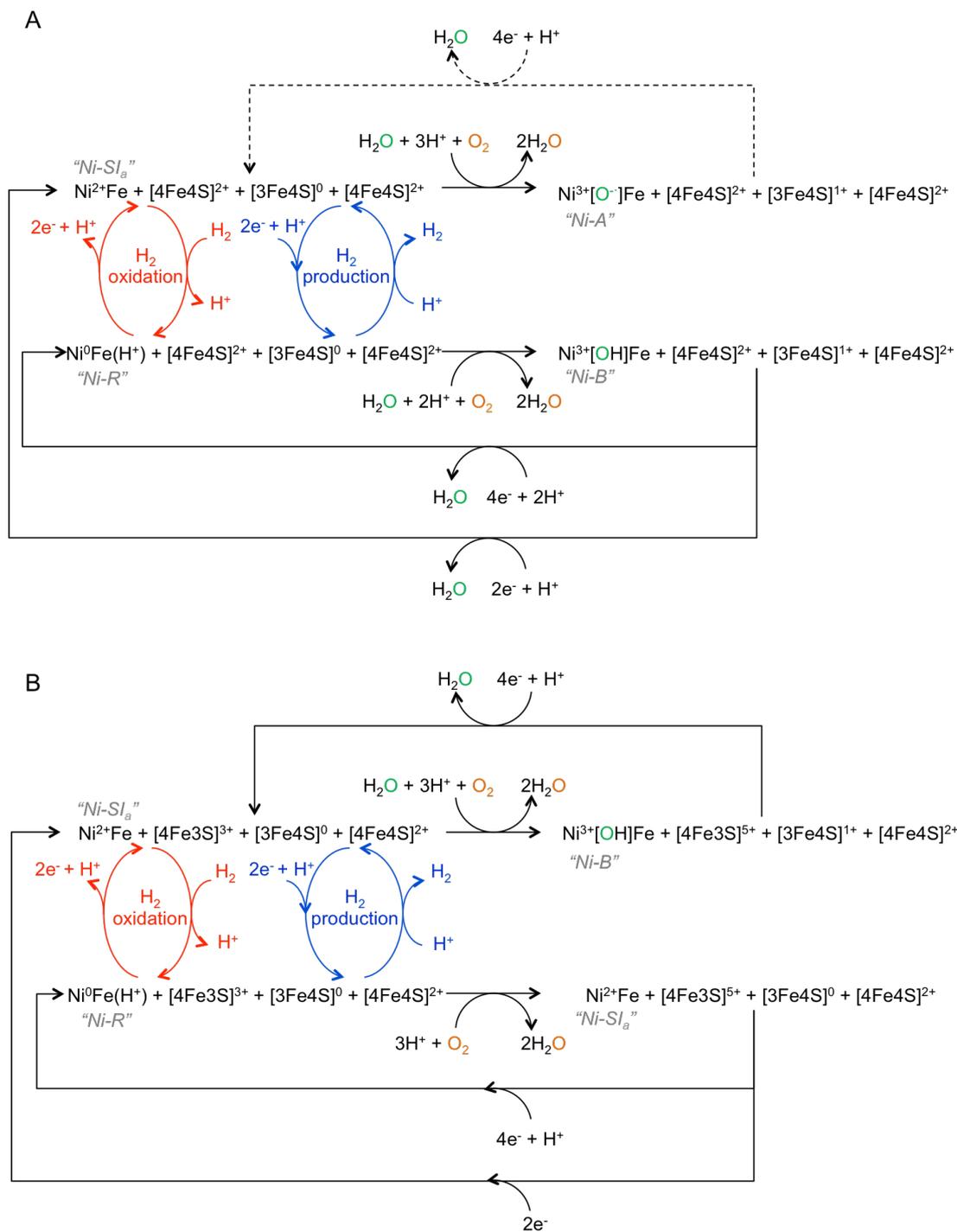
Figure 1.10 Possible states formed on reaction with O_2 at different stages of catalysis. A: O_2 sensitive NiFe hydrogenases and B: O_2 tolerant MBH. Red and green shows the proposed origin of the different oxygen atoms.

1.3 *Salmonella enterica* and *Escherichia coli* hydrogenases

1.3.1 Hydrogenases in the human gut

The focus on the role of hydrogenases in biotechnology has sometimes distracted attention from consideration of the roles of the enzymes within their parent microbes, and within the wider context of the ecosystem that they occupy.

The gut flora is formed of a complicated community of microorganisms, with a great diversity of species[83] and a high variability between hosts[84] depending on many factors including diet[85], age and geography[86]. The role of the gut flora in metabolism and human health is now thought to be so crucial that it has even been proposed that commensals influence the tendency of humans to develop of obesity[87]. Many other beneficial health effects have been associated with a person sustaining a gut microbiome consisting of normal commensal bacteria[88] including the competitive exclusion of pathogens[88], the development of a healthy immune system[89], the natural production of antibodies[90] and the breakdown of polysaccharides which humans are incapable of digesting[91-92]. Conversely, dysregulation in gut microbial communities has been implicated in a range of diseases. For example the establishment of the *Clostridium difficile* infection[93], which causes a great healthcare burden[94], has been attributed to the disruption in commensal flora causing a lack of competition. Autoimmune and inflammatory diseases[95] such as inflammatory bowel disease and asthma[96] have also been linked to gut bacteria.
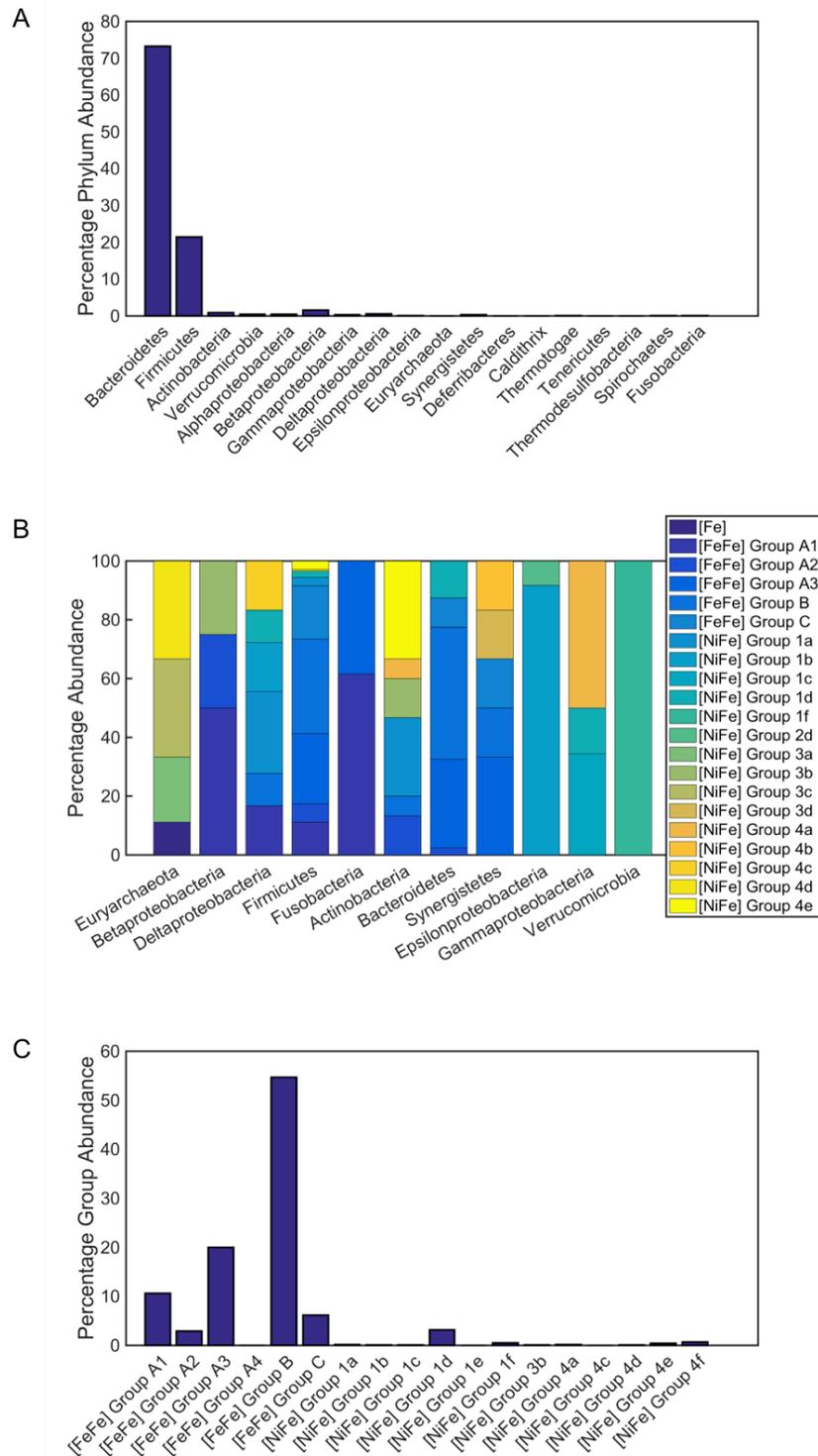
Figure 1.11 Dominant phyla and the distribution of hydrogenases in the human gut flora. Data from the work by Wolf et al[97]. A: The percentage abundance of different phyla across a sample of 20 human microbiomes. B: The distribution of different subgroups of hydrogenase according to different phyla, from a phylogenetic study. C: Percentage abundance of different hydrogenase subgroups as an average of 20 healthy human microbiomes.

The composition of the gut microbiota is thus of great interest to medical research, suggesting that understanding the metabolic enzymes which are key to bacterial survival in this environment is also important. Over 70% of the microbiome encodes a hydrogenase[97], and the ability to utilise the levels of H_2 in the gut, which may reach up to 160 μM[98], can give pathogenic bacteria a competitive advantage against commensals[99-101]. FeFe hydrogenases are more highly abundant than NiFe hydrogenases because the dominant phyla present in this environment are the Bacteroidetes and the Firmicutes[97] (as illustrated in Figure 1.1). However, the Bacteroidetes also possess genes for the group 1d hydrogenases, the O_2 tolerant membrane bound hydrogenases. This class of enzymes is also produced by the Enterobacteriaceae, Gram-negative rod shaped bacteria with facultative aerobic metabolism[102] that also form part of the commensal gut flora[103], but can cause a large proportion of the cases of enteric fever and diarrhoea cases that lead to millions of deaths each year[104]. Mice colonised with commensal gut Enterobacteriaceae have been shown to become more susceptible to infection with pathogenic Enterobacteriaceae[105]. In addition, antibiotic resistance may transfer between commensal and pathogenic Enterobacteriaceae[106].

Two well-known genii of Enterobacteriaceae are *Salmonella enterica* and *Escherichia coli* and they will be the main organisms discussed in this thesis. *Salmonella* species are facultative intracellular pathogens[107]. Strains of *Salmonella* can cause typhoid fever[108] and food poisoning[109]. *Salmonella* infection is associated with upregulation of its hydrogenase genes, in particular the group 1 hydrogenases[9, 98, 110]. These membrane bound, periplasmically orientated, "H_2-uptake" NiFe hydrogenases (MBH) oxidise molecular hydrogen to protons and electrons. Deletion of the *Salmonella* uptake hydrogenases renders the strain incapable of infecting mice[98], a process which may be reversed by complementation with any of the hydrogenase genes on a plasmid.

Many strains of *Escherichia coli* are harmless, and indeed may have a beneficial role in the human host by producing vitamin K_2[111]. However, pathogenic strains

can cause urinary tract infections[112], gastroenteritis[113] and neonatal meningitis[114]. *E. coli* also has group 1 hydrogenases, but it is not yet known whether these contribute to infection. In particular, the role of the group 1d hydrogenase in *E. coli,* known as Hyd-1, is as yet unclear, and this will be a subject of investigation in this thesis.

1.3.2 Similarity and difference in the *Salmonella enterica* and *Escherichia coli* NiFe hydrogenases

E. coli expresses two uptake hydrogenases, one from group 1d (Hyd-1) and one from 1c (Hyd-2), alongside the H_2 producing group 4a hydrogenase Hyd-3, which forms part of the formate hydrogenlyase complex[115], and Hyd-4, a putative hydrogenase not proposed to have a function in *E. coli*[116].

The genome of *Salmonella enterica* also encodes a group 4 hydrogenase and two group 1 hydrogenases[101], similar to *E. coli*. Indeed, the *S. enterica* hydrogenases are referred to by the same names. However, *S. enterica* Typhimurium also encodes an additional group 1d hydrogenase, referred to as Hyd-5. The percent sequence identity of conserved residues between the *E. coli* and *S. enterica* membrane bound uptake hydrogenases (MBH) are reported in Table 1.2. It may be seen that *E. coli* Hyd-1 and *E. coli* Hyd-2 enzymes are similar to their *S. enterica* namesakes. However, despite belonging to the same enzyme sub-group the large subunit of *S. enterica* Hyd-5 is more distinct from *E. coli* Hyd-1, suggesting it has been optimised for a different function.

Table 1.2 Percent sequence identity of conserved residues between the hydrogenases of *S. enterica* serovar typhimurium and *E. coli* K12 as calculated by BLAST® searching[117].

			Salmonella enterica serovar typhimurium					
			Hyd-1		Hyd-2		Hyd-5	
			Large	Small	Large	Small	Large	Small
Escherichia coli	Hyd-1	Large	91		42		66	
		Small		92		42		73
	Hyd-2	Large	43		94		45	
		Small		37		97		41

The Hyd-1, Hyd-2 and Hyd-5 MBH of *E. coli* and *S. enterica* are encoded by the gene clusters listed in Table 1.3. The complex maturation of the NiFe hydrogenases expressed by these operons can lead to complex regulatory effects.

Table 1.3 The subunits coded for by the *E. coli* and *S. enterica* MBH operons

Subunit	Hyd-1	Hyd-2	Hyd-5
Large	*hyaB*	*hybC*	*hydB*
Small	*hyaA*	*hybO*	*hydA*
Cytochrome	*hyaC*	*hybB*	*hydC*
Ferredoxin	-	*hybA*	-
Maturation Proteins	*hyaD, hyaE, hyaF*	*hybD, hybE, hybF, hybG*	*hydD, hydE, hydF, hydG, hydH, hydI*

1.3.3 Hydrogenase regulation in *S. enterica*

Kröger et al[118] released a database with a search tool to allow the *in vitro* expression conditions of any *Salmonella* gene of interest to be quickly found. Use of this search tool showed that the Hyd-1 genes are expressed at lower cell density and induced by anaerobic conditions. The Hyd-2 genes are expressed at higher cell densities and induced by anaerobic conditions. The Hyd-5 genes, by contrast, are induced by aerobic conditions. This correlates well with earlier work by Maier and co-workers studying the differential expression of different *S. enterica* typhimurium MBH *in vivo*[119]. In particular, Hyd-1 and Hyd-5 are expressed in different parts of the body and at different stages of infection[119]. In addition, the expression of the Hyd-5 genes is strongly upregulated inside macrophages, and also in liver cells, whilst Hyd-1 shows a lesser upregulation, and then only in macrophages. In contrast, the expression of Hyd-2 is largely unchanged by the exposure to the mammalian cells.

1.3.4 Hydrogenase regulation in *E. coli*

Due to the well-studied nature of *E. coli*, the expression of the MBH genes in this organism are well characterised, and a summary is presented in Figure 1.12. The expression of both the Hyd-1 and Hyd-2 operons, *hya* and *hyb*, are induced by a transition to anaerobiosis[120]. This is partly suggested to be an effect of the regulator Fnr, although it is suggested to be an indirect effect, and has been

disputed by Brøndsted et al[121]. The proteins AppY and ArcA directly regulate *hya* expression in *E. coli* during anaerobiosis, but mutation of *appY* has seemingly no effect on *hyb* regulation. The presence of the anaerobic electron acceptor nitrate downregulates both *hya* and *hyb*, a process in which ArcA and Fnr have been found to have no involvement. This effect is instead mediated by the concerted actions of the paired nitrate response regulators NarL/NarP and NarQ/NarX in a redundant manner. For these regulators, only the double NarLP or NarQX deletion mutants relieve nitrate repression and individual deletion mutation of NarL or NarP has little effect[120]. This is likely due to the crosstalk that exists in the response regulators of the Nar system, where NarL and NarP both recognize and activate the same *nirB* promoter[122].

Deletion strains of sigma factor RpoS have been found to reduce expression levels of *hya* in all conditions tested[123]. RpoS was shown to have no role in the mediation of the pH effect of *hya* expression, where levels peak at pH 4.7 and decline at higher pH values. In minimal medium the pH effect is even more pronounced in comparison to LB[123]. The pH response of *hya* is likely due to the effects of ArcA and AppY, as genetic deletion of either of these factors causes expression of *hya* to be greater in alkaline medium compared to acidic. In contrast, King et al found that expression of *hyb* was not subject to pH control by either ArcA or AppY, but was more strongly induced by alkaline pH[123].
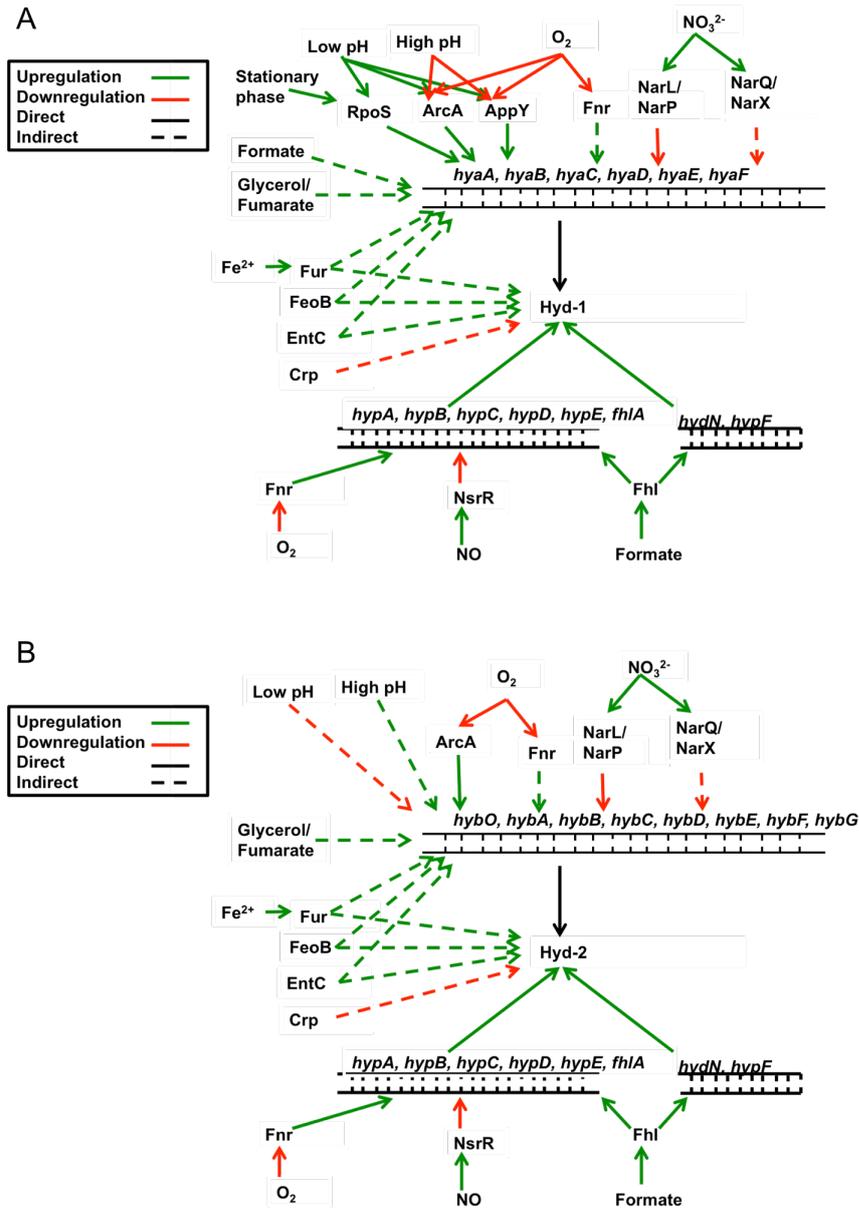
Figure 1.12 Regulation of A: Hyd-1 and B: Hyd-2 in *E. coli*.

Hyd-1 requires incorporation of iron ions, and thus gene expression is affected by their abundance. However, this is largely on a posttranscriptional level[124-125]. Although mutation of the iron homeostasis regulator Fur[126] showed significantly lower levels of the Hyd-1 and Hyd-2 protein than the wild type strain, this was shown not to be a transcriptional effect[127]. In addition, mutations to the iron transporters FeoB and EntC reduced levels of the *E. coli* MBH, whilst a double knockout shows next to no mature large subunit despite only minimal effect on transcriptional levels[125]. These findings concerning post-transcriptional control are as expected, as metal insertion occurs after translation, and is required to

mature the holoenzyme. The NikABCDE transporter transports nickel into *E. coli* in the form Ni(L-His)$_2$[128]. It has been suggested that this is a hydrogenase-specific transporter due to overlapping expression conditions such as nitrate repression and pH dependance[129], although mutational studies to confirm this have not been conducted.

The levels of Hyd-1 are affected by the growth medium. Although there has been some debate about the effects of supplementation with formate, with Brøndsted and Atlung seeing greater *hya* expression[121], Sawers et al observing increased presence of the protein[130] and Richard et al observing no difference in expression on supplementation[120], it is agreed that growth in a glycerol/fumarate medium increases *hya* expression[120-121]. This is likely due to the fermentation of glycerol, which is associated with formate hydrogen lyase activity[131]. As FHL in *E. coli* is coupled with the H$_2$-producing Hyd-3, activity results in an increase in molecular hydrogen, and thus an increased need for Hyd-1 activity. Expression of *hya* is not increased with growth on ribose, which was taken by Richard et al to indicate a lack of susceptibility to catabolite repression[120]. This is perhaps justified by the work of Brøndsted et al., who saw no effect of cAMP supplementation on *hya* expression[121]. However, Pinske et al in 2012 found that in a *crp* mutant strain in fermentative growth on glucose, increased levels of Hyd-1 were seen after six to twelve hours of growth[132]. The regulation of Hyd-2, in contrast, shows evidence of strong catabolite repression, although it is suggested to be indirect. The expression of this hydrogenase is upregulated by growth in glycerol and fumarate medium[120].

Certain aspects of the regulatory observations surrounding Hyd-1 and Hyd-2 can be explained by the regulation of the *hyp* and *hyd* operons, which are responsible for many of the maturation processes[133-134]. Both of these contain binding sites for FhlA in the promoter region, which acts as a transcriptional activator when bound to formate[135]. In this way, in the presence of formate, it forms a positive feedback loop, as the *fhlA* gene is contained on the *hyp* operon. The *hyp* operon is also activated by Fnr[136], which could explain how levels of

Hyd-1 and Hyd-2 are affected by this regulator despite the lack of a promoter site in the *hya/hyb* operons. Nitric oxide, bound to NsrR, has been identified as a repressor of the *hyp* operon[137]. Once more, there could be an involvement of *hyp* in Hyd-1 regulation, as nitric oxide is a product of the reduction of nitrate[138], known to suppress Hyd-1 and Hyd-2 activity[130].

1.3.5 Biosynthesis of the *E. coli* hydrogenases

In contrast to the FeFe hydrogenases, which have a well-understood biosynthesis pathway, the precise detail of how NiFe hydrogenase maturation proceeds is still under debate, but the system where it is best studied is *E. coli*. The active site maturation proteins used to synthesise all *E. coli* NiFe hydrogenases are from the *hyp* operon, which encodes the proteins HypA to HypF[139]. The major role of these proteins is to synthesise the NiFe active site with attached ligands, as summarised in Figure 1.13 and reviewed by Lacasse and Zamble[140]. In brief, HypF converts carbamoyl phosphate to an AMP adduct, and transfers the carboxamide moiety to the cysteine terminus of HypE[141-143]. On the scaffold formed by the interaction of these two, the carboxamide is reduced to a cyano group. HypE then interacts with a HypD-HypC complex transferring the cyano group to the iron centre contained within[144], although the main scaffold protein for the cofactor assembly is proposed to be HypD[145]. Whether the transfer of the cyano ligands occurs before addition of the carbon monoxide group is not yet established, although it is proposed that it is HypC (or the Hyd-2 accessory protein HybG) which transfers an Fe-CO_2 complex to HypD for reduction to carbon monoxide[146].

After two cycles of HypE interaction, in order to add both cyano groups to the iron, the HypC-HypD complex interacts with the hydrogenase large subunit and the $Fe(CN)_2CO$ moiety is transferred[147-149]. Meanwhile nickel, transported into the cell via the ATP-binding cassette (ABC) transporter NikABCDE[150], binds to a dimer of HypB and in a process mediated by GTP hydrolysis[151]. In the maturation of Hyd-3, this Ni containing dimer binds to zinc containing HypA[152], and this

HypB-HypA complex binds to the large subunit, where SlyD mediates the release of Ni and HypA from HypB by modulating the Ni binding affinity[153-154]. As Ni complexes the iron moiety, HypA is released. HypA is, however, specific for Hyd-3[133] and in Hyd-1 and Hyd-2 maturation, the homologue of HypA, Hyd-2 accessory protein HybF performs this role[155-156].
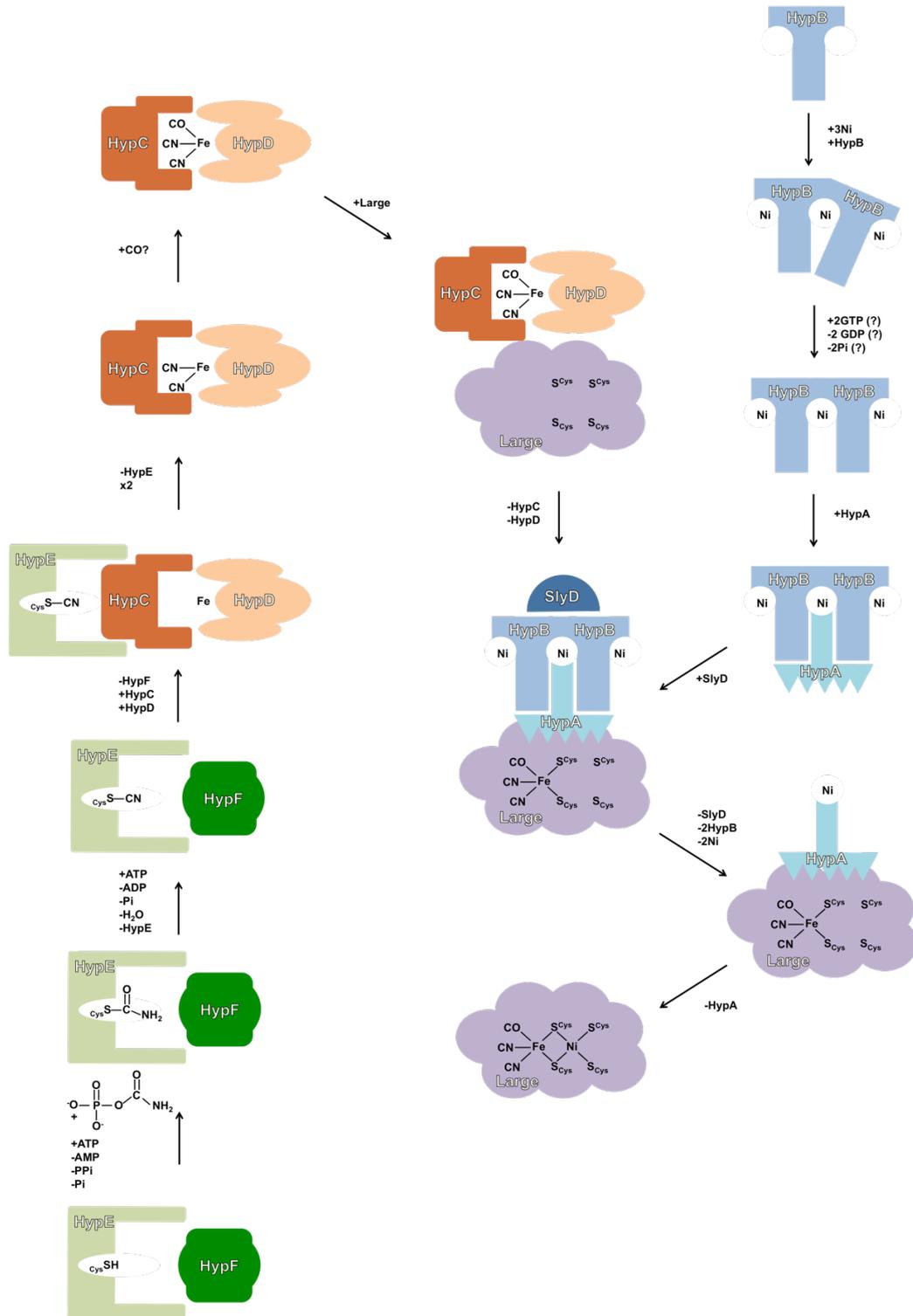
Figure 1.13 Role of the *hyp* operon in the biosynthesis of the NiFe active site.

Simultaneously to insertion of the active site into the large subunit, iron-sulfur clusters are assembled and ligated into the small subunit. This process is less well understood than the active site assembly. The iron may be transported into the cell by a number of transporters, including FeoB and EntC. *E. coli* then possesses several general mechanisms for cluster insertion, and Pinske and Sawers identified that in null mutants of the iron-sulfur cluster binding proteins IscA or ErpA there is no detectable activity of Hyd-1 or Hyd-2[157]. However these carriers have previously exhibited functional redundancy in anaerobiosis[158], convoluting the issue. A homologue of Hyd-1 accessory protein HyaF, HydG in *S. enterica* has been shown to have an important role in iron sulfur cluster insertion[159], suggesting that in *E. coli* the maturation of the small subunit could be individual to each hydrogenase, making this a complex issue to disentangle.

Following incorporation of the cofactors, further processing of NiFe hydrogenases is necessary, as shown in Figure 1.14. The unprocessed form of the large subunit is 15 amino acids longer at the C-terminal end than the processed form. The accessory protein HyaD, co-expressed with the large and small subunits of Hyd-1, is predicted to act as an endopeptidase, due to homology with HybD, which is the confirmed endopeptidase for Hyd-2[160]. Endopeptidase activity only occurs after detachment of HypC from the Ni-containing large subunit and is Ni-dependent[161], which supports the finding that insertion of Ni only takes place in the pre-processed form of the large subunit[162].

Transportation and insertion of the mature enzyme further depends on a cleavable N-terminal signal peptide in the small subunit which contains a SRRxFLK motif[163]. Such twin-arginine signal peptides target proteins towards the membrane embedded twin-arginine translocation (Tat) complex[164], a system which uses proton motive force (Δp) to transport fully folded proteins across the membrane together[165]. It has been shown for Hyd-2 that although only the small subunit contains the signal motif, both subunits are transported across the membrane[166]. Accessory proteins HyaE and HybE interact with the small subunit only when the signal peptide is present and are thus thought to act as non-

essential chaperones that perhaps act in a "proofreading" fashion[167]. The N-terminus of the small subunit containing the twin-arginine signal is cleaved after insertion into the membrane, in Hyd-1 this is at position A45[168].
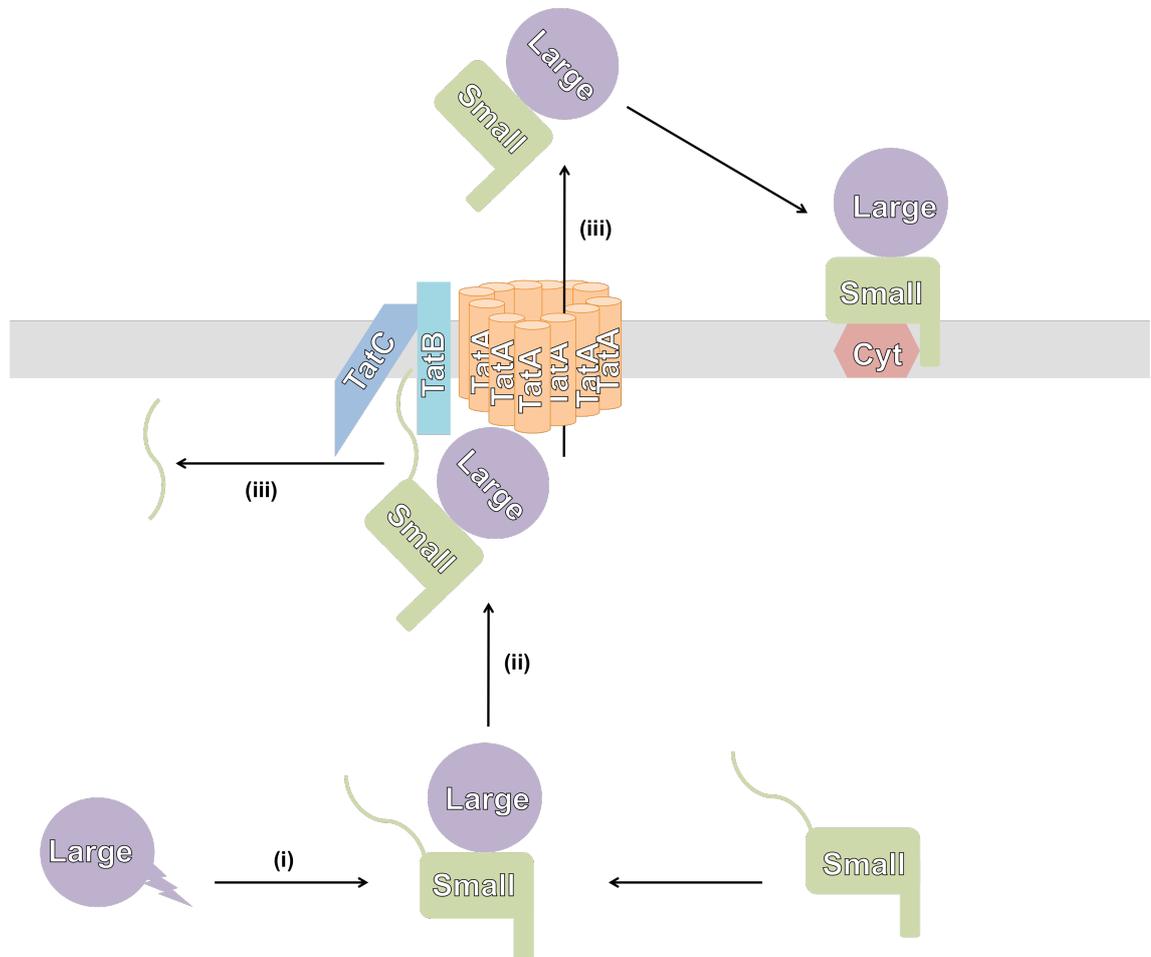
Figure 1.14 Processing and transportation of the periplasmic membrane bound NiFe hydrogenase. (i) The C-terminal peptide of the large subunit is cleaved, prompting association with the small subunit. (ii) The N-terminal peptide of the small subunit, containing the Tat signal motif, is recognised by TatB and TatC. (iii) The N-terminal peptide is cleaved and the large-small heterodimer is transported with intact secondary structure through the pore formed by a multimer of TatA.

1.4 Catalytic enzyme electrochemistry

1.4.1 Gas-activating redox enzymes and enzyme electrochemistry

Besides hydrogen, biology has evolved metalloenzymes to also activate the diatomic gas molecules N_2, CO, and O_2. Nitrogenases are enzymes expressed by multiple bacteria, for example cyanobacteria, and catalyze the conversion of N_2 to ammonia[169]. Carbon monoxide dehydrogenases (CODH) catalyze the reversible conversion between carbon dioxide and carbon monoxide[170]. Laccases, enzymes found in plants, fungi and microorganisms[171], use O_2 as a secondary substrate in the oxidation of a variety of phenolic substrates[172]. Photosystem II (PSII), catalyses light driven water splitting, providing high energy electrons in photosynthesis and generating all the O_2 in the atmosphere via water oxidation[173].

The structures of these enzymes are shown in Figure 1.15. All contain multiple transition metal active sites. While a subset of carbon monoxide dehydrogenases are comparable to hydrogenases, with both containing nickel and iron at the active site[174], laccases have copper O_2-reaction centres[175], the best characterized nitrogenases have molybdenum and iron reaction centres[176], although vanadium containing nitrogenases also exist[177], and PSII uses manganese[178] as the site of catalysis. The ability of biology to harness the redox activity of a variety of metal ions is therefore well demonstrated. The need for multiple metal centres can be rationalised as allowing for a distribution of electrons so that when reduction or oxidation catalysis occurs, the change in charge is shared across the cluster meaning that redox reactions can proceed more rapidly. In addition, coordination of the metals by the surrounding amino acids allows reactive properties to be tuned by the ligands, also contributing to rapid and efficient catalysis[179].

In order to transport electrons to/from the buried active sites all the enzymes employ electron transfer relays. For nitrogenase[180] and CODH[170] these take the form of iron-sulfur clusters, comparable to the hydrogenase structure, while

laccase simply uses more copper centers. For PSII this "wire" involves non-transition metal cofactors[181].

By connecting to the electron transfer relays such redox enzymes can be studied by electrochemistry. The simplest type of enzyme electrochemistry experiment involves immersing an electrode into a solution of enzyme in the absence of substrate, as carried out to measure reversible electron transfer in and out of the type 2 copper site of laccase[182]. This technique was also used to study nitrogenase, enabling identification of the midpoint potentials of the $[FeMoco^{red}] \rightleftharpoons [FeMoco^{semi-red}]$ and $[FeMoco^{semi-red}] \rightleftharpoons [FeMoco^{ox}]$ active site transitions[183]. Such experiments are not useful for catalytic studies because the observed turnover rate is limited by diffusion and not the biochemical activity of the enzyme.

A (i)

(ii)

Fe protein
4Fe4S cluster

e⁻

MoFe protein
P-cluster

e⁻

MoFe protein
FeMoco cluster

$N_2 \longrightarrow$ NH_3

B (i)

(ii)

$CO \longleftrightarrow$ CO_2

C-cluster

e⁻

B-cluster

e⁻

D-cluster

B-cluster

e⁻

C-cluster

e⁻

$CO \longleftrightarrow CO_2$

C (i)

(ii)

T1

substrate – OH $\longrightarrow$
substrate = O

e⁻

T3

T2

$O_2 \longrightarrow H_2O$

T2

D (i)

(ii)

Chlorophyll

Oxygen evolving
complex

Plastoquinone

Pheophytin

e⁻

$H_2O \longrightarrow O_2$
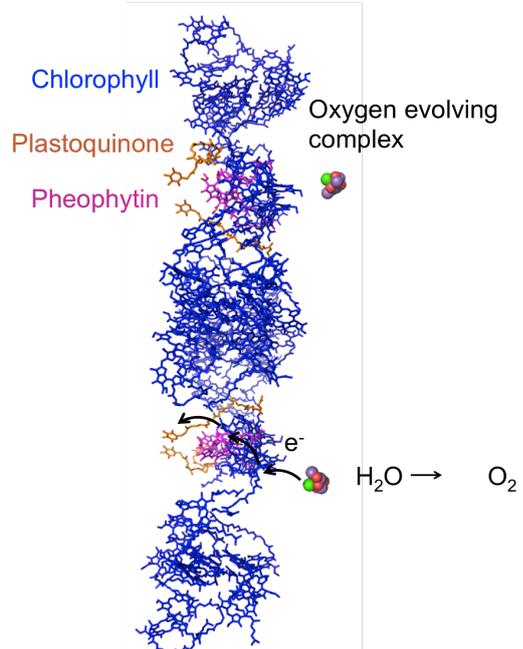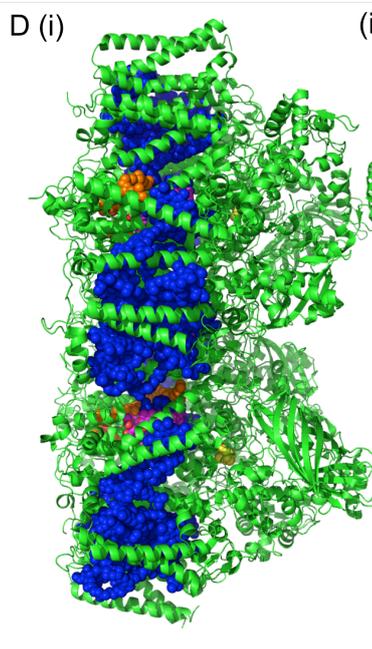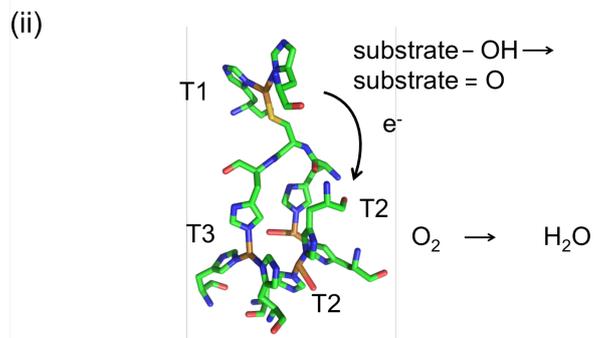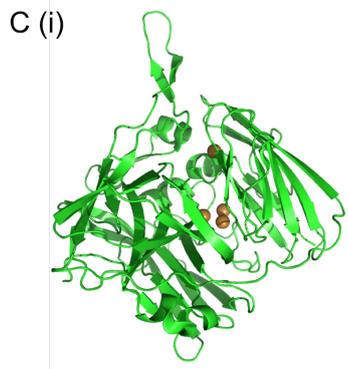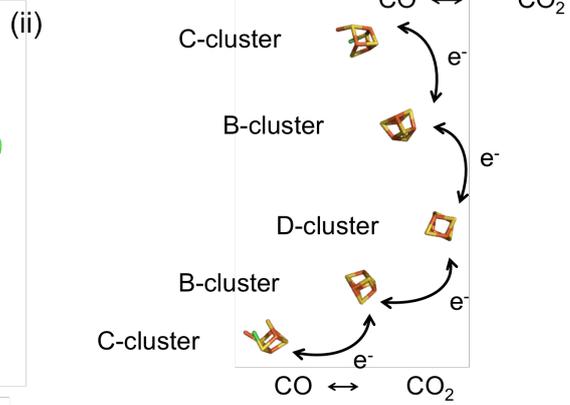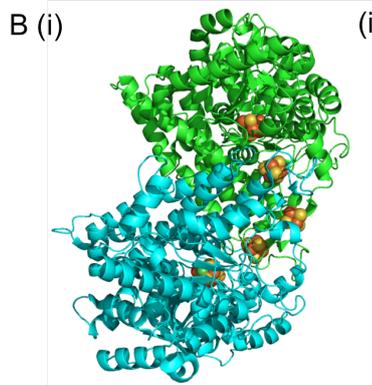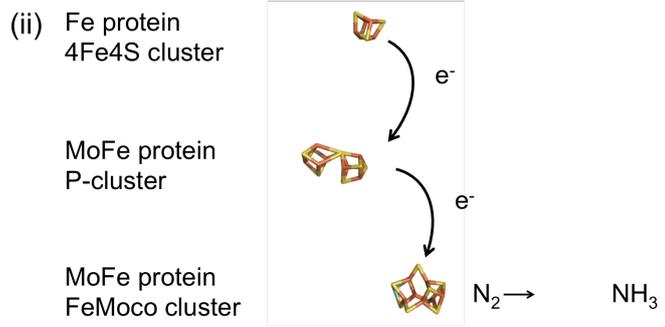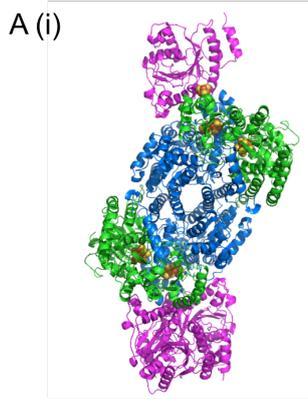
Figure 1.15 Structures of gas activating enzymes. A: Nitrogenase from *Azotobacter vinelandii* (PDB: 1N2C[176]). (i) Nitrogenase secondary structure. Colours: magenta, Fe Protein; blue, beta subunit of MoFe protein; green, alpha subunit of MoFe subunit; orange sphere, iron; yellow sphere, sulfur. (ii) Structure of the reactive clusters. Colours: orange, iron; yellow, sulfur; cyan, molybdenum. B: Carbon monoxide dehydrogenase from *Moorella thermoacetica* (PDB: 3I01[174]). (i) CODH secondary structure. Colours: green, monomer A; cyan, monomer B; orange sphere, iron; yellow sphere, sulfur; green sphere, nickel. (ii) Structure of the reactive clusters. Colours: orange, iron; yellow, sulfur; green, nickel. C: Laccase from *Thermus thermophilus* HB27 (PDB: 2XU9[175]). (i) Laccase secondary structure. Spheres: copper. (ii) Structure of the copper sites. Colours: brown, copper; blue, nitrogen; red, oxygen; green, carbon; yellow, sulfur. D: Photosystem II from *Thermosynechococcus vulcanus* (PDB: 4UB6[178]). (i) PSII secondary structure. Sphere colours: blue, cholorphyll; magenta, pheophytin; orange, plastoquinone; yellow, oxygen evolving complex. (ii) Cofactors of PSII. Colours: blue, chlorophyll; magenta, pheophytin; orange, plastoquinone; purple sphere, manganese; red sphere, oxygen; green sphere, calcium.

An alternative approach is to directly attach proteins to the surface of the working electrode. This is referred to as protein film electrochemistry (PFE). A typical setup is illustrated in Figure 1.16 with hydrogenase as an example. The cell is designed to facilitate temperature control using a water jacket and the buffer inside the cell determines the pH. A "three-electrode" setup is used where the potential of the working electrode is raised and lowered with respect to the reference electrode (often saturated calomel or Ag/AgCl) in order to give more reducing or oxidizing conditions, and the counter electrode (usually Pt) completes the circuit by countering the electron flow at the working electrode.
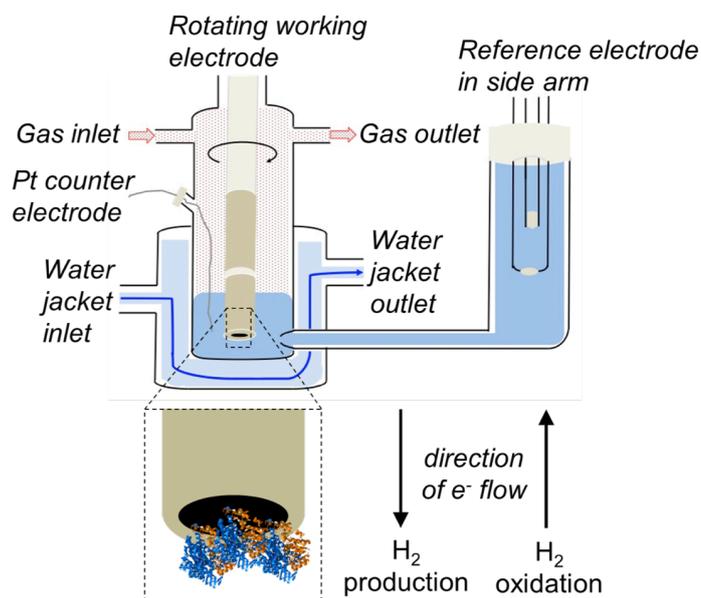
Figure 1.16 Protein film electrochemistry setup. Adapted from Flanagan and Parkin[24]. Hydrogenase is applied to an electrode as represented by the cartoon inset and placed into an electrochemical cell to form a three-electrode setup. The electrode rotates to avoid diffusion effects and temperature and gas composition is controlled.

PFE is useful for the characterisation of redox-active enzymes. For example, by sweeping the potential of a working electrode with a film of carbon monoxide dehydrogenase up and down (to oxidizing and reducing potentials respectively, known as cyclic voltammetry) the bidirectionality can be assessed by examining the positive and negative current, where positive current corresponds to CO oxidation and negative current CO_2 reduction[184]. The ability to hold the electrode at a constant potential (referred to as chronoamperometry) allows assessment of the impact of external factors such as inhibitors on the reactivity of the enzymes[185]. In some electrochemical setups the working electrode is able to rotate, which allows for minimization of diffusion effects. This can be important for supplying substrate, for example in analysis of the reduction of O_2 by laccase[172], or oxidation of H_2 by hydrogenases, and also for removing product, for example in H_2 production hydrogenase experiments and PSII O_2-producing photo-reduction experiments[186]. Hydrogenase electrochemistry will be the focus of the remainder of this chapter and a large component of this thesis.

1.4.2 Protein film electrochemistry of hydrogenases

In PFE of hydrogenases, positive current corresponds to the movement of electrons from the enzyme into the electrode (H_2 oxidation), and negative current corresponds to movement of electrons from the electrode into the enzyme (H_2 production). Equation 1.1 below states that the catalytic current, i_{cat}, is given as a function of the turnover rate, k_{cat}, the area of the electrode, A, the surface density of electroactive and correctly orientated enzyme on the electrode, Γ, the number of electrons, n, and Faraday's constant, F[187].

$$i_{cat} = k_{cat} \times nFA\Gamma$$

Equation 1.1

Translating a measurement of catalytic current into an enzyme turnover rate is therefore complex. Firstly this requires knowledge of the surface area of the electrode. One of the common surfaces used for this technique is pyrolytic graphite[57], which is cleaned by abrasion with sandpaper. This means that although the diameter of the electrode surface may be known, the surface area itself may actually be much greater as the surface will not be perfectly flat due to the scoring effects of this technique[188]. Indeed, the greater area of graphite relative to the same diameter of gold electrode may be why the graphite electrode is often preferred, as more enzyme may be adsorbed and thus yield greater currents. Secondly, the coverage density of electroactive and correctly orientated enzyme on the electrode is required. In theory, "non-turnover" enzyme electrochemical measurements, made in the absence of substrate, should reveal this parameter, but in most studies the signal from the enzyme in the absence of substrate is too small to see relative to the background electrode charging and discharging processes[189]. Additionally, hydrogenases react with protons, an unavoidable substrate when water is the solvent.

1.4.3 Electrochemical definitions of O_2 tolerance

Electrochemistry has proved an important technique in defining hydrogenase O_2 tolerance. Figure 1.17 shows a chronoamperometric experiment showing how the O_2 tolerant *E. coli* Hyd-1 and the O_2 sensitive *E. coli* Hyd-2 react to the presence of oxygen. In this experiment the potential is held at a constant voltage whilst the electrochemical cell is exposed to (i) 3% H_2 (ii) 3% H_2 and 3% O_2 and (iii) 3% H_2. It is seen that whilst the activity of Hyd-1 under O_2 reaches a plateau, the activity of Hyd-2 tends towards zero as exposure to O_2 increases. After O_2 is removed from the system, the activity of Hyd-1 quickly returns to almost 100% of the initial activity. By contrast, during the 30-minute reactivation period after O_2 is removed from the system, Hyd-2 regains only 80% of the initial activity. This loss of activity is due to formation of the Ni-A state, which is spectroscopically detectible in samples of O_2 sensitive enzyme exposed to air[190].
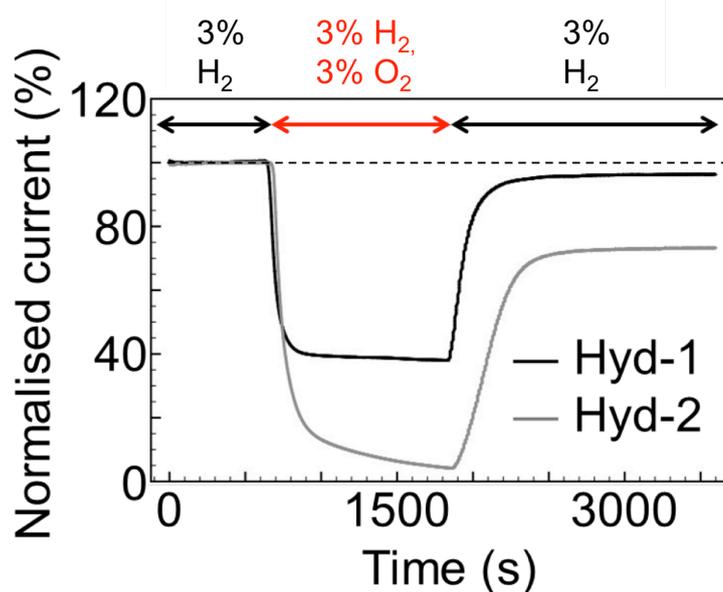
Figure 1.17 Chronoamperometry experiment showing the effect of O_2 inhibition on *E. coli* Hyd-1 (black) and Hyd-2 (grey). Adapted from Flanagan and Parkin[24]. The potential was held at a constant value whilst the system was exposed to 10 minutes of 3% H_2, 20 minutes of 3% H_2 and 3% O_2, then 30 minutes of 3% H_2. The dotted line shows the initial activity, which has been normalized to 100%.

1.4.4 The electrochemistry of hydrogen catalysis and catalytic bias

The ability of electrochemistry to investigate both H_2 production and H_2 oxidation has proved useful for investigating whether a hydrogenase has a catalytic bias either towards H_2 oxidation or H_2 production[191]. An example of this is shown in Figure 1.18, which shows cyclic voltammograms of Hyd-1 and Hyd-2 as the potential is swept from reducing to oxidizing conditions and back again. At more oxidizing, higher potentials, both Hyd-1 and Hyd-2 show approximately 3 μA of H_2 oxidation. However, at lower, more reducing potentials, only Hyd-2 shows 2 μA of H_2 production, whilst Hyd-1 has a negligible negative current. In other words, Hyd-1 has a strong bias towards H_2 oxidation, whilst Hyd-2 is a more bidirectional catalyst.
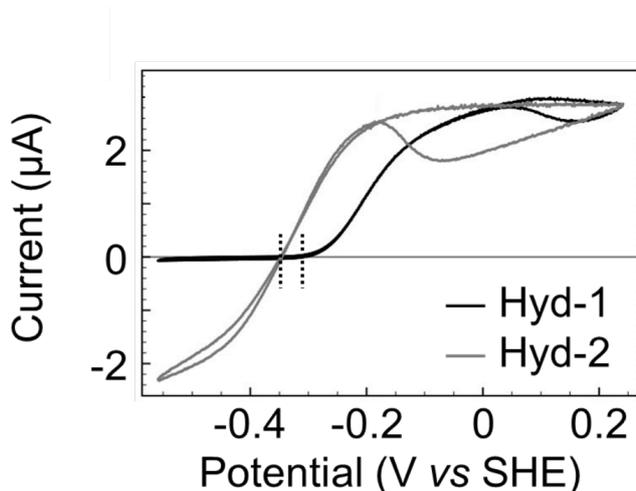
Figure 1.18 Cyclic voltammetry experiment showing catalysis under 3% H_2 for Hyd-1 (black) and Hyd-2 (grey). Adapted from Flanagan and Parkin[24]. The potential is swept from -0.558 V vs SHE to +0.242 V vs SHE and back again at pH 6. Resulting current is proportional to hydrogenase activity. Vertical dotted lines show the potential of onset of H_2 oxidation.

This catalytic bias towards H_2 oxidation has been observed in all O_2 tolerant hydrogenases, as has the overpotential requirement, the additional ~0.05 V of potential required for the onset of H_2 oxidation to commence in Hyd-1 relative to Hyd-2[68]. It is thought that this overpotential requirement and the catalytic bias are dependent on the point of electron exit and entry into the enzyme, and thus the potential of the distal 4Fe4S cluster[192-193], which has not yet been observed

through EPR in Hyd-1. However, as defined by Murphy et al[68], at pH values below 5, the overpotential for Hyd-1 begins to approach the standard $2H^+/H_2$ reduction potential, and Hyd-1 becomes a more reversible catalyst. The exact ratio of H_2 production to H_2 oxidation in that study could not be quantified as significant H_2 production is only seen when a large amount of protein film is applied to the electrode. This means that at low partial pressures of H_2, diffusion limitation causes a current plateau that prevents determination of the exact H_2 oxidation current, whilst at high partial pressures of H_2 the diffusion limitations are avoided, but the extent of product inhibition lowers the H_2 production current.

During investigations into *Desulfovibrio vulgaris* hydrogenase variants, Hamdan et al found that narrowing gas channels can also alter catalytic bias[191]. Mutations to a valine at the mouth of the gas channel in O_2 sensitive hydrogenases increases the O_2 tolerance by restricting O_2 access, but also increases the catalytic bias towards H_2 oxidation[191]. This observed effect was attributed to slower rates of H_2 release in H_2 production, but not H_2 binding in H_2 oxidation, and thus may be described as decreasing H_2 production rather than increasing H_2 oxidation.

1.4.5 Anaerobic inactivation

Even with a low electroactive film coverage on the electrode, as in Figure 1.18, as the scan goes from low potential to high, a plateau is reached, with the current continuing to decrease during the backwards scan. As the backwards scan continues towards lower potentials, the current increases once again. Spectroscopic evidence indicates the reason for this decrease in current is the high potential formation of the Ni-B state[194-195]. It may be seen that the extent of this inactivation is much greater for Hyd-2 than it is for Hyd-1. Slow scan rates, where the system is at oxidizing potentials for longer, have been used to measure a parameter called E_{switch}, defined by the point of greatest rate of reactivation in the scan from high to low potentials[195]. This parameter has been

used to compare different hydrogenases and variants of hydrogenases. For example, in the work by Evans et al discussed earlier, the R509K (*E. coli* numbering) mutation which significantly lowered the turnover did not adjust the E_{switch} parameter, whilst the mutation of the nearby aspartate residues to asparagine had less effect on the turnover but significantly lowered the E_{switch}[67]. This suggests that the reactivation from the Ni-B state is able to occur at more oxidizing potentials when in proximity to the negatively charged aspartate residues than when in proximity to the neutral asparagines. The E_{switch} has previously been used to determine Ni-B reduction potentials, acidity constants and reaction enthalpies and entropies. However, work by Fourmond et al suggests that the E_{switch} parameter should not be used in this manner[196]. They instead use a chronoamperometry experiment where they switched between inactivating and activating potentials in order to determine that, at least for *Aquifex aeolicus* NiFe hydrogenase, the inactivation constant k_I, is potential independent, whilst the activation constant, k_A, decreases exponentially with potential, until it reaches a limit. This limit at oxidizing potentials and under H_2 has been interpreted to mean that at these potentials, a process not involving transfer of electrons from the electrode causes reactivation of the Ni-B state. As a long incubation with H_2 can reactivate an O_2 sensitive hydrogenase after O_2 exposure[197], it has been hypothesized that this reactivation process is H_2 driven. From the analysis in this work, they hypothesized that the formation for the Ni-B $Ni^{III}OHFe^{II}$ state proceeds via $Ni^{II}H_2OFe^{II}$ and $Ni^{III}H_2O$ intermediates[196]. This proposal would fit the previous evidence that the bridging hydroxide is solvent derived[76].

The previously discussed gas channel mutants of *Desulfovibrio fructosovorans* hydrogenases show an increased O_2 tolerance and catalytic bias towards H_2 oxidation[191], but analysis using the potential step methodology also showed that the reactivation rate, k_A, compared favorably with the O_2 tolerant *Aquifex aeolicus* hydrogenase[198], higher than the k_A of the wild type hydrogenase. They showed that the O_2 tolerance was positively correlated with both the rate of activation and the rate of inactivation. This could mean that the variant enzymes

formed a protective Ni-B state more quickly than the native hydrogenase but also reactivated more quickly from Ni-B to an active state. The evidence in the work was used to hypothesize that the aerobic inactivation is related to the anaerobic inactivation. However, as stated previously, a variant of *R. eutropha* MBH with impaired O_2 tolerance in fact reactivated more quickly after O_2 exposure[199]. This work did not encompass analysis of anaerobic inactivation, for reasons that will be discussed later in this chapter. The disparity between the two hypotheses and whether it is preferable that k_A would be higher or lower will be discussed further in Chapter 5.

1.4.6 Electrochemistry of multimeric structures

As mentioned earlier, most electrochemical experiments and crystal structures of hydrogenases feature only the large and small subunits[33, 56-57, 71], whilst in the cell the membrane bound NiFe hydrogenase usually co-expresses with at least one additional cytochrome *b*-type subunit embedded in the membrane which transports the electrons between the enzyme and other cellular components such as ubiquinones[48]. At the time of writing, the only crystal structure published which features the cytochrome subunit is that of *E. coli* Hyd-1, and shows a (large)$_2$(small)$_2$cyt arrangement, where the dimer of heterodimers is arranged so that the distal cluster of each small subunit is within electron transfer distance[200] from the heme group of the cytochrome[35]. However, it is not known whether this is representative of the true state of the enzyme in the *E. coli* cell, or whether it is representative of other NiFe hydrogenases. In particular it has been shown that the *R. eutropha* NiFe hydrogenase can be extracted in a lipid bilayer as a trimer of heterotrimers[201], with a (large)$_3$(small)$_3$(cyt)$_3$ arrangement. Furthermore, electrochemistry of this supercomplex does not show anaerobic Ni-B formation, as seen when the large and small subunits are isolated, and O_2 tolerance of the heterotrimeric complex is also enhanced[199]. The lack of a current plateau at high potentials has, in part, been explained by the need to use mediated electrochemistry with ubiquinol in order to monitor electron transfer whilst the hydrogenase is in its multimeric form in the lipid bilayer. Radu et al[199]

state that when the cytochrome b is in equilibrium with its ubiquinone partners the active site is prevented from permanently resting in the Ni-B state, even when the ubiquinone pool is fully oxidized. Also, O_2 inactivated hydrogenase is quickly reactivated even under high potentials. They propose that the trimeric complexes can form large supercomplexes, and that electron transfer between these complexes can assist reactivation even when the ubiquinone pool is exhausted.

Formation of larger complexes is thus important to consider when investigating the electrochemical properties of hydrogenases, however there are issues with these investigations. The first issue is attaching the enzyme to the electrode, necessitating that the complex is embedded in a lipid bilayer, and that this bilayer is attached to the electrode with a mixed self-assembled monolayer (SAM) formed from tether and spacer molecules [199]. The second issue is the need to use ubiquinone mediators in order to conduct electron transfer. In addition to the aforementioned effects on the O_2 tolerance and anaerobic inactivation which may obscure the differences between enzyme variants, at low currents, the catalytic wave-shape is dominated by the redox transitions of the ubiquinone[202], which could lead to misinterpretation of the transitions which occur.

Chapter 2

Large subunit variants of *Salmonella enterica* membrane bound NiFe hydrogenase-5

2.1 Introduction

The three *S. enterica* membrane bound NiFe hydrogenases (MBH) have been implicated in pathogen virulence[98]. Hyd-1 and Hyd-2 share a high degree of homology with the hydrogenases of the same name in *E. coli* and are expressed anaerobically *in vitro,* like the *E. coli* hydrogenases (see Section 1.3 of Chapter 1). Hyd-5, whilst most closely resembling *E. coli* Hyd-1, has no direct equivalent in *E. coli* and is preferentially expressed under aerobic conditions *in vitro*[9]. Expression of both Hyd-1 and Hyd-5 is upregulated in murine macrophages, and deletion of these enzymes prevents colonisation of mice[119]. It has been hypothesised that the O_2 tolerance of the hydrogenases is important in bacterial macrophage survival, and thus understanding this property could be beneficial in the design of new anti-microbials.

Much research has been conducted on the role of the small subunit in the O_2 tolerance of MBH. The clusters proximal and medial to the active site have both been shown to have vital roles in the ability of hydrogenase to oxidise H_2 in the presence of O_2[32, 56-57]. However, despite the fact that these clusters lie close to the large-small subunit interface, and the possible need for communication between the clusters and the active site, the role of large subunit residues have been largely neglected in the study of O_2 tolerance.
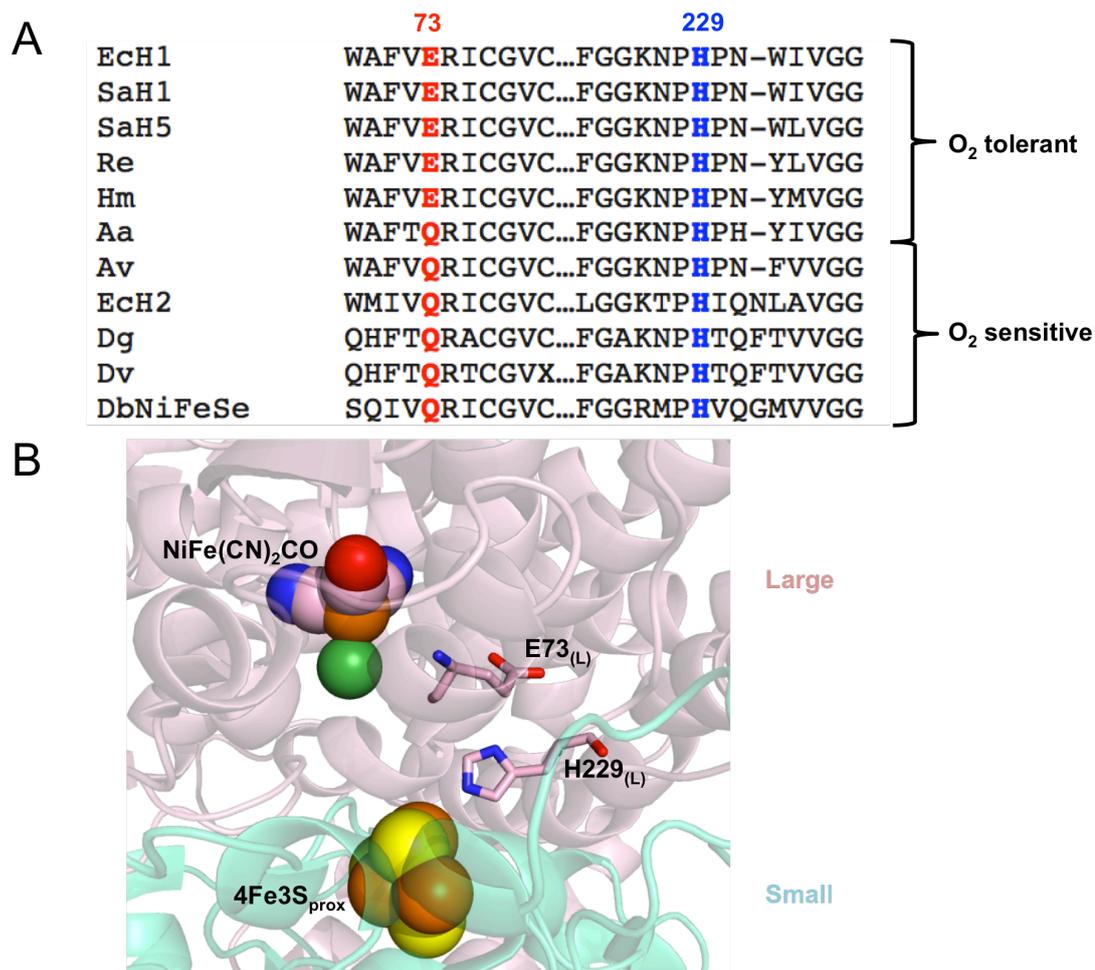
Figure 2.1 Conservation of residues 73 and 229. Adapted from Bowman et al[36]. A: Sequence alignment of sections of large subunit sequences. The sequences of O_2 tolerant hydrogenases (Sa5, *S. enterica* Hyd-5; EcH1, *E. coli* Hyd-1; Re, *R. eutropha* MBH; Hm, *Hydrogenovibrio marinus* MBH; and Aa, *Aquifex aeolicus*) are compared with sequences from standard O_2 sensitive hydrogenases (EcH2, *E. coli* Hyd-2; Av, *Allochromatium vinosum*; Dv, *Desulfovibrio vulgaris*; and DbNiFeSe, *Desulfomicrobium baculatum* NiFeSe hydrogenase) showing the conservation of the histidine 229 and glutamate 73. B: Crystal structure of *S. enterica* Hyd-5 (PDB: 4C3O[36]) showing relative location of histidine 229 and glutamate 73 (detailed residues) to each other, the proximal cluster, and the NiFe active site. Atoms associated with cofactors are depicted as spheres and coloured according to type: yellow, sulfur; orange, iron; green, nickel; red, oxygen; pink, carbon; blue, nitrogen. The secondary structure of the small subunit is traced in cyan, whereas the secondary structure of the large subunit is traced in pink.

A recent crystal structure of *S. enterica* typhimurium Hyd-5 shows a large subunit histidine, 229, within hydrogen bonding distance of the proximal 4Fe3S cluster[36] (Figure 2.1 B). Sequence alignment shows that this histidine is completely conserved amongst all NiFe hydrogenases, whether O_2 sensitive or O_2 tolerant (Figure 2.1 A). Another residue, glutamate 73, was identified as of potential interest as the glutamate is only conserved amongst O_2 tolerant MBH. All other NiFe hydrogenases have a conserved glutamine at this position. It was thus hypothesised that residues 229 and 73 would have an impact on either the catalysis or the O_2 tolerance of Hyd-5.

2.2 Methods

Native, E73A variant and H229A variant Hyd-5 were created by chromosomal mutation and purified from *S. enterica* by Lisa Bowman[36] (at the time, PhD student at the Division of Biological Chemistry and Drug Discovery, College of Life Sciences, University of Dundee). These were transported on dry ice to the University of York and frozen in liquid N_2. The protein samples were transferred into the anaerobic glove box whilst still frozen. Protein film electrochemistry was performed according to the methods described in Chapter 8.

For the methylene blue assay, Hyd-5 was purified from the same Native and variant strains by Julia Walton (Research Technician at the University of York) according to the method described in Chapter 8. The methylene blue assay was performed by David Lloyd (Project student at the University of York) according to the method described in Chapter 8 immediately after taking the enzymes into the anaerobic glove box. The enzymes were then diluted 100-fold in H_2 saturated buffer and left for a period of at least 24 hours before the assay was performed once more.

2.3 Results and discussion

2.3.1 The role of glutamate 73 and histidine 229 in Hyd-5 catalysis in the absence of O_2

Chromosomal mutations of Hyd-5 in *S. enterica* were created and purified by a collaborator, Dr Lisa Bowman, under the supervision of Prof. Frank Sargent (Division of Biological Chemistry and Drug Discovery, College of Life Sciences, University of Dundee). The parent *S. enterica* strain contains an altered promoter which upregulates the Hyd-5 operon and a stop codon that truncates the small subunit before the transmembrane helix. The latter design feature ensures that the Hyd-5 enzyme is devoid of a membrane anchor, and the large-small heterodimer is therefore soluble in the periplasm, enabling purification without the need for membrane solubilisation steps[36]. The parent strain was used to create alanine variants of histidine 229 (H229A) and glutamate 73 (E73A) and the enzymatic properties were compared to those of the Native Hyd-5.

Methylene blue assays were performed by undergraduate student David Lloyd (Project student, University of York) to determine the turnover rate (k_{cat}) at pH 6 for H_2 oxidation. These assays showed that both variants had lower activity than the native enzyme in their as-isolated form (k_{cat} for Native Hyd-5: 18 s^{-1}, E73A variant: 6 s^{-1}, H229A variant: 5 s^{-1}). This could, in part, be due to a portion of the enzyme used to measure concentration not being mature hydrogenase containing the correct metal ions. However, the E73A variant activated by a sustained period under a H_2 atmosphere had the same H_2 oxidation activity as the Native Hyd-5 (Native Hyd-5: 20.8±0.1 s^{-1}, E73A variant: 20.1±0.1 s^{-1}) and thus it is likely that the difference in initial turnover was due to mature but inactive MBH. In contrast, although turnover of the H229A variant increased with activation, the variant continued to have poor activity compared to the Native Hyd-5 (12.6±0.5 s^{-1}). These results would suggest that the E73A variant is susceptible to O_2 inhibition during the aerobic purification procedure, and that this inhibition is reversed during activation by incubation with H_2, as documented previously for O_2 sensitive NiFe hydrogenases[195, 197]. As the turnover

rate of the H229A Hyd-5 variant also increases following H_2 activation, it is likely that some of the same O_2 inhibition also occurs in this variant. However, the reason why the maximum post-activation turnover rate does not equal Native levels are not determinable through the use of assays and suggests that more in-depth mechanistic experiments are needed.

In order to explore further, the activated enzymes were investigated using protein film electrochemistry. Figure 2.2 shows cyclic voltammetry plots for the H_2 oxidation activity of Native Hyd-5 and the E73A and H229A variants in the absence of O_2. In these experiments, the potential is swept from low to high (forward sweep) and then reversed (back sweep). As previously reported, the voltammogram for Native Hyd-5 is representative of H_2 oxidation processes in other O_2 tolerant MBH[9]. As illustrated in Figure 2.3 D, Hyd-5 exhibits the characteristic overpotential requirement of O_2 tolerant MBH, where the potential of onset of H_2 oxidation is greater than required by the $2H^+/H_2$ Nernst couple (denoted by the vertical bar). During the forward scan of Native Hyd-5 under 10% H_2 (Figure 2.2), above -0.3 V vs standard hydrogen electrode (SHE) the current begins to rapidly increase before reaching a plateau at potentials more positive than -0.05 V vs SHE. During the backwards sweep, the current decreases in the potential region from +0.2 to +0.1 V vs SHE. This decrease in current at high potential is attributed to anoxic inactivation of the enzyme due to Ni-B formation[194-195]. The current increase, observed as the potential is lowered between +0.1 and -0.05 V vs SHE, is attributed to the reverse reaction, the conversion of oxidatively inactivated Ni^{III}-B back to catalytically active Ni^{II} through the addition of a proton and an electron[195]. By differentiating the cyclic voltammogram, an approximation of the potential of the fastest rate of reactivation from Ni-B, may be determined. The position of this potential, the E_{switch}, is indicated by the dotted red circle in Figure 2.2 A.

As with Native Hyd-5, the E73A variant has an overpotential requirement (Figure 2.2 D). The inactivation and reactivation for E73A also occurs at the same potentials as in Native Hyd-5 (Figure 2.2 B), and although at high

potentials the H_2 oxidation current from the E73A variant does not plateau in the forward sweep as extensively as observed in Native Hyd-5 experiments, overall the differences in catalytic waveshape are not significant, and likely due to the higher film of Native Hyd-5 on the electrode, as indicated by the maximum H_2 oxidation current observed in each. In contrast, the H229A variant shows a markedly altered voltammetric waveshape. Rather than observing a current plateau during the forward potential sweep, the current sharply declines so that the activity at +0.2 V vs SHE is less than half that at 0 V vs SHE. This experiment can therefore explain the lower turnover rate in the methylene blue H_2 oxidation assays of H229A, as the redox potential of methylene blue at pH 6 is around +0.047 V vs SHE[203], in the region where the H229A variant is more extensively inactivated relative to the other two variants, as indicated in Figure 2.2.

Although it is possible that film loss is a factor in the shape of the voltammogram of the H229A variant, it would be expected that this would result in a lower maximum current of H_2 oxidation than the Native Hyd-5, whereas this is not the case. Furthermore, the sharp increase in current during the reverse potential sweep of H229A from +0.1 to -0.05 V vs SHE indicates that the loss in current at high potential is reversible[8, 204]; suggesting that the inactivation/reactivation process involves the reversible formation of the rapidly-reactivating Ni-B state. There is also only 15 mV of difference between the E_{switch} of the H229A variant and Native Hyd-5, supporting the notion that similar states are involved. However mechanistic reasons for the difference in the extent of inhibition cannot be provided by just voltammetric experiments and therefore this issue is returned to in Chapter 5.
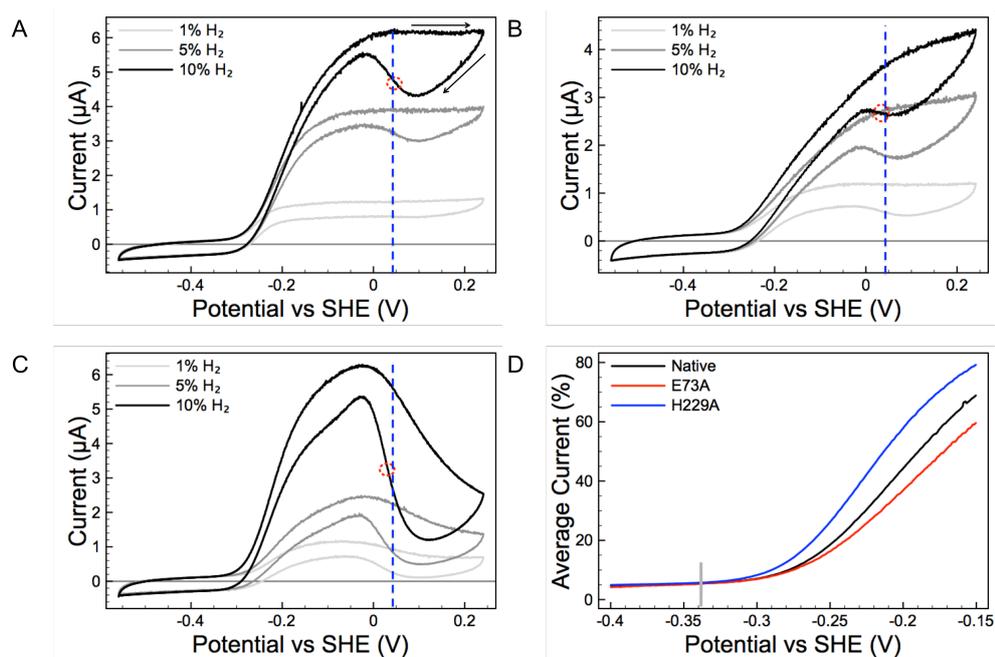
Figure 2.2 Anoxygenic H_2 oxidation catalysis. Adapted from Bowman et al[36]. The plots show the catalytic response to H_2 of Hyd-5 A: Native, B: E73A variant and C: H229A variant at pH 6.0, 37°C. Cyclic voltammograms were performed under different percentages of H_2 as indicated. A N_2 carrier gas was used to give a total gas mixture flow rate of 100 standard cubic centimeters (scc) min^{-1}. The potential was increased from -0.56 to $+0.24$ V vs SHE, and then the scan direction was reversed at a rate of 5 mV s^{-1} (direction indicated by arrows in A). The dotted red circle shows the potential of fastest reactivation from Ni-B, E_{switch}, for each voltammogram at 10% H_2 and 5 mV s^{-1} The blue dotted line indicated the methylene blue redox potential, $+0.047$ V vs SHE[205]. D: To emphasize the overpotential for catalytic onset the voltammograms measured at 10% H_2 for each enzyme are compared. The current during the forward and back potential sweep has been averaged and then normalized relative to the current at 0 V vs SHE. The grey vertical line shows the calculated Nernstian onset potential, $E(H^+,H_2)$, under the experimental conditions.

Figure 2.3 shows experiments conducted to determine the H_2 affinity of the Hyd-5 variants. In this experiment, the potential was maintained at $+0.06$ V vs SHE and the percentage of H_2 was adjusted according to the dotted line. The current response to this H_2 concentration may be used to construct a Hanes-Woolf plot, as described in Chapter 8, which gives a value for the

Michaelis constant, K_M. The value of K_M is $7.1 \pm 2.7\ \mu$M for the E73A variant and $5.9 \pm 1.2\ \mu$M for the H229A variant. The value of the K_M for Native Hyd-5 measured in an earlier study was slightly higher at $9\ \mu$M[9], but this is likely due to the higher pH value of 7.4 at which the study was conducted. Cracknell et al observed K_M values of 8 to 15 in the O_2 tolerant MBH of *R. eutropha*, which varied with pH[206]. Since the amino acid substitutions in the variants are away from the proposed H_2 gas channel[71] (see Section 1.2.4 of Chapter 1), changes to the H_2 affinity of the enzymes are not expected.
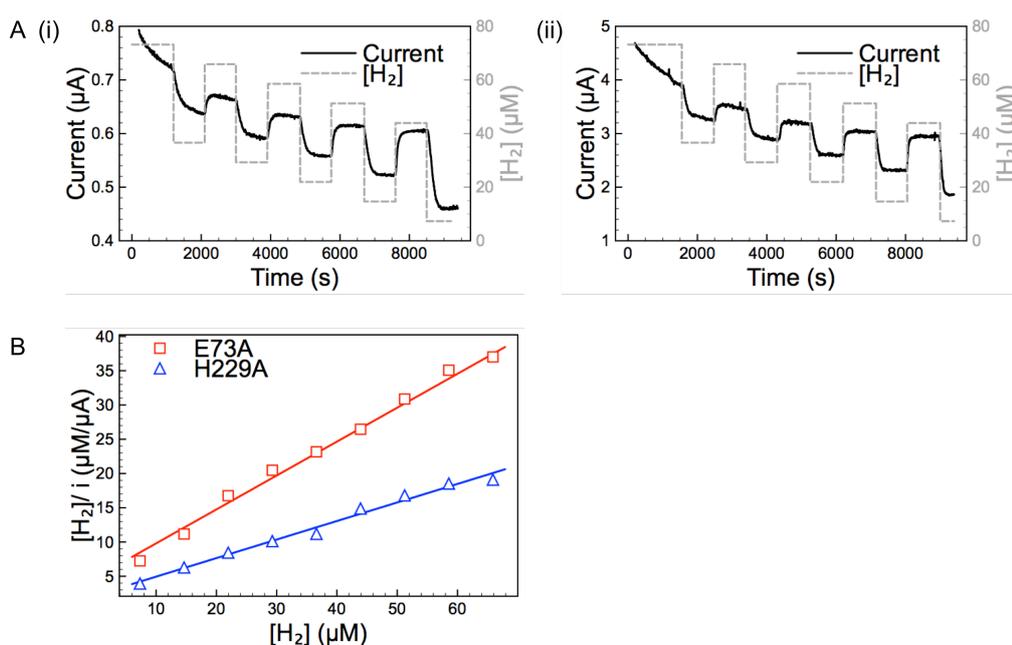
Figure 2.3 Determination of the Michaelis constant. A: The current response was monitored (black, unbroken line) at varying concentrations of H_2 (grey, dotted line) for the Hyd-5 (i) E73A variant and (ii) H229A variant. The plots shown have been corrected for film loss. B: Hanes-Woolf plot, used to determine the Michaelis constant for the E73A variant (red triangles) and the H229A variant (blue circles).

2.3.2 The role of glutamate 73 and histidine 229 in Hyd-5 catalysis in the presence of O_2

Since glutamate 73 is generally a conserved residue in O_2 tolerant MBH, the sensitivity of the Native and variant Hyd-5 enzymes to O_2 inhibition was probed by chronoamperometry experiments, shown in Figure 2.4. The current response was monitored at +0.06 V vs SHE under 3% H_2 before switching to a 3% H_2 3% O_2 mixture, then finally the system was returned to 3% H_2. Native Hyd-5 shows little inhibition under O_2 and almost 100% of the initial activity is recovered once O_2 is removed. An ability to maintain activity under O_2 is the marker of O_2 tolerance, and an essential requirement of an aerobically expressed hydrogenase[207]. As with other O_2 tolerant hydrogenases, the small amount of inactive state which is formed under O_2 is attributed to formation of the Ni-B state[208], because the enzyme quickly reactivates once O_2 is removed from the system.
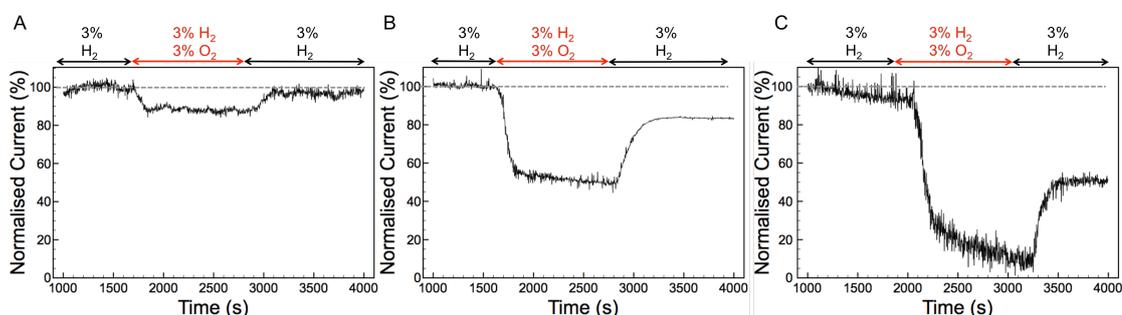
Figure 2.4 Sensitivity to O_2 inhibition. Chronoamperometric traces showing the inhibition by O_2 and recovery from O_2 inhibition for A: Native Hyd-5, B: E73A and C: H229A. The potential was held at +0.06 V vs SHE and the system was held under 3% H_2, before the gas was switched to 3% H_2 and 3% O_2, after which the system was returned to 3% H_2. Current is normalized to the activity immediately before O_2 exposure. Grey dotted line represents the maximum possible activity. Other conditions: pH 6, N_2 carrier gas at 100 scc min^{-1}, 4000 rev per minute (rpm) rotation rate.

In contrast to Native Hyd-5, the E73A variant (Figure 2.4 B) shows an approximate 50% drop in H_2 oxidation activity under O_2, and 80% of the initial activity is recovered after O_2 is removed from the system. The fact that not all of the inhibited enzyme recovers from O_2 inhibition rapidly suggests that some of the E73A enzyme inactives to form either the long lasting "unready" Ni-A state,

or a "dead" state. The methylene blue assays reported earlier in this chapter demonstrate that the E73A variant shows recovery after a long period of incubation with H_2, suggesting that the state formed under O_2 is Ni-A. This is an indication that the E73A variant is more O_2 sensitive than Native Hyd-5.

The chronoamperometry trace for the Hyd-5 H229A variant (Figure 2.4 C) shows strong O_2 inhibition. Whilst the H_2 oxidation activity of Native Hyd-5 rapidly stabilizes under O_2, the activity of the H229A variant tends towards zero. Although there is likely some film loss, as observable in the slight decline in current in the first stage of the chronoamperometry experiment, the trajectory under O_2 is much more negative, comparable to the behavior of O_2 sensitive hydrogenases[8]. Furthermore, the variant recovers no more than 50% of the initial activity when O_2 is removed from the system, a much lower current than could be explained merely by extrapolating the film loss. As with the E73A variant, it is likely that H229A forms a mixture of Ni-B and Ni-A under O_2.

Cyclic voltammetry experiments showing activity before, during and after O_2 exposure (Figure 2.5) reveal that under O_2 (black trace) the variant enzymes show little (E73A) or no (H229A) activity above +0.05 V vs SHE, whilst the Native Hyd-5 retains some activity even at +0.25 V. The negative current measured at potentials more negative than -0.3 V vs SHE in O_2 is due to O_2 reduction on the carbon surface and is not due to enzyme activity. The grey dashed line in Figure 2.5 shows the potential at which the chronoamperometry experiments in Figure 2.4 were conducted.
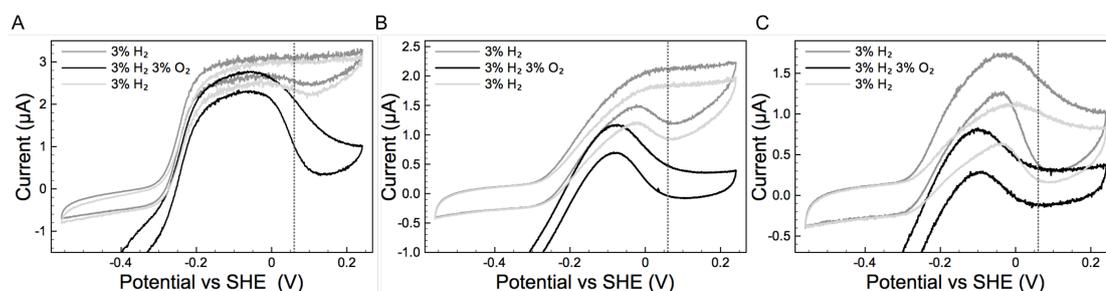
Figure 2.5 Cyclic voltammetry of Hyd-5 A: Native, B: E73A variant and C: H229A variant before, during and after exposure to O_2. The potential was swept from -0.56 to +0.24 V vs SHE and back again at a rate of 5 mV s^{-1} 5 times under 3% H_2 (dark grey) followed by five times under 3% H_2 and 3% O_2 (black) before five cycles once more under 3% H_2 (light grey). The fifth cycle of each is shown. Grey dotted line represents shows the potential at which the chronoamperometric experiments in Figure 2.4 were conducted. Other conditions: pH 6, N_2 carrier gas at 100 scc min^{-1}, 4000 rpm rotation rate.

Again, the Native Hyd-5 voltammogram measured after exposure of the enzyme to O_2 (Figure 2.5 A, light grey) shows 90% of the H_2 oxidation activity is recovered following O_2 exposure. The same voltammogram for the E73A variant (Figure 2.5 B, light grey) exhibits less than 80% of the original activity, confirming that this variant is more susceptible to long lasting inactivation. The H229A variant shows the least recovery after O_2 exposure (~50%), suggesting that half of this enzyme forms a long lasting inactive state during exposure to O_2. These results therefore support the chronoamperometry measurements, confirming that both the E73A and the H229A Hyd-5 variant form a mixture of Ni-A and Ni-B under O_2 exposure. Both variants thus have diminished O_2 tolerance.

2.3.3 Confirmation of observed results and hypotheses on the role of glutamate 73 and histidine 229 in MBH

Shortly after the *S. enterica* Hyd-5 work was published, Frielingsdorf et al released a paper that showed the crystal structure of the proximal cluster of *R. eutropha* MBH in reduced, oxidised and superoxidised states[33]. An oxygen atom, proposed to originate from either water or hydroxide, was bound to the superoxidised cluster but not to the reduced cluster. This oxygen bridged the gap between the proximal cluster and residue H229 in a way that suggested involvement of the residue in the reactivity of the superoxidised state (Figure 2.6).
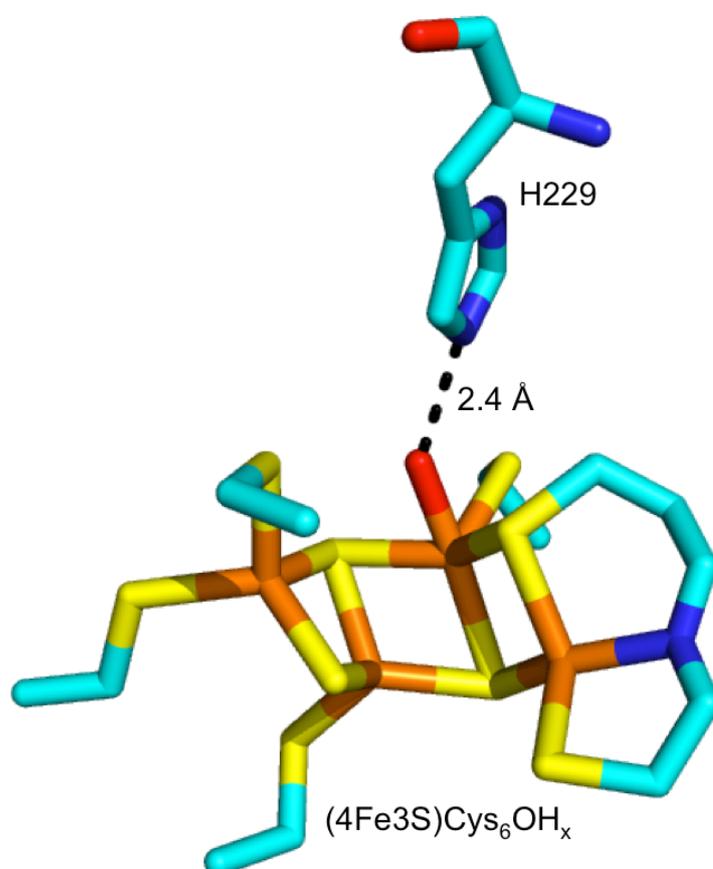
Figure 2.6 Structure of superoxidised proximal cluster of *R. eutropha* (PDB: 4IUC) showing distance of bound oxygen to histidine 229. Colours: green, carbon; red, oxygen; blue, nitrogen; yellow, sulfur; orange, iron.

Strains of *R. eutropha* that expressed H229A, H229M and H229Q variants of MBH could not grow on H_2 in the presence of O_2[33], confirming that histidine 229 is crucial for O_2 tolerance across MBH enzymes, not just *S. enterica* Hyd-5. In addition, methylene blue assays showed lowered specific activity for the variant strains with regards to the strains expressing Native MBH, although this does not appear to have been investigated further and no electrochemistry of the MBH variants was reported. It is likely that at a pH of 5.5, the pH value at which the assay was previously performed by the group[209], the redox potential for methylene blue (+0.047 V vs SHE[205]) would fall within the region of greater anoxic inactivation for the H229A variant[203]. This would lower the specific activity in the same way that the turnover measured by methylene blue was lower for the Hyd-5 H229A variant than for the Native Hyd-5.

Dance used the published work which resulted from this chapter[36] and the work by Frielingsdorf et al[33] as a basis for density functional theory calculations in order to propose a mechanism by which the proximal cluster changes from the closed structure of the reduced state to the open structure of the super-oxidised state[210]. In this mechanism, the transfer of a proton from the large subunit to the proximal cluster via histidine 229 is a crucial step in cluster opening. This would support the finding that O_2 tolerance is impacted when the proton transfer capability of this residue is removed via amino acid substitutions. Dance hypothesised that glutamate 73 could be a source of the protons for this process as the side chain of this residue is seen to rotate in different crystal structures, and in many structures is seen as binding to a water molecule. Alternatively, the glutamate residue was hypothesised to communicate structural changes at the active site to the proximal cluster. Either of these hypotheses could explain why the replacement of glutamate 73 with alanine diminishes the O_2 tolerance of Hyd-5 at pH 6. Exploration of these hypotheses is discussed in more detail in Chapters 4 and 5 of this thesis.

2.4 Conclusions

E73A and H229A variants of *S. enterica* Hyd-5 were investigated with protein film electrochemistry. Both variants showed markers of reduced O_2 tolerance, suggesting that the residues both play a role in the H_2 oxidation activity under O_2, although the role of histidine 229 is more significant than that of glutamate 73. Histidine 229 also showed involvement in anoxic inactivation at high potentials in the absence of O_2. It has been hypothesised as a result of this work that glutamate 73 and histidine 229 are part of the proton transfer pathway to the proximal cluster.

The work in this chapter has important implications for hydrogenase research. Focus on exploring catalytic activity and O_2 tolerance has usually been on the metal sites themselves. However, the work presented here demonstrates that residues in the secondary and tertiary coordination sphere of the metals can also impact the activity of hydrogenases. This finding will need to be taken into account when creating synthetic hydrogenase mimics, which are likely to have very different catalytic properties depending on the size and type of the ligands used.

Chapter 3

Development of a protocol to create NiFe hydrogenase variants in *E. coli*

3.1 Introduction

The maturation processes of MBH, as detailed in Section 1.3.5 of Chapter 1, are complex. Biosynthesis of an intact MBH requires the expression of at least two separate gene operons. The first operon encodes the subunits of the hydrogenase of interest and several accessory proteins which act as endopeptidases and chaperones[140, 211]. The second operon is the Hyp operon, which encodes the proteins that synthesise the complex structure of the hydrogenase active site. Further to this are the proteins, not yet fully understood, that perform the synthesis and insertion of the iron-sulfur clusters[159, 212]. For this reason MBH intended for purification are either expressed from plasmids harbouring all genes for synthesis, maturation and regulation[213] or from the chromosome, under the control of natural regulation[57].

The current methodology used to create chromosomal mutations of MBH in *E. coli* relies on the Hamilton method[48, 214]. This involves constructing a plasmid containing the intended sequence of the gene flanked by homology sequences (600 base pairs according to Hamilton at al[214]). Homologous recombination is then used to effect gene replacement. This construction involves the use of multiple plasmid constructs and thus multiple steps of polymerase chain reaction (PCR) amplification, restriction, ligation and verification[48]. Not only is this time consuming but Hamilton et al[214] admitted that there is no guarantee that the mutation will be transferred, meaning that screening of several isolates may be necessary.

In 2008 Heerman et al[215] published a methodology to create scarless chromosomal mutation in *E. coli* via Red®/ET® recombination. This method,

depicted in Figure 3.1, relies on the *rpsL*150 allele present in many laboratory strains of *E. coli* to perform streptomycin counter-selection. This allele gives streptomycin resistance, but may be repressed by a second wild type *rpsL* gene to give streptomycin sensitivity. Red®/ET® recombination uses the pRed/ET plasmid to provide the ability to insert a strand of linear DNA into the chromosome, provided that there are 50 base pairs of homology on the fragment to the chromosome on either side of the site of interest[216-218]. In the Heerman methodology[215], a fragment of DNA containing a wild type *rpsL* gene and a gene for neomycin/kanamycin resistance is inserted into the site of interest. This *rpsL-neo* cassette is removed by a further strand of DNA containing only the 50 base pairs of homology and the intended mutation. The selective pressure applied for this step is the return to streptomycin resistance with the removal of the wild type *rpsL* gene alongside the cassette.

This chapter will focus on adapting the Heerman methodology[215] to create single site variants of the *E. coli* membrane bound hydrogenases, and expansion of the methodology to include the addition of polyhistidine tags.
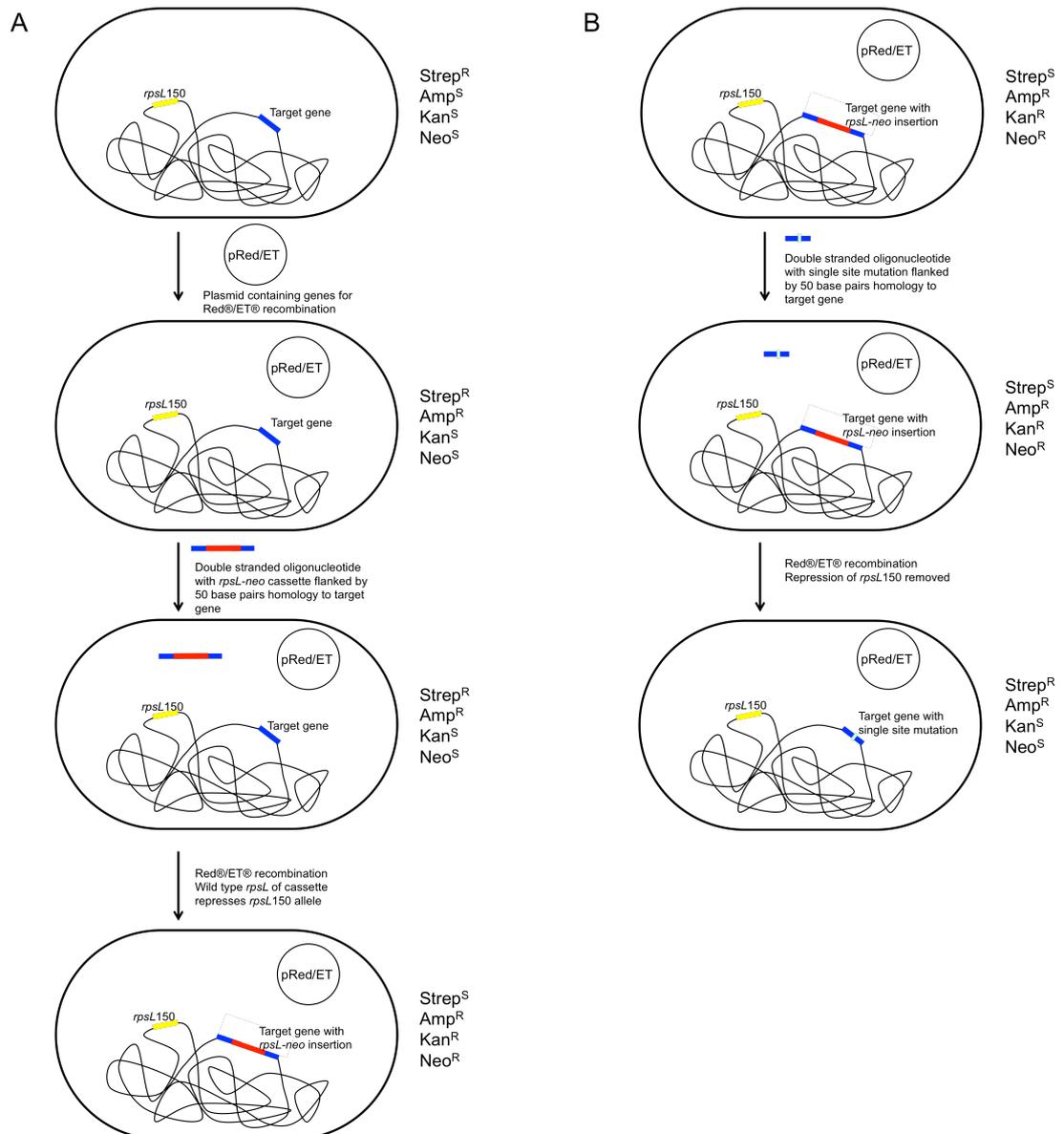
Figure 3.1 Use of Red®/ET® recombination to insert a single site mutation into the *E. coli* chromosome with streptomycin counter-selection. Adapted from Heerman et al[215]. A: Insertion of the *rpsL-neo* cassette into target gene. B: Replacement of *rpsL-neo* cassette to leave target gene with single site mutation. Selective pressure is given by the antibiotic resistance profiles to the right of each step. Strep: streptomycin, amp: ampicillin, kan: kanamycin, neo: neomycin.

3.2 Methods

3.2.1 Strains, plasmids, primers and oligomers

The *E. coli* strains used and created in this chapter are listed in Table 3.1. Plasmid pRed/ET(amp) was obtained from the "Quick and Easy *E. coli* Gene Deletion Kit" (Gene Bridges, Cambio). The *rpsL-neo* template was obtained from the "Counter-Selection BAC Modification Kit" (Gene Bridges, Cambio). All primers used in the study are listed in Table 3.2 and Table 3.3. Oligonucleotides were obtained from Sigma-Aldrich in a salt-free grade.

Table 3.1 Genotypes of strains W3110[219], MC1061[220] and those created in this study.

Strain name	Genotype
W3110	F⁻ lambda⁻ IN(rrnD-rrnE)1 rph-1 (StrepS)
MC1061	araD139 Del(araA-leu)7697 Del(lac)X74 galK16 galE15(GalS) lambda⁻ e14⁻ mcrA0 relA1 rpsL150 spoT1 mcrB1 hsdR2 (StrepR)
LAF-001	F⁻ lambda⁻ IN(rrnD-rrnE)1 rph-1 rpsL150 (StrepR)
LAF-002	F⁻ lambda⁻ IN(rrnD-rrnE)1 rph-1 rpsL150 hyaA(histag):rpsL-neo (KanR StrepS)
LAF-003	F⁻ lambda⁻ IN(rrnD-rrnE)1 rph-1 rpsL150 hyaA(histag) (StrepR)
LAF-004	F⁻ lambda⁻ IN(rrnD-rrnE)1 rph-1 rpsL150 hyaB(E73Q):rpsL-neo (KanR StrepS)
LAF-005	F⁻ lambda⁻ IN(rrnD-rrnE)1 rph-1 rpsL150 hyaBE73Q (StrepR)
LAF-006	F⁻ lambda⁻ IN(rrnD-rrnE)1 rph-1 rpsL150 hyaBE73Q hyaA(histag):rpsL-neo (KanR StrepS)
LAF-007	F⁻ lambda⁻ IN(rrnD-rrnE)1 rph-1 rpsL150 hyaBE73Q hyaA(histag) (StrepR)
LAF-008	F⁻ lambda⁻ IN(rrnD-rrnE)1 rph-1 rpsL150 hyaB(E73A):rpsL-neo (KanR StrepS)
LAF-009	F⁻ lambda⁻ IN(rrnD-rrnE)1 rph-1 rpsL150 hyaA(histag) hyaBE73A (StrepR)
LAF-010	F⁻ lambda⁻ IN(rrnD-rrnE)1 rph-1 rpsL150 hyaA(histag) hyaBE73K (StrepR)
LAF-011	F⁻ lambda⁻ IN(rrnD-rrnE)1 rph-1 rpsL150 hyaA(histag) hyaBE73N (StrepR)
LAF-012	F⁻ lambda⁻ IN(rrnD-rrnE)1 rph-1 rpsL150 hyaB(E73A):rpsL-neo (KanR StrepS)
LAF-013	F⁻ lambda⁻ IN(rrnD-rrnE)1 rph-1 rpsL150 hyaBE73A (StrepR)
LAF-014	F⁻ lambda⁻ IN(rrnD-rrnE)1 rph-1 rpsL150 hyaB(H229A):rpsL-neo (KanR StrepS)
LAF-015	F⁻ lambda⁻ IN(rrnD-rrnE)1 rph-1 rpsL150 hyaBH229A (StrepR)
LAF-016	F⁻ lambda⁻ IN(rrnD-rrnE)1 rph-1 rpsL150 hyaA(polyhis):rpsL-neo (KanR StrepS)
LAF-017	F⁻ lambda⁻ IN(rrnD-rrnE)1 rph-1 rpsL150 hyaBH229A hyaA(histag):rpsL-neo (KanR StrepS)
LAF-018	F⁻ lambda⁻ IN(rrnD-rrnE)1 rph-1 rpsL150 hyaBH229A hyaA(histag) (StrepR)
LAF-019	F⁻ lambda⁻ IN(rrnD-rrnE)1 rph-1 rpsL150 hybO(polyhis):rpsL-neo (KanR StrepS)
LAF-020	F⁻ lambda⁻ IN(rrnD-rrnE)1 rph-1 rpsL150 hybO(hisΔTM):rpsL-neo (KanR StrepS)
LAF-021	F⁻ lambda⁻ IN(rrnD-rrnE)1 rph-1 rpsL150 hybC(H214A):rpsL-neo (KanR StrepS)
LAF-022	F⁻ lambda⁻ IN(rrnD-rrnE)1 rph-1 rpsL150 hybCH214A (StrepR)
LAF-023	F⁻ lambda⁻ IN(rrnD-rrnE)1 rph-1 rpsL150 hyabCH214A hybO(polyhis):rpsL-neo (KanR StrepS)

Table 3.2 Primers used to create DNA to be transformed into cells. Inserted or mutated nucleotides are represented in bold and nucleotides homologous to the *rpsL-neo* cassette are in italics.

Stage	Used to create strain	Name	Sequence (5' to 3')
Amplification of *rpsL* gene	LAF-001	rpsl_up1	CTTGACACACCTTTTCGGCCATCGC
	LAF-001	rpsl_down1	CGTGTTAATTCAGGATTGTCC
Insertion of *rpsL-neo* cassette into target gene	LAF-002, LAF-006, LAF-016, LAF-017	hyaA_histag_neo_sense	CCAGCAACCTACAGAAACCGAACATCAGCCAGGCAATGAGGATAAACAGGCA**CATCATCATCATCATCATCATTGA**GGCCTGGTGA
	LAF-002, LAF-006, LAF-017	hyaA_his2_neo_antisense	GGCGGCGGTCCGGCATTATTGATGGTGTATCCCTGAGTTTCGTACTGAGTGCT**CATGCCTGTTTATCCTCATT**CAGAAGAACTCGTCAAGAAGGCG
	LAF-019, LAF-023	hybO_histag_neo_sense	GATGGCGGGGGATCG… CATCATCATCATCATCATCAT… **…**GTCAGAAGAACTCGTCAAGAAGGCG
	LAF-019, LAF-023	hybO_his2_neo_antisense	GTCAGCAATGCCCCGCAGGAGGAGGCTGCTTAATAAAATTACGTCTGTTCACGGTCAGAAGAACTCGTCAAGAAGGCG
	LAF-014	hyaB_h229a_neo_sense	GCTTTCGTCAATGTTGATGGCGCAAGGCATCCCGCCGACAATCCAGTTTGGA**AGC**TCAGAAGAACTCGTCAAGAAGGCG
	LAF-014	hyaB_h229a_neo_antisense	CGTGAACTGGGTCGTCAGCAAAAGAAAGATAAACGTGACTCACGGGGAGAAAC**ATCATCATCATCATCATCATTAA**GGCCTGGTGAT
	LAF-008, LAF-012	hyaBe73a_neo_sense	GATGGGGTAAACCGAAGGCAGGGGCGGTGTACGCCGACCCGCAGATACGTT**GTCAGAGAGAACTCGTCAAGAAGGCG**
	LAF-008, LAF-012	hyaBe73a_neo_antisense	TTCCAGCGTGAAATTGTCAAAATCACGCGGTCTTTGGCGGTAAAAACCCGGGTC**CATCATCATCATCATCATTAA**GGCCTGGTGAT
	LAF-004	hyaBe73q_neo_sense	GCTGGAGATCATCCTACAAAGGGGCGGGGGACCCGCGACCCGCAGATACGTT**CAGGAAGAACTCGTCAAGAAGGCG**
	LAF-004	hyaBe73q_neo_antisense	TCCGGCATTATTGATGGTGTATCCCTGAGTTTCGTACTGAGTGCT**CATGCCTGTTTATCCTCATT**CAAATGATGATGAGGATAAA
	LAF-016	hyaA_histag_neo_antisense	TACAGAAACCGAACATCAGCCAGGCAATGAGGATAAACAGGCA**CATCATCATCATCATCATCATTGA**GGCCTGGTGA
	LAF-020	hybO_hisdTM_neo_sense	CCAACCAACCACACCGCCGAGCAAACCAATAGCGCCTGCAGAGAACGTTGCCGCCTCAGAGAGAACTCGTCAAGAAGGCG
	LAF-020	hybO_hisdTM_neo_antisense	GTCGAAAATCAAACTCCGCGTTCACAGAAACCGGATGTTAAGCGTAAAGAGC**ATCATCATCATCATCATCATTAA**GGCCTGGTGAT
Removal of *rpsL-neo* cassette to create single site variant	LAF-003, LAF-007, LAF-018	hyaA_his2_olap_sense	GATGGCGGGGGATCG
	LAF-003, LAF-007, LAF-018	hyaA_his2_olap_antisense	TCCGGCATTATTGATGGTGTATCCCTGAGTTTCGTACTGA GTGCT**CATGCCTGTTTATCCTCATT**CAAATGATGATGAGGATAAA
	LAF-021	hybC_h214a_neo_sense	AACCGTCGAGGTTGATCGGGTTCGCGACAACCACTACCGCCCAGTTCT GAATGGC**TCAGAAGAACTCGTCAAGAAGGCG**
	LAF-021	hybC_h214a_neo_antisense	GTGCCAGCGTGACGCTAACCGCGTCGTCGGCGGTAAACGCCGGCC**ATCATCATCATCATCATCATTAA**GGCCTGGTGAT
	LAF-005	hyaBe73q_olap_sense	GCGTAAACCGAAGCCAGGGGCGGTGTACGCCGACCCGCAGATACGTTGAACGAACGCCCAC
	LAF-005	hyaBe73q_olap_antisense	GCTGGAGATCATCCTACAAAGGGGCGGGGGACCCGCGACCCGCAGATACGTT**GCACGTATCTG**
	LAF-009, LAF-013	hyaBe73a_olap_sense	GCGTAAACCGAAGCCAGGGGCGGTGTACGCCGACCCGCAGATACGTTGCGAACGAACGCCCAC
	LAF-009, LAF-013	hyaBe73a_olap_antisense	GCTGGAGATCATCCTACAAAGGGGCGGGGGACCCGCGACCCGCAGATACGTT**GCAACGTATCTG**
	LAF-010	hyaBe73k_olap_sense	GCGTAAACCGAAGCCAGGGGCGGTGTACGCCGACCCGCAGATACGTT**AAACGTATCTG**
	LAF-010	hyaBe73k_olap_antisense	GCGTGGAGATCATCCTACAAAGGGGCGGGGGACCCGCGACCCGCAGATACGTTCGTT**AAACGTATCTG**
	LAF-011	hyaBe73n_olap_sense	GCGTAAACCGAAGCCAGGGGCGGTGTACGCCGACCCGCAGATACGTTCGTT**AACCGTATCTG**
	LAF-011	hyaBe73n_olap_antisense	GCTGGAGATCATCCTACAAAGGGGCGGGGGACCCGCGACCCGCAGATACGTTCGTT**AACCGTATCTG**
	LAF-015	hyaBH229A_olap_sense	TTCCAGCGTGAAATTGTCAAAATCCACGCGGTCTTTGGCGGTAAAAAACCCGG**CTC**CAAACTGG
	LAF-015	hyaBH229A_olap_antisense	GCTTTCGTCAATGTTGATGGCGCAAGGCATCCCGCCGACAATCCAGTTTGG**AGC**CGGGGTTTTTACC
	LAF-022	hybC_H214A_olap_sense	GTGCCAGCGTGACGCTAACCGCGTCGTCGGCGGTAAATCCAGGTTCTGAAT**GGC**CATTCAGAAC
	LAF-022	hybC_H214A_olap_antisense	AACCGTCGAGGTTGATCGGGTTCGCGACAACCACTACCGCCGACCAGGTTCTGAAT**GGC**CGGCGGGTTTTACC

Table 3.3 Primers used to check for PCR verification and sequencing of derived strains

Strains verified	Name	Sequence (5' to 3')
LAF-016	counter_hyaA_histag_sense	TTGACCAGCGCAGAGACGTCATAA
LAF-016	counter_hyaA_histag_antisense	GCGTAATCGGGGTCGACCACCA
LAF-004, LAF-005, LAF-012, LAF-013, LAF-014, LAF-015	hyaB_sense	ATGAGCACTCAGTACGAAACT
LAF-002, LAF-003, LAF-006, LAF-007, LAF-008, LAF-009, LAF-010, LAF-011, LAF-017, LAF-018	counter_hyaA_hisdTM_sense	TCGTTCTACAGCCGCGCGTGGTC
LAF-002, LAF-003, LAF-006, LAF-007, LAF-008, LAF-009, LAF-010, LAF-011, LAF-014, LAF-015, LAF-017, LAF-018	forseq_hyaB_H229A_antisense	AGGCGTTCCATATTGACTGCC
LAF-004, LAF-005, LAF-012, LAF-013	hyaB_antisense	GTTTTGTACGTCGAAGAAATA
LAF-019, LAF-020, LAF-023	counter_hybO_hisdTM_sense	CTTGCCAACGTCGAAAATCAA
LAF-019, LAF-020, LAF-023	hybA_antisense	GTTGTTGTAGTCGTACTTCGG
LAF-021, LAF-022	hybC_sense	ATGAGCCAGAGAATTACTATT
LAF-021, LAF-022	forseq_hybC_H214A_antisense	AACCTTATAAACCTGCTCAAC

3.2.2 Transformation of pRed/ET(amp) plasmid into W3110

The pRed/ET(amp) plasmid was transformed into *E. coli* strain W3110 with electroporation according to the instructions given in the technical manual of the "Quick and Easy *E. coli* Gene Deletion Kit" (Gene Bridges, Cambio). Briefly, a 1 mL overnight culture was grown in LB medium in a microfuge tube, of which the lid was punctured with a needle, at 37 °C with shaking. 30 μL of this was used to inoculate 1.4 mL LB in a 2 mL microfuge tube and this was shaken at 37 °C for 3 hours. The tube was centrifuged for 30 seconds at 11000 rev per minute (rpm) in a bench-top microfuge, the supernatant was discarded and the pellet was washed by resuspension in 1 mL chilled 10% (v/v) glycerol solution. The centrifugation and washing was repeated twice more. After the supernatant was discarded the third time, the pellet was resuspended in ~30 μL of supernatant which was left in the tube. 1 μL pRed/ET plasmid was added to the resuspension and the mixture was transferred to a 1 mm chilled GenePulser®/MicroPulser™ electroporation cuvette (Bio-Rad). The cuvette was placed in a Bio-Rad MicroPulser™, and the Ec1 pulse setting (V=1.8 kV, 5 msec) was used to electroporate the cells. The cells were resuspended in 1 mL LB medium, and returned to the 2 mL microfuge tube. The tube was incubated with shaking at 30 °C for 70 minutes, before 100 μL was plated on LB agar with 50 μg/mL ampicillin and incubated at 30 °C overnight.

3.2.3 Transformation of *rpsL*150 into W3110 to create LAF-001

MC1061 and W3110 were grown on LB agar with 50 μg/mL streptomycin to verify phenotype. The *rpsL* gene was purified from MC1061 by PCR using the rpsL_up1 and rpsL_down1 primers (Table 3.2, Heerman et al[215]) and KOD polymerase. The QIAquick PCR Purification Kit was used to purify 30 μL DNA at ~220 ng/mL.

Starter cultures of W3110 + pRed/ET were gown overnight at 30 °C in 1 mL LB media with 50 μg/mL ampicillin. 30 μL of this was transferred to 1.4 mL LB

media in a 2 mL hole-punched microfuge tube. The tube was shaken at 30 °C for 2 hours. After this time, 50 μL 10% (w/v) L-arabinose solution was added and the tube was shaken at 37 °C for 1 hour. The tube was centrifuged and washed with 10% glycerol as above. The pellet was mixed with 2 μL of the purified *rpsL* PCR product and electroporated on the same settings as above. After electroporation the cells were returned to the tube and the tube was shaken for 70 minutes at 37 °C. The cells were centrifuged for 1 minute at 11000 rpm in a bench-top microfuge, the majority of the supernatant was discarded, and the cells were resuspended in ~100 μL of the remaining supernatant. This was spread onto an LB agar plate with 50 μg/mL ampicillin and 50 μg/mL streptomycin and the plate was grown at 30 °C overnight.

PCR was used to purify the *rpsL* gene of the resulting strain and in-house sequencing at the University of York with the rpsL_up1 primer was used to confirm the adenine to guanine mutation characteristic of insertion of the *rpsL*150 allele from strain MC1061.

3.2.4 Chemical competence protocol

The Red®/ET® recombination plasmid replicates at 30 °C and expresses recombination proteins at 37 °C, in the presence of L-arabinose. All other strains were created using a chemical competence protocol designed to respect both conditions.

In order to create competent stocks of a strain the strain was grown at 30 °C overnight in 1 mL LB media plus 50 μg/mL ampicillin and 50 μg/ml kanamycin or streptomycin depending on the stage of the protocol. The entire 1 mL was used to inoculate 50 mL LB plus 50 μg/mL ampicillin in a 250 mL conical flask. The flask was shaken at 30 °C for three hours. 1.8 mL 10% L-arabinose was added and the flask was shaken for 45 minutes at 37 °C. The culture was transferred to a 50 mL falcon tube and this was centrifuged at 4000 rpm at 4 °C for 20 minutes in an Allegra X-22R benchtop centrifuge (Beckman Coulter). The

supernatant was discarded and the pellet was resuspended in 10 mL chilled buffer RF1 (300 mM potassium chloride, 100 mM magnesium chloride, 60 mM potassium acetate, 20 mM calcium chloride, 20% v/v glycerol, pH 5.8). The suspension was incubated on ice for 15 minutes and centrifuged once again for 10 minutes. The pellet was then resuspended in 5 mL chilled buffer RF2 (10 mM MOPS, 40 mM potassium chloride, 150 mM calcium chloride, 15% v/v glycerol, pH 6.8). The mixture was incubated on ice for a further 15 minutes before dividing into 400 μL of aliquots and transferring into a -80 °C freezer.

To transform the cells the stocks were thawed on ice and divided into 100 μL aliquots in 2 mL microfuge tubes. 10-20 μL purified DNA was added to each tube before incubation on ice for 30 minutes. The tubes were heat-shocked at 42 °C for 45 seconds before being incubated on ice once more for 2 minutes. 1 mL LB media was added to each and the tubes were shaken at 37 °C for 60 minutes. The tubes were centrifuged at 11000 rpm in a microfuge and the majority of the supernatant was discarded. The pellet was resuspended in 100 μL of the remaining supernatant and the mixture was streaked on an LB plate with 50 μg/mL ampicillin and 50 μg/mL of either kanamycin or streptomycin depending on the experiment. The plate was grown at 30 °C for a minimum of 16 hours.

3.2.5 Creation of *rpsL-neo* cassette

The double stranded fragment of DNA containing the *rpsL-neo* cassette and homology arms was amplified with blunt-ended PCR and Q5 polymerase. 1 μL *rpsL-neo* was used per 50 μL reaction and the primers used to create the cassette for each target are given by the "neo" primers in Table 3.2. Successful amplification was verified by running 5 μL of the product on a 0.7% w/v agarose gel in with SYBR® Safe- DNA gel stain. 5 μL 3 M sodium chloride (pH 7) and 150 μL 100% ethanol was added to each reaction and the DNA was precipitated at -80 °C for 5 minutes. The tubes were centrifuged at 13000 rpm for 5 minutes in a benchtop microfuge to pellet the DNA. The liquid was discarded and the pellet was washed with 500 μL 70% ethanol. The pellet was dried at 37 °C and

resuspended in 10 μL buffer EB from the Qiagen PCR purification Kit. DNA concentration was measured on a Nanodrop 1000 spectrophotometer.

3.2.6 Creation of oligonucleotide for single-site variant

The double stranded oligonucleotide containing the intended mutation and homology arms for site of interest was amplified by blunt ended PCR and Q5 polymerase. 1 μL of each 100 μM overlap ("olap" in Table 3.2) primer was used per 50 μL reaction. These primers contain ~20 base pairs of overlapping sequence meaning that the resulting amplification consists of the intended mutation flanked by homology sequences to the gene of interest. Agarose gels and ethanol precipitation were used to purify DNA as above.

3.2.7 Verification of successful transformation

Colony PCR of the transformed strains was as described in Chapter 8 with primers given in Table 3.3. The distance between the chromosomal sequences with homology to these primers is large enough to enable verification of mutations at multiple gene positions, but also to enable easy detection on an agarose gel. Presence of the *rpsL-neo* cassette was detected by increase in amplified fragment size by at least 1.5 kilobase pairs. QIAquick gel purification kit was used to purify DNA from gel bands. This purified DNA was used for sequencing, initially in-house at the University of York, and subsequently by GATC biotech. Gene sequences are visualised with program FinchTV (Geospiza).

3.2.8 Western blot protocol

5 mL starter cultures in LB media were grown at 37 °C in 50 mL falcon tubes throughout the day. These were added to 45 mL LB media in 50 mL falcon tubes and these were grown overnight at 37 °C. Each culture was centrifuged at 4000 rpm at 4 °C for 20 minutes in a benchtop centrifuge. The supernatant was discarded and the pellet was resuspended in 1 mL lysis buffer (50 mM Tris, 10% v/v glycerol, 2% v/v Triton X-100, lysozyme, EDTA-free protease inhibitor). This mixture was left for 30 minutes on ice before sonication on ice with a sonic

dismembrator (Model 505, Fisher Scientific) fitted with a 1/8" microtip probe (5 minutes on the power setting of 0.5 with pulses of 5 seconds on followed by 5 seconds off). The lysate was transferred to a 2 mL microfuge tube and spun at 12000 rpm for 20 minutes at 4 °C. The supernatant was removed to a clean tube and the pellet was resuspended in lysis buffer without lysozyme and protease inhibitor.

These soluble and insoluble fractions were used to run an SDS-PAGE gel as detailed in Chapter 8. The gel was transferred onto a nitrocellulose membrane for 90 minutes at 80 V using a Tetra blotting module (Bio-Rad). In order to keep the system cool, the transfer tank was placed in an ice bucket and falcon tubes containing frozen water were submerged in the tank. The success of the transfer was verified by staining with Ponceau S and destaining with water. Stain was removed by washing with TBST (25mM Tris, pH 7.4, 3.0mM potassium chloride, 140mM sodium chloride and 0.05% Tween® 20). The blocking buffer (0.5 g EasyBlocker (GeneTex) in 10 mL TBST) was made up fresh and shaken at room temperature for 30 minutes. After removing stain, the membrane was blocked with 5 mL blocking buffer for 1 hour at room temperature. 5 μL anti-6xHis primary antibody (GeneTex) was diluted in 5 mL blocking buffer and after the blocking step the membrane was incubated with the antibody for 1 hour at room temperature. The membrane was washed 3 x 7 minutes at room temperature with TBST, 5 μL horseradish peroxidase (HRP) anti-rabbit antibody was diluted in blocking buffer and incubated with the membrane for 1 hour at room temperature before the membrane was again washed for 3 x 7 minutes at room temperature with TBST. 1 mL of each reagent in the West Dura Trial Kit (Invitrogen) was applied to the membrane with slow pipetting and this was left for 5 minutes before the membrane was sealed between two pieces of transparency film and bubbles were removed. X-ray film (Fuji medical) was exposed to the membrane in a dark room and developed to show bands.

3.3 Results and discussion

3.3.1 Creation of an *rpsL*150 strain

Strain *E. coli* K12 strain W3110[219] was chosen as the parent strain for the molecular biology because that strain has few additional natural mutations other than those which make it safe for laboratory usage. This strain does not contain a natural *rpsL*150 allele. For this reason, the *rpsL* gene from W3110 was swapped for the *rpsL*150 allele from MC1061[220] in the W3110 chromosome by Red®/ET® recombination using streptomycin as a selective pressure. Figure 3.2 shows the single site mutation characteristic of successful insertion of the *rpsL*150 allele into the W3110 chromosome. This LAF-001 (W3110 *rpsL*150) strain is the parent strain for all other molecular biology.
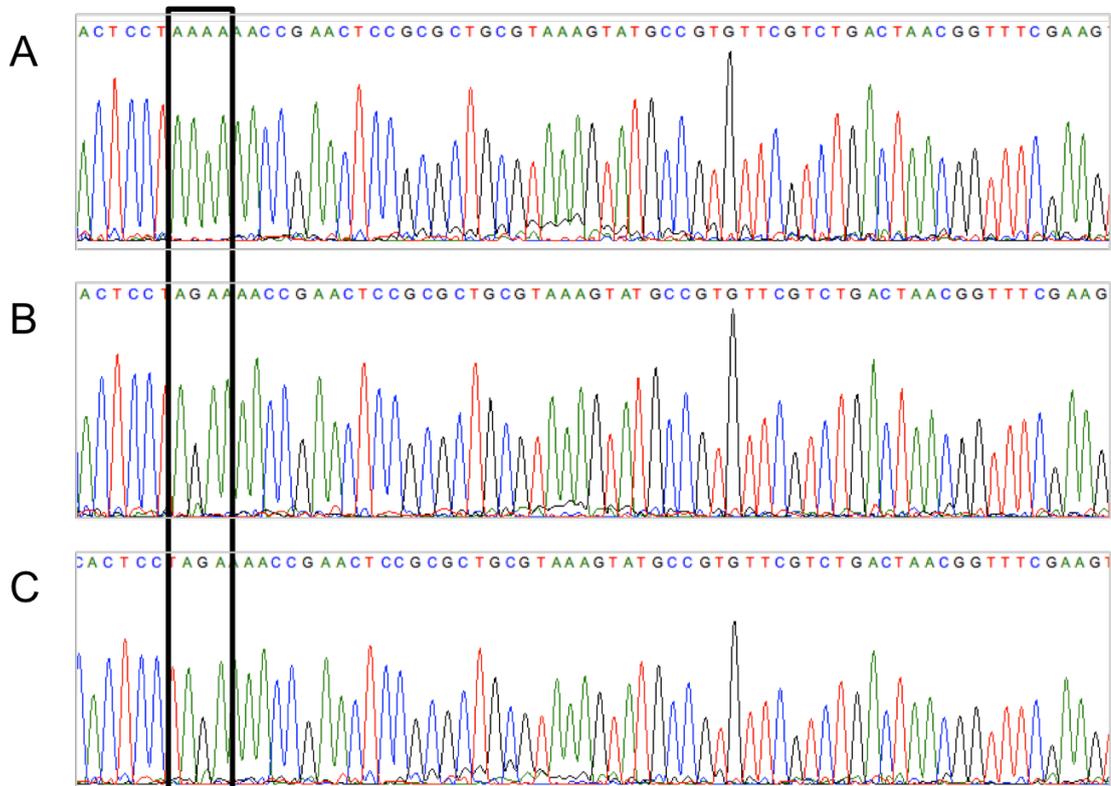
Figure 3.2 Creation of LAF-001, a W3110 *rpsL*150 strain. Sequence of the *rpsL* gene of A: wild type W3110, B: MC1061 and C: LAF-001. Black box shows codon that is mutated in the *rpsL*150 allele.

3.3.2 Creation of single site variants in the Hyd-1 and Hyd-2 large subunit

As the same procedure is used in order to create all variants, the creation of the Hyd-1 H229A variant will be used to illustrate the method development, and this is shown in Figure 3.3. The double stranded *rpsL-neo* cassette specific to the site of interest was synthesised by PCR, using the *rpsL-neo* cassette and primers composed of 50 base pairs of homology to the site of interest and 20 base pairs of homology to the cassette to create a ~1.5 kilobase fragment (Figure 3.3 A (i)). Due to the poor success of the electroporation protocol for recombination described the GeneBridges manual, a protocol was designed, as described in the methods section, which combined the methodology of Hanahan[221] with the requirements of pRed/ET plasmid expression and replication. This protocol gave much higher success rate for the insertion of linear DNA into the chromosome. Insertion into the chromosome was verified by using colony PCR of the resulting LAF-014 strain. Primers binding on either side of the side of interest were used to confirm presence of additional bases (Figure 3.3 A (iii)). Synthesis of double stranded fragment was conducted by PCR, using primers containing 50 base pairs of homology, the intended mutation, and 20 base pairs of overlap with the other primer (Figure 3.3 A (ii)). Replacement of the *rpsL-neo* cassette with this fragment was confirmed by verifying removal of the 1.5 kilobase fragment in the LAF-015 strain using the same checking primers. Sequencing confirmed replacement of wild type histidine codon (CAT) with mutant alanine codon (GCT).
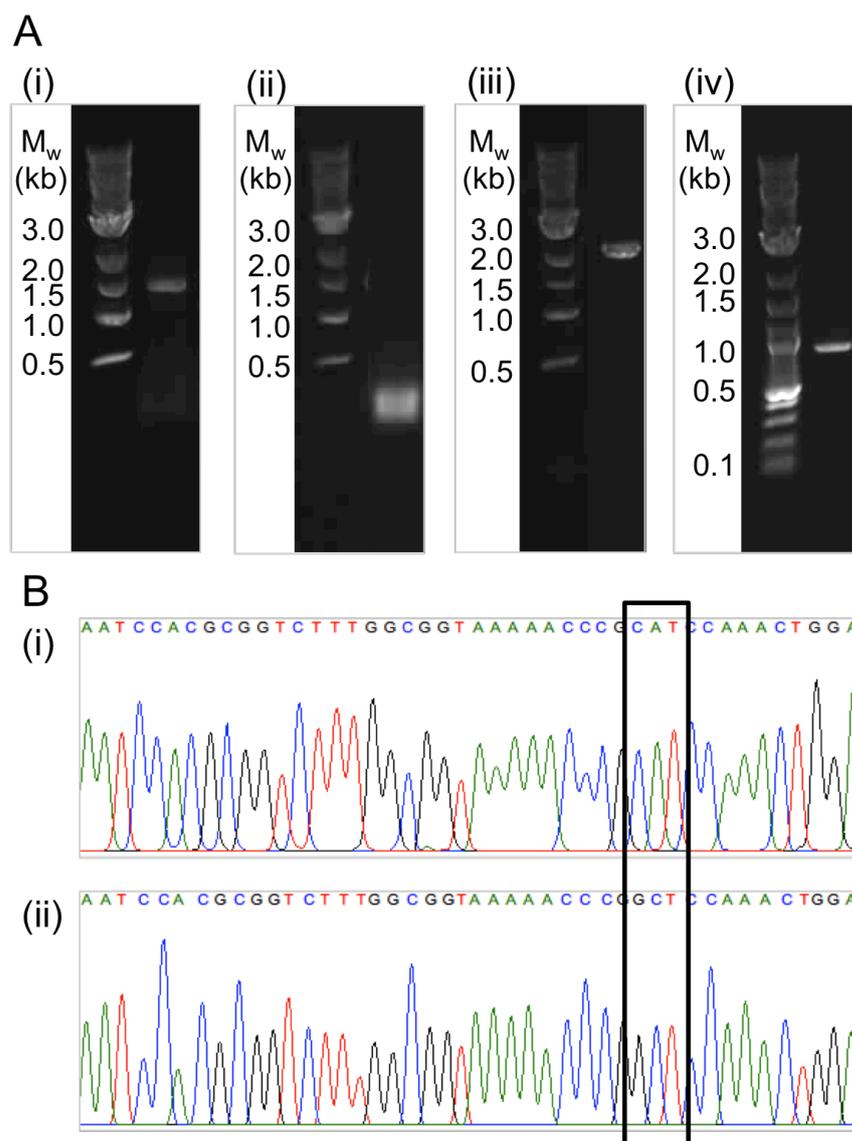
Figure 3.3 Creation of H229A single site variant in the Hyd-1 large subunit. A: Agarose gel electrophoresis showing: (i) PCR synthesis of ~1.5 kilobase pair double stranded oligonucleotide containing the *rpsL-neo* cassette flanked by 50 base pairs of homology upstream and downstream to the codon coding for position 229 of Hyd-1 in the gene *hyaB*; (ii) PCR synthesis of ~100 base pair double stranded oligonucleotide containing the codon coding for the H229A mutation flanked by 50 base pair of homology to the correct region of the *hyaB* gene; (iii) colony PCR of LAF-014 with checking primers to verify successful insertion of the cassette into the desired site of *hyaB*; (iv) colony PCR of LAF-015 with checking primers to verify successful removal of the cassette from *hyaB*. B: Sequencing to verify successful replacement of histidine codon (CAT) in Native strain LAF-001 (i) with alanine codon (GCT) in H229A strain LAF-015. Black box shows *hyaB* codon coding for position 229.

This procedure of insertion and removal of specific *rpsL-neo* cassettes was repeated to create Hyd-1 E73Q and E73A variants (LAF-005 and LAF-013) and a Hyd-2 H214A variant (LAF-022). The sequencing verification of successful codon substitution is shown in Figure 3.4. It may be seen that this procedure allows mutation at any chromosomal position without need for specific restriction enzymes or any scarring in the gene of interest.
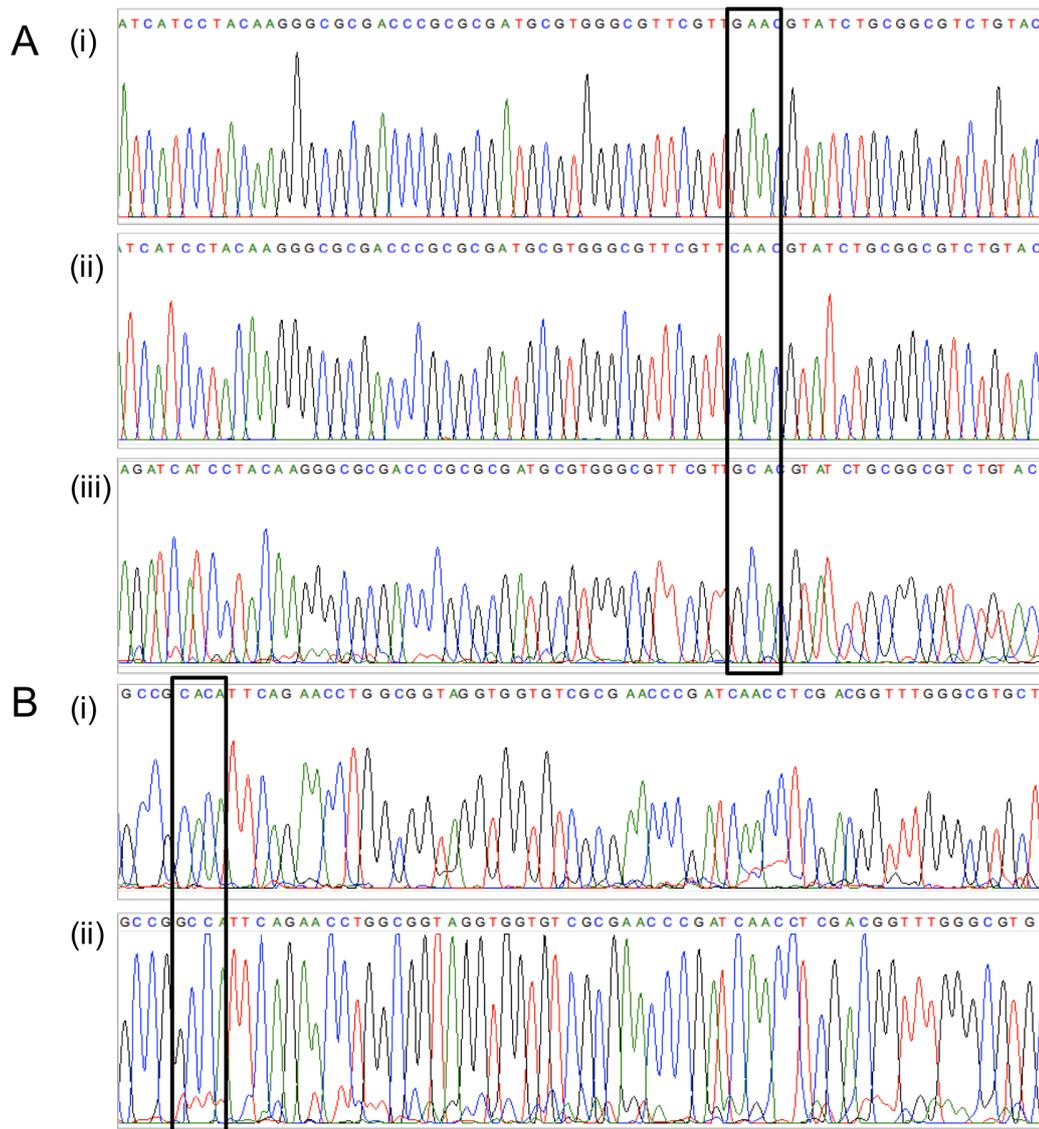
Figure 3.4 Creation of other single site variants in A: Hyd-1 and B: Hyd-2. A: Replacement of (i) glutamate codon (GAA) in Native *hyaB* (LAF-001) with (ii) glutamine codon (CAA) in E73Q variant (LAF-005) and (iii) alanine codon (GCA) in E73A variant (LAF-013). B: Replacement of (i) histidine codon (CAC) of Native *hybC* (LAF-001) with (ii) alanine codon (GCC) in H214A variant (LAF-022).

3.3.3 Incorporation of polyhistidine tags into Hyd-1 and Hyd-2

Following the success of the single site mutations, the protocol was expanded to accommodate addition of polyhistidine tags to enable purification of the Native and variant membrane bound hydrogenases via immobilised metal-affinity chromatography. This was not done in the Heerman work[215], but is a vital procedure if the methodology is to be adapted for future hydrogenase work. As the large and small subunit of the MBH are transported together, it was only necessary to add the tag to one of the subunits. The small subunit was chosen for this purpose as the C-terminus of the large subunit is cleaved during maturation. Figure 3.5 shows the arrangement of the large and small subunit genes of Hyd-1 and Hyd-2 in relation to the different strategies of where to add the polyhistidine tag. The Hyd-2 large and small subunit genes (*hybC* and *hybO* respectively) are separated by other subunits of the hydrogenase (*hybA* and *hybB,* Figure 3.5 B (i)) which when expressed are only loosely associated with the core HybOC heterodimer[48]. As these subunits are of no interest to the protein characterisation performed in this thesis, no special care need be taken to ensure that *hybA* is adequately expressed. For this reason the Hyd-2 Native and H214A Hyd-2 variant proteins were both purified at the stage where the chromosome contained nucleotides coding for the polyhistidine tag immediately followed by the *rpsL-neo* cassette (Figure 3.5 B (ii)).
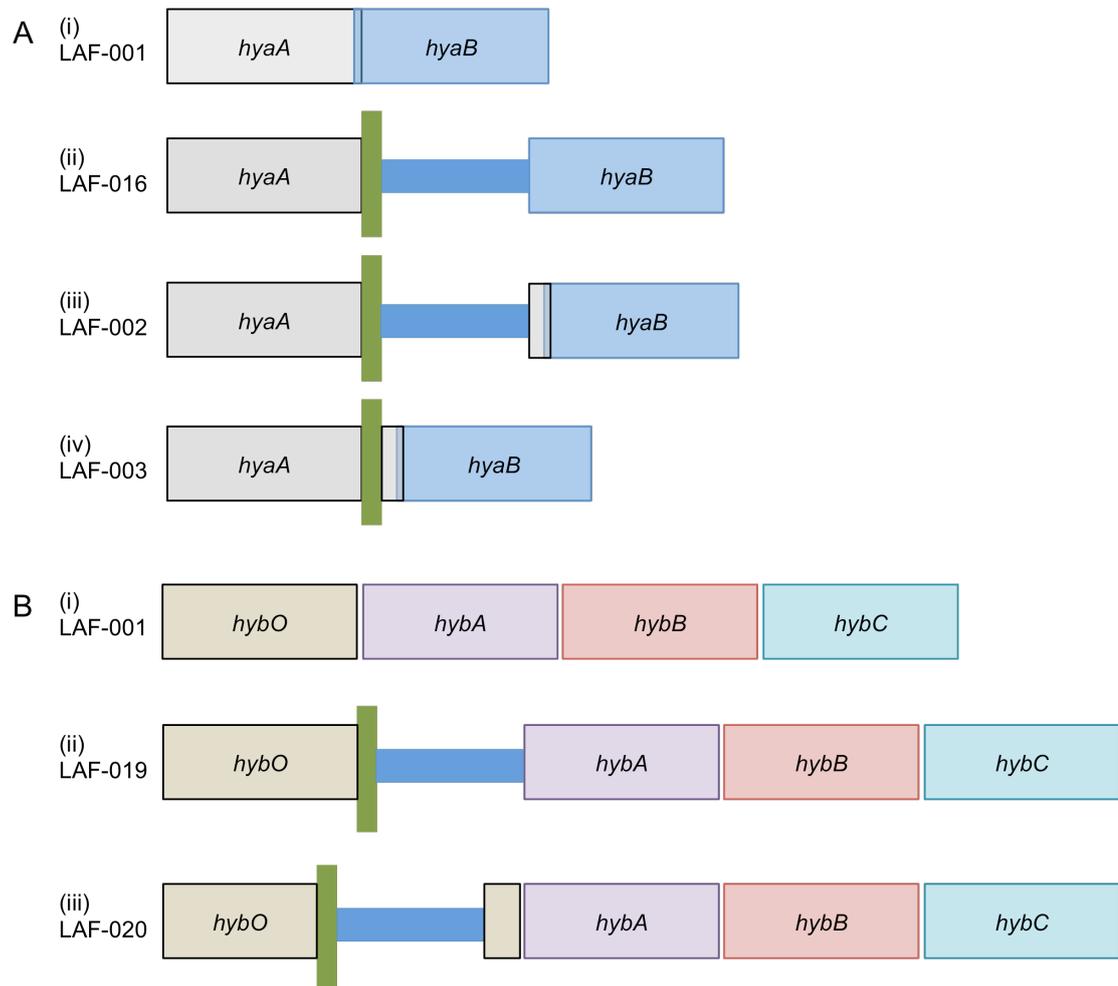
Figure 3.5 Schemes for the insertion of a polyhistidine tag into the gene operons of A: Hyd-1 and B: Hyd-2. Vertical green bar represents the nucleotides coding for the polyhistidine tag plus stop codon whilst horizontal blue bar represents *rpsL-neo* cassette. A: (i) small and large subunit Hyd-1 genes *hyaA* and *hyaB*, representing the overlap of stop and start codons in LAF-001; (ii) insertion of nucleotides coding for polyhistidine tag and cassette at terminus of *hyaA* in LAF-016; (iii) insertion of nucleotides coding for polyhistidine tag, cassette and 20 base pairs duplicated from the terminus of *hyaA* in LAF-002; (iv) removal of cassette to give insertion of nucleotides coding for polyhistidine tag and 20 base pairs duplicated from the terminus of *hyaA* in LAF-003. B: (i) separation of small and large subunit Hyd-2 genes *hybO* and *hybC* in the Hyd-2 gene operon in LAF-001; (ii) insertion of nucleotides coding for polyhistidine tag and cassette at terminus of *hybO* in LAF-019; (iii) insertion of nucleotides coding for polyhistidine tag and cassette directly before the *hybO* nucleotides coding for the small subunit transmembrane helix in LAF-020.

In contrast, the gene for the large subunit of Hyd-1 (*hyaB*) immediately follows the gene for the small subunit (*hyaA*), and indeed the stop codon for *hyaA* overlaps with the start codon for *hyaB* (Figure 3.5 A (i)). For this reason, the histidine tag insertion (Figure 3.5 A (ii)) which in Hyd-2 gives good expression does not show any expression of Hyd-1 (Figure 3.6 A). It was hypothesised that by placing the polyhistidine tag before the small subunit transmembrane helix the resulting construct would not only avoid disruption to the *hyaB* start codon, but would result in soluble protein. This was tested using the Hyd-2 operon (Figure 3.5 B (iii)), because LAF-019 could be used as a positive control. However, as shown in Figure 3.6 B, expression of Hyd-2 in the resulting strain (LAF-020) was undetectable in comparison to that in strain LAF-019. It is likely that much of the hydrogenase that is not anchored to the membrane is degraded by cellular proteases.

In order to overcome the issue, a further strain was created where the codons for the polyhistidine tag are located after the bases coding for the C-terminus of *hyaA*, but the final 20 bases of *hyaA* are duplicated after the *rpsL-neo* cassette in order to preserve the start codon of *hyaB* (Figure 3.5 A (iii)). The *rpsL-neo* cassette was replaced by a double stranded oligomer coding for 50 base pairs of homology to the terminus of *hyaA* followed by the polyhistidine tag, the 20 base pair repeat of the *hyaA* terminus and 50 base pairs of homology to the start of *hyaB* (Figure 3.5 A (iv)). This strain was shown to give good expression of Hyd-1 (Figure 3.6 C).
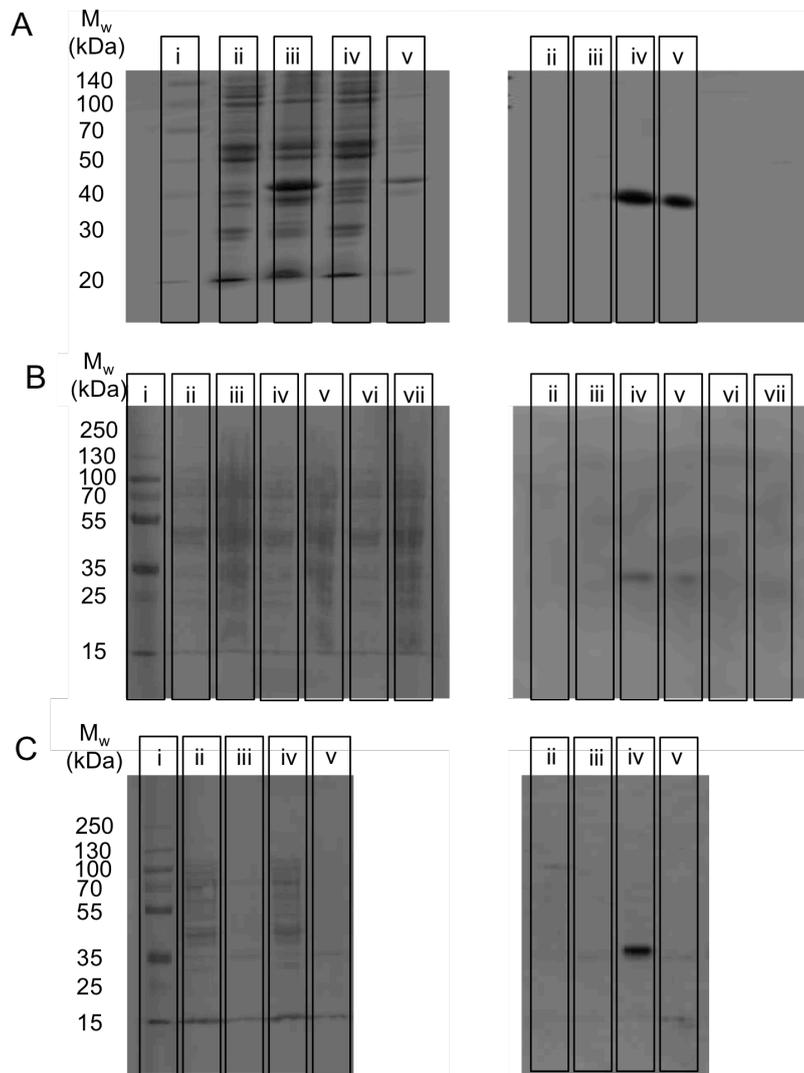
Figure 3.6 Expression of the small subunit with different strategies of insertion of the polyhistidine tag. Left: Ponceau S stained membranes. Right: western blots with antibodies against His$_6$. A: Expressions of strains created with strategy shown in Figure 3.5 A (ii) and B (ii). Lanes: (i) molecular weight size markers; (ii) LAF-016 (Hyd-1) soluble fraction; (iii) LAF-016 (Hyd-1) insoluble fraction; (iv) LAF-019 (Hyd-2) soluble fraction; (v) LAF-019 (Hyd-2) insoluble fraction. B: Comparison of expression of strains depicted in Figure 3.5 B (i), (ii) and (iii). Lanes: (i) molecular weight size markers; (ii) native strain LAF-001 soluble fraction; (iii) LAF-001 insoluble fraction; (iv) LAF-019 soluble fraction; (v) LAF-019 insoluble fraction; (vi) pre-transmembrane polyhistidine tagged Hyd-2 strain LAF-020 soluble fraction (vii) LAF-020 insoluble fraction. C: Comparison of expression of strains depicted in Figure 3.5 A (i) and (iv). Lanes: (i) molecular weight size markers; (ii) LAF-001 soluble fraction; (iii) LAF-001 insoluble fraction; (iv) polyhistidine tagged Hyd-1 with duplicated *hyaA* terminal nucleotides (LAF-003) soluble fraction; (v) LAF-003 insoluble fraction.

This version of the polyhistidine tag was also successfully inserted into the variant strains of Hyd-1, and this is demonstrated for the creation of a histidine tagged H229A variant (LAF-018) in Figure 3.7. The synthesis of the *rpsL-neo* cassette and oligomer containing the intended mutation proceeded in the same manner as discussed in Section 3.3.2 (Figure 3.7 A (i) and (ii)). Insertion and removal of this cassette were confirmed by checking primers and agarose gel electrophoresis (Figure 3.7 A (iii) and (iv)). Sequencing was used to verify that the polyhistidine tag codon insertion and duplication of the *hyaA* bases was successful, and this is shown in Figure 3.7 B where the inserted sequence is highlighted by the black box.
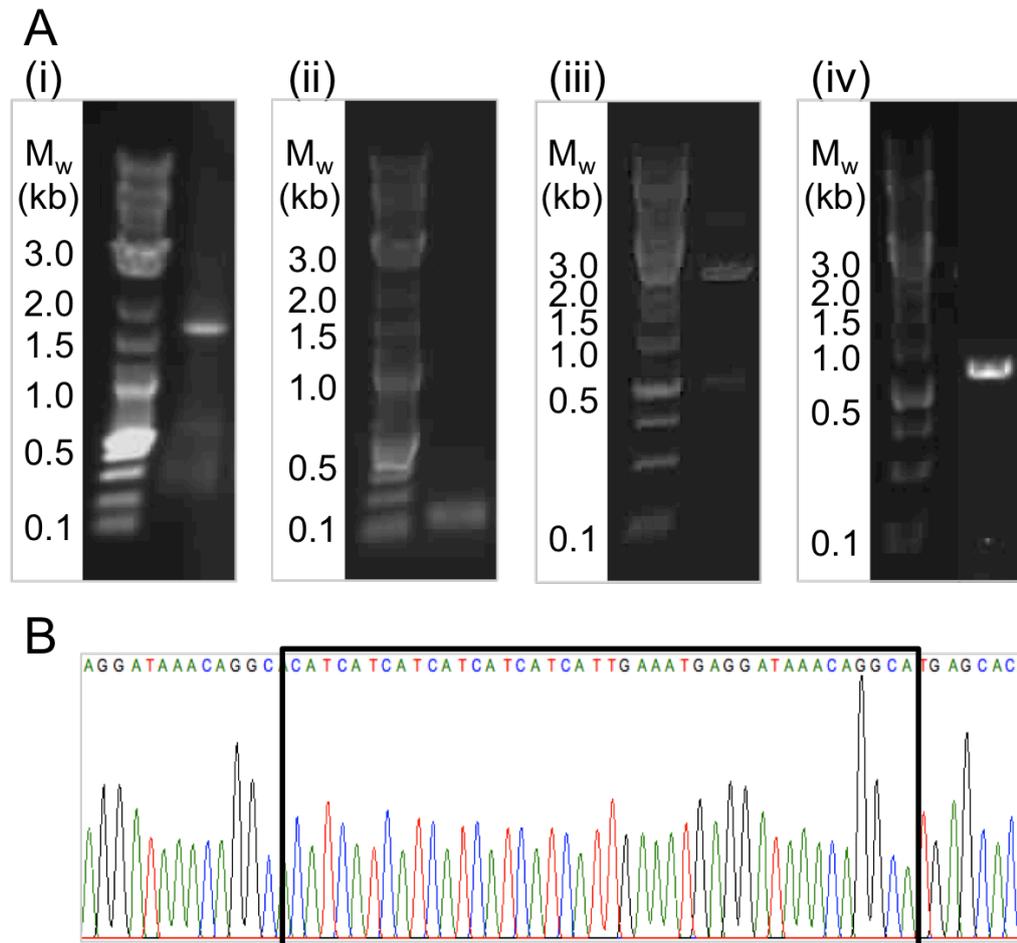
Figure 3.7 Insertion of the polyhistidine tag into the Hyd-1 H229A variant. A: Agarose gel electrophoresis showing: (i) PCR synthesis of ~1.5 kilobase pair double stranded oligonucleotide containing 50 base pairs of homology to the terminus of *hyaA*, nucleotides coding for the polyhistidine tag and stop codon, the *rpsL-neo* cassette, the 20 base pairs duplicated from the *hyaA* terminus and 50 base pairs of homology to the strart of *hyaB*; (ii) PCR synthesis of ~100 base pair double stranded oligonucleotide containing 50 base pairs of homology to the terminus of *hyaA*, nucleotides coding for the polyhistidine tag and stop codon, the 20 base pairs duplicated from the *hyaA* terminus and 50 base pairs of homology to the strart of *hyaB*; (iii) colony PCR of LAF-017 with checking primers to verify successful insertion of the polyhistidine tag, cassette and duplicated genes in between *hyaA* and *hyaB*; (iv) colony PCR of LAF-018 with checking primers to verify successful removal of the cassette between the polyhistidine tag and duplicated bases. B: Sequencing to verify successful insertion of polyhistidine tag, stop codon and 20 duplicated bases (black box) in strain LAF-018.

80

3.3.4 Use of one parent strain to create multiple child strains

As the *rpsL-neo* cassette was removed in order to create the Hyd-1 polyhistidine tag sequence, strain LAF-003 could be used to create single site variants, which would all be polyhistidine tagged. Because the mutation causing the amino acid substitution is only created during the final step where the *rpsL-neo* cassette is replaced by the double-stranded oligonucleotide, the same *rpsL-neo* strain may be used to create substitutions with any amino acid. This is demonstrated in Figure 3.8, where the same *rpsL-neo* strain (LAF-008) was used to create three different variants (LAF-009, LAF-010 and LAF-011) in a short amount of time, merely by using different oligonucleotides.
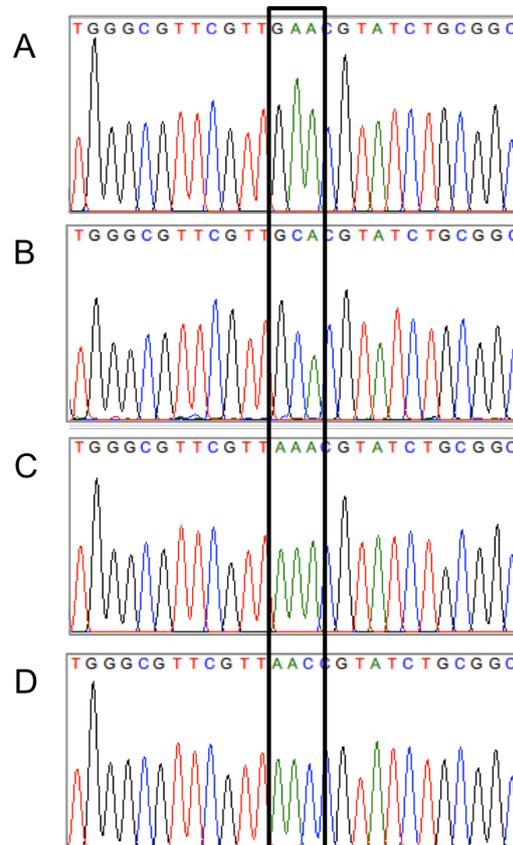
Figure 3.8 Creation of polyhistidine tagged Hyd-1 E73 variants from one parent strain. Replacement of A: glutamate codon (GAA) in Native *hyaB* (LAF-003) with B: alanine codon (GCA) in polyhistidine tagged E73A variant (LAF-009), C: lysine codon (AAA) in polyhistidine tagged E73K variant (LAF-010) and D: asparagine codon (AAC) in polyhisditine tagged E73N variant (LAF-011).

Figure 3.9 shows the parent and child strains of all strains discussed in this thesis. It may be seen that insertion and removal of the cassette allows multiple rounds of mutation, which allows the possibility of creating double and triple amino acid substitutions easily, although this is not explored here. One limitation of this method is that it has only been explored in mutation of the *E. coli* MBH, and relies on the mechanics of this host to perform recombination. It would be desirable to explore whether it may be expanded to encompass the incorporation of mutations in hydrogenases of other organisms.
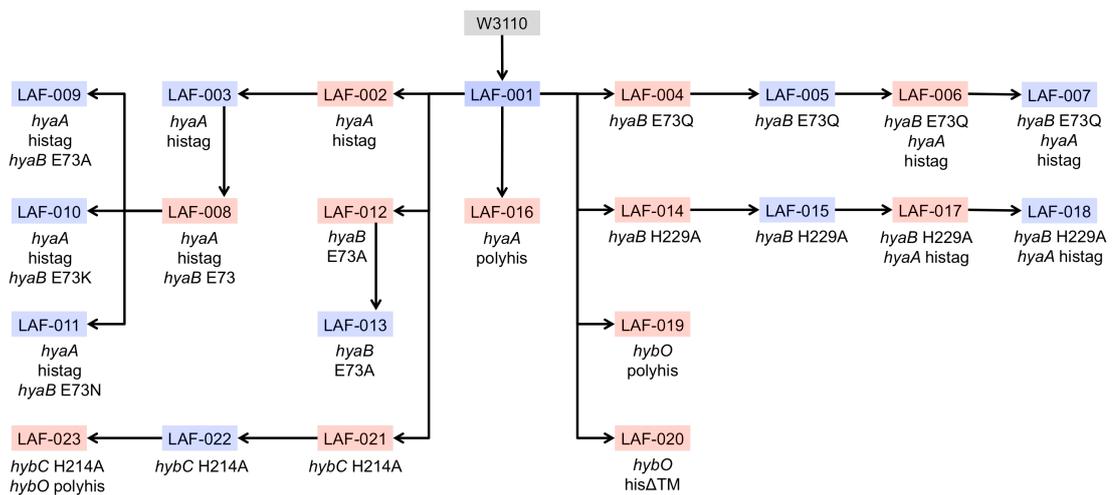
Figure 3.9 Scheme depicting the origin of each strain discussed in this work. Red indicates presence of *rpsL-neo* cassette, and blue indicates absence of the cassette. Text below the strain name indicates the position of the cassette or the mutation accordingly.

3.4 Conclusions

A method of incorporating mutations into the *E. coli* chromosome has been employed for the first time in the creation of NiFe hydrogenase variants. Multiple iterations of the process allows incorporation of more than one mutation. Nucleotides coding for polyhistidine tags were added in a way that allowed good expression of the protein. This functionality of the Red®/ET® methodology has not previously been explored.

It is considered that use of the method discussed here could save man-hours and allow exploration of many hydrogenase variants at the same site rather than necessitating that a group focus on creating one variant only. In addition, the ability of the method to insert a polyhistidine tag into the chromosome could allow proteins with complex maturation other than hydrogenases to be successfully purified.

Chapter 4

Role of large subunit residue 73 in H_2 production and catalytic bias of *E. coli* Hyd-1

4.1 Introduction

The iron-sulfur clusters and their amino acid ligands have been shown to play an important role in controlling fundamental properties of the NiFe hydrogenases. For example, as discussed in Section 1.2.6 of Chapter 1, the proximal and medial clusters have been shown to be of vital importance to the O_2 tolerance of membrane bound NiFe hydrogenases (MBH)[56-57]. It is thought that these centres play a vital role in donating electrons to reduce inhibitory reactive oxygen species bound at the NiFe catalytic site to water ($O_2 + 4e^- + 4H^+ \rightarrow 2H_2O$)[25, 222]. The distal cluster, as the point of entry/exit of the hydrogenase, has been hypothesised to control the onset potential for H_2 oxidation, and thus the catalytic bias between H_2 oxidation and proton reduction (H_2 production)[68]. However, it was established in Chapter 2 and other works[33, 210], that residues in the secondary and tertiary coordination sphere of the iron-sulfur clusters may also have a role in tuning the properties of hydrogenases, and this will be the focus of this chapter.
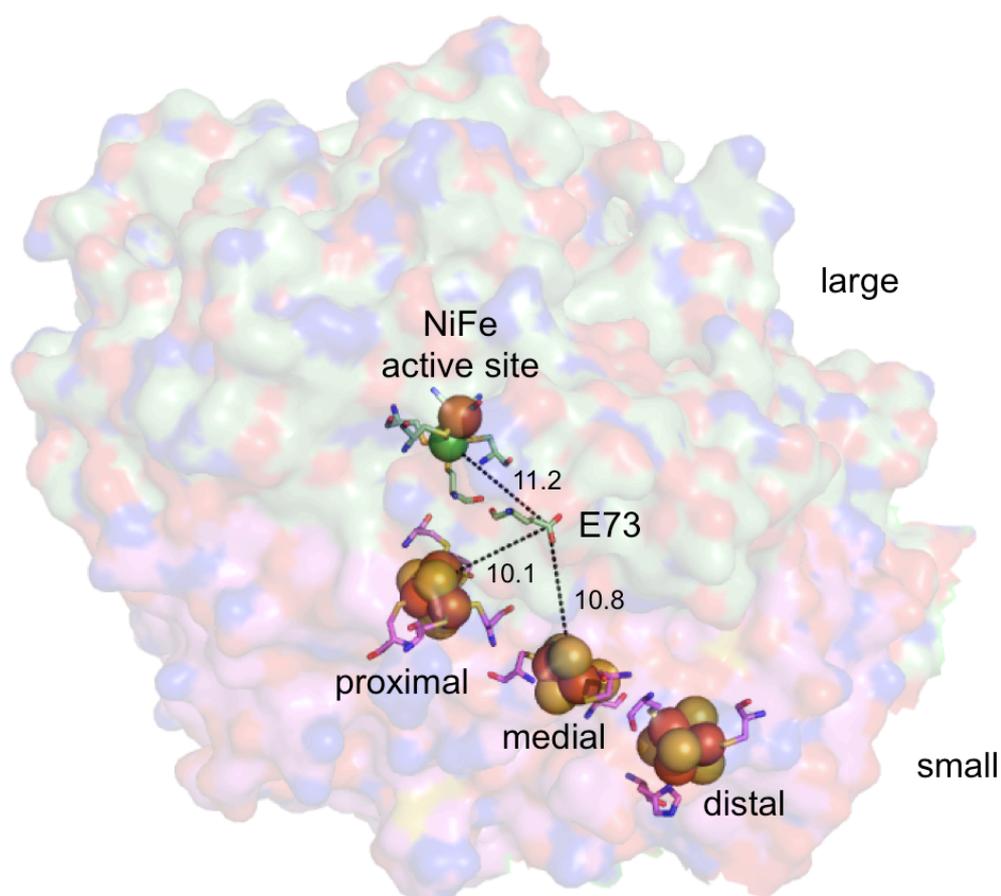
Figure 4.1 Location of glutamate 73 within the large-small heterodimer of *E. coli* Hyd-1 (PDB: 3UQY[34]). Transparent surface represents the protein subunits, iron-sulfur clusters and nickel and iron of the active site shown as spheres and the ligands and E73 are shown as sticks. Number next to the dashes shows the distance in Å. Colours: pale green, carbon of large subunit; magenta, carbon of small subunit; red, oxygen; blue, nitrogen; yellow, sulfur; orange, iron; green, nickel.

Residue 73 in the large subunit of Hyd-1 is at a similar distance from the active site and both the proximal and medial iron-sulfur clusters (Figure 4.1). This residue is a conserved glutamate in the majority of O_2 tolerant MBH. It was seen in Chapter 2 that mutation of glutamate 73 to alanine in O_2 tolerant MBH *S. enterica* Hyd-5 slightly reduced the O_2 tolerance. This was used by Dance[210] to propose two possible roles of the residue. Firstly, the carboxylic acid group could be part of the proton transfer pathway, passing H^+ between water molecules and histidine 229, causing a proton driven structural change, triggering formation of the superoxidised state of the proximal cluster. Alternatively, the glutamate

85

could form part of a hydrogen-bonding network, where structural transitions at the active site could be communicated through the hydrogen bonds to the proximal cluster, triggering formation of the superoxidised state in a proton-independent manner. Alanine, with a methyl group as a side chain, represents a truncation of glutamate to eliminate all functionality. However, glutamine is the conserved residue that replaces glutamate in this position in all O_2 sensitive hydrogenases. Glutamine is uncharged but is able to participate in hydrogen bonding, although with a different hydrogen-bonding pattern than the carboxylic acid of glutamate. To explore the impact of changing proton transfer capability/ hydrogen-bonding patterns in this way, an E73Q variant was created in *E. coli* Hyd-1. In addition, an E73A variant was created in order to verify that the properties seen in *S. enterica* Hyd-5 are conserved in the equivalent *E. coli* Hyd-1 variant. To discover the impact of a positive charge on the residue, an E73K variant was created, and an E73N variant was created in order to further elaborate on the effect of changing hydrogen bonding in this region of the protein.

4.2 Method

4.2.1 Purification and activity measurements.

Hydrogenase was purified from strains LAF-003, LAF-007, LAF-009, LAF-010 and LAF-011 and electrochemistry was performed as described in Chapter 8. The methylene blue assay measurement of H_2 oxidation was performed at pH 4.5 according to the method described in Chapter 8.

4.2.2 Computational measurements of variant stability and structure

In order to model the effect of the amino acid substitution, the SDM server was used (http://www-cryst.bioc.cam.ac.uk/~sdm/sdm.php)[223] on the 3UQY protein data bank structure file of Hyd-1[34]. The L chain and position 73 were selected. For each variant a different iteration of submission to the server was used.

4.2.3 EPR spectroscopy

EPR spectroscopy was performed by John Wright (PhD student in Dr Maxie Roessler's group at Queen Mary University of London) on samples of enzyme supplied from York. Hyd-1 E73Q variant was prepared and concentrated as detailed in Chapter 8. It was diluted in the EPR buffer (pH 7, 50 mM HEPES, 50 mM sodium phosphate, 150 mM sodium chloride and 30% w/v glycerol) and concentrated to 12 μM, 250 μL before shipping on dry ice to Queen Mary University London, where it was frozen at -80 °C until needed. A redox titration was performed on the sample and 9 μL aliquots were transferred to 1.6 OD quartz EPR tubes (Wilmad) by John Wright. All EPR was performed by John Wright as described previously[224]. Measurements were performed using an X/Q-band Bruker Elexsys E580 Spectrometer (Bruker BioSpin GmbH, Germany) at 9.68 GHz, equipped with a closed-cycle cryostat. All measurements were carried out at 20 K in an X-band split-ring resonator module with 2 mm sample access (ER 4118X-MS-2W). The samples were positioned in the resonator guided by the microwave frequency and the Q-value (typically 700), as reported by the built in Q-indicator. EPR measurement conditions used for all samples were 2 mW power, 100 kHz modulation frequency and 1.0 mT modulation amplitude.

4.3 Results and discussion

4.3.1 Purification of Native and E73 variant Hyd-1
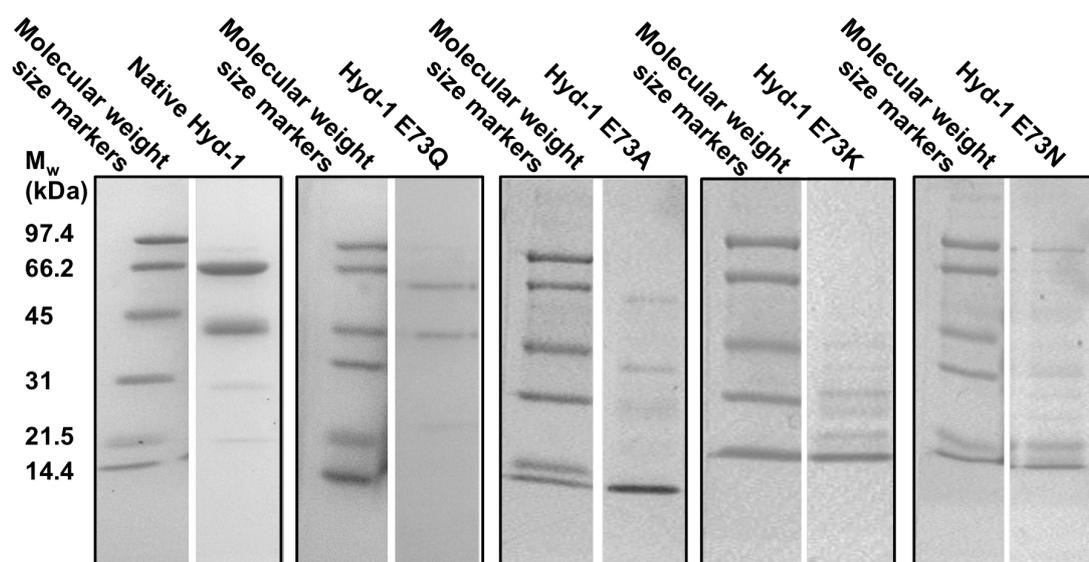
Figure 4.2 SDS-PAGE of eluted protein on 10% acrylamide gel. Presence of hydrogenase is indicated by presence of bands at 66 kDa (large subunit) and 41 kDa (small subunit).

Native, E73Q and E73A variant Hyd-1 were successfully purified from strains LAF-003, LAF-007 and LAF-009 respectively. E73Q and Native Hyd-1 purified with a good yield, and gave pure hydrogenase as seen in Figure 4.2. E73A purified with a lower yield, and impurities were detected in the gel of the elution fractions. Unfortunately, despite using the same purification protocol, no large subunit was detectable in the gel of the elution fractions of E73K or E73N. As seen in Figure 4.3, in O_2 tolerant MBH, residue 73 is close to both a proline and an arginine. It is possible that the positive charge of the lysine could repulse the arginine and attract the backbone oxygen of the proline in a way that might disrupt the folding of the large subunit. As asparagine may form hydrogen bonds but is shorter than glutamate or glutamine, the E73N variant may have similarly disrupted folding.
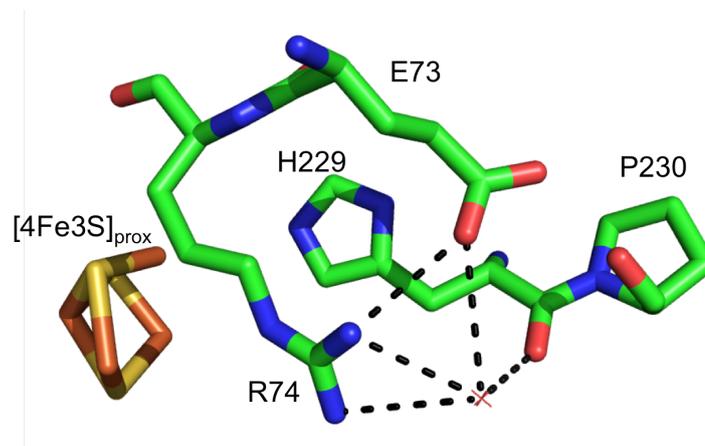
Figure 4.3 Proximity of glutamate 73 to proline 230 and arginine 74 (structure of *R. eutropha* MBH PDB: 3RGW[32]). Colours: blue, nitrogen; red, oxygen; green, carbon; yellow, sulfur; orange, iron. Dashes show polar contacts and red cross shows water.

This hypothesis was testing by using the SDM server[223] to computationally build the mutations into the Hyd-1 protein structure. The resulting values for the stability measure pseudo $\Delta\Delta G$ are given in Table 4.1. Whilst the E73A variant is expected to be slightly more stable and the E73Q variant neutral for stability, the E73K and E73N variants are expected to be destabilised by the amino acid substitution. This suggests that the reason that purification of the E73N and E73K variants was unsuccessful was that these variants did not form stable hydrogenase.

Table 4.1 Calculated effect of amino acid substitution on pseudo $\Delta\Delta G$ (kcal mol^{-1})

Variant	Pseudo $\Delta\Delta G$	Effect
E73Q	-0.32	Neutral
E73A	0.96	Slightly stabilising
E73K	-3.27	Highly destabilising
E73N	-1.66	Destabilising

4.3.2 Effect of the amino acid substitution on catalysis

The catalytic activity and O_2 tolerance of Native Hyd-1 and E73A and E73Q variants at pH 6 is shown in Figure 4.4. These are the conditions that were used in Chapter 2 to investigate the *S. enterica* Hyd-5 E73A variant. As expected, the *E. coli* Hyd-1 E73A variant has similar catalytic activity to Native Hyd-1 but diminished O_2 tolerance both in terms of the H_2 oxidation activity under O_2 and in terms of the recovery after O_2 is removed from the system. In contrast, the E73Q variant shows similar O_2 tolerance to Native Hyd-1. As glutamine does not participate in formal proton transfer, this nullifies the hypothesis that glutamate 73 mediates O_2 tolerance by participating in proton transfer to the proximal cluster, causing proton-dependant structural transitions[210]. However, the alternative hypothesis is that glutamate 73 communicates structural changes that occur at the active site in the presence of O_2 to the proximal cluster in a proton-independent fashion via a hydrogen-bonding network. This hypothesis could explain the difference in the O_2 tolerance of the E73A and E73Q variants, as the glutamine side chain is able to form hydrogen bonds whilst the alanine side chain is not. Therefore, only glutamine would be able to maintain a hydrogen-bonding network of structural communication between the active site and the proximal cluster.
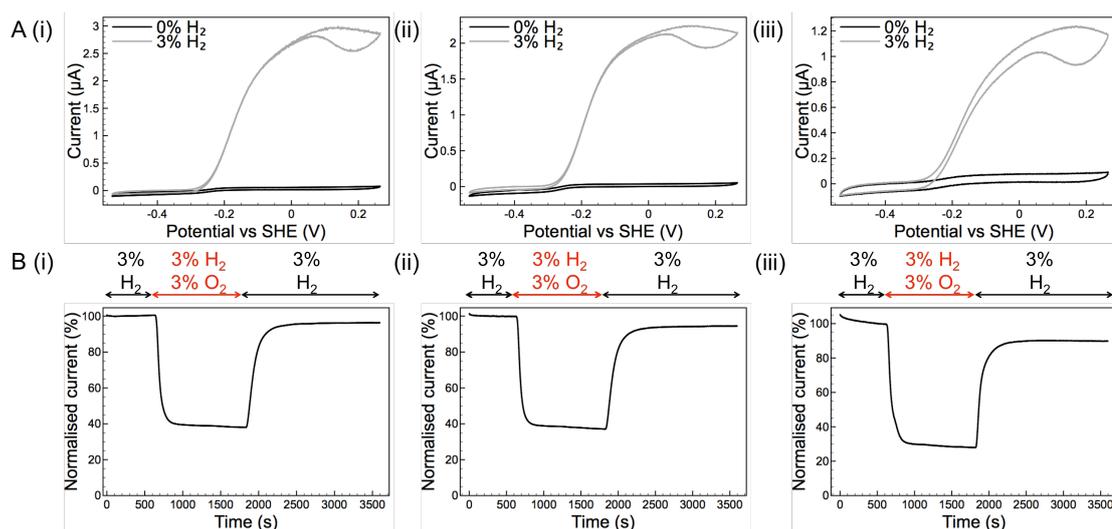
Figure 4.4 A: Catalytic ability and B: O_2 tolerance of Hyd-1 (i) Native, (ii) E73Q variant and (iii) E73A variant at pH 6. A: The potential was swept from -0.535 to +0.265 V vs SHE and back again at 5 mV s^{-1} and 100 % N_2 (black) or 3% H_2 97% N_2 (grey). B: The potential was held at -0.06 V vs SHE at pH 6 whilst the gas mixtures indicated above the plot were flowed through the cell. Current normalised to the H_2 oxidation current just prior to the addition of oxygen.

Although the H_2 oxidation activity of the E73Q variant at 3% H_2 is not visibly altered relative to Native Hyd-1, at pH 6 and 0% H_2 more negative current is produced by this variant at low potentials, indicating greater H_2 production activity (Figure 4.4). In order to probe these differences, the cyclic voltammetry experiments were repeated at pH 4.5, as seen in Figure 4.5. Lower pH has been shown to be a crucial factor in H_2 production activity of O_2 tolerant hydrogenases, partly because of a greater supply of substrate, but also because of the non-linear change in the overpotential of H_2 oxidation with pH[68].
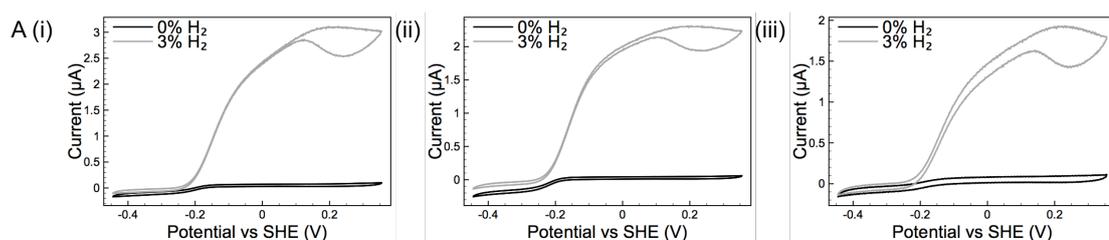
Figure 4.5 A: Catalytic ability of Hyd-1 (i) Native (ii) E73Q variant and (ii) E73A variant at pH 4.5. The potential was swept from -0.445 to +0.355 V vs SHE and back again at 5 mV s^{-1} and 100 % N_2 (black) or 3% H_2 97% N_2 (grey).

In the pH 4.5 experiments, the catalysis of E73A variant and Native Hyd-1 is again comparable under either 3% or 0% H_2. The E73Q variant shows no difference in the H_2 oxidation activity at 3% H_2 but at low potential and 0% H_2 there is visibly more negative current from E73Q than Native Hyd-1. Indeed, when the voltammetry traces are overlaid, the E73Q variant has double the H_2 production current of the Native Hyd-1 (Figure 4.6). This represents a shift in the catalytic bias towards H_2 production.
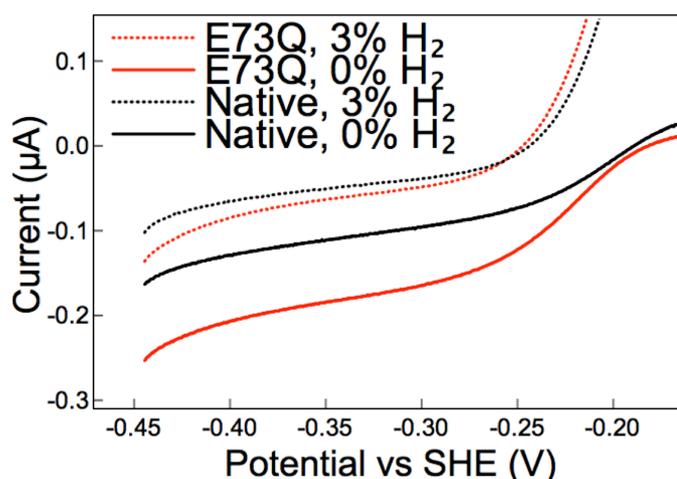
Figure 4.6. Overlay of low potential H_2 production emphasised for Hyd-1 Native (black) and E73Q variant (red) at 100% N_2 (solid line) and 3% H_2 97% N_2 (dotted line). Line shown is the average of the forwards and backwards scans in Figure 4.5.

In order to confirm that a shift in the catalytic bias is an intrinsic property of the E73Q variant and not an artefact due to, for example, a film effect, a chronoamperometry experiment was designed to explore H_2 production at low potential relative to H_2 oxidation at high potential for the Native Hyd-1 and E73 variants. This is shown in Figure 4.7. By switching between reducing and oxidising potentials (Figure 4.7 A (i)) the H_2 production current could be monitored at both 100% N_2 and 3% H_2 97% N_2. This was normalised to the H_2 oxidation current at 3% H_2 97% N_2. There is a clear gap between the normalised H_2 production currents of the Native Hyd-1 and E73Q variant at low potential and 100% N_2, indicating that under these conditions, the increased catalytic bias towards H_2 production is conserved in the E73Q variant. The gap is absent in the plot of the E73A variant, suggesting that the catalytic bias of this variant is unchanged with respect to Native Hyd-1. When these data are extracted in Figure 4.7 C, it is seen that the E73Q variant has double the normalised H_2 production current of both the Native and E73A variant Hyd-1. A t-test confirmed that this was statistically significant, giving $p=0.0053$ for the comparison of Native and E73Q variant Hyd-1. In contrast, the difference between the E73A variant and Native Hyd-1 was not significant, at $p=0.1226$.

By adjusting the rotation rate of the working electrode during the course of the experiment (Figure 4.7 A (ii)), it was shown that there was adequate diffusion of H_2, as there was very little increase in either H_2 production or H_2 oxidation current when the rotation rate was increased from 3000 to 3500 rev per minute (rpm). When the rotation rate is ceased, there is a large drop-off in current (Figure 4.7 B). This is expected for H_2 oxidation, due to a lack of substrate supply. However, at pH 4.5 there is a large supply of protons available as a substrate for H_2 production. The decrease in H_2 production current under conditions of no rotation is thus indicative of the product inhibition. This is clarified by the current at -0.385 V vs SHE and 3% H_2, where no difference is seen between the current produced by the Native Hyd-1 and the current produced by the E73Q variant. This suggests that the variant shows strong product inhibition. This property is explored later in this chapter.
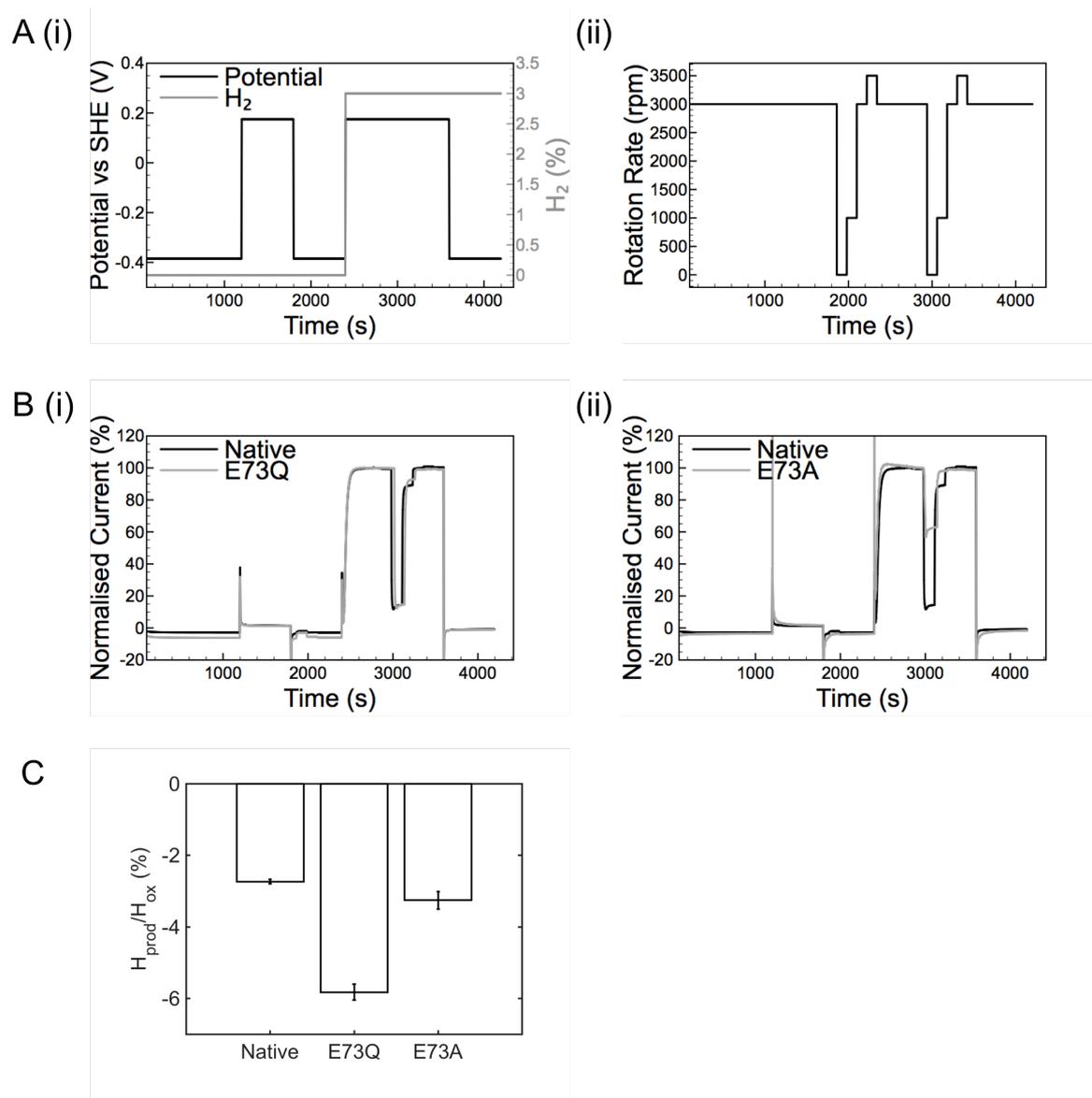
Figure 4.7 Chronoamperometry experiment to measure catalytic bias in Native and variant Hyd-1 at pH 4.5. A: Experimental design. (i) The potential (black line) was held at either -0.385 V vs SHE or +0.175 V vs SHE as the gas mixture (grey line) was switched between 100 % N_2 and 3% H_2 97% N_2. (ii) The rotation of the working electrode was ceased at the times shown on the plot before being resumed in increments. B: Resulting current comparison for (i) Hyd-1 Native (black) and E73Q variant (grey) and (ii) Hyd-1 Native (black) and E73A variant (grey), normalised to the H_2 oxidation current at 2939 seconds. C: Extracted normalised H_2 production current at 2399 seconds over an average of three repeats. Error bars show the standard error.

The alteration of the catalytic bias in the E73Q variant is somewhat unexpected as the position of residue 73 is conducive to neither of the catalytic control mechanisms discussed by previous works[191-192]. Firstly, being a large subunit residue, the glutamine at position 73 is highly unlikely to alter the reduction potential of the distal proximal cluster, which is located in the small subunit. Secondly, residue 73 is not located in the gas channel[71] and thus is unlikely to narrow the channel in a way that could restrict H_2 entry or exit, as was previously demonstrated to alter the catalytic bias of *Desulfovibrio vulgaris* NiFe hydrogenase[191]. The properties of the E73Q Hyd-1 variant were thus explored further.

A change in catalytic bias towards H_2 production could either represent a higher H_2 production or a lower H_2 oxidation. This is an important thing to consider before offering any mechanistic explanations. H_2 oxidation rates cannot be simply determined from electrochemical measurements because the number of hydrogenase molecules adsorbed onto the electrode is not known (see Section 1.4.2 of Chapter 1). This was first assessed by performing a H_2 oxidation assay using methylene blue. The rate of catalysis (k_{cat}) was 21 ± 4 s^{-1} for Native Hyd-1 and 22 ± 3 s^{-1} for Hyd-1 E73Q. This difference was found not to be significant. This indicates that at the methylene blue redox potential (determined as $+0.113$ V vs SHE, at pH 4.5, 25 °C by cyclic voltammetry (Chapter 8)) the amino acid exchange does not impact the ability of the enzyme to perform H_2 oxidation.
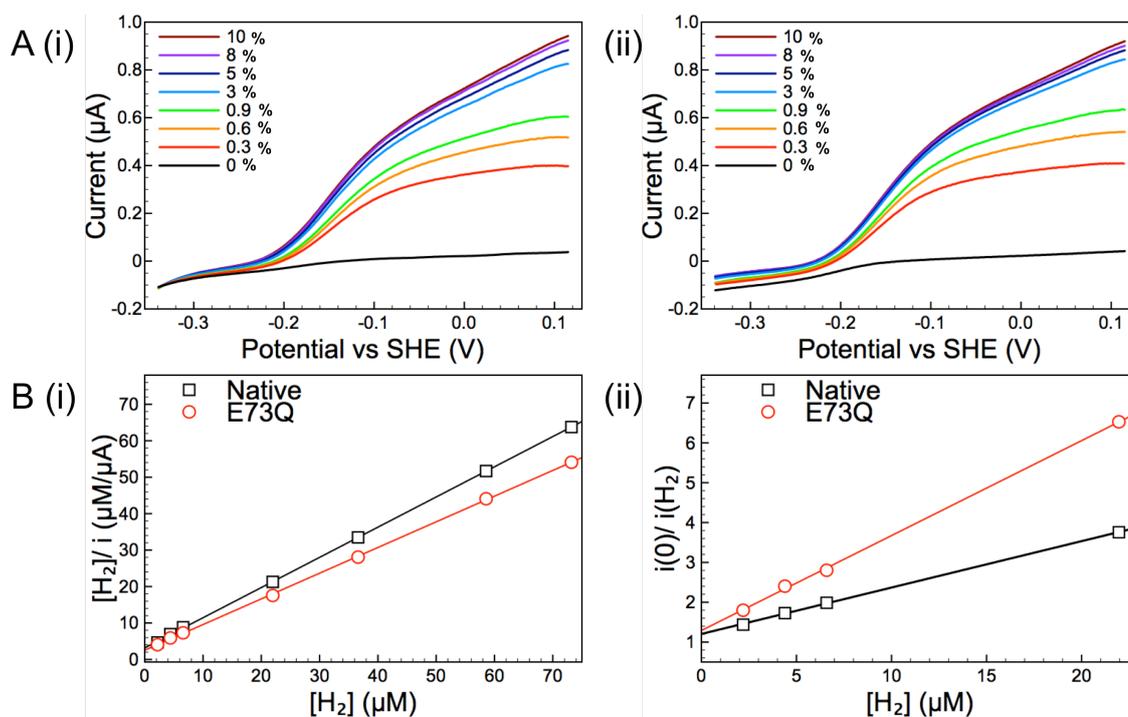
Figure 4.8 Determination of the K_M constant of H_2 oxidation and the K_i constant of H_2 production. A: Averaged forward and backward scans of Hyd-1 (i) Native and (ii) E73Q variant at different percentages of H_2 as indicated by the legend. The values produced by these scans were used for the data analysis shown in B. B: The (i) Hanes-Woolf analysis of Native (black square) and E73Q variant (red circle) Hyd-1, used to determine the Michaelis constant at +0.113 V vs SHE and (ii) the inhibition plot to determine the inhibition constant at -0.285 V vs SHE.

This result suggests that the substitution of glutamate with glutamine has not significantly adjusted the rate of H_2 oxidation. Therefore, the Michaelis constants (K_M) for H_2 oxidation and inhibition (K_i) constants for H_2 production were calculated by performing a series of cyclic voltammetry experiments at different levels of H_2 as shown in Figure 4.8 A. A representation of the plots generated from this experiment are shown in Figure 4.8 B and Table 4.2 shows the coefficients generated from each of the three repeats. The K_M was found to be 4.2±1.0 μM for Native Hyd-1 and 3.8±1.7 μM for E73Q variant Hyd-1. This difference is not significant, suggesting that H_2 affinity is not changed. This is an expected result as the amino acid exchange was not located in the site of the H_2 gas channel[71]. Therefore, it is highly likely that the change in catalytic bias is due to an increase in H_2 production.

Table 4.2 Experimental repeats for the Hanes-Woolf plot

Experiment	Gradient	Intercept	Calculated K_M
Native 1	1.02	3.99	3.9
Native 2	0.43	2.91	6.8
Native 3	0.85	2.62	3.1
Native 4	1.02	3.12	3.1
E73Q 1	0.72	1.73	2.4
E73Q 2	0.52	2.41	4.6
E73Q 3	1.05	3.30	3.1
E73Q 4	0.53	2.65	5.0

Table 4.3 Experimental repeats for the inhibition plot

Experiment	Gradient	Intercept	Calculated K_I
Native 1	0.14	1.04	7.2
Native 2	0.16	1.26	6.3
Native 3	0.10	1.25	10.4
Native 4	0.07	1.27	13.9
E73Q 1	0.37	1.44	2.7
E73Q 2	0.16	1.42	6.4
E73Q 3	0.20	1.16	5.0
E73Q 4	0.23	1.14	4.3

It is known that O_2 tolerant hydrogenases have very strong product inhibition in H_2 production[225]. It may be hypothesised that if the variant was less product inhibited then greater H_2 production could arise. However, the K_i for the Native Hyd-1 is 9.5 ± 1.7 μM whilst the K_i for the E73Q variant Hyd-1 is 4.6 ± 0.8 μM. This suggests that the variant is in fact slightly more product inhibited than the Native Hyd-1. Product inhibition is likely the reason that the difference in H_2 production by the Native and variant Hyd-1 is much larger at 100% N_2 than 3% H_2. However, increased product inhibition is more likely to lead to decreased H_2 and this property cannot explain the difference in the catalytic bias of the E73Q Hyd-1 variant compared to Native Hyd-1.

4.3.3 Properties of the E73Q variant
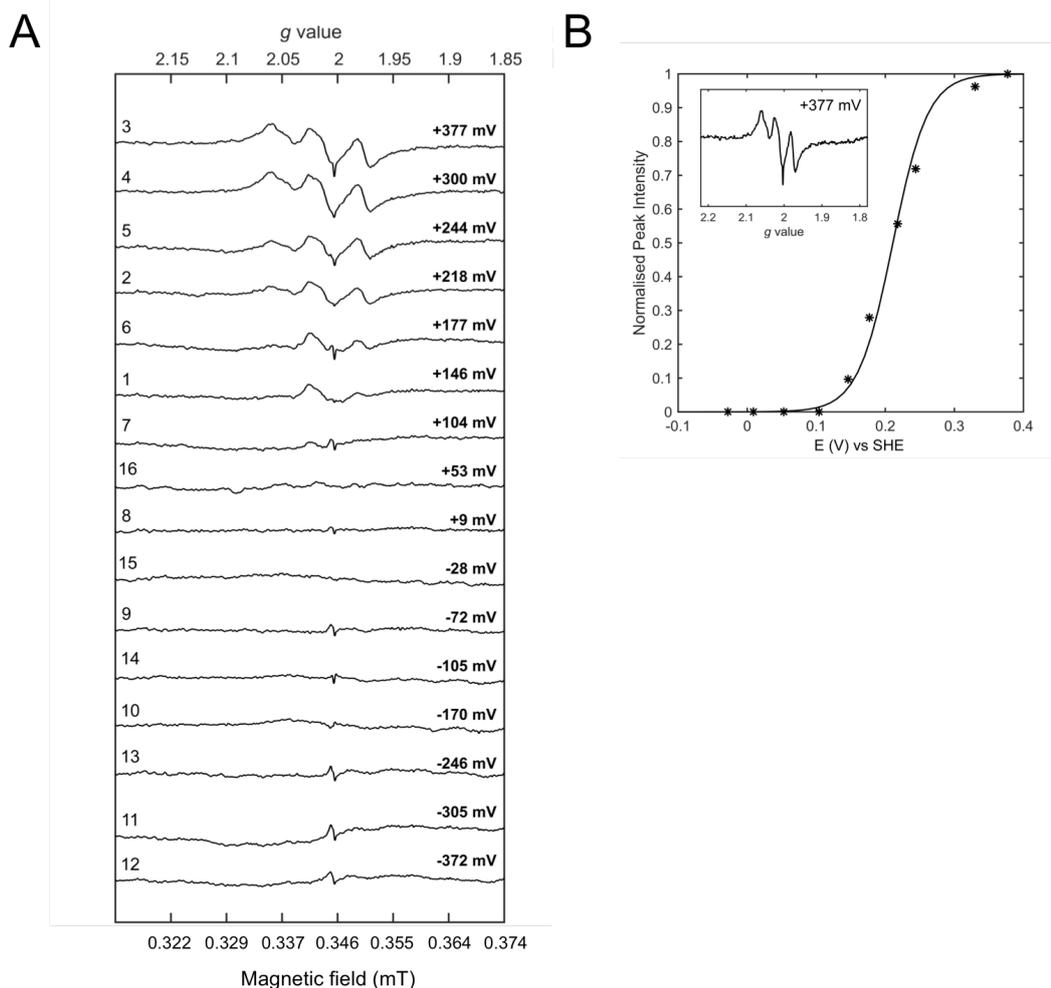
Figure 4.9 EPR spectroscopy of the Hyd-1 E73Q variant (from John Wright, Queen Mary University of London). Adapted from Flanagan et al[226]. A: Full potentiometric titration using small volume (9 μL) samples. Potential (right) and order of sample titration (left) indicated on graph. B: Fit of the potentiometric titration of the g=1.97 [4Fe3S]$^{5+/4+}$ peak (inset) to the one-electron Nernst equation (solid line). All spectra were baseline subtracted.

In the model proposed by Hexter et al[192], the catalytic bias is controlled by the reduction potentials of the iron-sulfur cluster relay. The substitution of glutamate for glutamine removes positive charge from the tertiary coordination sphere of the proximal cluster, which could have an effect on the redox potential. In order to investigate this, electron paramagnetic resonance (EPR) spectroscopy of the E73Q Hyd-1 variant poised at different solution redox

potentials was performed by John Wright (PhD student, Queen Mary University London) and this is shown in Figure 4.9. The midpoint reduction potential for the $[4Fe3S]^{4+}$ to $[4Fe3S]^{5+}$ proximal cluster transition is 211 mV$\pm$10 mV, which compares favourably to previously seen values of 230 mV $\pm$ 15 for Native enzyme[227]. The medial cluster signal also developed as a function of potential in a way that was comparable with previous measurements of *E. coli* Hyd-1[227]. Unfortunately, quantitative analysis of lower potential transitions than the proximal cluster was not possible as the enzyme concentration was too low. The Hyd-1 distal cluster is invisible by EPR[227], but it is considered unlikely that the potential of such a distant centre[34] (see Figure 4.1) would be affected by the amino acid substitution.
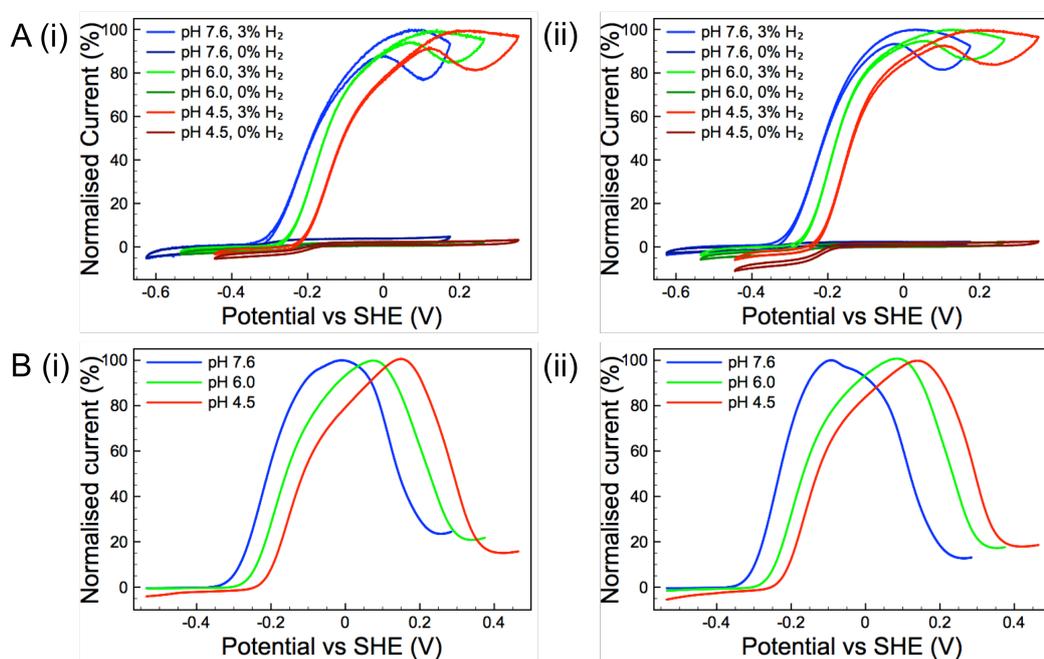
Figure 4.10 Impact of pH on A: catalysis and B: reactivation from Ni-B for Hyd-1 (i) Native and (ii) E73Q variant. A: The potential was swept from -0.625 V vs SHE (pH 7.6, blue), -0.535 V vs SHE (pH 6, green) or -0.445 V vs SHE (pH 4.5, red) and swept to +0.175 V vs SHE (pH 7.6), +0.265 V vs SHE (pH 6) or +0.355 V vs SHE (pH 4.5) at 5 mV s^{-1} and 0 or 3% H$_2$ before being swept back to the low potential. This scan was repeated four times and the fourth cycle is shown. B: The potential was held at +0.465 V vs SHE in pH 4.5 (red), or +0.375 V vs SHE in pH 6.0 (green), or +0.285 V vs SHE in pH 7.6 (blue) for 5 hours at 3% H$_2$ before the potential was scanned to -0.535 V vs SHE at a scan rate of 0.1 mV s^{-1}.

A mechanism proposed by Dance[210] on the role of glutamate 73 is that it forms part of the proton transfer relay between a proton reservoir and the proximal cluster. This was shown not to contribute to O_2 tolerance (above), since there was no difference in the O_2 tolerance of Native and E73Q variant Hyd-1. However, as H_2 production depends on proton reduction this process could be altered by the availability of protons. Thus the impact of pH on the catalytic activity of the Native and E73Q variant Hyd-1 was investigated and the results of this are shown in Figure 4.10. There is no visible difference seen in the voltammetric curves of Figure 4.10 A, showing there is no substantial disparity in the pH profile of H_2 oxidation catalysis between Native and E73Q Hyd-1. When the catalytic onset potentials (Eonset) are extracted from such experiments, these are also shown not to change upon exchanging glutamate 73 for glutamine (Figure 4.11 B).
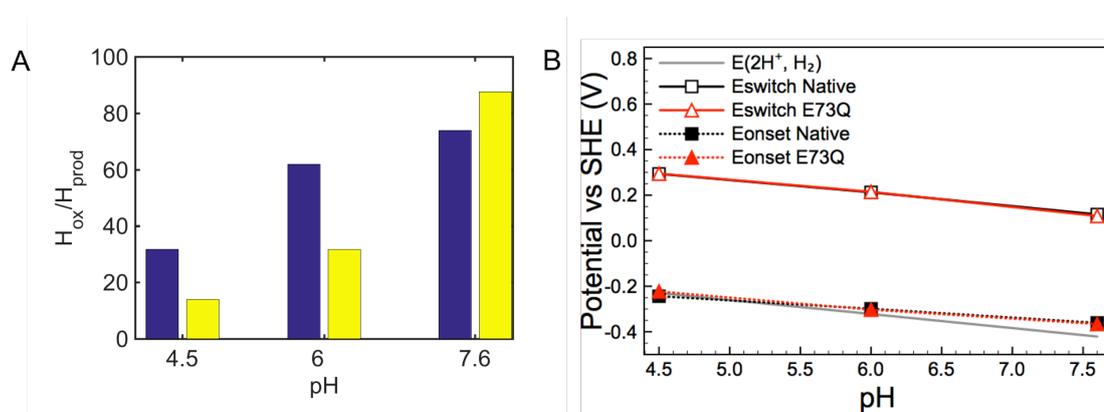
Figure 4.11 Extracted data from plots in Figure 4.10 to show pH effect. A: H_2 oxidation to H_2 production ratios for Native Hyd-1 (blue bars) and E73Q variant (yellow bars). Calculated from $i_{Hox}/-i_{Hprod}$ at -0.285 and +0.113 V vs SHE at pH 4.5, -0.375 and +0.023 V vs SHE at pH 6 and -0.465 and -0.067 at pH 7.6. B: the potential of onset of H_2 oxidation (Eonset, filled shaped) and potential of fastest reactivation from Ni-B (Eswitch, open shapes) for Hyd-1 Native (squares) and E73Q variant (triangles). Grey line shows the $2H^+/H_2$ couple calculated from the Nernst equation ($E(2H^+,H_2)$).

To specifically probe the involvement of glutamate 73 in proton transfer during the formation or reactivation of the Ni-B state a measurement of E_{switch}, a parameter which describes the ease of Ni-B reduction in hydrogenase enzymes[196], was also conducted (Figure 4.8 B). Specifically, the electrode potential was held at a positive value to fully inactivate the enzyme under anaerobic conditions, then the voltage was slowly lowered to produce a voltammetric curve which was differentiated to yield E_{switch}. When the E_{switch} is thus extracted, there is no difference between the E73Q variant and Native Hyd-1 (Figure 4.11 B).

At pH 6 and pH 4.5, proton reduction occurs in both the Native and E73Q variant Hyd-1, and for both these pH points the E73Q variant has half the H_2 oxidation to H_2 production (H_{ox}/H_{prod}) ratio of the Native Hyd-1 (Figure 4.11 A). This value cannot be calculated for the pH 7.6 data because O_2 tolerant MBH do not produce H_2 at such alkaline levels[68]. The H_2 production current of Native Hyd-1 doubles from pH 6 to pH 4.5, causing the H_{ox}/H_{prod} ratio to half. At both pH values the E73Q variant has double the H_2 production current of the Native Hyd-1. This means that H_{ox}/H_{prod} of E73Q at pH 6 is equal to H_{ox}/H_{prod} of the Native Hyd-1 at pH 4.5.

The pH effect on H_2 production by O_2 tolerant MBH has been linked to the control of the onset potential by the distal cluster[68]. As the onset potential is unchanged in the E73Q variant (above) and glutamate 73 is distant from the distal cluster (Figure 4.1), it is unlikely that this property is responsible for the difference in H_2 production. However, changing pH has been associated with changes in the proportions of the Ni-C and Ni-L states present in the active site by EPR and infrared (IR) spectroscopy[228]. At more acidic pH values, Ni-C dominates, and at more alkaline pH values, Ni-L dominates. It is perhaps unsurprising that H_2 production occurs when Ni-C is dominant, as this is the state which contains a bridging hydride[62], and needs only one proton and one electron to produce H_2 and Ni-SI$_a$. In Hyd-1 glutamate 73 is connected to the NiFe active site via a hydrogen-bonding network as seen in Figure 4.12. It is

possible that the glutamine amino acid substitution causes a shift in the hydrogen-bonding network which could promote Ni-C to be more dominant and that it is for this reason that H_2 production is increased.
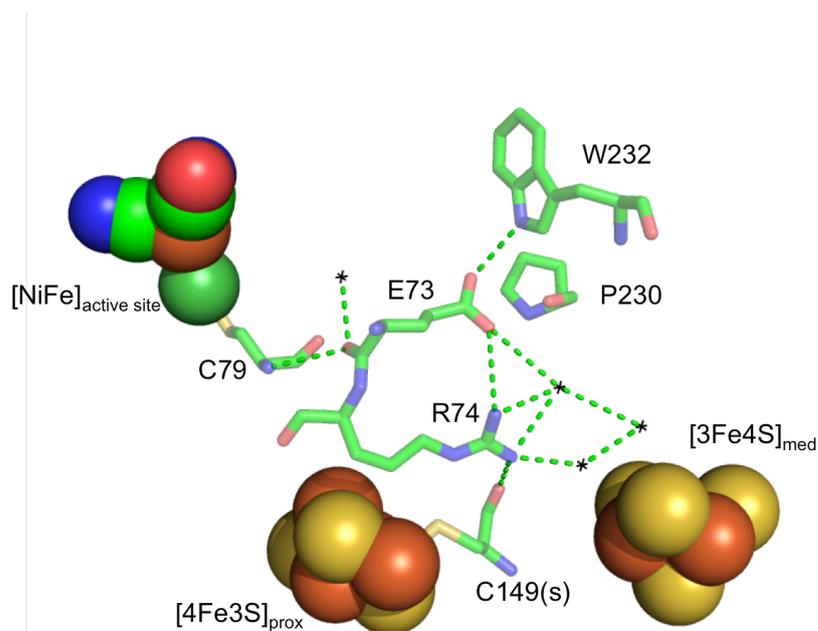
Figure 4.12 Network of polar contacts (green dashes) connecting the active site to the proximal and medial iron-sulfur clusters in *E. coli* Hyd-1 (PDB: 3UQY[34]). Colours: dark green, nickel; bright green, carbon; blue, nitrogen; red, oxygen; orange, iron; yellow, sulfur. Asterisks represent water.

There are several ways that this could be investigated that are beyond the scope of this study. The first is to create the same amino acid substitution in an O_2 tolerant MBH from another species, such as *R. eutropha*. In this species, residue 232 is a tyrosine[32] rather than a tryptophan, and so the hydrogen-bonding network is likely to be different. Another approach would be to use QM/MM (quantum mechanics/ molecular mechanics) in order to perform an energy minimisation on a computed glutamine substitution and to monitor changes to the NiFe site. This could be confirmed with the use of spectroelectrochemistry such as the Fourier transformed infrared work demonstrated by Hidalgo et al[65]. This technique could illustrate the proportions of each nickel state (Ni-C, Ni-R etc.) present at different potentials and pH values and allow investigation about whether they change in the E73Q variant with respect to Native Hyd-1.

4.4 Conclusions

The findings of this study have implications for biotechnology. One method of increasing rates of H_2 production in photosynthetic organisms is the expression of a non-native hydrogenase[229]. However, these often also require the incorporation of the associated maturation proteins of the non-native species, which could limit the ability to use the organisms on an industrial scale. The results suggested by this chapter indicate that good performance may be achieved by instead making amino acid substitutions of the hydrogenases belonging to the photosynthetic organism, thereby changing their catalytic properties. As these belong to the organism, no special processes would be required to ensure their replication or maturation. This work thus expands the possible strategies for biotechnological aspects of H_2 production.

Chapter 5

The role of the conserved histidine adjacent to the proximal cluster in O_2 tolerant and O_2 sensitive membrane bound NiFe hydrogenase of *Escherichia coli*

5.1 Introduction

For several years it has been suspected that there is a relationship between O_2 tolerance and anaerobic inactivation in NiFe hydrogenases[198], but the nature of this relationship is a disputed topic. Relative to O_2 sensitive hydrogenases, the O_2 tolerant MBH have a more positive E_{switch} values (the potential of the rate of fastest reactivation from Ni-B) and faster rates of Ni-B reactivation. Hamdan et al[198] showed that in a series of hydrogenase variants, the ones with a higher Ni-B reactivation rate had greater O_2 tolerance. This would suggest that rapid Ni-B reactivation reflects the ability of the hydrogenase to achieve facile reduction of reactive oxygen species and thus protection against O_2. However, more recently, Radu et al[202] claimed that O_2 tolerance is dependant on the slow reduction of the superoxidised proximal cluster. Both of these studies relied on dramatic changes in the protein, either by narrowing the gas channel[198], which also has an effect on catalytic bias, or by converting the 4Fe3S proximal cluster to 4Fe4S[202], the full impact of which on protein stability is unknown.

On the basis of the work discussed in Chapter 2 and the work by Frielingsdorf et al[33], Dance[210] proposed an O_2 tolerance mechanism (Figure 5.1) which relies heavily on the chemistry of the large subunit histidine adjacent to the proximal iron sulphur cluster. Dance hypothesised that structural transitions at the active site under O_2 cause proton transfer via the histidine to the S3 sulfur of the cluster, and this triggers breaking of the S3-Fe4 bond and thus opening of the proximal cluster from reduced to superoxidised form.
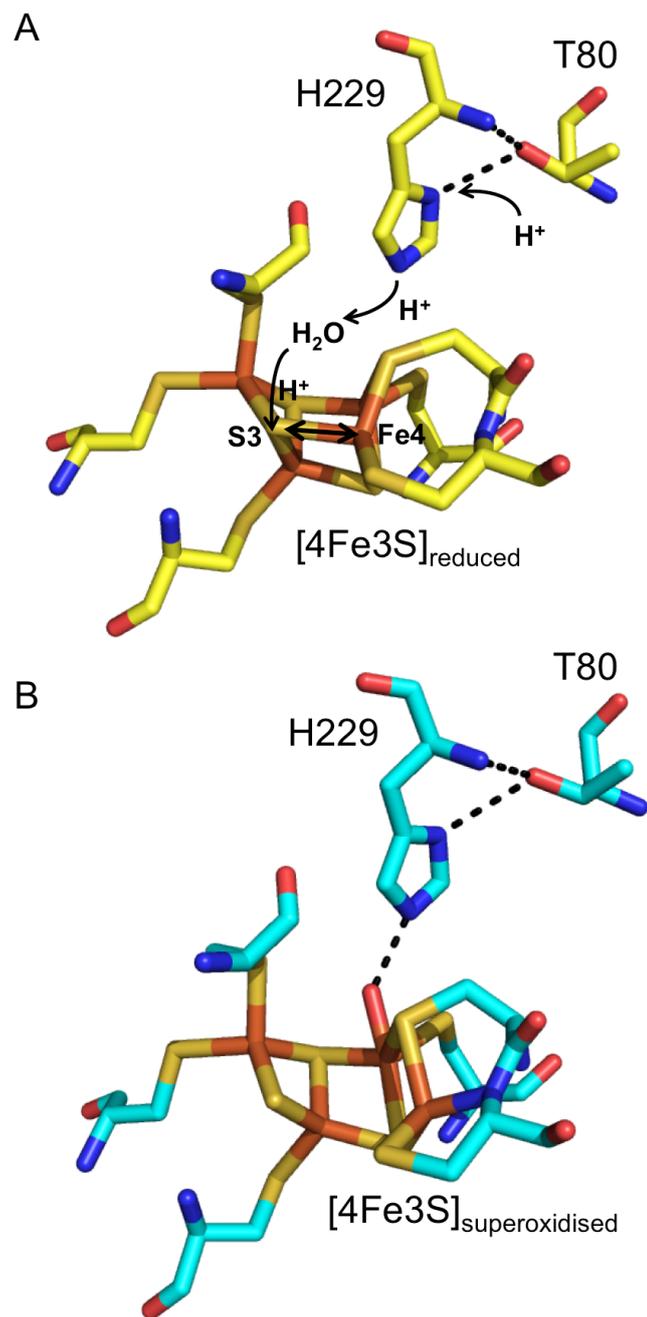
Figure 5.1 Mechanism proposed by Dance[210] of how histidine 229 could assist opening of the proximal cluster from reduced to superoxidised state. A: The reduced form of O_2 tolerant MBH from *R. eutropha* (PDB: 3RGW[32]). Curved arrows show proton transfer whilst double headed arrow shows site of cluster opening. Yellow: carbon, dark blue: nitrogen, red: oxygen, orange: iron, gold: sulphur. B: Superoxidised, open, form of the cluster (PDB: 4IUD[33]), showing an oxygen atom bound to the proximal cluster hydrogen bonding to H229. Colours: light blue, carbon; dark blue, nitrogen; red, oxygen; orange, iron; gold, sulphur. All numbering used is *E. coli* Hyd-1.

A notable oversight is that the works of Dance[210] and Frielingsdorf et al[33] neglected to investigate the role of the histidine in high potential anaerobic conditions, despite the detection of the superoxidised state in anaerobic EPR samples[230]. It has also been shown that at high potentials and under anaerobic conditions Ni-A is formed in samples of O_2 sensitive hydrogenases[80]. Therefore it may be proposed that the superoxidised state also has a role under O_2 free conditions. It may thus be hypothesised that the reason the cyclic voltammogram shape of the *S. enterica* Hyd-5 H229A variant changes relative to the native enzyme at high potentials is due to changes in the rate of formation of the superoxidised state. This hypothesis is supported by close examination of the work by Lukey et al[56], where greater inactivation is seen at high potentials in a Hyd-1 variant where the 4Fe3S cluster was replaced with a 4Fe4S cluster that could not form the superoxidised state.

Despite the strong evidence linking the histidine to O_2 tolerance[33], this residue is conserved across all NiFe hydrogenases. This also raises the question as to whether this histidine has a role in the function of O_2 sensitive hydrogenases. In order to resolve this question of the precise role of the proximal cluster histidine in O_2 tolerant and O_2 sensitive enzymes, alanine variants of histidine 229 of *E. coli* Hyd-1 and also of the respective position in Hyd-2, histidine 214, were created as discussed in Chapter 3. These Hyd-1 H229A and Hyd-2 H214A variants have been tested with protein film electrochemistry in order to assess their reactive properties with H_2 and O_2.

5.2 Methods

5.2.1 Protein purification

Native Hyd-1, Hyd-1 H229A, Native Hyd-2 and Hyd-2 H229A were purified from strains LAF-003, LAF-015, LAF-016 and LAF-019 respectively as described in Chapter 8.

5.2.2 Protein film electrochemistry

Protein film electrochemistry was performed in a N_2-filled glove box (Faircrest) as detailed in Chapter 8. A chronoamperometric potential step experiment, first detailed by Fourmond et al[196], was used to probe the inactivation and reactivation rate of the Hyd-1 Native and variant hydrogenase. The potential steps of this experiment are shown in Figure 5.2 against a typical cyclic voltammogram of Native Hyd-1. At the blue potential, the enzyme is assumed to be completely active. The red potentials are the inactivating steps and the green potentials represent a partial reactivation. The resulting chronoamperometric traces were fit to the equations of Fourmond[196] as detailed in Section 5.2.3.
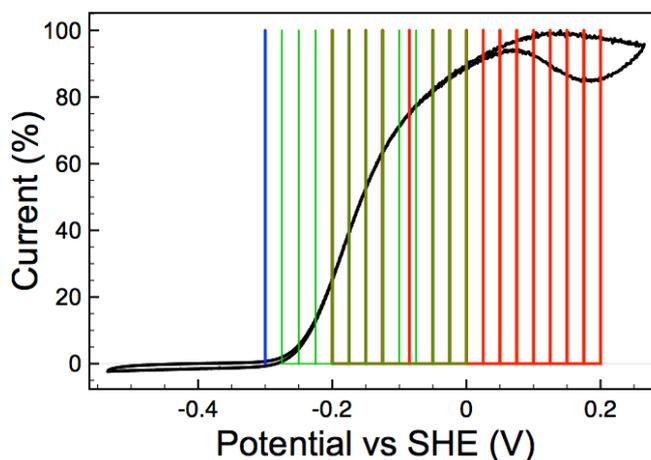
Figure 5.2 Potentials investigated with chronoamperometry to determine inactivation and reactivation rates. Black trace shows cyclic voltammetry of Native Hyd-1 at pH 6 and 3% H_2. Vertical lines show potentials monitored in the chonoamperometry experiment, where blue is fully activating, red is inactivating and green is partially activating.

5.2.3 Data modelling

The rates of Ni-B inactivation (k_A) and reactivation (k_I) were calculated for the potential region of +0.1 to +0.2 V vs SHE by using MATLAB 2016a software (MathWorks) to fit the inactivation steps (red lines, Figure 5.2) to Equation 5.1. In order to do this, the experiments were first separated into individual potential steps by establishing the timespans as a condition using the "cond" function and assigning the start point of each timepoint as 0 seconds and the end point as 300 seconds. The code below was then used to fit each step to a curve given by Equation 5.1, where xdata is the time in seconds and the ydata is the experimental current data of each potential step. Equation 5.1 is defined in the fittype function, where a is i_0, b is i_∞ and c is k_{tot}. The typical fit given by this method is shown in Figure 5.3, and it may be seen that the data (blue) and fit (red) overlap closely. The MATLAB coeffvalues function allowed the coefficients a, b and c of the best fit for each potential step to be to be written to a table.

$$i(t) = (i_0 - i_\infty) \exp[-k_{tot}E(t)] + i_\infty \qquad \text{(Equation 5.1)}$$

MATLAB code:

```
fo = fitoptions('Method','NonlinearLeastSquares',...
        'Lower',[0,0],...
        'Upper',[Inf,max(xdata)],...
        'StartPoint',[1 1 1]);
ft = fittype('((a-b)*exp(-c*x)+b )','options',fo);
 [curve2,gof2] = fit(xdata,ydata,ft);
c=coeffvalues(curve2);
t=table(43,c(1),c(2),c(3),'VariableNames',{'E' 'i0' 'iinf' 'ktot'});
```
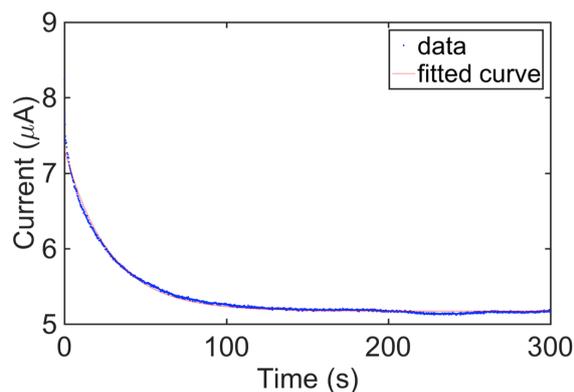
Figure 5.3 Fit versus data for the inactivation curve. The fit of Equation 5.1 (red line) against the current data (blue trace) for Native Hyd-1 when the potential is stepped to +0.2 V vs SHE from -0.3 V vs SHE and sustained at +0.2 V vs SHE for 300 seconds.

The separate tables of coefficients for each variant and repeat were aggregated by compiling them into a MATLAB datastore and then writing the contents of the datastore as an Excel workbook (Microsoft). This table was then opened in Excel in order to assign potentials corresponding to the coefficients generated for each step. The potential dependant inactivation rate (k_A) and reactivation rate (k_I) values were calculated using the timepoints when the potential was stepped from a low to high potential, by using the calculated coefficents to solve Equations 5.2 and 5.3[196] using a value of $A_0 = 1$. This value assumes that the enzyme is 100% active, because the inactivation immediately followed the step to the blue, reducing, potential in Figure 5.2, which is assumed to be fully activating.

$$k_A(E) = A_0 \frac{i_\infty}{i_0} k_{tot}(E) \qquad \text{(Equation 5.2)}$$

$$k_I(E) = k_{tot}(E) - k_A(E) \qquad \text{(Equation 5.3)}$$

5.3 Results and discussion

5.3.1 Role of the histidine in protein stability
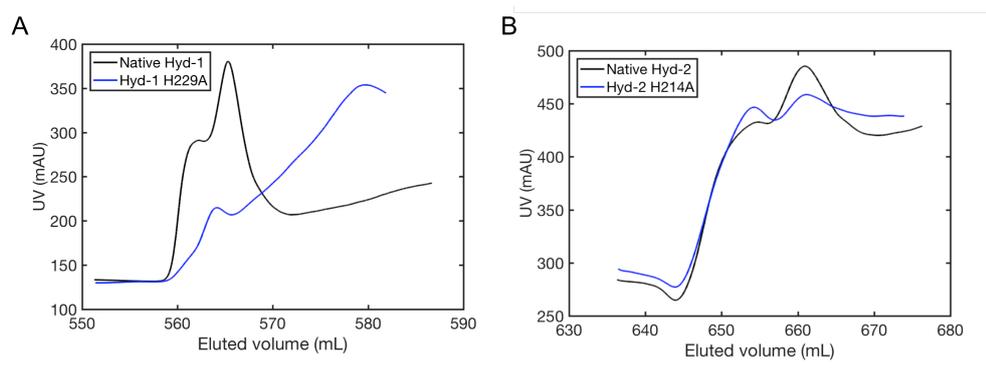
Figure 5.4 Akta Start UV traces for the elution of A: Hyd-1 Native and H229A variant and B: Hyd-2 Native and H214A variant from the nickel affinity column. A peak in the UV absorbance at fraction represents the elution of the hydrogenase, with the size of the peak representing the amount of protein eluted.

Native Hyd-1 was purified from strain LAF-003, as described in Chapter 4 using the method described in Chapter 8. The same method was used to purify Hyd-1 H229A, Native Hyd-2 and Hyd-2 H214A from strains LAF-015, LAF-016 and LAF-019. The yields are reported in in Table 5.1. The elution fractions of Native Hyd-1 were visibly brown, and thus in the interest of purity only a small amount was retained (2 x 3 mL fractions). In contrast, Native Hyd-2 and Hyd-2 H214A had less brown elution fractions and thus more elution fractions were retained (5 or 6 x 3 mL) in order to conserve as much active enzyme as possible. Hyd-1 H229A variant elution fractions were colourless, and thus the volume and concentration given in Table 5.1 are the result of concentration with a centrifugal filter after a large amount of elution fractions were retained.

Table 5.1 Protein yields from 18 L purification protocol

Hydrogenase	Concentration (mg/ml)	Volume (ml)	k_{cat} (s^{-1})
Native Hyd-1	0.091	6	300 ±111
Hyd-1 H229A	0.229	1.5	27 ±2
Native Hyd-2	0.270	25	
Hyd-2 H214A	0.150	18	

The difference in the amount of the Hyd-1 H229A variant produced relative to the native Hyd-1 is particularly substantial, as shown by the purification traces in Figure 5.4, where the peaks for Native Hyd-2 and Hyd-2 H214A are of similar height, but the peak at fraction 6 where the Hyd-1 H229A variant elutes is much smaller than the peak for the Native Hyd-1, despite using the same purification protocol. This was not noted for the purification of the *S. enterica* Hyd-5 H229A variant by Lisa Bowman[36], but this variant also contained an overexpression promoter at the start of the operon which might have masked this characteristic. It might be hypothesised that because histidine 229 spans the large-small subunit interface, the residue might play an important role in determining the stability of the heterodimer. Lack of stability could, in part, explain the drastic difference in turnover (k_{cat}) of the H229A variant relative to Native Hyd-1 determined by methylene blue assay, shown in Table 5.1. Any dissociated monomers would contribute to the determination of the concentration, but not the H_2 oxidation activity.
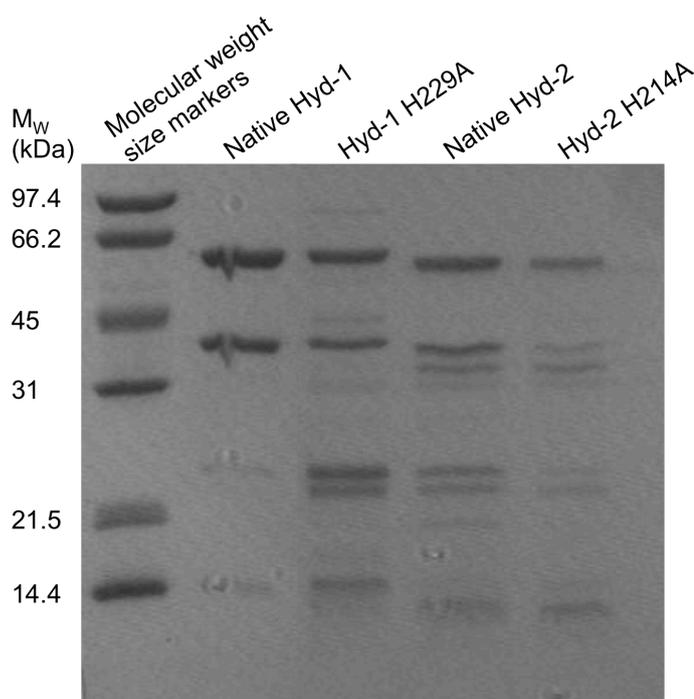
Figure 5.5 SDS PAGE gel loaded with concentrated Hyd-1 and Hyd-2 Native and variant hydrogenase. The strong band at 65 kDa corresponds to the large subunit whilst the strong band at 40 kDa corresponds to the small subunit.

As seen in Figure 5.5, all purified enzymes contained a band at ~65 kDa and a band at ~40 kDa, denoting the large and small subunits. As expected, the Native Hyd-1 is more pure than the variant or Hyd-2 hydrogenases, due to the care taken to only retain elution fractions containing pure hydrogenase. It is likely that the additional band below the small subunit for the Hyd-2 variants is due to a degradation product formed during the O_2-exposed dialysis or centrifugation steps. The band at ~25 kDa has been identified in other hydrogenase samples and has been characterised by Hope Adamson (PhD student, University of York) as cAMP Receptor Protein, which has been named as one of the most common "contaminant" proteins seen in Ni-affinity chromatography[231].

Figure 5.6 shows protein film electrochemistry of catalysis at 3% H_2 as the same film of hydrogenase is transferred between buffers at different pH values for Native and variant Hyd-1 and Hyd-2, where each scan shown is the last of four cycles. For both the Hyd-2 H214A variant, difficulty forming a stable film at high or low pH led to the commencement of experiments in pH 6. The Hyd-1 H229A variant was able to form a film on the electrode at pH 4.5, but at lower current densities than the Native Hyd-1. Native Hyd-1 shows lower current densities after prolonged immersion in pH 7.6 buffer, but it is capable of forming a stable film at pH 4.5, which fits the expression profile of Hyd-1 in *E. coli,* which largely expresses at low pH[123]. By contrast, Native Hyd-2 demonstrates almost no current loss at pH 7.6, which fits the expression profile in *E. coli* as expressing at high pH[123]. For both of the histidine to alanine substitutions, the current diminishes with transfer to a new buffer. The Hyd-1 H229A scan in pH 6 buffer is approximately 80% the current of the scan in at pH 6, and the Hyd-2 H214A scan in pH 7.6, is about a third lower in current than at pH 6. This substantial film loss of both variants relative to the native hydrogenases once again suggests a role for the histidine in protein stability. Histidine has previously been noted as an important residue for protein stability[232], particularly as it may form multiple hydrogen bonds and exist in two tautomeric states. The lack of ability to perform this role in the alanine substitution is thus likely a contributor to instability in

the variant enzymes, suggesting a primary reason that this residue has been conserved across all hydrogenases.
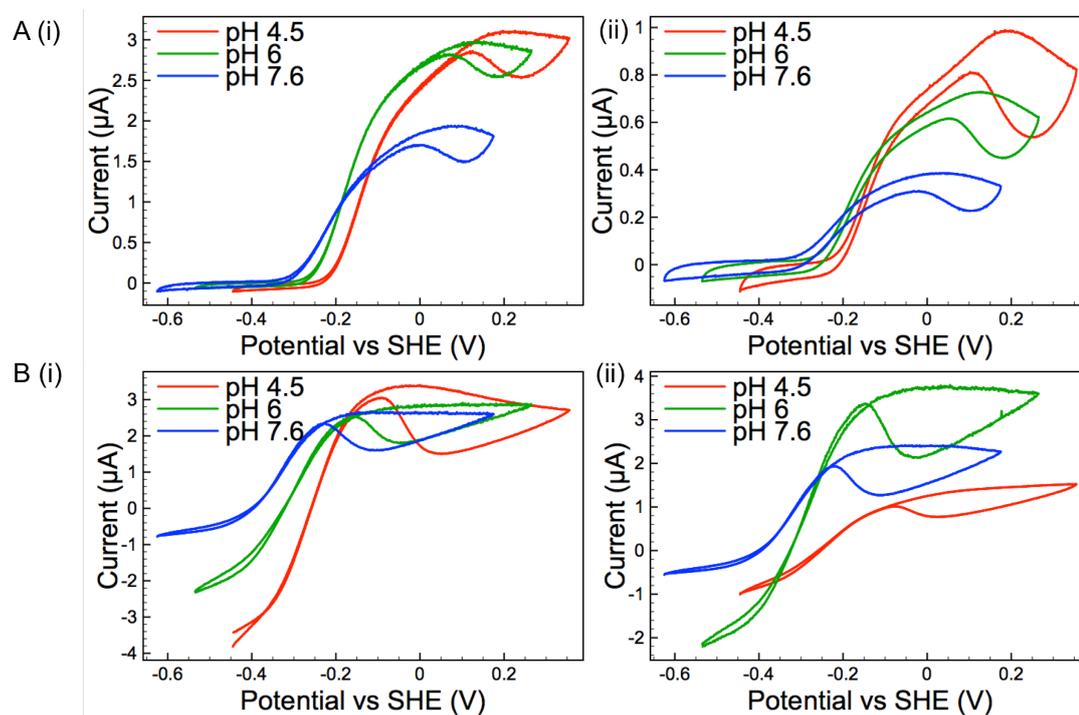
Figure 5.6 Film loss in Native and variant Hyd-1 and Hyd-2. Cyclic voltammetry experiments at 3% H_2 for A: Hyd-1 (i) Native and (ii) H229A variant and B: Hyd-2 (i) Native and (ii) H214A variant at pH 4.5 (red trace), pH 6 (green trace) and pH 7.6 (blue trace). The same film of enzyme was used for all three pH points. Voltammogram at highest maximum current shows first buffer used and voltammogram at lowest maximum current shows last buffer used. The potential was swept from -0.625 V vs SHE (pH 7.6), -0.535 V vs SHE (pH 6) or -0.445 V vs SHE (pH 4.5) and swept to +0.175 V vs SHE (pH 7.6), +0.265 V vs SHE (pH 6) or +0.355 V vs SHE (pH 4.5) at 5 mV s^{-1} before being swept back to the low potential. This scan was repeated four times and the fourth cycle is shown.

5.3.2 Effect of substitution of histidine 229 with alanine on Hyd-1 catalysis

Figure 5.7 shows an overlay of chronoamperometry experiments of native Hyd-1 and Hyd-1 H229A. In these experiments the potential is switched from reducing to oxidising and back again at 0% H_2, then to oxidising potential followed by reducing potential at 3% H_2. The traces were normalised to the current of maximum H_2 oxidation. Under conditions of 100% N_2 and low potential, the H_2 production current clearly overlaps for the variant and native enzyme. This suggests that the substitution of histidine with alanine does not cause a shift in catalytic bias as seen for the glutamate to glutamine substitution in Chapter 4[226].
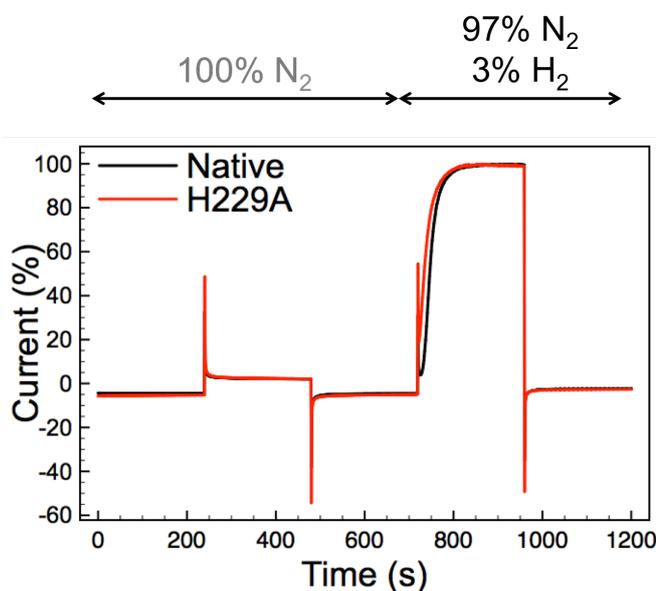
Figure 5.7 Chronoamperometric trace overlay of H_2 production in Hyd-1 Native (black) and H229A variant (red). The potential was switched between reducing (-0.4 V vs SHE) and oxidising (+0.175 V vs SHE) values at pH 4.5 and the gas in the cell was switched from 100% N_2 to 97% N_2 3% H_2. Current trace is normalised to the activity at +0.175 V vs SHE and 3% H_2. Current below 0 represents H_2 production.

Figure 5.8 A shows the H_2 oxidation activity of the Native and H229A variant Hyd-1 at 3% H_2, normalised to maximum activity. At lower potentials at 3% H_2, there is seemingly no difference between Native Hyd-1 and the Hyd-1 H229A variant. However, at high potentials, the native Hyd-1 shows only a small decline during the forward scan, meaning that the highest potential in these experiments has a current which is only 5% less than that at the maximum. On the other hand, the H229A variant current is 15% less at the highest potential scanned than at the maximum. During the scan back down to lower potentials the current of the variant declines by a further 25% for the H229A variant but only by a further 10% for the Native Hyd-1. This suggests that the H229A variant is inactivated by high potentials to a greater extent than the native Hyd-1. The complete reactivation during the scan back to low potentials suggests that the inactive state is Ni-B[8, 204]. This is consistent with what was seen in Chapter 2 using the *S. enterica* Hyd-5 H229A variant[36]. The degree of inactivation in the Hyd-1 H229A variant shows less pH senstivity than the Native Hyd-1. It is difficult to know the exact pK_a of this histidine, as buried histidines are known to have a variable pK_a[233] and the nearby presence of the metal-rich proximal cluster is likely to influence this property further. Nonetheless, it is likely that the ability of the histidine to access different tautomeric states is important to Ni-B formation and reduction.
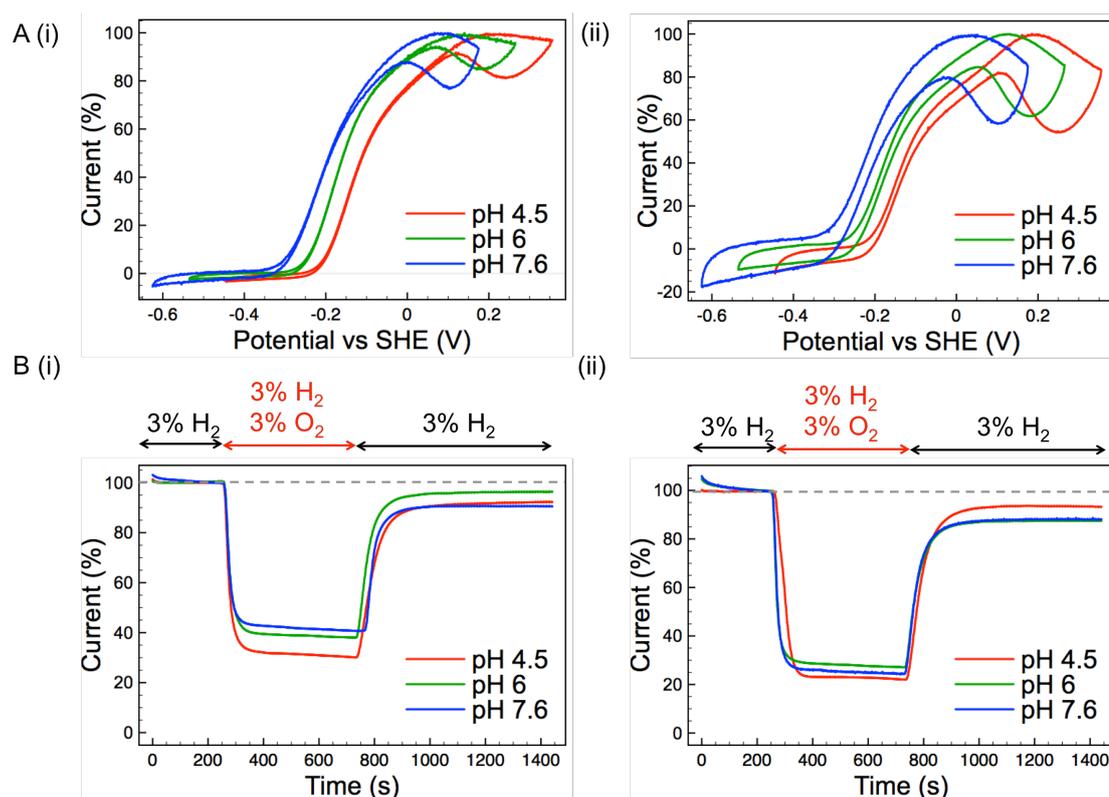
Figure 5.8 Catalytic activity of Hyd-1 (i) Native and (ii) H229A variant. A: H_2 oxidation catalysis at 3% H_2. The same film of enzyme was used for all three pH points and the traces are normalised to the maximum current of H_2 oxidation. The potential was swept from -0.625 V vs SHE (pH 7.6), -0.535 V vs SHE (pH 6) or -0.445 V vs SHE (pH 4.5) to +0.175 V vs SHE (pH 7.6), +0.265 V vs SHE (pH 6) or +0.355 V vs SHE (pH 4.5) at 5 mV s^{-1} before being swept back to the low potential. This scan was repeated four times and the fourth cycle is shown. B: Chronoamperometric traces showing the O_2 tolerance. The H_2 oxidation was monitored at 3% H_2 before, during and after O_2 exposure at a constant potential of +0.175 V vs SHE (pH 4.5), +0.085 V vs SHE (pH 6) or -0.05 V vs SHE (pH 7.6). Current traces were corrected for film loss and normalised to the H_2 oxidation current immediately before the addition of O_2.

Figure 5.8 B shows the chronoamperometric experiment designed to measure O_2 inhibition of H_2 oxidation. At pH 6, the Hyd-1 H229A variant shows less activity under O_2 and a lower extent of reactivation after removal of O_2 than the native Hyd-1. Again, this is consistent with what was seen in Chapter 2. At all pH values studied, the Hyd-1 H229A inactivated under O_2 to 20-30% of the original activity, lower than for the Native Hyd-1. The proportion of inactivation is

insensitive to pH for the variant whilst Native Hyd-1 shows greater inactivation in pH 4.5 than at pH 6 or 7.6. It is possible that the greater proton availability at pH 4.5 causes formation of the superoxidised cluster to be triggered more easily than at a higher pH value, via the proton-dependant mechanism proposed by Dance[210]. Trapping the proximal cluster in the superoxidised state is suggested by Radu et al[202] to protect the hydrogenase from O_2 damage. This would explain why the Hyd-1 H229A shows a less permanent inactivation at pH 4.5 than at pH 6 or 7.6. In the Native Hyd-1 there is greater reactivation after O_2 is removed from the system at pH 6 than at pH 7.6, which is not seen in the Hyd-1 H229A variant. It is likely that the pK_a of the histidine, and thus the pH of maximum proton donor ability, lies closer to pH 6 than pH 7.6. These results thus suggest that the ability of the histidine to participate in proton transfer plays a role in the O_2 tolerance, as was previously proposed by Dance[210].

5.3.3 Effect of histidine 214 substitution with alanine in Hyd-2
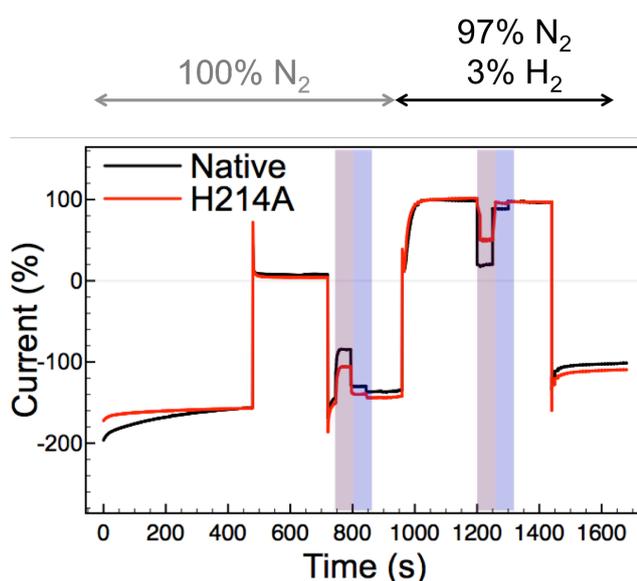
Figure 5.9 Chronoamperometric trace overlay of H_2 production in Hyd-2 Native (black) and H214A variant (red). The potential was switched between reducing (-0.4 V vs SHE) and oxidising (-0.045 V vs SHE) potentials at pH 4.5 and the gas in the cell was switched from 100% N_2 to 97% N_2 3% H_2. Transparent bars show where rotation was stepped to 0 rev per min (purple) and then to 1000 rev per min (blue). Current trace is normalised to the activity at -0.045 V vs SHE and 3% H_2. Current below 0 represents H_2 production.

Figure 5.9 shows the equivalent chronoamperometry experiment to that shown for Hyd-1 in Figure 5.7. As both Native Hyd-2 and the Hyd-2 H214A variant are bidirectional hydrogenases[8], there is a large negative current indicating substantial H_2 production at low potential under both 0 and 3% H_2. Both the Native and the variant maintain H_2 production when the rotation of the working electrode is ceased (red bar), indicating that Hyd-2 is less product inhibited than Hyd-1, something which has been described previously[8]. Although there is a small gap between the H_2 production level of Native Hyd-2 and that of Hyd-2 H214A, this is slight compared to the doubling in H_2 production relative to H_2 oxidation seen in the Hyd-1 E73Q variant. It is possible that the difference originates as a correction effect, as the actual H_2 oxidation current of Hyd-2 H214A was half that of the Native Hyd-2, due to the acid sensitivity of the variant. Overall, it is concluded that the catalytic bias of Hyd-2 has not been changed to any significant degree as a result of the histidine to alanine amino acid substitution.
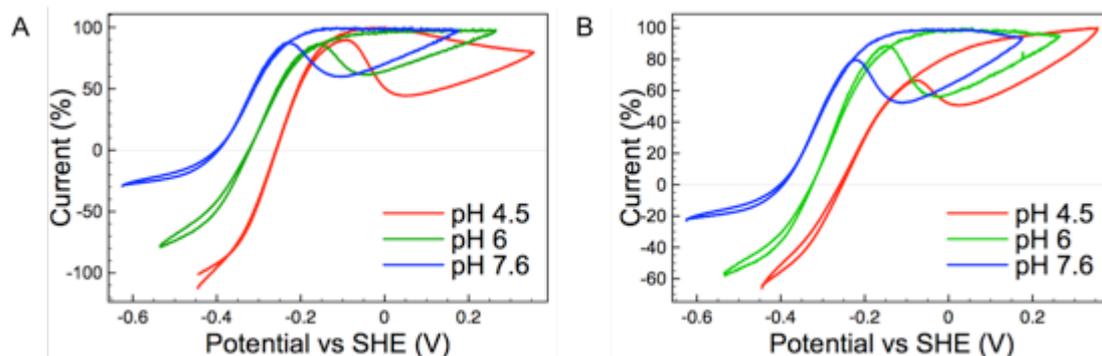
Figure 5.10 H_2 oxidation catalysis of Hyd-2 A: Native and B: H214A variant at 3% H_2. The same film of enzyme was used for all three pH points and the traces are normalised to the maximum current of H_2 oxidation. The potential was swept from -0.625 V vs SHE (pH 7.6), -0.535 V vs SHE (pH 6) or -0.445 V vs SHE (pH 4.5) to +0.175 V vs SHE (pH 7.6), +0.265 V vs SHE (pH 6) or +0.355 V vs SHE (pH 4.5) at 5 mV s^{-1} before being swept back to the low potential. This scan was repeated four times and the fourth cycle is shown.

Figure 5.10 shows catalytic activity of Native Hyd-2 and Hyd-2 H214A at 3% H_2. There is no clear difference in the catalytic waveshapes of Native Hyd-2 and Hyd-2 H214A at pH 6 or pH 7.6. The current of Native Hyd-2 shows a high potential decrease during the scan to high potentials at pH 4.5, whilst the Hyd-2 H214A variant shows an increase in the same region. However, this is most probably due to the pH instability of the variant causing lower film density than for the Native Hyd-2. Indeed, Figure 5.11 shows catalytic activity at different H_2 levels at much lower film densities at pH 4.5 for both the Native and variant Hyd-2, and similar shapes are observed. This suggests that histidine 214 plays no role in controlling the degree of Ni-B formation during O_2-free catalysis by Hyd-2. Interestingly, the catalytic waveshapes at pH 6 and 7.6 are almost identical for Native Hyd-2 in Figure 5.10, whilst for Native Hyd-1, in Figure 5.8, different shapes are observed. It is likely that Ni-B is formed too quickly in Hyd-2 for pH differences to become apparent and a slower scan rates would be needed to probe these differences.
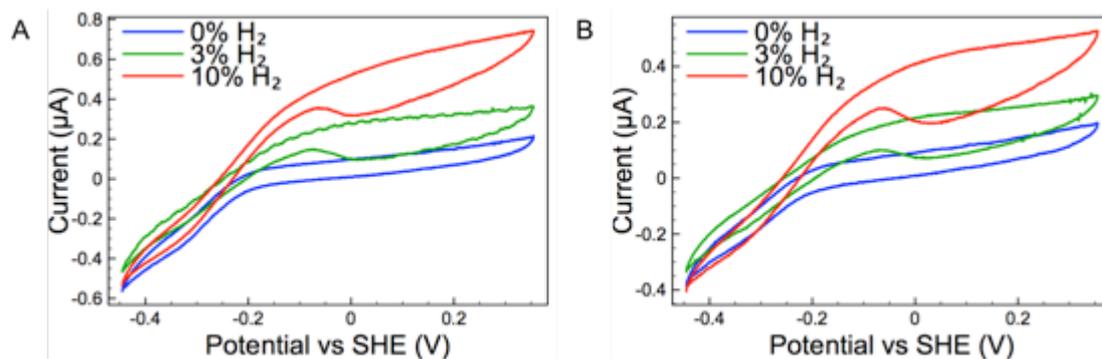
Figure 5.11 H_2 oxidation catalysis of Hyd-2 A: Native and B: H214A variant at pH 4.5. Blue: 0% H_2, green: 3% H_2 and red: 10% H_2. The potential was swept from -0.445 V vs SHE to +0.355 V vs SHE at 5 mV s^{-1} before being swept back to the low potential. This scan was repeated four times for each percentage of H_2 and the fourth cycle is shown.

Figure 5.12 shows the chronoamperometry experiment designed to monitor the extent of O_2 inhibition. As Hyd-2 forms Ni-B at lower potentials than Hyd-1[8], the potential at which this experiment was conducted was conducted was -0.135 V vs SHE, in order to determine that any inactivation was solely the result of O_2 exposure, and not simply high potential Ni-B formation. The activity of O_2

sensitive hydrogenases activity tends towards zero under O_2[8] and both the Native and H214A variant Hyd-2 exhibit this property. There is no significant difference in the extent of reactivation for Native Hyd-2 and Hyd-2 H214A, suggesting that the histidine does not act in a protective manner against formation of Ni-A under O_2 in Hyd-2.
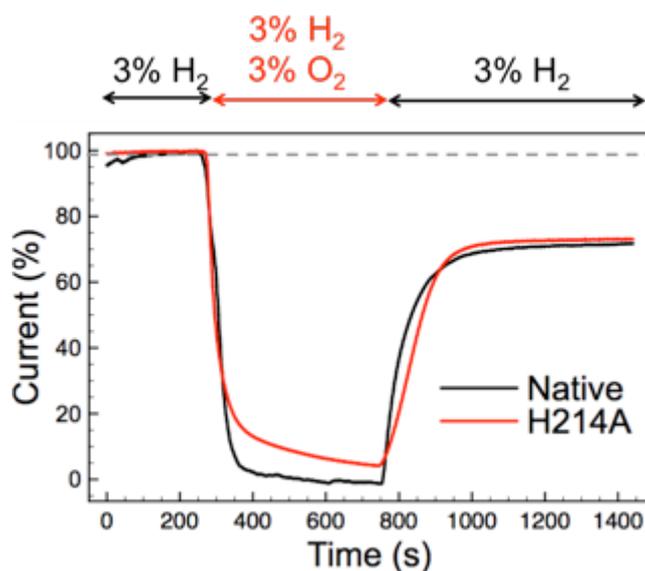
Figure 5.12 Chronoamperometric trace over lay of Hyd-2 Native (black) and H214A variant (red) showing the O_2 sensitivity. The H_2 oxidation was monitored at 3% H_2 before, during and after O_2 exposure at a constant potential of -0.135 V vs SHE. Current traces were corrected for film loss and normalised to the H_2 oxidation current immediately before the addition of O_2.

The fact that exchanging conserved histidine for alanine decreases O_2 tolerance in Hyd-1 but not in Hyd-2 suggests that the histidine plays an important role in the formation of the superoxidised state of the 4Fe3S proximal cluster, which is a unique feature of O_2 tolerant MBH[32]. These results therefore agree with previous *S. enterica* Hyd-5 work (Chapter 2) and support the Dance mechanism[210] outlined in the introduction to this chapter. The histidine also limits Ni-B formation in Hyd-1 under anaerobic conditions, but does not affect Ni-B formation in Hyd-2. This strongly suggests that the manner in which the histidine protects against inactivation at high potentials in the absence of O_2 is also via interaction with the superoxidised cluster.

5.3.4 Source of the difference between Native Hyd-1 and Hyd-1 H229A

In order to quantify the difference between Native Hyd-1 and Hyd-1 H229A, further investigations were conducted which go beyond the qualitative assessment described previously. Firstly, an investigation was conducted into the E_{switch} values at various pH points. The parameter E_{switch} defines the point of fastest reactivation during a scan to low potential after a period at which the potential is sustained at a high value in order to anaerobically inactivate the enzyme[204]. A study by Fourmond et al[196] concluded that this parameter is a feature of scan rate and reactivation rate k_A, where a 10-fold increase in k_A shifts the E_{switch} by +80 mV. Figure 5.13 shows the scan from high to low potential for Native and H229A Hyd-1 at pH 4.5, pH 6 and pH 7.6 after 5 hours at high potential. After this high potential inactivation step the current for Native Hyd-1 still remains at around 20% of its maximum. By contrast the high potential current for the H229A variant is only 5% of its maximum. This confirms that the period of time at high potential inactivates a higher proportion of the H229A enzyme than the Native Hyd-1.
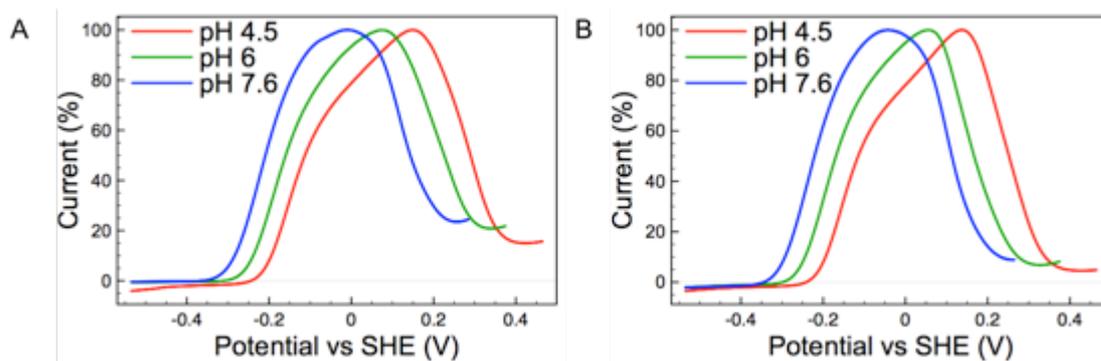
5.13 E_{switch} experiments on Hyd-1 A: Native Hyd-1 and B: H229A variant at pH 4.5 (red), pH 6 (green) and pH 7.6 (blue) at 3% H_2. The potential was held at +0.465 V vs SHE (pH 4.5), +0.375 V vs SHE (pH 6) or +0.285 V vs SHE (pH 7.6) for 5 hours before the potential was swept to -0.535 V vs SHE at 0.2 mV s^{-1}. Current is normalised to the maximum current.

Figure 5.14 shows the switch and onset potentials (Eswitch and Eonset respectively) calculated from the differentiation of the curves in Figure 5.13. This figure shows that whilst the potentials for the onset of H$_2$ oxidation of the Native and H229A variant Hyd-1 are the same at all three pH values, the E$_{switch}$ is only the same at pH 7.6. At pH 6 and 4.5 the H229A variant reactivates at potentials that are 50 mV lower than the values for Native Hyd-1. This would correspond to a decrease in the reactivation constant[196]. It was discussed earlier that the catalytic waveshape of the Native Hyd-1 is more pH sensitive than for Native Hyd-2. Dance proposed that proton transfer via histidine 229 could trigger opening of the superoxidised cluster during Ni-B formation[210] (Figure 5.1). The results shown in Figure 5.14 suggest that the pK_a of the histidine lies somewhere between 4.5 and 6, and this could be the source of pH sensitivity of the Hyd-1 catalytic waveshape.
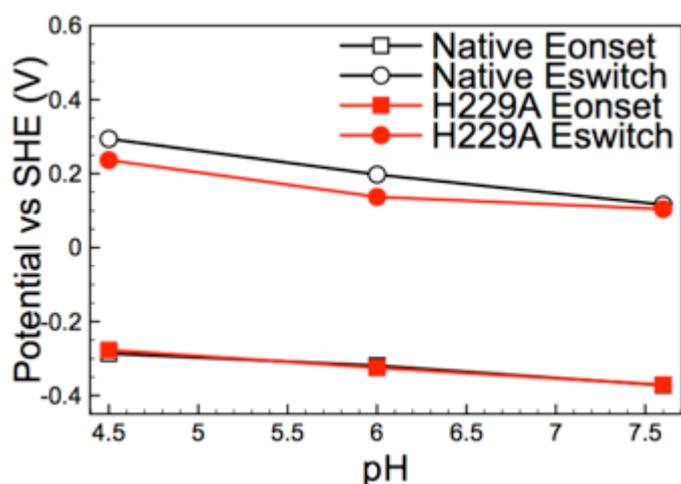
Figure 5.14 Plot of onset potential (Eonset, square) and E$_{switch}$ (Eswitch, circle) against pH for Hyd-1 Native (open black) and H229A variant (filled red). Values calculated from differentiation of the curves in Figure 5.13. Onset potential is the potential at which H$_2$ onset commences and switch potential is the potential at which the reactivation rate is the greatest.

$$\frac{dA(t)}{dt} = -k_I(E)A(t) + k_A(E)(1 - A(t))$$ (Equation 5.4)

The extent of inactivation seen in cyclic voltammetry is a function of the rate of activation (k_A) and the rate of inactivation (k_I) as given by equation 5.4, where A is the proportion of active to inactive enzyme at time t and $dA(t)/dt$ is the rate of change in the proportion of active to inactive enzyme[198]. A potential step experiment was employed as first described by Fourmond et al[196] in order to extract the k_I and k_A constants for Native Hyd-1 and the Hyd-1 H229A variant at pH 6 and 10% H_2, described in Sections 5.2.2 and 5.2.3. The potential steps and resulting current traces of Native Hyd-1 and Hyd-1 H229A are shown in Figure 5.15. The method involves steps to low potential where the enzyme is presumed 100% active[196] and then to high potential where the slope of the current decrease due to inactivation is monitored. Even by eye it may be seen that the H229A variant inactivates more at high potential than the Native Hyd-1, which is to be expected from previous cyclic voltammetry experiments.
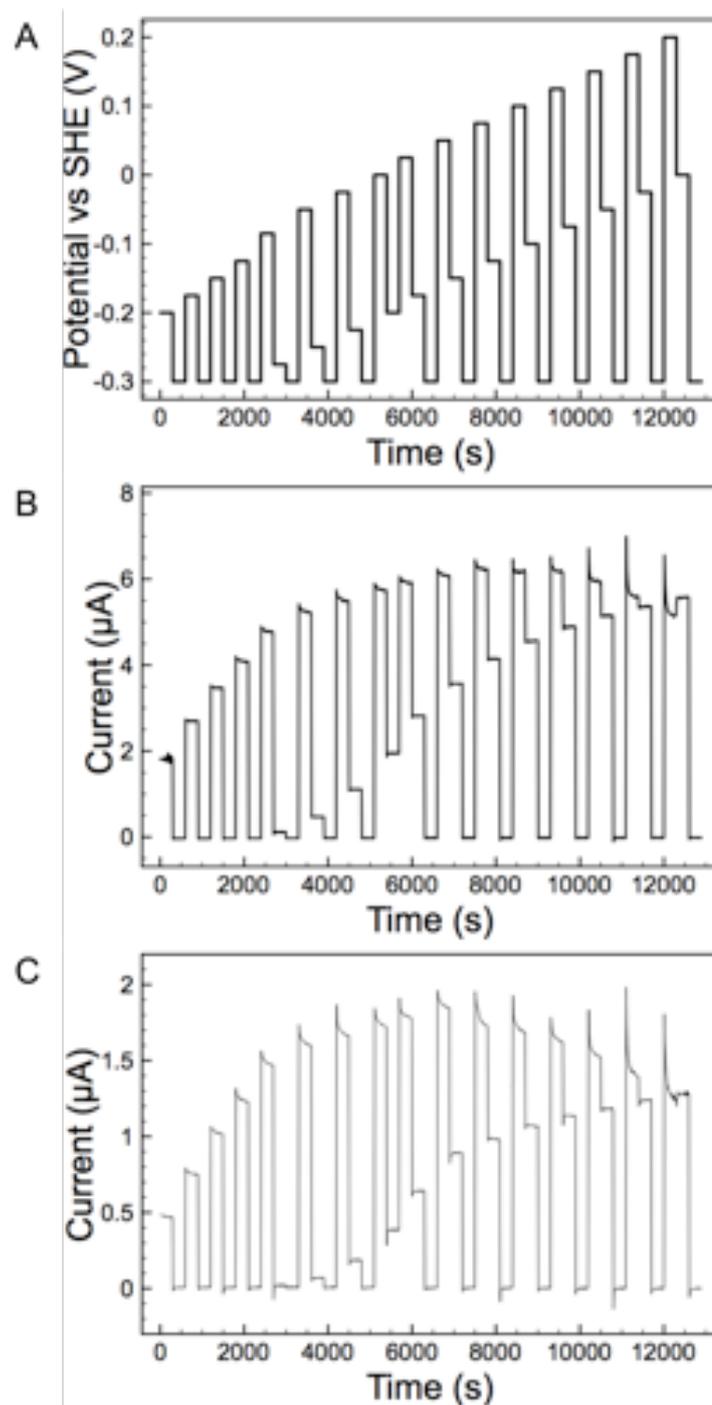
Figure 5.15 Potential step experiment to measure activation and inactivation rates at pH 6. A: The potential steps which occurred at each timepoint. B: Resulting chronoamperometric trace for Native Hyd-1. C: Resulting chronoamperometric trace for Hyd-1 H229A variant. The experiments were conducted at 10% H_2.

Each step up to high potential was then fit to Equation 5.1[196] using the MATLAB software. The constants found from the fit were used to solve Equations 5.2 and 5.3[196] in order to derive the k_I and k_A constants. The value of k_I is shown in Figure 5.16 as an average of three repeats. There is no consistent difference between the k_I of the Native and H229A variant of Hyd-1 that may explain the difference in high potential Ni-B formation. However, the value of k_I is very small and it is likely charging current on the electrode will dominate. Figure 5.15 B shows that even on a blank electrode potential steps cause jumps in the current. This is due to rearrangement of the double layer of charge, which acts as a capacitor in the electrochemical cell. This capacitor must be charged before a desired potential is reached at the working electrode, causing a capacitive current[234-235]. It is likely that capacitive current is dominating at low potentials, where a lower k_I is seen.
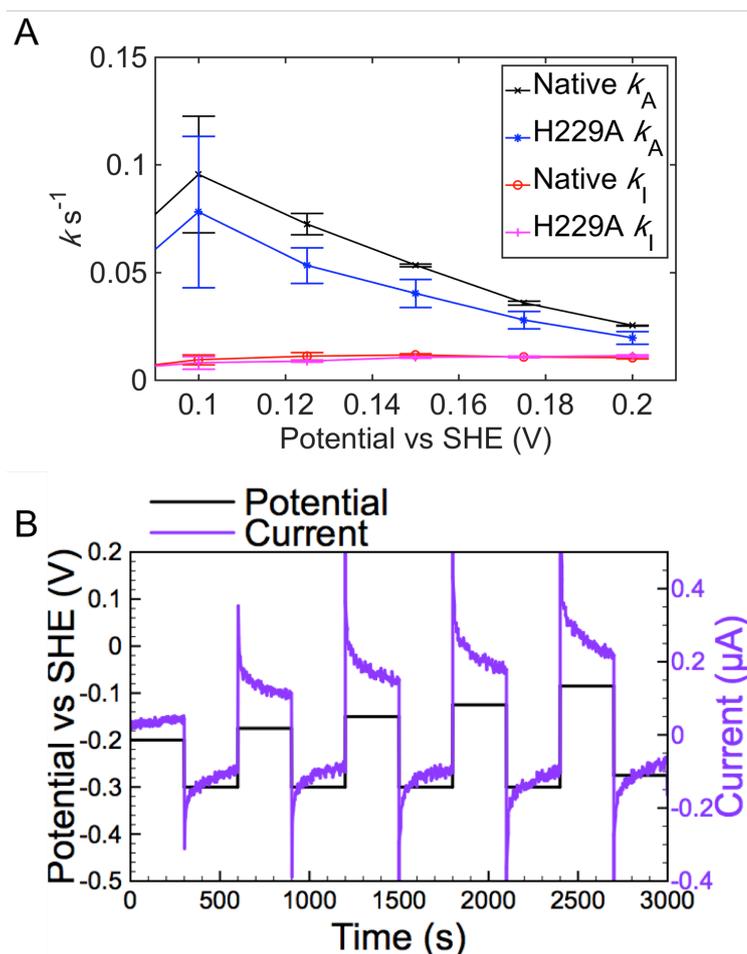
Figure 5.16 A: Calculated k_I and k_A values. k_I values of Hyd-1 red: Native and pink: H229A variant and k_A values of Hyd-1 black: Native and blue: H229A variant. Points show an average of three repeats and error bars show standard error. B: Effect of potential switching on a blank electrode under the same conditions as the experiments in Figure 5.15. Black trace shows the steps in electrode potential. Purple trace shows resulting current on a blank electrode.

Figure 5.16 A shows the plot of the k_A against potential in the region where Hyd-1 reactivates. Across these potentials the value of k_A for the H229A variant is consistently lower than that of the Native Hyd-1. This correlates with the E_{switch} values shown in Figure 5.14. The k_A difference suggests the H229A variant is slower to reactivate from Ni-B than Native Hyd-1[196]. This would agree with the finding of Hamdan et al[198] that increased k_A increases O_2 tolerance. However, they contradict the finding by Radu et al[202] that O_2 tolerance associated with

slow reactivation after O_2 exposure. A possible explanation for this may lie in the fact that the work by Radu et al was conducted on the heterotrimeric complex in an artificial membrane using ubiquinone mediated electron transfer[202], whilst the work by Hamdan et al[198] and the work here was conducted on the isolated large-small heterodimer using direct electron transfer. The heterotrimeric complex is known to protect against O_2[199], but it also causes a delay between the injection of H_2 and the onset of H_2 oxidation. When H_2 was injected into the 4Fe4S proximal cluster variant of *R. eutropha* MBH after O_2 exposure this variant showed rapid reactivation relative to the slow reactivation of the Native MBH[202]. However, the K_M of this variant was not quoted. It is possible that the faster reactivation of the variant was thus not a function of reduction of the superoxidised cluster but rather increased H_2 access, perhaps due to destabilisation of a multimeric form of the complex.

Table 5.2 Expected oxidation state of the proximal and medial iron-sulfur clusters at differing potentials for O_2 tolerant[227] and O_2 sensitive[236] hydrogenase.

Potential (mV)	O_2 tolerant	O_2 sensitive
-400	$[4Fe3S]^{3+} [3Fe4S]^0$	$[4Fe4S]^{1+} [3Fe4S]^0$
-300	$[4Fe3S]^{3+} [3Fe4S]^0$	$[4Fe4S]^{2+} [3Fe4S]^0$
0	$[4Fe3S]^{3+} [3Fe4S]^0$	$[4Fe4S]^{2+} [3Fe4S]^0$
100	$[4Fe3S]^{4+} [3Fe4S]^0$	$[4Fe4S]^{2+} [3Fe4S]^{1+}$
200	$[4Fe3S]^{4+} [3Fe4S]^{1+}$	$[4Fe4S]^{2+} [3Fe4S]^{1+}$
300	$[4Fe3S]^{5+} [3Fe4S]^{1+}$	$[4Fe4S]^{2+} [3Fe4S]^{1+}$

The proximal and medial clusters have different midpoint potentials in O_2 tolerant and O_2 sensitive hydrogenase. The expected states of these clusters at different potentials are shown in Table 5.2. The transition of the O_2 tolerant proximal cluster to superoxidised state would be predicted to occur at high potentials and during reaction with O_2[227]. If this high potential transition was impeded, for example by the amino acid substitution discussed here, then there would be less electrons available for the reduction of Ni-B, which could cause the lower reactivation rate observed. Because the proximal cluster of O_2 sensitive hydrogenase is fully oxidised above -300 mV vs SHE[236], the reactivation rate of these hydrogenases is already lower and this could by why the anaerobic

inactivation and O_2 tolerance of Hyd-2 are unaffected in the H214A variant. This hypothesis could be confirmed by EPR titrations of the Hyd-1 H229A variant, although it might be important to ensure that this was performed at a pH where histidine participates in proton transfer.

5.4 Conclusions

In conclusion, the role of the histidine in both O_2 tolerant and O_2 sensitive hydrogenases is likely to be maintaining stability of the large-small heterodimer with regards to pH. In the O_2 tolerant hydrogenase, this residue also contributes to O_2 tolerance and high potential anaerobic inactivation. It is hypothesised that proton movement involving the histidine, as suggested by Dance[210], is involved in this activity.

The work in this chapter is strong evidence that the superoxidised form of the proximal cluster is not only has a role in tolerance to O_2, but is also involved in high potential anaerobic inactivation. This comparison has largely been neglected when characterising O_2 tolerant hydrogenases. However, this relationship provides a marker that could enable new hydrogenases to be classified as O_2 tolerant or O_2 sensitive through the use of simple voltammetry experiments under anaerobic conditions. Furthermore, there is interest from a biotechnological perspective. There are many hydrogenase variants in which a change in the O_2 tolerance is a side effect of a change to the H_2 oxidation catalysis[67, 191]. The work here suggests that altered inactivation at higher potentials could be another consequence which might limit applications.

Chapter 6

The role of membrane bound NiFe hydrogenase Hyd-1 in the growth and competitive ability of *E. coli*

6.1 Introduction

The ability to adapt to a different environmental condition is often an evolutionary advantage to a species in a diverse ecosystem[237]. In the ecosystem of the mammalian gut, the export of molecular hydrogen as a waste product by commensal bacteria is exploited by pathogen *S. enterica* during colonisation[99]. This pathogen utilises its 3 periplasmically orientated membrane bound NiFe hydrogenases (MBH) in order to utilise H_2 which may reach levels of 40 μM in the gut lumen[98]. As discussed in Chapter 1, the related bacterium *E. coli*, which is also responsible for a great burden of disease[112-114], expresses two MBH with high identity to those of *S. enterica*[115].

The role of these MBH, Hyd-1 and Hyd-2, in *E. coli* has been generally established as H_2 oxidation[8, 238]. This has been contested by Trchounian et al, who have stated that at high pH the Hyd-1 and Hyd-2 act as H_2 producers whilst the cytoplasmically orientated Hyd-3 is a H_2 oxidizer[239]. However, these findings have been largely ignored firstly because isolated Hyd-1 enzyme only shows H_2 production at low pH[240] and secondly because there was no investigation of regulatory effects which may have offered an alternative explanation for the observed changes in H_2 production. Nonetheless, there are still questions about the role of the MBH in *E. coli*. Hyd-2 is suggested to function as the main *E. coli* H_2 uptake enzyme[241], which echoes findings that it is Hyd-2 in *S. enterica* that permits H_2 dependent growth of this organism[242]. However, the role of Hyd-1 has not been well established in either of these organisms, in particular the reason that this enzyme is induced by anaerobiosis and yet is O_2 tolerant, although there is a suspected role in micro-aerobic conditions[243]. Due to the acidity profile, it has been suggested that Hyd-1 is responsible for H_2 uptake at

low pH[123], and sensitivity to acid was increased in a *S. enterica* Hyd-1 knockout[119]. Hyd-1, has also been indicated to have a role during fermentative growth[241]. More recently, a study by Pinske et al[132] found that carbon starvation lead to an increase in levels of Hyd-1, and that addition of a utilizable carbon source led to a return to lower levels of the protein, indicating that a function of Hyd-1 is to allow H_2 consumption as an energy source when other fuels are scarce. Nonetheless, the exact nature of the Hyd-1 function in *E. coli* has proved elusive and will be a subject of investigation in this chapter.

The experiments in this chapter have taken advantage of the cytoplasmic NiFe hydrogenase Hyd-3, which is a major part of the formate hydrogen lyase complex, and acts as a H_2 producer[12-13]. This hydrogenase is an important part of the formate cycle, but is also responsible for the majority of H_2 produced by *E. coli*, much of which is then recycled by the H_2 uptake hydrogenases[8].

6.2 Methods

6.2.1 Investigation of the growth rate of single site variants of *E. coli* Hyd-1

Growth curves were performed by University of York summer project student Hamid-Reza Danesh-Azari. 20 mL autoclaved glass bottles fitted with a cap containing a rubber stopper were filled with either 20 mL sterile LB medium or 20 mL M9 minimal medium[244] (47 mM sodium phosphate, 22 mM monopotassium phosphate, 19 mM ammonium chloride, 9 mM sodium chloride) supplemented with filter sterilised 2% w/v glucose, 0.1 mM calcium chloride, 2 mM magnesium chloride, and 0.1% v/v 1000x metals solution[245] (50 mM iron (III) chloride, 20 mM calcium chloride, 10 mM magnesium chloride, 10 mM zinc sulphate, 2 mM cobalt (II) chloride, 2 mM copper (II) chloride and 2mM nickel (II) chloride). Bottles were purged with filter sterilised nitrogen gas (BOC) using a needle, before inoculation with starter cultures of the strains diluted to the same optical density. The bottles were placed at 37 °C. Each hour, a 1 mL sample was taken with a needle and syringe and placed in a 1 mL cuvette in a Jenway 6305 UV/Vis spectrometer and the optical density at 600 nm was measured with reference to sterile media.

6.2.2 Batch culture experiments

A sterile ~1.2 L glass vessel with metal lid containing ports was filled with 1 L of M9 medium supplemented with filter sterilised 10 μM calcium chloride, 1 mM magnesium chloride, 0.1% v/v 1000x metals and either 40 mM fumarate and 0.2% v/v glycerol or 0.1% w/v glucose. A colony of the strain to be grown was picked from a fresh plate with a pipette tip and dropped in to 10 mL of the M9 medium plus supplement in a sterile 30 mL Sterilin™ pot. Two of these starter cultures for each strain were shaken for approximately 24 hours at 37 °C. The starter cultures were combined and centrifuged at 4000 rpm for 15 minutes and the pellet was resuspended in 11 mL of the fresh medium. 1 mL was transferred to a 1.5 mL cuvette and the optical density was measures on a Jenway 6305 UV/Vis spectrometer. The solution was diluted to an optical density of 0.25 with

fresh medium and 10 mL was added to the vessel with a sterile syringe and needle through a rubber septum in a port of the top plate. A temperature probe maintained the temperature at 37 °C and a stirrer stirred the vessel continuously at ~100 rev per minute. The pH was monitored with a pH probe (Fermprobe, F-615, Broadly-James) and O_2 was monitored with an oxygen probe (Oxyprobe® II, D540, Broadly-James) connected to a potentiostat (built in house by the Biology Electronics Workshop, University of York) that held the potential of the probe at -0.6 V vs SHE and transmitted the recorded reading to a voltmeter. The pH showed no drift across the experiments and the O_2 reading was calibrated using readings in air, 100% argon, and 100% O_2. Samples were taken using a sterile 120 mm needle and 1 mL syringe according to the markers indicated in Figure 6.2. The sample was transferred to a 1.5 mL cuvette and the optical density was monitored with a Jenway 6305 UV/Vis spectrometer.

6.2.3 Competition experiments

The batch culture vessel was prepared with supplemented M9 media as described in Chapter 8. Two starter cultures for each of the strains LAF-001 and LAF-012 were prepared as above and grown for 24 hours at 37 °C. the cultures for each strain were combined, centrifuged and the pellets resuspended in 10 mL fresh medium. 1 mL of each was taken and the optical density was recorded as above. Equal proportions of each strain were taken so that the 10 mL solution at an optical density of 0.25 contained the equivalent of an optical density of 0.125 of each LAF-001 and LAF-012. This 10 ml culture was added to the vessel as above. The optical density was monitored by taking samples with a needle and syringe every hour for twelve hours and again at 24 hours. For experiments with the addition of hydrogen peroxide, 1.5 mL of either 3% or 6% peroxide solution was added directly after the 8 hour timepoint was removed. At the timepoints indicated by the markers in Figure 6.3 C, a further 1 mL sample was removed and this was used to create serial dilutions in fresh media. The dilution was streaked on plates of LB agar and LB agar plus 50 μg/mL kanamycin, and these were placed at 37 °C until visible colonies formed. The proportion of Hyd-1

knockout was calculated by dividing the number of colonies on the kanamycin plate (which grew only LAF-012) by the number of colonies on the plate without antibiotics (which grew both strains).

6.2.4 Chemostat experiment

Batch culture competition experiments were prepared and run as in Section 6.2.3, except that tubes capped with aluminium foil were autoclaved alongside the vessel. After 10 hours under flame sterile conditions the foil cap was removed from the inlet tube and the tube was placed in a 1.5 L conical flask filled with sterile media and sealed with foil. A peristaltic pump added the media to the vessel at a rate of 120 mL per hour. Excess culture was removed by placing an outlet tube connected to a fast running peristaltic pump just above the level of the surface of the culture. Every time the culture rose to the level of the tube, media would be removed through the outlet until the volume was lowered once more. Every 12 hours, fresh media was added to the inlet flask and the outlet flask was emptied. The optical density was monitored at the timepoints indicated in Figure 6.4 A. At the timepoints indicated in Figure 6.4 C, an additional 1 mL sample was taken and three separate serial dilutions were made. The remainder of the initial sample was frozen at -80 °C. Each serial dilution was streaked on an LB agar plate with 50 μg/mL streptomycin and an LB agar plate with 50 μg/mL kanamycin. The proportion of Hyd-1 was calculated by dividing the number of colonies on the kanamycin plate (where only LAF-012 grows) by the number of colonies on the streptomycin plate (where only LAF-001 grows) and dividing this number by 2. From the 48 hour timepoint, 1.5 mL 6% hydrogen peroxide was added every two hours, and the reading of the oxygen probe was monitored every 5 minutes.

6.2.5 Quantitative reverse-transcription PCR (RT-qPCR)

The samples taken from the chemostat experiment above were thawed on ice and the RNA was extracted using the GeneJet® RNA purification kit (ThermoFisher Scientific) according to the instructions in the manual. cDNA was

synthesised from the extracted RNA using the Maxima First Strand cDNA Synthesis Kit for RT-qPCR with dsDNAse (ThermoFisher Scientific). 2 μL of the reaction product was used directly in each 20 μL reaction with TaqMan® Fast Advanced Master Mix (ABI Applied Biosystems). Primers and TaqMan® probes for small subunit genes of Hyd-1 and Hyd-2, *hyaA* and *hybO* and for endogenous controls *rssA, cysG, hcaT,* and *idnT* are given in Table 6.1. The primers were designed using the OligoArchitecht™ Online Design Tool (Sigma-Aldrich) and ordered from Sigma-Aldrich in a salt free grade. Thermal cycling of the 96-well plate containing TaqMan® reactions was performed using the StepOnePlus™ system and analysis was performed with the StepOnePlus™ software.

Table 6.1 Primers and probes for RT-qPCR

Gene	Primer/Probe	5' Modification	3' Modification	Name	Sequence (5' to 3')
hyaA	Sense primer	None	None	hyaA_qPCR_sense	GTCGATATTCCGCAAATG
	Antisense primer	None	None	hyaA_qPCR_antisense	GTAGGTTGCTGGTTATGA
	TaqMan probe	JOE	BHQ1	hyaA_probe	TACTCATTCCACCGCCGATACC
hybO	Sense primer	None	None	hybO_qPCR_sense	CCAGAAACTTACGGCAAC
	Antisense primer	None	None	hybO_qPCR_antisense	GATGGATGCCTTTATGGAA
	TaqMan probe	JOE	BHQ1	hybO_probe	ATACCTTCTTCGTTACAGCCATAGCA
rssA	Sense primer	None	None	rssA_qPCR_sense	TAGGCAGCATAACGACAC
	Antisense primer	None	None	rssA_qPCR_antisense	GGCAAACAGGTTGAATCA
	TaqMan probe	JOE	BHQ1	rssA_probe	CAACGGCAACAGAGATTATGACCAC
cysG	Sense primer	None	None	cysG_qPCR_sense	ACGCTGGTGTTCTATATG
	Antisense primer	None	None	cysG_qPCR_antisense	TACCGTTTTCGACAATTG
	TaqMan probe	JOE	BHQ1	cysG_probe	TGGCATTCCGTGTTCAATCAGC
hcaT	Sense primer	None	None	hcaT_qPCR_sense	TGCTGACACTTCTCTTTG
	Antisense primer	None	None	hcaT_qPCR_antisense	GTACCAGTGGTGAGAAAA
	TaqMan probe	JOE	BHQ1	hcaT_probe	CCAATCATCACCAGCATCAGCC
idnT	Sense primer	None	None	idnT_qPCR_sense	CAAGCTGATTTCTGATACG
	Antisense primer	None	None	idnT_qPCR_antisense	GATGCTACGATGGTAAATAC
	TaqMan probe	JOE	BHQ1	idnT_probe	TCGCCACTACGCTGATTGCTA

6.3 Results and discussion

6.3.1 Effect of single site Hyd-1 mutants on growth of *E. coli*

Hydrogenases are energetically expensive enzymes, as they require many steps of maturation to form the intact final structure[140, 246]. Therefore it is possible that any loss that would be generated by the deletion of the enzymes is recuperated by the saving in "production costs". The enzymatic properties of the E73Q and H229A Hyd-1 variants discussed in the previous chapters are different from the Native Hyd-1. In particular, E73Q shows enhanced bidirectionality, and H229A shows reduced O_2 tolerance and lower catalytic activity at high potentials. The question of whether these differences in enzymatic function when added to the energetic expense of their expression and maturation was tested using strains LAF-005 and LAF-015, which differ from the W3110 *rpsL150* strain LAF-001 only in the codon corresponding to their respective amino acid substitution (ie. the stage before the addition of the histidine tag). The growth of the strains was monitored by undergraduate summer project student Hamid-Reza Danesh-Azari in tubes filled with media and purged with nitrogen before the start of the experiment and these are shown in Figure 6.1. No significant difference was observed between the growth rate of any of the strains in either rich LB media (Figure 6.1 A) or minimal M9 media (Figure 6.1 B) supplemented with glucose.
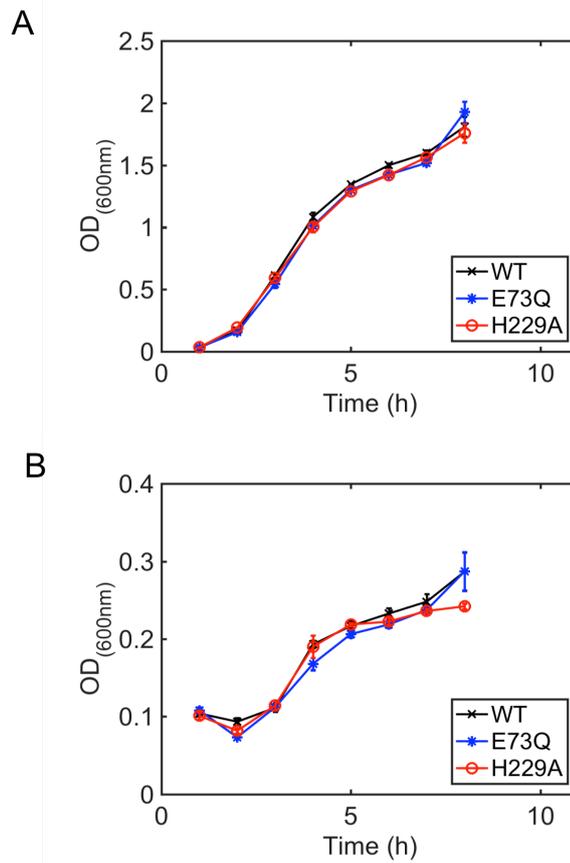
Figure 6.1 Growth curves for *E. coli* strains expressing Hyd-1 single site variants. Growth of Hyd-1 large subunit E73Q and H229A single site mutant strains LAF-005 and LAF-015 compared to the parent strain LAF-001 in A: LB and B: M9 glucose media in sealed tubes purged with N_2. Error bars show the standard deviation divided by the square root of the number of repeats.

It is possible that the changes caused by the single site mutation do not have a large enough effect to be detrimental. However, in the creation of the single site E73A mutant, an intermediate (LAF-012) is formed which contains the *rpsL-neo* cassette[215] interrupting the *hyaB* gene in a position between nucleotides which code for different residues of the active site. This strain should not be able to form mature Hyd-1 (as seen for strain LAF-016 in Chapter 3) and thus is considered a Hyd-1 knockout strain. In addition, the antibiotic resistance profile of the strain is distinct from parent strain LAF-001, allowing its use in competition experiments. LAF-012 was thus used to investigate the effect of a Hyd-1 knockout on the growth rate and competitive ability of *E. coli*.

6.3.2 Role of Hyd-1 on *E. coli* growth in batch culture

In order to minimise experimental drift due to sampling, a 1 L vessel was used for the following sections of the chapter, where removal of a 1 mL sample corresponds to only 1/1000 of the culture, and is less likely to impact the overall growth conditions. The setup also contains a probe to control the temperature and a probe to monitor the level of O_2. The system was stirred at ~100 rev per minute to prevent the bacteria settling out of the culture. Samples were taken with a 12 cm needle through a septum in the lid of the vessel.

The ability to take a greater number of samples allows the possibility of monitoring the strains in minimal media from a very low optical density (OD) until the stationary phase is reached in order to examine for any differences between the wild type and Hyd-1 knockout strain. As growth of *E. coli* in minimal media is slow, different biological replicates starting from the same optical density were used to examine a variety of sampling times for growth in M9 media with glucose (0.1%), which is hypothesised to induce expression of Hyd-1, and with glycerol and fumarate (0.2% and 40 mM respectively), which is hypothesised to induce expression of Hyd-2[247]. These are shown as the scatter plots in Figure 6.2 A and B. The preference of the strains for glucose media is immediately obvious, as the growth of both strains in these experiments plateaus after 10 hours of growth, compared to 23-24 hours in glycerol and fumarate media. In the glucose media, the O_2 is largely depleted within 6 hours. In the glycerol and fumarate media, the O_2 is comparably depleted in 7-8 hours of growth. This slightly slower depletion is likely due to the slower growth rate in glycerol and fumarate relative to glucose media (0.41 h^{-1} in glycerol and fumarate versus 0.63 h^{-1} in glucose). After O_2 is depleted, the growth rate in both medias decreases, but more substantially for glycerol and fumarate (0.16 h^{-1}) than in glucose media (0.41 h^{-1}). The switch to anaerobic respiration is why the lag between the growths of glucose and glycerol and fumarate media grows greater over time.

The final OD in glucose media is lower than the final OD in glycerol and fumarate media. This is because 0.1% w/v glucose is 5.5 mM, below the optimum 11 mM required for optimum growth of *E. coli*[248]. This system is thus nutrient limited for carbon. This is a preferred condition for the investigation of Hyd-1, because it is expected that the use of H_2 as an energy source would be more important in conditions of low carbon[249].
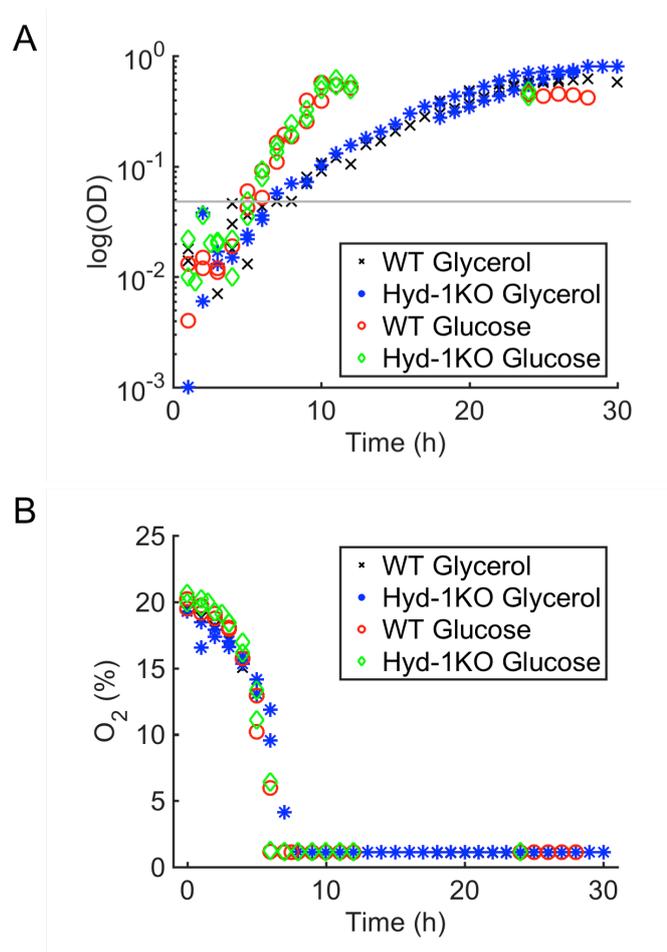
Figure 6.2 Optimisation of batch culture conditions and sampling times. A: Logarithmic scatter plot of the change in optical density of wild type parent strain LAF-001 and Hyd-1 knockout strain LAF-012 in M9 media with glycerol and fumarate (black cross and blue asterisk) and M9 media with glucose (red circle and green diamond). Grey line shows the optical density below which the spectrometer measurements are not reliable. B: Scatter plot of the change in O_2 with time for the experiments shown in Figure 6.2 A. At least two biological replicates measured at a variety of time-points are shown for each experiment.

There is no clear difference in the optical density or O_2 utilisation between the wild type and Hyd-1 knockout strains in either media. This suggests that knocking out the Hyd-1 protein does not change the growth rate of *E. coli* under these conditions. It is possible that the expression of Hyd-1 instead acts as a competitive advantage over other organisms in the gut. As mentioned earlier, whilst there are many theories on the role of Hyd-1 in *E. coli*[8, 123, 249-250], none have fully explained why the enzyme is O_2 tolerant but is induced by anaerobiosis. It may be hypothesised that the O_2 tolerance of Hyd-1 is not due to any role in growth under O_2, but resistance to a sudden oxidative shock when the bacteria are under anaerobic conditions.

6.3.3 Effect of Hyd-1 on competitive ability in batch culture with oxidative shock

In order to test these hypotheses equal amounts of the wild type and Hyd-1 knockout strain were grown in co-culture and the proportion of the Hyd-1 knockout present in the culture was monitored for changes over time due to a competitive disadvantage. Furthermore, different concentrations of hydrogen peroxide were added to the system immediately after the 8 hour sample was taken. This is two hours after O_2 depletion, in order to ensure that anaerobiosis has induced Hyd-1 expression. The two concentrations of hydrogen peroxide chosen have been documented to be detrimental to *E. coli* survival due to DNA damage[251] but can be added without any large change in culture volume.
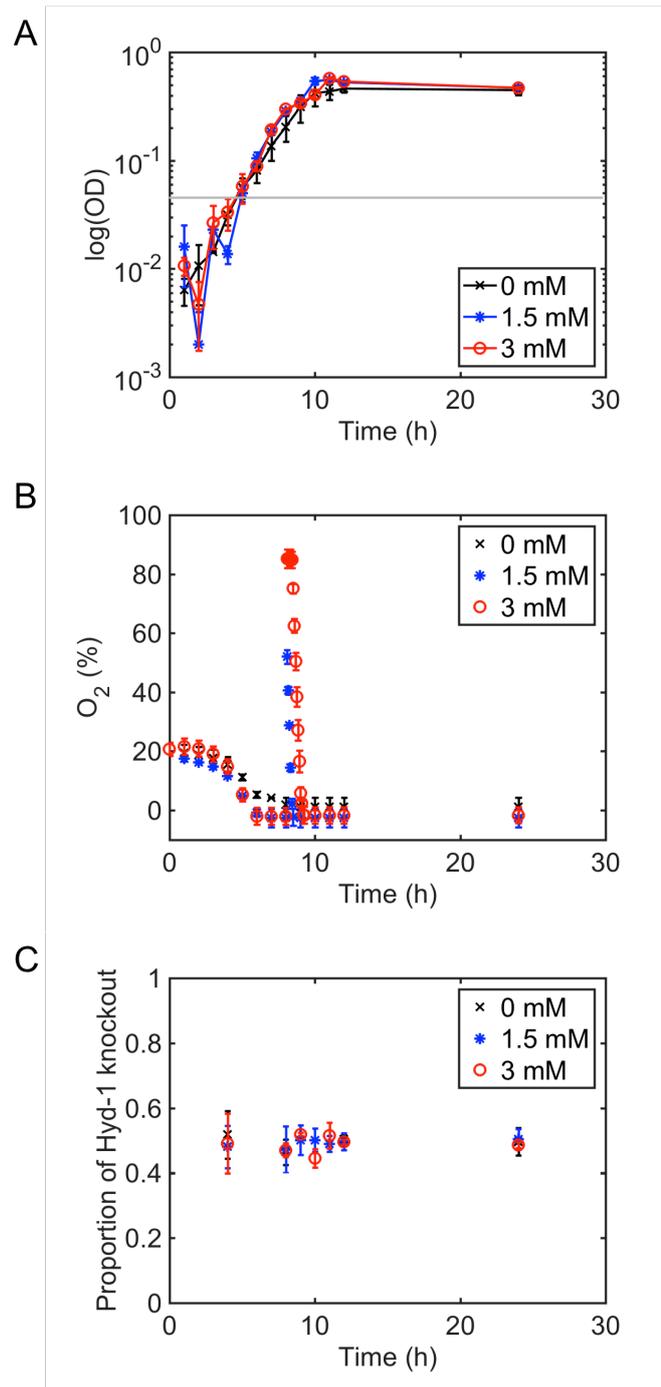
Figure 6.3 Competitive ability of a Hyd-1 knockout with and without oxidative shock. Competition experiments of LAF-001 and LAF-012 in batch culture with the addition of 0 (black cross), 1.5 (blue asterisk) and 3 (red circle) mM hydrogen peroxide after the 8 hour sample was taken. A: Logarithmic plot of the change in optical density. B: Change in O_2 content. C: Proportion of the culture composed of the Hyd-1 knockout strain as measured by the colony count on antibiotic plates. Error bars show the standard error across three biological replicates.

Figure 6.3 shows an average of three biological replicates for all concentrations of hydrogen peroxide added. When 1.5 mM hydrogen peroxide is added, there is a spike in the O_2 reading to approximately 50% saturation, and there is a one hour lag in the optical density before the exponential phase is resumed. When 3 mM hydrogen peroxide is added to the culture, the O_2 is raised to the maximum detectable by the O_2 probe, and there is a two hour lag in growth before exponential phase is resumed. Despite these effects, there is no significant change to the proportion of the Hyd-1 knockout strain in the culture, and at the end of all the growths, regardless of the amount of hydrogen peroxide added, this is approximately 50% of the culture.

6.3.4 Effect of Hyd-1 in a chemostat setup

As the hydrogen peroxide is added only two hours after the O_2 in the system is depleted, it is possible that there is sufficient O_2 in the culture to prevent the addition of hydrogen peroxide to have the effect of a "shock". Furthermore, because the addition occurs shortly before stationary phase, the impact on growth rate is difficult to detect. Therefore, a setup was used where after 10 hours of batch culture growth, media was added at a low dilution rate, and excess culture removed at the same rate to keep the volume of the system constant. This chemostat setup is depicted in Figure 6.4. After the constant media flow was initiated, the dilution rate, and thus the specific growth rate, was 0.12 h^{-1}. As the maximum growth rate, as mentioned above, is 0.63 h^{-1} in the medium, the dilution rate allowed steady state to be reached, with a doubling time of 5.7 h. Thus, a constant OD was achieved where new carbon source was enough to prevent cell death, but not enough to allow the growth rate to increase. This permitted the strains to adapt to low O_2 conditions before successive additions of hydrogen peroxide. The first addition at 48 hours causes an immediate reduction in the optical density, which declines further, although to a lesser extent, with each addition. The optical density then rises once more with the recovery from this oxidative shock, although in part this may be due to the O_2 levels, which remain at approximately 5% until the end of the

experiment. Once again, there is no significant change in the proportion of the Hyd-1 knockout strain with the addition of hydrogen peroxide.
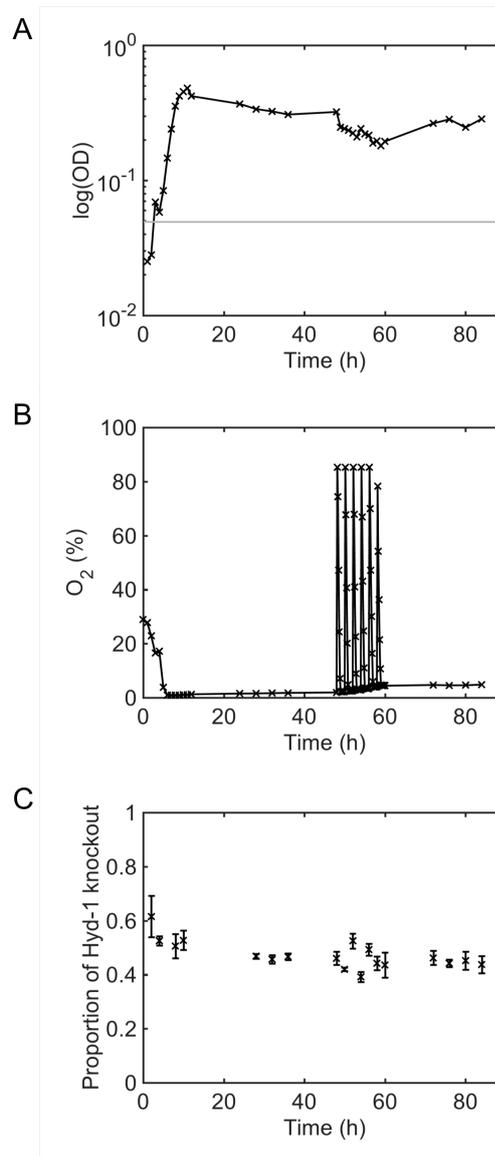
Figure 6.4 Competitive ability of a Hyd-1 knockout in a chemostat. LAF-001 (wild type, streptomycin resistant) and LAF-012 (Hyd-1 knockout, kanamycin resistant) strains were grown in co-culture under batch conditions for 10 hours before a chemostat system was established by the continuous addition of fresh media and the continuous removal of excess culture. Six additions of 3 mM hydrogen peroxide at two hour intervals commenced immediately after removal of the 48 hour sample. A: Logarithmic plot of the change in optical density. B: Change in O_2 content. C: Proportion of the culture composed of the Hyd-1 knockout strain as measured by the colony count on antibiotic plates. Error bars show standard error across three technical replicates.

In order to verify that the reason there was no difference between the wild type and knockout strains was not simply due to a lack of hydrogenase expression, the expression of Hyd-1 and Hyd-2 during the batch culture phase was investigated with RT-qPCR. The *hyaA* and *hybO* genes (Hyd-1 and Hyd-2 small subunit) were monitored using TaqMan probes. *hyaA* is before *hyaB* on the hydrogenase operon and the expression of this gene is less likely to be affected by the presence of the cassette in the chromosome. Four different endogenous controls, *rssA*, *cysG*, *hcaT*, and *idnT*, were chosen due to their stability of expression across various conditions[252-253]. As expected, expression of both Hyd-1 and Hyd-2 was upregulated at 6 hours, when O_2 in the system is largely depleted (Figure 6.5). The upregulation is 50-fold in Hyd-1 but only 7-fold in Hyd-2, which confirms that glucose supplementation induces Hyd-1 rather than Hyd-2. Hyd-1 has a further large upregulation between 6 and 8 hours of growth, whilst the change in Hyd-2 is only a slight upregulation. This is because 6 hours is during exponential phase, where Hyd-2 is known to express[120], whilst 8 hours is the onset of stationary phase, where Hyd-1 is known to express[121]. These results confirm that expression of the MBH is induced by the experimental conditions.
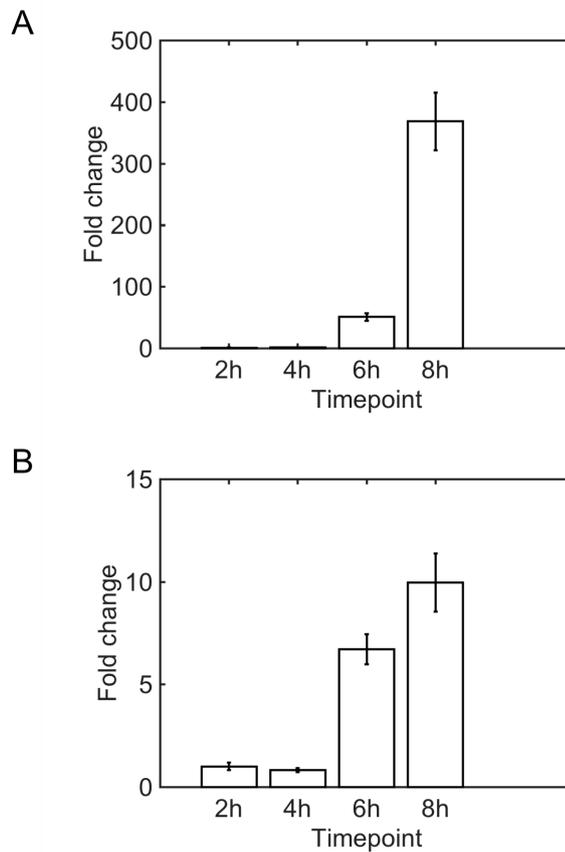
Figure 6.5 *hyaA* and *hybO* expression during batch culture phase. Fold change in expression of A: the Hyd-1 gene *hyaA* and B: the Hyd-2 gene *hybO* relative to the level of expression at the 2 hour timepoint as measured by RT-qPCR, normalised to the average expression of the control genes. Error bars show the propagation of the uncertainty across three technical replicates.

The expression of the genes was also monitored at the later stages of the experiment. Between the onset of the chemostat mode and the first addition of hydrogen peroxide, the expression of *hyaA* shows a 3-fold reduction in level, whilst the *hybO* gene shows a slight upregulation (Figure 6.6). This could imply that Hyd-1 is more important during nutrient depletion at the end of batch culture growth than during chemostat operation when nutrients are added at a constant rate. The expression of both hydrogenases does not decrease between 48 hours and 60 hours, suggesting that the oxidative shock of the peroxide additions does not cause expression of anaerobiosis genes to cease.
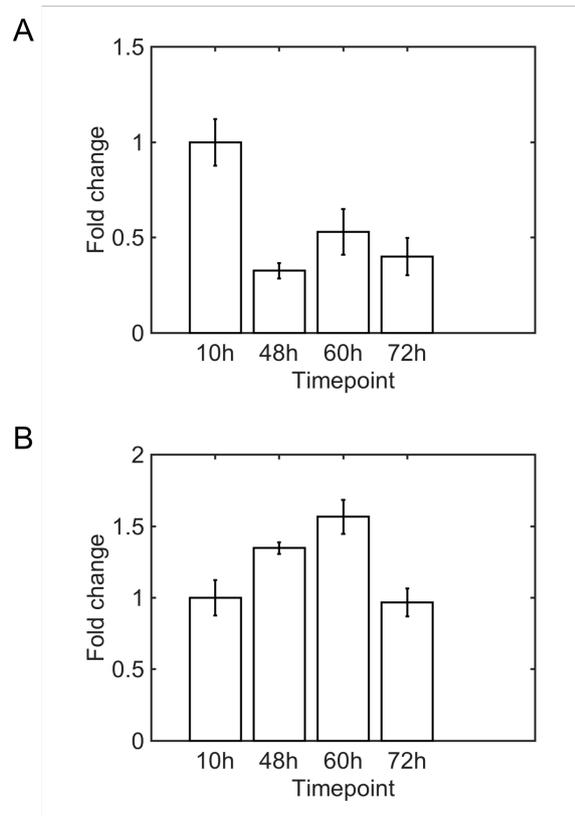
Figure 6.6 *hyaA* and *hybO* expression during chemostat phase. Fold change in expression of A: the Hyd-1 gene *hyaA* and B: the Hyd-2 gene *hybO* relative to the level of expression at the 10 hour timepoint as measured by RT-qPCR. Error bars show the propagation of the uncertainty across three technical replicates.

The extensive investigations in this chapter were unable to show any significant contribution of NiFe hydrogenase Hyd-1 to bacterial growth or competition, although the gene showed clear expression which could indicate an underlying role. This is perhaps unsurprising as investigations into the role of the *S. enterica* hydrogenases suggest that Hyd-2 is the most important hydrogenase with regards to bacterial virulence[242]. However, the hydrogenases of *S. enterica* are expressed differentially at different stages of infection[119]. It could be that to draw out any differences in a Hyd-1 *E. coli* knockout strain the bacterium would need to be exposed to different types of mammalian cells. Alternatively, as Hyd-2 is expressed under the conditions investigated, this enzyme could be compensating for Hyd-1 in the deletion strain. In this case, a Hyd-2 knockout strain could be used as the "wild-type" and a Hyd-1/Hyd-2 double knockout could be used to test for the role of Hyd-1 in *E. coli*.

6.4 Conclusions

Single site variants and knockouts of *E. coli* Hyd-1 have been assessed for changes in growth rate or competitive ability. No significant difference was found either in batch culture or chemostat operation. However, using RT-qPCR, it was found that the expression of Hyd-1 and Hyd-2 was induced under the conditions investigated, suggesting that *E. coli* is employing the hydrogenases, despite the role of Hyd-1 not being discernible.

Chapter 7

Discussion and future perspectives

Hydrogen is an ancient fuel, a modern fuel and a fuel of the future. Hydrogenases are possessed by a large variety of organisms, that utilise hydrogen as an energy source in diverse environments[5, 11, 97]. Humanity also aims to exploit hydrogen as an energy source in order to counteract the crises of depleting fossil fuels and global warming. However, challenges yet remain in this industry, and hydrogen production is still both costly and energetically expensive[1]. For this reason, research has turned to the hydrogenases in the hopes of understanding how their function relates to their biochemical properties.

The membrane bound NiFe hydrogenases (MBH) of enteric bacteria are of great interest for two main reasons. The first is that both *Salmonella enterica* and *Escherichia coli* posses hydrogenases belonging to a special subset of MBH, the O_2 tolerant MBH[8-9]. This subset is able to sustain catalytic H_2 oxidation in the presence of O_2, which is a desirable property for industrial applications, where maintaining anoxygenic conditions could be costly. The second reason is that the MBH of *S. enterica* have been identified as virulence factors[98] and thus characterisation of the structure and function of these MBH is of interest to understanding the pathogenesis of enteric bacteria and the development of novel antimicrobials.

Hyd-5 is an O_2 tolerant MBH of *S. enterica* that is expressed under aerobic conditions[118]. It is thus considered a useful subject for investigations into the biochemistry of O_2 tolerance. Prior to the work described here, investigations into this property had focussed almost entirely on the roles of the iron-sulfur clusters of the small subunit in protection of the MBH from O_2 inhibition[56-57, 209]. Chapter 2 describes the electrochemical characterisation of two Hyd-5 large

subunit variants. Glutamate 73 is a conserved glutamate only in O_2 tolerant MBH. Protein film electrochemistry showed that an E73A Hyd-5 variant had relatively similar turnover and H_2 oxidation catalysis to the Native Hyd-5, but diminished O_2 tolerance. Histidine 229 is fully conserved in hydrogenases, and in crystal structures lies close to the proximal iron-sulfur cluster[36], which has previously been strongly implicated in O_2 tolerance[57]. Protein film electrochemistry (PFE) of a H229A Hyd-5 variant found that not only was the O_2 tolerance severely impaired relative to Native Hyd-5, but that at high potentials the H229A variant showed greater anaerobic inactivation than the Native MBH. These results demonstrated that large subunit residues removed from the primary coordination sphere of the metal centres may have a significant impact on the properties of the hydrogenase. This is an important consideration when using synthetic models to emulate MBH activity.

Frielingsdorf et al confirmed that the findings in Chapter 2 on the H229A variant were also applicable to the MBH of *R. eutropha*[33]. They also published a crystal structure that showed H229 interacting with the superoxidised state of the proximal cluster formed under O_2. Dance used the work in Chapter 2 and the work by Frielingsdorf et al to propose a mechanism of formation of the superoxidised state which involved proton transfer via H229 triggering a structural change at the proximal cluster[210]. Dance also suggested that glutamate 73 could either be part of the proton transfer pathway for this process or could be forming part of a hydrogen bonding network which would communicate structural changes at the active site to the proximal cluster. In order to test these hypotheses, large subunit variants of another O_2 tolerant MBH, Hyd-1, were created in *E. coli.*

Prior to this work, there were two main methods of creating MBH variants. The first method involves introducing a large plasmid containing genes for the variant hydrogenase, its maturation and its regulation[213]. This method would require the plasmid to be maintained during protein expression, but also requires the cell to transport iron and nickel at sufficient levels to express and

mature the MBH. The second method involves creating a plasmid containing the gene of the variant hydrogenase and 600 base pairs of homology and then performing recombination[8, 48]. This method would not require plasmid maintenance during protein expression, but could require screening of multiple clones[214]. Both methods require plasmid construction, which entails many steps of restriction, PCR amplification, ligation and verification, which can be extremely time consuming.

Chapter 3 aimed to streamline the process of creation of MBH variants in *E. coli* by optimising the Red®/ET® recombination and streptomycin counter selection protocol first demonstrated by Heerman et al[215]. This process requires only two steps for the creation of each chromosomal single site mutations. The work in this thesis demonstrates the first time that this protocol has been applied to hydrogenases, allowing the rapid creation of variants in *E. coli* MBH O_2 tolerant Hyd-1 and O_2 sensitive Hyd-2. Furthermore, nucleotides coding for polyhistidine tags were inserted into the genes coding for the small subunit, allowing purifications of the variants. This functionality was not explored by Heerman et al[215], but has the potential to allow purification of other protein complexes which would be troublesome to express from a plasmid. The methodology developed in Chapter 3 could thus speed up the process of variant creation in *E. coli*, potentially enabling a more in-depth exploration of the properties of variants. Ideally, this protocol would be trialled in other organisms in order to further improve its application.

Native Hyd-1 and E73Q, E73A, E73N and E73K Hyd-1 variants of *E. coli* were created and purification was attempted. As described in Chapter 4, only the purification of Native Hyd-1 and the E73Q and E73A variants was successful. Computationally calculated structures of the E73K and E73N variants showed that these amino acid substitutions had a destabilising effect on the protein structure. The E73A Hyd-1 variant had similar properties to the Hyd-5 E73A variant in *S. enterica* as described in Chapter 2. In contrast, the Hyd-1 E73Q variant had an identical O_2 tolerance profile to Native Hyd-1. This suggests that

glutamate 73 does not participate in proton transfer during the reaction with O_2. However, the results in Chapter 4 could suggest that glutamate 73 is involved a hydrogen-bonding network which could allow communication between the active site and the proximal cluster upon reaction with oxygen[210].

Despite the unchanged O_2 tolerance profile in the Hyd-1 E73Q variant, this enzyme exhibited a change in a different fundamental property, the catalytic bias. Under conditions of 100% N_2 and pH 4.5 or pH 6, the Hyd-1 E73Q variant had double the H_2 production to H_2 oxidation ratio of the Native Hyd-1. This has never before been achieved without consequence to the O_2 tolerance. The work in Chapter 4 thus demonstrates a potential avenue of exploration for biotechnology, in which small changes could be made to the hydrogenases native to photosynthetic organisms, perhaps with dramatic consequences.

Investigations into the Hyd-1 E73Q variant found no changes to the iron-sulfur cluster potentials, reactivation from Ni-B or onset potential that would explain the change in catalytic bias. However, glutamate 73 is at similar distances from the NiFe active site, proximal cluster and medial cluster[34]. It could be that the NiFe site has been altered by the amino acid substitution in a way that affects the relative proportions of the intermediate states of the catalytic cycle. This could be investigated firstly by quantum mechanics/ molecular mechanics (QM/MM) to simulate changes of the active site when glutamine is at position 73 rather than glutamate. Spectroelectrochemistry could also be used to demonstrate which states are present at the active site at different potentials and pH values.

In order to investigate the hypothesis regarding the histidine, variants Hyd-1 H229A and Hyd-2 H214A were created and purified alongside Native Hyd-1 and Hyd-2 in Chapter 5. The Hyd-1 H229A variant was purified at lower yields than the Native Hyd-1, suggesting a role for the residue in heterodimer stability. This was supported by the finding that both the Hyd-1 H229A and Hyd-2 H214A variants formed less stable films on the electrode at both low and high pH

values. The reason that the histidine is conserved across all hydrogenases was previously unknown. It is hypothesised that the reason is that the histidine residue bridges the large-small interface in order to stabilise the heterodimer. This could be tested by performing calorimetric analysis of thermal stability.

By investigation with PFE, it was seen that the properties of diminished O_2 tolerance and increased anaerobic inactivation seen in the *S. enterica* Hyd-5 H229A variant are also seen in the *E. coli* Hyd-1 H229A variant. This variant was shown to have a lower rate of reactivation than Native Hyd-1. In contrast, the Hyd-2 H214A variant is unchanged from Native Hyd-2, both in terms of the reaction with O_2 and in terms of the extent of anaerobic inactivation. It is hypothesised that in Hyd-1 histidine 229 participates in proton transfer to the proximal cluster, triggering opening to the superoxidised state[210]. This would not be possible in Hyd-2, which is why the reactivity is unchanged in the H214A variant. Investigation of this hypothesis with EPR could show whether the transitions of the proximal cluster have been impacted in the variant MBH.

An important implication of the work in Chapter 5 is that the superoxidised state of the proximal cluster has a vital role in O_2 tolerant MBH not only in the presence of O_2 but also in catalysis at high potentials in the absence of oxygen. Although anaerobic inactivation has previously been linked to O_2 tolerance[198], in general aspects of O_2 tolerance have previously been considered as completely separate from the catalytic activity of MBH. The work presented here demonstrates that these properties may in fact be intimately connected, and this should be considered in further research of either property. Furthermore, the anaerobic inactivation may act as a fingerprint for NiFe hydrogenases, meaning that much can be determined about the enzymes with simple cyclic voltammetry experiments, without needing to introduce oxygen into the system.

The effect of the E73Q and H229A variants on the growth of *E. coli* was tested in Chapter 6, but no impact was found. Furthermore, across a series of growth and competition experiments, a Hyd-1 knockout strain consistently performed

equally well as the wild type strain, despite clear expression of the Hyd-1 genes under the experimental conditions. The role of Hyd-1 in *E. coli* thus remains elusive. Research often reports changing levels of gene expression with the implication that information has been gleaned about the role of the protein in the cell[249]. The work in Chapter 6 demonstrates that this is not necessarily the case.

The reason that no difference in growth rate or competitive ability was seen in a Hyd-1 knockout could be that Hyd-1 acts in a functionally redundant manner with Hyd-2 and that in the knockout strain Hyd-2 compensates for the activity of Hyd-1. In order to investigate this strains would need to be created where Hyd-2 is also knocked out, which could cause the absence of Hyd-1 to have a more significant effect. Alternatively, the effect may only be seen as in *S. enterica*, where MBH contribute to the colonisation of mammals. It may thus be advantageous to conduct *in vivo* competition experiments.

The work in this thesis clearly demonstrates that MBH have been specifically optimised by evolution to perform their functional roles. In the case of *E. coli* Hyd-1 and *S. enterica* Hyd-5 this is O_2 tolerant H_2 oxidation. Residues of the large subunit at up to 10 Å distance from the metal sites contribute to both of these functionalities, whilst also ensuring protein stability. However, this work also demonstrates that this is an opportunity that may be exploited, for, just as each residue has a functional role, each small change and substitution allows exploration of new functionality which may open new avenues into the research of hydrogenases and their relationship to biotechnology.

Chapter 8

Experimental Materials and Methods

8.1 Preparation of protein structure images

Protein structures were downloaded from the protein data bank[254] in text format. The program PyMOL[255] (SCHRÖDINGER) was used to visualise protein structures. Individual features were selected by using the "sele" function. Polar contacts were found by right-clicking on a residue, and selecting "actions", "find", "polar contacts", and "to other atoms within object". Dotted lines were created by picking atoms by double clicking with the right mouse button and using the "dist pk1 pk2" operation. The "Ray" function was used to render the image of the structure on the screen and the image was exported as a png file.

8.2 Preparation of antibiotic stocks, plates and cultures

Antibiotic stocks of kanamycin, ampicillin and streptomycin at 50 mg/ mL were made by dissolving 0.5 g of solid antibiotic in 10 mL pure water and using an 0.2 micron syringe filter to aliquot the solution into 2 mL sterile microfuge tubes under flame sterile conditions. The tubes were frozen at -20 °C and thawed as needed.

To make antibiotic plates, 500 mL bottles of LB agar were sterilised in a benchtop autoclave and left to cool in a water bath at 60 °C whilst the antibiotic stocks were thawed on ice. 500 μL of each antibiotic (usually kanamycin and ampicillin or streptomycin and ampicillin) was added to each bottle with a pipette under flame sterile conditions. The bottle was swilled to mix and the plates were poured in flame sterile conditions (usually ~20 mL per plate) before the lid was closed and the plates were left to set for 10-20 minutes. The plates were dried in a laminar flow cabinet and stored at 4 °C until needed.

Liquid LB was made in 500 mL bottles and sterilised using a benchtop autoclave. The bottle was stored at room temperature. In order to make liquid cultures, smaller volumes were measured into a 15 mL or 50 mL Falcon tube (Fisher Scientific) to prevent contamination of the larger stock and the correct antibiotics were added in flame sterile conditions. Cultures were created by picking a single colony from a plate with a pipette tip and then either stirring the media with it (small volume) or dropping the tip in. Unless stated otherwise, the cultures were grown at 30 °C and on ampicillin (50 μg/mL) in order to maintain the pRed/ET plasmid.

In order to make glycerol stocks a liquid culture was grown overnight as above. 1 mL of this was combined with 1 mL 50% v/v glycerol in a 2 mL microfuge tube and mixed by pipetting up and down. The stocks were frozen at -80 °C. in order to plate out a particular strain, the stock was scraped with a metal loop whilst still frozen and quickly returned to the freezer. The loop was used to streak the plate in a G pattern, holding the loop in the flame until red hot and leaving to cool for 30 seconds before streaking each new section.

Four transformations would ordinarily be plated onto each antibiotic plate by taking care to remain within drawn sections of the plate whilst streaking. Any colonies that grew would be streaked out to single colonies on a fresh plate, and the single colonies would be streaked out once more, all on ampicillin plus either kanamycin or streptomycin as needed and at 30 °C. The colonies of this plate would be the ones used for PCR verification, but also to check that the strains were only resistant for the correct antibiotics. Streaked plates were stored at 4 °C.

8.3 PCR reactions for checking and sequencing

Colony PCR was performed by dipping a sterile pipette tip into a colony and using it to stir the reaction mixture before vortexing to mix. PCR was performed using Q5® High-Fidelity Master Mix (New England Biolabs) at 98 °C for 30 seconds followed by 35 cycles of: 98 °C, 10 seconds; 50-70 °C, 30 seconds; 72 °C, 30 seconds/kilobase and a 5 minute final extension at 72 °C. Where the reaction was to be purified, 5 μL was taken from each 50 μL reaction and combined with 1 μL 6X Gel Loading Dye (New England Biolabs) and 5 μL was loaded onto an agarose gel. Where the purpose of the reaction was solely for gel verification, 5 μL of 6X Gel Loading Dye was added to the 25 μL completed reaction and mixed by vortexing, and 10 μL was added onto the agarose gel.

Agarose gels were prepared by dissolving 0.5 g agarose into 70 mL 0.5 x TBE buffer (110 mM Tris pH 8.3, 90 mM borate, 2.5 mM EDTA) in a 250 mL conical flask and adding 7 μL SYBR® Safe DNA Gel Stain. The flask was microwaved until a rolling boil was observed (approx. 1 min). The flask was left until it could be handled without burning and the gel was poured into a container sealed at the edges with masking tape. A comb of the correct size was added to the container and the gel was left to set. Once set the tape was removed and the gel was placed into a horizontal electrophoreisis tank filled with 0.5 x TBE buffer. The comb was removed, topping up the buffer as necessary and PCR product pipetted into the wells. Electrophoreisis was performed for 60 minutes at 90 V before the gel was imaged on a transilluminator. Where necessary, gel bands were cut out with a scalpel and DNA was purified using a QIAquick Gel Extraction Kit. DNA was stored at -20 °C until used.

The concentration of DNA in the purified PCR product was measured using a Nanodrop 1000 spectrometer. In order to prepare DNA for sequencing, DNA was diluted with pure water (Purite) to the correct concentration, for LIGHTRUN sequencing (GATC Biotech): 20-80 ng/μL. A primer at least 50 base pairs away from the region of interest was diluted to 5 μM with pure water and 5 μL was

added to 5 μL of DNA in a 1.5 mL microfuge tube. The mixture was dispatched for LIGHTRUN sequencing (GATC Biotech). Sequence was visualised with FinchTV (Geospiza).

8.4 Batch culture and competition experiments in minimal media

For the experiments in Chapter 6, 5x stocks of M9 salts (bought as 5x M9 powder from Sigma Aldrich), pure water (purite), 100 mM calcium chloride, 1 M magnesium chloride, and glycerol (where necessary) were autoclaved. The vessel in which experiments were conducted was autoclaved whilst empty. The day before the inoculation with starter culture, the vessel was opened in a laminar flow cabinet to ensure sterility and 1 L media was added at 1x M9 salts (47 mM sodium phosphate, 22 mM monopotassium phosphate, 19 mM ammonium chloride, 9 mM sodium chloride), 10 μM calcium chloride, 1 mM magnesium chloride, 0.1% v/v 1000x metals (50 mM iron (III) chloride, 20 mM calcium chloride, 10 mM magnesium chloride, 10 mM zinc sulphate, 2 mM cobalt (II) chloride, 2 mM copper (II) chloride and 2mM nickel (II) chloride) and either 40 mM sodium fumarate and 0.2% v/v glycerol or 0.1% w/v glucose. The metals, sodium fumarate and glucose were filter sterilised through a 0.2 micron filter. The vessel was transferred to the apparatus which would allow the stirrer and probes to be connected, and the media was stirred and heated until the commencement of the experiment. For the chemostat experiment, media was prepared at the correct composition in 2 L bottles in the laminar flow cabinet and poured into the conical flask containing the inlet tube under flame sterile conditions at the required time.

The growth rate was calculated according to Equation 8.1[256], where N is the concentration of cells, t is the time and k is the growth rate. Integrating this gives equation 8.2. The concentration of cells was calculated according to an OD_{600} of 1 corresponding to 8 x 10^8 cells per mL. The natural log of this was plotted against time and the growth rate was derived from the gradient.

$$\frac{dN}{dt} = kN \qquad \qquad \text{(Equation 8.1)}$$

$$\ln\left(\frac{N2}{N1}\right) = k(t2 - t1) \qquad \qquad \text{(Equation 8.2)}$$

Plates for colony counting in competition experiments were prepared without ampicillin and stored at 4 °C until an hour before use, when they were placed at room temperature to pre-warm. Serial dilutions were performed by taking 100 μL of the culture and using it to inoculate 900 μL of fresh media in a sterile 2 mL microfuge tube. 100 μL of this dilution was used to inoculate the next tube and so on until the correct dilution was achieved. 10 or 100 μL of the correct dilution was spread on the plate using a glass spreader which had been sterilised by dipping in 100 % ethanol, passing through a flame and allowing to cool for a few seconds before making circular motions over the surface of the plate. The plates were incubated at 37 °C until colonies were evident by eye. The android app Click Counter Free was used to assist colony counting.

8.5 Purification of *E. coli* MBH

The protein purification protocol was adapted from Lukey et al[8]. 10 mL starter cultures of histidine tagged strains (see Chapter 3) were grown in LB plus streptomycin (50 μg mL^{-1}) at 37 °C with shaking throughout the day. 3 mL of this was used to inoculate each 6 L bottle. The bottles contained LB plus glycerol (1% v/v), sodium fumarate (0.4% w/v) and streptomycin (50 μg ml^{-1}). The sodium fumarate and streptomycin were sterilised by vacuum filtration through a 0.2 micron filter paper (Whatman). The bottles were filled to leave only 5 mL headspace and placed in a standing incubator at 37 °C overnight until an optical density (OD) of ~1 was reached.

All bottles were removed from the incubator at once, and the cells were harvested by spinning at 5500 g for 15 minutes on a Beckman Avanti centrifuge (JA10 rotor) at 4 °C. After each 15 minutes, the supernatant was discarded and more culture was added, so that the pellet grew larger each time. The ~50 g collected pellet was resuspended in ~125 mL chilled buffer (100 mM Tris pH 7.6, 300 mM NaCl). Sucrose (20% w/v) was added to the resuspension and this mixture was stirred at 4 °C for at least 45 minutes. This was pelleted once more by centrifugation at 6500 g for 20 minutes on a Beckman Avanti centrifuge (JA25.50 rotor) at 4 °C. The pellet was lysed with osmotic shock by resuspension in 300 mL ice-cold water (Purite). The resuspension was stirred in the fridge for at least 30 minutes before overnight solubilisation by making the mixture up to 100 mM Tris pH 7.6, 300 mM NaCl, and 9% Triton X-100, with Lysozyme from chicken egg white (Sigma Aldrich), Deoxyribonuclease I (Sigma Aldrich) and Pierce™ Protease Inhibitor Mini Tablets, EDTA-free (Thermo Scientific). After this overnight stirring in the fridge, the mixture was divided between 150 mL Sterilin® sample containers (Thermo Scientific), and each pot underwent a final lysis step by sonication with a 20 mm probe using a Soniprep 150 (MSE) at a power of 15-20 on ice for 10 x 30 s, swapping pots between each sonication. The pots were then combined and stirred for 30 minutes at 4 °C. The mixture was then centrifuged at 20000 g for 30 minutes at 4 °C on a Beckman Avanti

centrifuge (JA25.50 rotor). The supernatant was diluted to 600 mL with 100 mM Tris pH 7.6, and in preparation for loading onto the column the mixture was made up to 50 mM imidazole. An Akta Start and 5 mL HisTrap Ni affinity column (GE Healthcare) was used for the purification. The supernatant was loaded at 4 mL min^{-1} and then the column was washed with 8 column volumes of buffer A (100 mM Tris, 150 mM NaCl, 50 mM imidazole, pH 7.6). The protein was eluted using a gradient elution (0-100% buffer B: 100 mM Tris, 1M imidazole, pH 7.6).

The presence of hydrogenase in the fractions corresponding to an elution peak was confirmed using SDS-PAGE. A 10% resolving gel and a 6% stacking gel were poured into gel plates with a 1 mm gap containing a 15 well comb. The gel was placed in a cassette and tank of a Mini-PROTEAN® System. 15 μL fraction was combined with 3 μL 6 x SDS loading buffer and 15 μL of the mixture was loaded into each well of the gel. The gel was run at 200 V for 40 minutes. It was then microwaved in water until a rolling boil was reached, rocked at room temperature for 5 minutes, microwaved in a Coomassie brilliant blue G-250 (70 μg) solution in water and hydrochloric acid (35 mM) until a rolling boil, rocked at room temperature until bands developed, and destained in water. Fractions containing hydrogenase were dialysed in the fridge overnight (100 mM Tris, 150 mM NaCl, pH 7.6) in 0.2 micron dialysis tubing. Where needed, the protein was concentrated using an Amicon Ultra centrifugal filter with 30 kDa cutoff (Merck Millipore). Protein was divided into 25 μL aliquots and stored at -80 °C until needed.

A UV-1061 (Shumadzu) UV-Vis spectrometer and Semi-Micro Cell 108B-QS cuvette (Hellma Analytics) were used to obtain a full spectrum of the purified enzymes (250-700 nm). A molar extinction coefficient of 171,335 M^{-1} cm^{-1} calculated using the ExPaSy ProtParam tool was used to calculate the protein concentration from the absorbance at 280 nm (A_{280}).

8.6 Hydrogenase buffer composition

Measurements of protein activity were performed in a "mixed hydrogenase" buffer. This was composed of 15 mM sodium acetate (Sigma Aldrich), CHES (N-Cyclohexyl-2-aminoethanesulfonic acid) (AMRESCO), MES (2-(N-morpholino)ethanesulfonic acid) (Sigma Aldrich), HEPES (4-(2-hydroxyethyl)-1-piperazineethanesulfonic acid) (Sigma Aldrich) and TAPS (N-tris(Hydroxymethyl)methyl-3-propanesulfonic acid sodium potassium salt) (Sigma Aldrich) and 100 mM NaCl.

8.7 Methylene blue assay for measurement of H_2 oxidation activity

An anaerobic glove box (Faircrest) filled with N_2 (BOC) was used to perform the assay measurements. The enzyme was diluted 100-fold in the "mixed hydrogenase" buffer, adjusted to the stated pH with HCl and NaOH. A 0.1 mM solution of methylene blue was made up in the same buffer and a flow of H_2 (BOC) at 100 standard cubic centimetres (scc) min^{-1}, controlled by a Sierra Smart-Trak 50 mass flow controller, was bubbled through for a minimum of one hour. 2 mL of this methylene blue solution was transferred to a 3 mL cuvette containing a 1 mm magnetic bead. The cuvette was placed in an LED-spectrometer (built in-house, Department of Chemistry Electronic Workshop, University of York) on top of a magnetic stirrer plate. A light blocking cuvette lid with an injection hole was placed over the cuvette and the stirrer was turned on. The solution was illuminated at 626 nm for 150 seconds before 50 μL diluted enzyme was injected via the hole in the cuvette lid. The absorbance was monitored using a voltmeter until the solution was completely decolourised. The protein concentrations, determined as above, and an in-house determined methylene blue extinction coefficient of 28000 μM^{-1} cm^{-1} were used to convert the fastest rate of absorbance change into rate of H_2 oxidation. The quoted assay rates were an average of three repeats.

8.8 Protein film electrochemistry

All electrochemistry measurements were performed in an anaerobic glove box filled with N_2. A gas tight electrochemical cell (built in-house by the University of York glassblowers) housed the three electrode configuration. A water jacket achieved control of the temperature, at 37 °C unless stated otherwise. The graphite working electrode and platinum counter electrode were in the main body of the cell whilst the saturated calomel reference electrode (SCE) was housed in a side arm filled with 0.1 M NaCl and connected to the main body of the cell by a Luggin capillary. The "mixed hydrogenase" buffer described above was adjusted to the correct pH using HCl and NaOH and approximately 2.5 mL was used to cover the electrodes in the main body of the cell. Gases (BOC) were flowed through the electrochemical cell and at a rate of 100 scc min^{-1} and the stated composition under the control of Smart-Trak mass flow controllers (Sierra Installations) connected to the electrochemical cell. N_2 was used as a carrier gas. In order to prepare the graphite electrode (electrodes manufactured in-house at the University of York) Norton P1200 abrasive sheets were used to stand the surface before application of 2 μL of the enzyme. A CompactStat potentiostat (Ivium Technologies) and the IviumSoft Program were used to control the electrochemical experiment and the electrode was rotated at 4000 rev min^{-1} using an Origatrod rotator (Origalys) to allow an adequate supply of substrate and removal of product. After applying the film of enzyme, a cyclic voltammogram was performed at 3% H_2 97% N_2. If a significant plateau in the current was shown at high potentials (Figure 8.1 A), the film was deemed to be in excess and cotton wool was used to remove excess film until the more characteristic waveshape appeared (Figure 8.1 B). All cyclic voltammetry was performed at 5 mV s^{-1} unless specified otherwise.
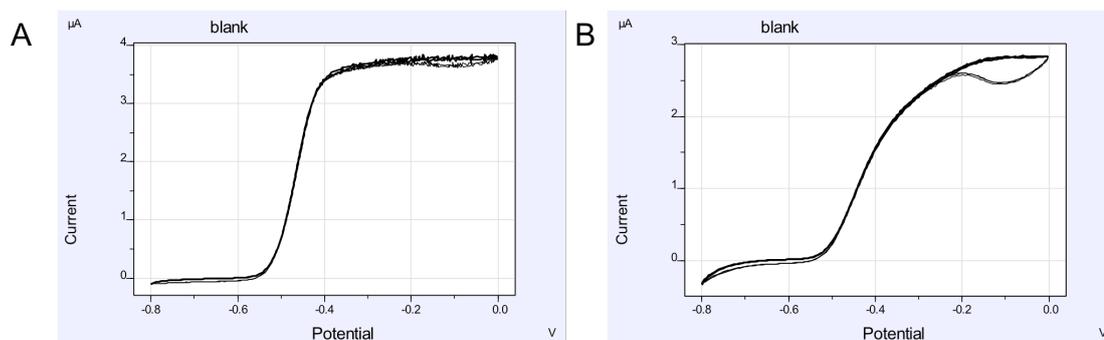
Figure 8.1 Effect of film density on voltammogram shape. Catalysis by Hyd-1 E73Q variant A: before and B: after abrasion with cotton wool to remove excess film. The potential was swept from -0.8 to 0 V vs SCE and back again at 3% H_2. 3 cycles are shown overlaid on the plots.

In order to ensure repeatability in cyclic voltammetry, the potential was cycled up and down at least four times and the data from final scan was taken as the experimental result. It is this scan that is shown in the Figures of Chapters 2, 4 and 5. As seen in Figure 8.1, the scans generally overlaid well and so the data shown is representative of the set.

For Chapter 2, a reference electrode correction factor of E(V vs SHE) = E(V vs Ref) +0.241 V according to literature values[257]. For chapters 4 and 5 a reference electrode correction factor determined with calibration measurements made using 100 μM methylene blue cyclic voltammetry at pH 7, 25 °C, using a platinum working electrode (Figure 8.2). The values given for the potentials of maximum current (E at imax), minimum current (E at imin), midpoint (Emid), and correction factor (Ecorrection) needed to give the value of Em,7 = +0.019 V vs SHE (calculated from published reference data[203]) is given in Table 7.1. The correction value used was E(V vs SHE) = E(V vs Ref) +0.265 V.
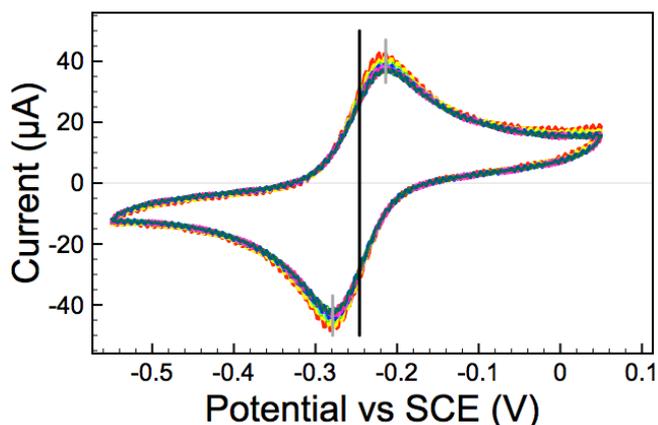
Figure 8.2 Calculation of the correction factor. The potential was swept from -0.56 to +0.06 V vs SCE and back again at 50 mV s^{-1} using the platinum wire as a working electrode. The potential of the maximum and minimum current are marked by grey lines and the midpoint potential of -0.246 V vs SCE is given by the black line.

Table 8.1 Values used to determine the PFE correction factor.

E at imax	E at imin	Emid	Ecorrection
-0.214	-0.282	-0.248	0.267
-0.214	-0.276	-0.245	0.264
-0.212	-0.278	-0.245	0.264
-0.216	-0.280	-0.248	0.267
-0.214	-0.276	-0.245	0.264
-0.218	-0.280	-0.249	0.268
-0.214	-0.276	-0.245	0.264
-0.212	-0.278	-0.245	0.264
-0.208	-0.282	-0.245	0.264

The midpoint of methylene blue at pH 4.5 was calculated by repeating the cyclic voltammetry at this pH value (Figure 8.3). The midpoint was given as -0.152 V vs SCE, and thus using the correction factor the methylene blue midpoint potential is given as +0.113 V vs SHE.
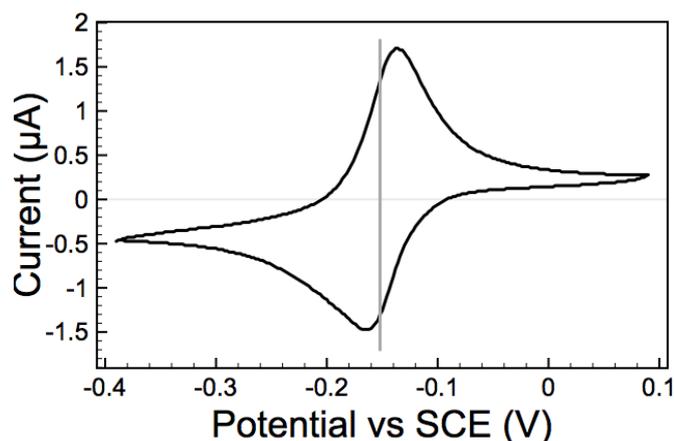
Figure 8.3 Calculation of the methylene blue midpoint potential at pH 4.5. The potential of a methylene blue solution was swept from -0.4 to +0.1 V vs SCE and back again at 10 mV s^{-1}. The midpoint potential, calculated as -0.152 V vs SCE, is given by the grey vertical line.

8.9 Calculation of K_M and K_i.

Chronoamperometry (Chapter 2) or cyclic voltammetry (Chapter 4) was performed at varying percentages of H_2 and the solubility of dissolved H_2 at 37 °C in solution at was calculated by the Van't Hoff equation. This is given by Equation 8.3 below, where $H(T)$ is Henry's law constant for H_2 at T, 310.15 K (37 °C), $H°$ is Henry's law constant for H_2 at $T°$, 298.15 K (25 °C), $\Delta_{sol}H$ is the enthalpy of dissolution and R is the gas constant. As for H_2 $H°$ is 7.8 x 10^{-4} M atm^{-1} and $-\Delta_{sol}H/R$ is 500 K[258], $H(T)$ is given as 7.32 x 10^{-4} M atm^{-1}. This value was multiplied by the partial pressure of H_2 at each percentage and then by 10^6 to give the concentration of H_2 in the solution in μM.

$$H(T) = H°{\times}exp\left[\frac{-\Delta_{sol}H}{R}\left(\frac{1}{T} - \frac{1}{T°}\right)\right]$$ Equation 8.3

As current is proportional to the rate of activity ($i \propto v$)[195], in order to calculate the Michaelis constant (K_M) a Hanes-Woolf diagram of [H_2] against [H_2]/i was plotted, representing a rearrangement of the Michaelis-Menten equation as given in Equation 8.4. The straight line depicted in the diagram yielded a slope of

165

1/maximum rate of activity ($1/V_{max}$) and the intercept of K_M/V_{max}, meaning that the value of K_M in μM was given by the intercept divided by the slope.

$$\frac{[S]}{v} = \frac{1}{V_{max}}[S] + \frac{K_M}{V_{max}}$$
<div align="right">Equation 8.4</div>

The product inhibition constant of H_2 production (K_i) was calculated by plotting $[H_2]$ against $i(0)/i(H_2)$ where $i(0)$ represents V_{max}, the H_2 production current under 100 N_2 and $i(H_2)$ represents v, the current at each H_2 concentration. The currents were first corrected so that $i(H_2)$ at 10% H_2 (fully inhibited) would equal 0. The K_i was given as 1/slope of the resulting straight-line plot.

Symbols and abbreviations

Δp	Proton-motive force
ABC	ATP-binding cassette
AMP	Adenosine monophosphate
amp	Ampicillin
cAMP	Cyclic adenosine monophosphate
CODH	Carbon monoxide dehydrogenase
cyt	Cytochrome
D. vulgaris	*Desulfovibrio vulgaris*
DFT	Density functional theory
E	Potential
E. coli	*Escherichia coli*
Ecorrection	Correction potential
Emid	Midpoint potential
ENDOR	Electron-nuclear double resonance spectroscopy
Eonset	Onset potential
EPR	Electron paramagnetic resonance
E_{switch}	Switch potential
FTIR	Fourier transform infrared spectroscopy
H_{ox}/H_{prod}	H_2 oxidation to H_2 production ratio
HRP	Horseradish peroxidase
Hyd-1	Hydrogenase-1
Hyd-2	Hydrogenase-2
Hyd-3	Hydrogenase-3
Hyd-4	Hydrogenase-4
Hyd-5	Hydrogenase-5
i	Current
imax	Maximum current
imin	Minimum current
IR	Infrared

k_A	Reactivation rate
kan	Kanamycin
k_{cat}	Turnover rate
k_I	Inactivation rate
K_i	Inhibition constant
K_M	Michaelis constant
MBH	Membrane bound NiFe hydrogenase
NADH	Nicotinamide adenine dinucleotide
neo	Neomycin
OD	Optical density
PCR	Polymerase chain reaction
PDB	Protein data bank
PFE	Protein film electrochemistry
PSII	Photosystem II
QM/MM	Quantum mechanics/ molecular mechanics
R. eutropha	*Ralstonia eutropha*
rpm	Rev per minute
S. enterica	*Salmonella enterica*
SAM	Self-assembled monolayer
scc	Standard cubic centimeters
SCE	Saturated calomel electrode
SDS-PAGE	Sodium dodecyl sulphate polyacrylamide gel electrophoreisis
SHE	Standard hydrogen electrode
strep	Streptomycin
Tat	Twin-arginine translocation
TBST	Tris buffered saline with Tween® 20
UV	Ultraviolet
v	Rate of activity
V_{max}	Maximum rate of activity

References

1.   Lauermann, G.; Häussinger, P.; Lohmüller, R.; Watson, A. M., Hydrogen, 1. Properties and Occurrence. In *Ullmann's Encyclopedia of Industrial Chemistry*, Wiley-VCH Verlag GmbH & Co. KGaA: 2000.

2.   McGlade, C.; Ekins, P., The geographical distribution of fossil fuels unused when limiting global warming to 2 degrees C. *Nature* **2015,** *517* (7533), 187-90.

3.   Tian, F.; Toon, O. B.; Pavlov, A. A.; De Sterck, H., A Hydrogen-Rich Early Earth Atmosphere. *Science* **2005,** *308* (5724), 1014-1017.

4.   Glueckauf, E.; Kitt, G. P., The hydrogen content of atmospheric air at ground level. *Quarterly Journal of the Royal Meteorological Society* **1957,** *83* (358), 522-528.

5.   Greening, C.; Constant, P.; Hards, K.; Morales, S.; Oakeshott, J. G.; Russell, R. J.; Taylor, M. C.; Berney, M.; Conrad, R.; Cook, G. M., Atmospheric hydrogen scavenging: from enzymes to ecosystems. *Applied and Environmental Microbiology* **2014,** *81* (4), 1190-9.

6.   Petersen, J. M.; Zielinski, F. U.; Pape, T.; Seifert, R.; Moraru, C.; Amann, R.; Hourdez, S.; Girguis, P. R.; Wankel, S. D.; Barbe, V.; Pelletier, E.; Fink, D.; Borowski, C.; Bach, W.; Dubilier, N., Hydrogen is an energy source for hydrothermal vent symbioses. *Nature* **2011,** *476* (7359), 176-80.

7.   Lubitz, W.; Ogata, H.; Rüdiger, O.; Reijerse, E., Hydrogenases. *Chemical Reviews* **2014,** *114*, 4081-4148.

8.   Lukey, M. J.; Parkin, A.; Roessler, M. M.; Murphy, B. J.; Harmer, J.; Palmer, T.; Sargent, F.; Armstrong, F. A., How *Escherichia coli* is equipped to oxidize hydrogen under different redox conditions. *The Journal of biological chemistry* **2010,** *285*, 3928-3938.

9.   Parkin, A.; Bowman, L.; Roessler, M. M.; Davies, R. A.; Palmer, T.; Armstrong, F. A.; Sargent, F., How *Salmonella* oxidises H_2 under aerobic conditions. *FEBS Letters* **2012,** *586*, 536-544.

10.   Burgdorf, T.; Lenz, O.; Buhrke, T.; van der Linden, E.; Jones, A. K.; Albracht, S. P. J.; Friedrich, B., [NiFe]-Hydrogenases of *Ralstonia eutropha* H16: Modular

Enzymes for Oxygen-Tolerant Biological Hydrogen Oxidation. *Journal of Molecular Microbiology and Biotechnology* **2005,** *10* (2-4), 181-196.

11.   Greening, C.; Biswas, A.; Carere, C. R.; Jackson, C. J.; Taylor, M. C.; Stott, M. B.; Cook, G. M.; Morales, S. E., Genomic and metagenomic surveys of hydrogenase distribution indicate H_2 is a widely utilised energy source for microbial growth and survival. *ISME J* **2016,** *10*, 761-777.

12.   McDowall, J. S.; Murphy, B. J.; Haumann, M.; Palmer, T.; Armstrong, F. A.; Sargent, F., Bacterial formate hydrogenlyase complex. *Proc Natl Acad Sci U S A* **2014,** *111* (38), E3948-56.

13.   McDowall, J. S.; Hjersing, M. C.; Palmer, T.; Sargent, F., Dissection and engineering of the *Escherichia coli* formate hydrogenlyase complex. *FEBS Lett* **2015,** *589* (20 Pt B), 3141-7.

14.   Takács, M.; Tóth, A.; Bogos, B.; Varga, A.; Rákhely, G.; Kovács, K. L., Formate hydrogenlyase in the hyperthermophilic archaeon, *Thermococcus litoralis*. *BMC Microbiology* **2008,** *8* (1), 1-12.

15.   Allakhverdiev, S. I.; Thavasi, V.; Kreslavski, V. D.; Zharmukhamedov, S. K.; Klimov, V. V.; Ramakrishna, S.; Los, D. A.; Mimuro, M.; Nishihara, H.; Carpentier, R., Photosynthetic hydrogen production. *Journal of Photochemistry and Photobiology C: Photochemistry Reviews* **2010,** *11* (2–3), 101-113.

16.   Kleihues, L.; Lenz, O.; Bernhard, M.; Buhrke, T.; Friedrich, B., The H_2 Sensor of *Ralstonia eutropha* Is a Member of the Subclass of Regulatory [NiFe] Hydrogenases. *Journal of Bacteriology* **2000,** *182* (10), 2716-2724.

17.   Wang, S.; Huang, H.; Kahnt, J.; Thauer, R. K., A Reversible Electron-Bifurcating Ferredoxin- and NAD-Dependent [FeFe]-Hydrogenase (HydABC) in *Moorella thermoacetica*. *Journal of Bacteriology* **2013,** *195* (6), 1267-1275.

18.   Zbell, A. L.; Maier, R. J., Role of the Hya Hydrogenase in Recycling of Anaerobically Produced H_2 in *Salmonella enterica* Serovar Typhimurium. *Applied and Environmental Microbiology* **2009,** *75* (5), 1456-1459.

19.   Vincent, K. A.; Cracknell, J. A.; Lenz, O.; Zebger, I.; Friedrich, B.; Armstrong, F. A., Electrocatalytic hydrogen oxidation by an enzyme at high carbon monoxide or oxygen levels. *Proceedings of the National Academy of Sciences of the United States of America* **2005,** *102*, 16951-16954.

20. Vincent, K. A.; Cracknell, J. A.; Clark, J. R.; Ludwig, M.; Lenz, O.; Friedrich, B.; Armstrong, F. A., Electricity from low-level H_2 in still air - an ultimate test for an oxygen tolerant hydrogenase. *Chemical Communications* **2006,** (48), 5033-5035.

21. Wait, A. F.; Parkin, A.; Morley, G. M.; dos Santos, L.; Armstrong, F. A., Characteristics of Enzyme-Based Hydrogen Fuel Cells Using an Oxygen-Tolerant Hydrogenase as the Anodic Catalyst. *The Journal of Physical Chemistry C* **2010,** *114* (27), 12003-12009.

22. Caputo, C. A.; Gross, M. A.; Lau, V. W.; Cavazza, C.; Lotsch, B. V.; Reisner, E., Photocatalytic Hydrogen Production using Polymeric Carbon Nitride with a Hydrogenase and a Bioinspired Synthetic Ni Catalyst. *Angewandte Chemie International Edition* **2014,** *53* (43), 11538-11542.

23. Lauterbach, L.; Lenz, O.; Vincent, K. A., H_2-driven cofactor regeneration with NAD(P)$^+$-reducing hydrogenases. *FEBS J* **2013,** *280* (13), 3058-68.

24. Flanagan, Lindsey A.; Parkin, A., Electrochemical insights into the mechanism of NiFe membrane-bound hydrogenases. *Biochemical Society Transactions* **2016,** *44* (1), 315.

25. Parkin, A.; Sargent, F., The hows and whys of aerobic H_2 metabolism. *Current opinion in chemical biology* **2012,** *16*, 26-34.

26. Volbeda, A.; Charon, M.-H.; Piras, C.; Hatchikian, E. C.; Frey, M.; Fontecilla-Camps, J. C., Crystal structure of the nickel–iron hydrogenase from Desulfovibrio gigas. *Nature* **1995,** *373*, 580-587.

27. van der Spek, T. M.; Arendsen, A. F.; Happe, R. P.; Yun, S.; Bagley, K. A.; Stufkens, D. J.; Hagen, W. R.; Albracht, S. P., Similarities in the architecture of the active sites of Ni-hydrogenases and Fe-hydrogenases detected by means of infrared spectroscopy. *Eur J Biochem* **1996,** *237* (3), 629-34.

28. Happe, R. P.; Roseboom, W.; Pierik, A. J.; Albracht, S. P. J.; Bagley, K. A., Biological activition of hydrogen. *Nature* **1997,** *385*, 126-126.

29. Bagley, K. A.; Duin, E. C.; Roseboom, W.; Albracht, S. P.; Woodruff, W. H., Infrared-detectable groups sense changes in charge density on the nickel center in hydrogenase from *Chromatium vinosum*. *Biochemistry* **1995,** *34* (16), 5527-35.

30. Bagley, K. A.; Van Garderen, C. J.; Chen, M.; Duin, E. C.; Albracht, S. P.; Woodruff, W. H., Infrared studies on the interaction of carbon monoxide with

divalent nickel in hydrogenase from *Chromatium vinosum. Biochemistry* **1994,** *33* (31), 9229-36.

31.   Shomura, Y.; Yoon, K.-S.; Nishihara, H.; Higuchi, Y., Structural basis for a [4Fe-3S] cluster in the oxygen-tolerant membrane-bound [NiFe]-hydrogenase. *Nature* **2011,** *479*, 253-256.

32.   Fritsch, J.; Scheerer, P.; Frielingsdorf, S.; Kroschinsky, S.; Friedrich, B.; Lenz, O.; Spahn, C. M. T., The crystal structure of an oxygen-tolerant hydrogenase uncovers a novel iron-sulphur centre. *Nature* **2011,** *479*, 249-252.

33.   Frielingsdorf, S.; Fritsch, J.; Schmidt, A.; Hammer, M.; Löwenstein, J.; Siebert, E.; Pelmenschikov, V.; Jaenicke, T.; Kalms, J.; Rippers, Y.; Lendzian, F.; Zebger, I.; Teutloff, C.; Kaupp, M.; Bittl, R.; Hildebrandt, P.; Friedrich, B.; Lenz, O.; Scheerer, P., Reversible [4Fe-3S] cluster morphing in an O_2-tolerant [NiFe] hydrogenase. *Nature Chemical Biology* **2014,** *10*, 378-385.

34.   Volbeda, A.; Amara, P.; Darnault, C.; Mouesca, J.-M.; Parkin, A.; Roessler, M. M.; Armstrong, F. A.; Fontecilla-Camps, J. C., X-ray crystallographic and computational studies of the O_2-tolerant [NiFe]-hydrogenase 1 from *Escherichia coli. Proceedings of the National Academy of Sciences of the United States of America* **2012,** *109*, 5305-5310.

35.   Volbeda, A.; Darnault, C.; Parkin, A.; Sargent, F.; Armstrong, F. A.; Fontecilla-Camps, J. C., Crystal structure of the O_2-tolerant membrane-bound hydrogenase 1 from *Escherichia coli* in complex with its cognate cytochrome b. *Structure (London, England: 1993)* **2013,** *21*, 184-190.

36.   Bowman, L.; Flanagan, L.; Fyfe, P. K.; Parkin, A.; Hunter, W. N.; Sargent, F., How the structure of the large subunit controls function in an oxygen-tolerant [NiFe]-hydrogenase. *Biochemical Journal* **2014,** *458*, 449-458.

37.   Volbeda, A.; Martin, L.; Cavazza, C.; Matho, M.; Faber, B. W.; Roseboom, W.; Albracht, S. P. J.; Garcin, E.; Rousset, M.; Fontecilla-Camps, J. C., Structural differences between the ready and unready oxidized states of [NiFe] hydrogenases. *JBIC Journal of Biological Inorganic Chemistry* **2005,** *10*, 239-249.

38.   Volbeda, A.; Martin, L.; Barbier, E.; Gutiérrez-Sanz, O.; Lacey, A. L. D.; Liebgott, P.-P.; Dementin, S.; Rousset, M.; Fontecilla-Camps, J. C., Crystallographic studies of [NiFe]-hydrogenase mutants: towards consensus structures for the

elusive unready oxidized states. *JBIC Journal of Biological Inorganic Chemistry* **2014,** *20*, 11-22.

39.   Volbeda, A.; Martin, L.; Liebgott, P.-P.; Lacey, A. L. D.; Fontecilla-Camps, J. C., [NiFe]-hydrogenases revisited: nickel–carboxamido bond formation in a variant with accrued O_2-tolerance and a tentative re-interpretation of Ni-SI states. *Metallomics* **2015,** *7*, 710-718.

40.   Abou-Hamdan, A.; Ceccaldi, P.; Lebrette, H.; Gutiérrez-Sanz, O.; Richaud, P.; Cournac, L.; Guigliarelli, B.; Lacey, A. L. D.; Léger, C.; Volbeda, A.; Burlat, B.; Dementin, S., A Threonine Stabilizes the NiC and NiR Catalytic Intermediates of [NiFe]-hydrogenase. *Journal of Biological Chemistry* **2015,** *290*, 8550-8558.

41.   Ogata, H.; Hirota, S.; Nakahara, A.; Komori, H.; Shibata, N.; Kato, T.; Kano, K.; Higuchi, Y., Activation Process of [NiFe] Hydrogenase Elucidated by High-Resolution X-Ray Analyses: Conversion of the Ready to the Unready State. *Structure* **2005,** *13*, 1635-1642.

42.   Ogata, H.; Mizoguchi, Y.; Mizuno, N.; Miki, K.; Adachi, S.-i.; Yasuoka, N.; Yagi, T.; Yamauchi, O.; Hirota, S.; Higuchi, Y., Structural Studies of the Carbon Monoxide Complex of [NiFe]hydrogenase from *Desulfovibrio vulgaris* Miyazaki F: Suggestion for the Initial Activation Site for Dihydrogen. *Journal of the American Chemical Society* **2002,** *124*, 11628-11635.

43.   Higuchi, Y.; Yagi, T.; Yasuoka, N., Unusual ligand structure in Ni–Fe active center and an additional Mg site in hydrogenase revealed by high resolution X-ray structure analysis. *Structure* **1997,** *5*, 1671-1680.

44.   Higuchi, Y.; Ogata, H.; Miki, K.; Yasuoka, N.; Yagi, T., Removal of the bridging ligand atom at the Ni-Fe active site of [NiFe] hydrogenase upon reduction with H_2, as revealed by X-ray structure analysis at 1.4 A resolution. *Structure (London, England: 1993)* **1999,** *7*, 549-556.

45.   Garcin, E.; Vernede, X.; Hatchikian, E. C.; Volbeda, A.; Frey, M.; Fontecilla-Camps, J. C., The crystal structure of a reduced [NiFeSe] hydrogenase provides an image of the activated catalytic center. *Structure (London, England: 1993)* **1999,** *7*, 557-566.

46.   Volbeda, A.; Amara, P.; Iannello, M.; Lacey, A. L. D.; Cavazza, C.; Fontecilla-Camps, J. C., Structural foundations for the O_2 resistance of *Desulfomicrobium baculatum* [NiFeSe]-hydrogenase. *Chemical Communications* **2013,** *49*, 7061-7063.

47.   Fritsch, J.; Scheerer, P.; Frielingsdorf, S.; Kroschinsky, S.; Friedrich, B.; Lenz, O.; Spahn, C. M., The crystal structure of an oxygen-tolerant hydrogenase uncovers a novel iron-sulphur centre. *Nature* **2011,** *479* (7372), 249-52.

48.   Dubini, A.; Pye, R. L.; Jack, R. L.; Palmer, T.; Sargent, F., How bacteria get energy from hydrogen: a genetic analysis of periplasmic hydrogen oxidation in *Escherichia coli. International Journal of Hydrogen Energy* **2002,** *27*, 1413-1420.

49.   Bagyinka, C., How does the ([NiFe]) hydrogenase enzyme work? *International Journal of Hydrogen Energy* **2014,** *39* (32), 18521-18532.

50.   Evans, R. M.; Armstrong, F. A., Electrochemistry of metalloproteins: protein film electrochemistry for the study of *E. coli* [NiFe]-hydrogenase-1. *Methods Mol Biol* **2014,** *1122*, 73-94.

51.   Frielingsdorf, S.; Fritsch, J.; Schmidt, A.; Hammer, M.; Lowenstein, J.; Siebert, E.; Pelmenschikov, V.; Jaenicke, T.; Kalms, J.; Rippers, Y.; Lendzian, F.; Zebger, I.; Teutloff, C.; Kaupp, M.; Bittl, R.; Hildebrandt, P.; Friedrich, B.; Lenz, O.; Scheerer, P., Reversible [4Fe-3S] cluster morphing in an O_2-tolerant [NiFe] hydrogenase. *Nat Chem Biol* **2014,** *10* (5), 378-85.

52.   Fritsch, J.; Lenz, O.; Friedrich, B., Structure, function and biosynthesis of O_2-tolerant hydrogenases. *Nat Rev Microbiol* **2013,** *11* (2), 106-14.

53.   Hidalgo, R.; Ash, P. A.; Healy, A. J.; Vincent, K. A., Infrared Spectroscopy During Electrocatalytic Turnover Reveals the Ni-L Active Site State During H_2 Oxidation by a NiFe Hydrogenase. *Angew Chem Int Ed Engl* **2015,** *54* (24), 7110-3.

54.   Reissmann, S.; Hochleitner, E.; Wang, H.; Paschos, A.; Lottspeich, F.; Glass, R. S.; Bock, A., Taming of a poison: biosynthesis of the NiFe-hydrogenase cyanide ligands. *Science* **2003,** *299* (5609), 1067-70.

55.   Dementin, S.; Belle, V.; Bertrand, P.; Guigliarelli, B.; Adryanczyk-Perrier, G.; De Lacey, A. L.; Fernandez, V. M.; Rousset, M.; Léger, C., Changing the ligation of the distal [4Fe4S] cluster in NiFe hydrogenase impairs inter- and intramolecular electron transfers. *Journal of the American Chemical Society* **2006,** *128*, 5209-5218.

56.   Evans, R. M.; Parkin, A.; Roessler, M. M.; Murphy, B. J.; Adamson, H.; Lukey, M. J.; Sargent, F.; Volbeda, A.; Fontecilla-Camps, J. C.; Armstrong, F. A., Principles of Sustained Enzymatic Hydrogen Oxidation in the Presence of Oxygen – The Crucial Influence of High Potential Fe–S Clusters in the Electron Relay of [NiFe]-Hydrogenases. *Journal of the American Chemical Society* **2013,** *135*, 2694-2707.

57.   Lukey, M. J.; Roessler, M. M.; Parkin, A.; Evans, R. M.; Davies, R. A.; Lenz, O.; Friedrich, B.; Sargent, F.; Armstrong, F. A., Oxygen-tolerant [NiFe]-hydrogenases: the individual and collective importance of supernumerary cysteines at the proximal Fe-S cluster. *Journal of the American Chemical Society* **2011,** *133*, 16881-16892.

58.   Volbeda, A.; Martin, L.; Liebgott, P. P.; De Lacey, A. L.; Fontecilla-Camps, J. C., [NiFe]-hydrogenases revisited: nickel-carboxamido bond formation in a variant with accrued O_2-tolerance and a tentative re-interpretation of Ni-SI states. *Metallomics* **2015,** *7* (4), 710-8.

59.   Ogata, H.; Hirota, S.; Nakahara, A.; Komori, H.; Shibata, N.; Kato, T.; Kano, K.; Higuchi, Y., Activation process of [NiFe] hydrogenase elucidated by high-resolution X-ray analyses: conversion of the ready to the unready state. *Structure* **2005,** *13* (11), 1635-42.

60.   Ogata, H.; Kramer, T.; Wang, H.; Schilter, D.; Pelmenschikov, V.; van Gastel, M.; Neese, F.; Rauchfuss, T. B.; Gee, L. B.; Scott, A. D.; Yoda, Y.; Tanaka, Y.; Lubitz, W.; Cramer, S. P., Hydride bridge in [NiFe]-hydrogenase observed by nuclear resonance vibrational spectroscopy. *Nat Commun* **2015,** *6*, 7890.

61.   Ogata, H.; Nishikawa, K.; Lubitz, W., Hydrogens detected by subatomic resolution protein crystallography in a [NiFe] hydrogenase. *Nature* **2015,** *520* (7548), 571-4.

62.   Pandelia, M.-E.; Ogata, H.; Lubitz, W., Intermediates in the Catalytic Cycle of [NiFe] Hydrogenase: Functional Spectroscopy of the Active Site. *ChemPhysChem* **2010,** *11*, 1127-1140.

63.   Pandelia, M. E.; Ogata, H.; Lubitz, W., Intermediates in the catalytic cycle of [NiFe] hydrogenase: functional spectroscopy of the active site. *Chemphyschem* **2010,** *11* (6), 1127-40.

64.   Ogata, H.; Nishikawa, K.; Lubitz, W., Hydrogens detected by subatomic resolution protein crystallography in a [NiFe] hydrogenase. *Nature* **2015,** *520*, 571-574.

65.   Hidalgo, R.; Ash, P. A.; Healy, A. J.; Vincent, K. A., Infrared Spectroscopy During Electrocatalytic Turnover Reveals the Ni-L Active Site State During H_2 Oxidation by a NiFe Hydrogenase. *Angewandte Chemie International Edition* **2015,** *54*, 7110-7113.

66.   Tai, H.; Nishikawa, K.; Inoue, S.; Higuchi, Y.; Hirota, S., FT-IR Characterization of the Light-Induced Ni-L2 and Ni-L3 States of [NiFe] Hydrogenase from Desulfovibrio vulgaris Miyazaki F. *J Phys Chem B* **2015,** *119* (43), 13668-74.

67.   Evans, R. M.; Brooke, E. J.; Wehlin, S. A.; Nomerotskaia, E.; Sargent, F.; Carr, S. B.; Phillips, S. E.; Armstrong, F. A., Mechanism of hydrogen activation by [NiFe] hydrogenases. *Nat Chem Biol* **2016,** *12* (1), 46-50.

68.   Murphy, B. J.; Sargent, F.; Armstrong, F. A., Transforming an oxygen-tolerant [NiFe] uptake hydrogenase into a proficient, reversible hydrogen producer. *Energy & Environmental Science* **2014,** *7* (4), 1426.

69.   Oteri, F.; Baaden, M.; Lojou, E.; Sacquin-Mora, S., Multiscale Simulations Give Insight into the Hydrogen In and Out Pathways of [NiFe]-Hydrogenases from *Aquifex aeolicus* and *Desulfovibrio fructosovorans. The Journal of Physical Chemistry B* **2014,** *118* (48), 13800-11.

70.   Dementin, S.; Burlat, B.; De Lacey, A. L.; Pardo, A.; Adryanczyk-Perrier, G.; Guigliarelli, B.; Fernandez, V. M.; Rousset, M., A glutamate is the essential proton transfer gate during the catalytic cycle of the [NiFe] hydrogenase. *J Biol Chem* **2004,** *279* (11), 10508-13.

71.   Kalms, J.; Schmidt, A.; Frielingsdorf, S.; van der Linden, P.; von Stetten, D.; Lenz, O.; Carpentier, P.; Scheerer, P., Krypton Derivatization of an O_2 -Tolerant Membrane-Bound [NiFe] Hydrogenase Reveals a Hydrophobic Tunnel Network for Gas Transport. *Angew Chem Int Ed Engl* **2016,** *55* (18), 5586-90.

72.   Oteri, F.; Baaden, M.; Lojou, E.; Sacquin-Mora, S., Multiscale simulations give insight into the hydrogen in and out pathways of [NiFe]-hydrogenases from *Aquifex aeolicus* and *Desulfovibrio fructosovorans. J Phys Chem B* **2014,** *118* (48), 13800-11.

73.   Liebgott, P.-P.; Leroux, F.; Burlat, B.; Dementin, S.; Baffert, C.; Lautier, T.; Fourmond, V.; Ceccaldi, P.; Cavazza, C.; Meynial-Salles, I.; Soucaille, P.; Fontecilla-Camps, J. C.; Guigliarelli, B.; Bertrand, P.; Rousset, M.; Léger, C., Relating diffusion along the substrate tunnel and oxygen sensitivity in hydrogenase. *Nature Chemical Biology* **2010,** *6*, 63-70.

74.   van Gastel, M.; Fichtner, C.; Neese, F.; Lubitz, W., EPR experiments to elucidate the structure of the ready and unready states of the [NiFe] hydrogenase

of *Desulfovibrio vulgaris* Miyazaki F. *Biochemical Society Transactions* **2005,** *33*, 7-11.

75.   Wulff, P.; Day, C. C.; Sargent, F.; Armstrong, F. A., How oxygen reacts with oxygen-tolerant respiratory [NiFe]-hydrogenases. *Proc Natl Acad Sci U S A* **2014,** *111* (18), 6606-11.

76.   Carepo, M.; Tierney, D. L.; Brondino, C. D.; Yang, T. C.; Pamplona, A.; Telser, J.; Moura, I.; Moura, J. J. G.; Hoffman, B. M., 17O ENDOR Detection of a Solvent-Derived Ni–(OHx)–Fe Bridge That Is Lost upon Activation of the Hydrogenase from *Desulfovibrio gigas. Journal of the American Chemical Society* **2002,** *124*, 281-286.

77.   Volbeda, A.; Martin, L.; Liebgott, P.-P.; Lacey, A. L. D.; Fontecilla-Camps, J. C., [NiFe]-hydrogenases revisited: nickel–carboxamido bond formation in a variant with accrued O_2-tolerance and a tentative re-interpretation of Ni-SI states. *Metallomics* **2015,** *7* (4), 710-8.

78.   Volbeda, A.; Martin, L.; Cavazza, C.; Matho, M.; Faber, B. W.; Roseboom, W.; Albracht, S. P.; Garcin, E.; Rousset, M.; Fontecilla-Camps, J. C., Structural differences between the ready and unready oxidized states of [NiFe] hydrogenases. *J Biol Inorg Chem* **2005,** *10* (3), 239-49.

79.   van der Zwaan, J. W.; Coremans, J. M.; Bouwens, E. C.; Albracht, S. P., Effect of $^{17}O_2$ and ^{13}CO on EPR spectra of nickel in hydrogenase from *Chromatium vinosum. Biochimica Et Biophysica Acta* **1990,** *1041*, 101-110.

80.   Abou Hamdan, A.; Burlat, B.; Gutiérrez-Sanz, O.; Liebgott, P.-P.; Baffert, C.; De Lacey, A. L.; Rousset, M.; Guigliarelli, B.; Léger, C.; Dementin, S., O_2-independent formation of the inactive states of NiFe hydrogenase. *Nature Chemical Biology* **2013,** *9*, 15-17.

81.   Barilone, J. L.; Ogata, H.; Lubitz, W.; Gastel, M. v., Structural differences between the active sites of the Ni-A and Ni-B states of the [NiFe] hydrogenase: an approach by quantum chemistry and single crystal ENDOR spectroscopy. *Physical Chemistry Chemical Physics* **2015,** *17*, 16204-16212.

82.   Krämer, T.; Kampa, M.; Lubitz, W.; van Gastel, M.; Neese, F., Theoretical Spectroscopy of the NiII Intermediate States in the Catalytic Cycle and the Activation of [NiFe] Hydrogenases. *ChemBioChem* **2013,** *14*, 1898-1905.

83.   Sears, C. L., A dynamic partnership: Celebrating our gut flora. *Anaerobe* **2005,** *11* (5), 247-251.

84.	Tap, J.; Mondot, S.; Levenez, F.; Pelletier, E.; Caron, C.; Furet, J.-P.; Ugarte, E.; Muñoz-Tamayo, R.; Paslier, D. L. E.; Nalin, R.; Dore, J.; Leclerc, M., Towards the human intestinal microbiota phylogenetic core. *Environmental Microbiology* **2009,** *11* (10), 2574-2584.

85.	Wu, G. D.; Chen, J.; Hoffmann, C.; Bittinger, K.; Chen, Y.-Y.; Keilbaugh, S. A.; Bewtra, M.; Knights, D.; Walters, W. A.; Knight, R.; Sinha, R.; Gilroy, E.; Gupta, K.; Baldassano, R.; Nessel, L.; Li, H.; Bushman, F. D.; Lewis, J. D., Linking Long-Term Dietary Patterns with Gut Microbial Enterotypes. *Science (New York, N.y.)* **2011,** *334* (6052), 105-108.

86.	Yatsunenko, T.; Rey, F. E.; Manary, M. J.; Trehan, I.; Dominguez-Bello, M. G.; Contreras, M.; Magris, M.; Hidalgo, G.; Baldassano, R. N.; Anokhin, A. P.; Heath, A. C.; Warner, B.; Reeder, J.; Kuczynski, J.; Caporaso, J. G.; Lozupone, C. A.; Lauber, C.; Clemente, J. C.; Knights, D.; Knight, R.; Gordon, J. I., Human gut microbiome viewed across age and geography. *Nature* **2012,** *486* (7402), 222-227.

87.	Turnbaugh, P. J.; Hamady, M.; Yatsunenko, T.; Cantarel, B. L.; Duncan, A.; Ley, R. E.; Sogin, M. L.; Jones, W. J.; Roe, B. A.; Affourtit, J. P.; Egholm, M.; Henrissat, B.; Heath, A. C.; Knight, R.; Gordon, J. I., A core gut microbiome in obese and lean twins. *Nature* **2009,** *457*, 480-484.

88.	Batt, R. M.; Rutgers, H. C.; Sancak, A. A., Enteric bacteria: Friend or foe? *Journal of Small Animal Practice* **1996,** *37* (6), 261-267.

89.	Sommer, F.; Backhed, F., The gut microbiota - masters of host development and physiology. *Nat Rev Micro* **2013,** *11* (4), 227-238.

90.	Mantis, N. J.; Rol, N.; Corthésy, B., Secretory IgA's Complex Roles in Immunity and Mucosal Homeostasis in the Gut. *Mucosal immunology* **2011,** *4* (6), 603-611.

91.	Clarke, G.; Stilling, R. M.; Kennedy, P. J.; Stanton, C.; Cryan, J. F.; Dinan, T. G., Minireview: Gut Microbiota: The Neglected Endocrine Organ. *Molecular Endocrinology* **2014,** *28* (8), 1221-1238.

92.	Gibson, G. R., Fibre and effects on probiotics (the prebiotic concept). *Clinical Nutrition Supplements* **2004,** *1* (2), 25-31.

93.	Milani, C.; Ticinesi, A.; Gerritsen, J.; Nouvenne, A.; Lugli, G. A.; Mancabelli, L.; Turroni, F.; Duranti, S.; Mangifesta, M.; Viappiani, A.; Ferrario, C.; Maggio, M.; Lauretani, F.; De Vos, W.; van Sinderen, D.; Meschi, T.; Ventura, M., Gut microbiota

composition and *Clostridium difficile* infection in hospitalized elderly individuals: a metagenomic study. *Scientific Reports* **2016,** *6*, 25945.

94.   Bouza, E., Consequences of *Clostridium difficile* infection: understanding the healthcare burden. *Clinical Microbiology and Infection 18*, 5-12.

95.   Guarner, F.; Malagelada, J.-R., Gut flora in health and disease. *The Lancet* **2003,** *361* (9356), 512-519.

96.   Shen, S.; Wong, C. H. Y., Bugging inflammation: role of the gut microbiota. *Clinical & Translational Immunology* **2016,** *5* (4), e72.

97.   Wolf, P. G.; Biswas, A.; Morales, S. E.; Greening, C.; Gaskins, H. R., H metabolism is widespread and diverse among human colonic microbes. *Gut Microbes* **2016,** *7* (3), 235-245.

98.   Maier, R. J.; Olczak, A.; Maier, S.; Soni, S.; Gunn, J., Respiratory hydrogen use by *Salmonella enterica* serovar Typhimurium is essential for virulence. *Infection and immunity* **2004,** *72*, 6294-6299.

99.   Lam, L. H.; Monack, D. M., Intraspecies competition for niches in the distal gut dictate transmission during persistent *Salmonella* infection. *PLoS Pathog* **2014,** *10* (12), e1004527.

100.   Maier, L.; Vyas, R.; Cordova, C. D.; Lindsay, H.; Schmidt, T. S. B.; Brugiroux, S.; Periaswamy, B.; Bauer, R.; Sturm, A.; Schreiber, F.; von Mering, C.; Robinson, M. D.; Stecher, B.; Hardt, W.-D., Microbiota-Derived Hydrogen Fuels *Salmonella Typhimurium* Invasion of the Gut Ecosystem. *Cell Host & Microbe* **2013,** *14*, 641-651.

101.   Lamichhane-Khadka, R.; Benoit, S. L.; Miller-Parks, E. F.; Maier, R. J., Host hydrogen rather than that produced by the pathogen is important for *Salmonella enterica* serovar Typhimurium virulence. *Infect Immun* **2015,** *83* (1), 311-6.

102.   Carroll, K. C., Chapter 15: Enteric Gram-Negative Rods (Enterobacteriaceae). In *Jawetz, Melnick, & Adelberg's Medical Microbiology*, 26 ed.; Brooks, G. F.; Carroll, K. C.; Butel, J. S.; Morse, S. A.; Mietzner, T. A., Eds. McGraw-Hill Medical: 2013.

103.   Schierack, P.; Walk, N.; Reiter, K.; Weyrauch, K. D.; Wieler, L. H., Composition of intestinal Enterobacteriaceae populations of healthy domestic pigs. *Microbiology* **2007,** *153* (Pt 11), 3830-7.

104.   Donnenberg, M. S., Pathogenic strategies of enteric bacteria. *Nature* **2000,** *406* (6797), 768-774.

105.   Littman, Dan R.; Pamer, Eric G., Role of the Commensal Microbiota in Normal and Pathogenic Host Immune Responses. *Cell Host & Microbe* **2011,** *10* (4), 311-323.

106.   Blake, D. P.; Hillman, K.; Fenlon, D. R.; Low, J. C., Transfer of antibiotic resistance between commensal and pathogenic members of the Enterobacteriaceae under ileal conditions. *Journal of Applied Microbiology* **2003,** *95* (3), 428 - 436.

107.   Jantsch, J.; Chikkaballi, D.; Hensel, M., Cellular aspects of immunity to intracellular *Salmonella enterica*. *Immunological Reviews* **2011,** *240* (1), 185-195.

108.   Kaur, J.; Jain, S. K., Role of antigens and virulence factors of *Salmonella enterica* serovar Typhi in its pathogenesis. *Microbiological Research* **2012,** *167* (4), 199-210.

109.   Yoon, H.; Ansong, C.; Adkins, J. N.; Heffron, F., Discovery of *Salmonella* Virulence Factors Translocated via Outer Membrane Vesicles to Murine Macrophages. *Infection and Immunity* **2011,** *79* (6), 2182-2192.

110.   Lamichhane-Khadka, R.; Kwiatkowski, A.; Maier, R. J., The Hyb hydrogenase permits hydrogen-dependent respiratory growth of *Salmonella enterica* serovar Typhimurium. *MBio* **2010,** *1* (5).

111.   Bentley, R.; Meganathan, R., Biosynthesis of vitamin K (menaquinone) in bacteria. *Microbiological Reviews* **1982,** *46* (3), 241-280.

112.   Johnson, J. R., Virulence factors in *Escherichia coli* urinary tract infection. *Clinical Microbiology Reviews* **1991,** *4* (1), 80-128.

113.   Robins-Browne, R. M.; Bordun, A.-M.; Tauschek, M.; Bennett-Wood, V. R.; Russell, J.; Oppedisano, F.; Lister, N. A.; Bettelheim, K. A.; Fairley, C. K.; Sinclair, M. I.; Hellard, M. E., *Escherichia coli* and Community-acquired Gastroenteritis, Melbourne, Australia. *Emerging Infectious Diseases* **2004,** *10* (10), 1797-1805.

114.   Gaschignard, J.; Levy, C.; Bingen, E.; Cohen, R., Pédiatrique Épidémiologie des méningites néonatales à *Escherichia coli*. *Archives de Pédiatrie* **2012,** *19*, S129-S134.

115.   Sawers, G., The hydrogenases and formate dehydrogenases of *Escherichia coli*. *Antonie van Leeuwenhoek* **1994,** *66*, 57-88.

116.   Self, W. T.; Hasona, A.; Shanmugam, K. T., Expression and Regulation of a Silent Operon, hyf, Coding for Hydrogenase 4 Isoenzyme in *Escherichia coli*. *Journal of Bacteriology* **2004,** *186*, 580-587.

117.   Altschul, S. F.; Gish, W.; Miller, W.; Myers, E. W.; Lipman, D. J., Basic local alignment search tool. *Journal of Molecular Biology* **1990,** *215* (3), 403-410.

118.   Kroger, C.; Colgan, A.; Srikumar, S.; Handler, K.; Sivasankaran, S. K.; Hammarlof, D. L.; Canals, R.; Grissom, J. E.; Conway, T.; Hokamp, K.; Hinton, J. C., An infection-relevant transcriptomic compendium for *Salmonella enterica* Serovar Typhimurium. *Cell Host Microbe* **2013,** *14* (6), 683-95.

119.   Zbell, A. L.; Maier, S. E.; Maier, R. J., *Salmonella enterica* Serovar Typhimurium NiFe Uptake-Type Hydrogenases Are Differentially Expressed In Vivo. *Infection and Immunity* **2008,** *76*, 4445-4454.

120.   Richard, D. J.; Sawers, G.; Sargent, F.; McWalter, L.; Boxer, D. H., Transcriptional regulation in response to oxygen and nitrate of the operons encoding the [NiFe] hydrogenases 1 and 2 of *Escherichia coli*. *Microbiology (Reading, England)* **1999,** *145 (Pt 10)*, 2903-2912.

121.   Brøndsted, L.; Atlung, T., Anaerobic regulation of the hydrogenase 1 (hya) operon of *Escherichia coli*. *Journal of Bacteriology* **1994,** *176*, 5423-5428.

122.   Yoshida, M.; Ishihama, A.; Yamamoto, K., Cross talk in promoter recognition between six NarL-family response regulators of *Escherichia coli* two-component system. *Genes Cells* **2015,** *20* (7), 601-12.

123.   King, P. W.; Przybyla, A. E., Response of hya expression to external pH in *Escherichia coli*. *Journal of bacteriology* **1999,** *181*, 5250-5256.

124.   Pinske, C.; Gary Sawers, R., The role of the ferric-uptake regulator Fur and iron homeostasis in controlling levels of the [NiFe]-hydrogenases in *Escherichia coli*. *International Journal of Hydrogen Energy* **2010,** *35*, 8938-8944.

125.   Pinske, C.; Sawers, G., Iron restriction induces preferential down-regulation of H_2-consuming over H_2-evolving reactions during fermentative growth of *Escherichia coli*. *BMC Microbiology* **2011,** *11*, 196.

126.   Hantke, K., Regulation of ferric iron transport in *Escherichia coli* K12: Isolation of a constitutive mutant. *Molecular and General Genetics MGG* **1981,** *182*, 288-292.

127.   Pinske, C.; Gary Sawers, R., The role of the ferric-uptake regulator Fur and iron homeostasis in controlling levels of the [NiFe]-hydrogenases in *Escherichia coli*. *International Journal of Hydrogen Energy* **2010,** *35* (17), 8938-8944.

128.   Chivers, P. T.; Benanti, E. L.; Heil-Chapdelaine, V.; Iwig, J. S.; Rowe, J. L., Identification of Ni-(L-His)$_2$ as a substrate for NikABCDE-dependent nickel uptake in *Escherichia coli. Metallomics: integrated biometal science* **2012,** *4*, 1043-1050.

129.   Rowe, J. L.; Starnes, G. L.; Chivers, P. T., Complex Transcriptional Control Links NikABCDE-Dependent Nickel Transport with Hydrogenase Expression in *Escherichia coli. Journal of Bacteriology* **2005,** *187*, 6317-6323.

130.   Sawers, R. G.; Ballantine, S. P.; Boxer, D. H., Differential expression of hydrogenase isoenzymes in *Escherichia coli* K-12: evidence for a third isoenzyme. *Journal of Bacteriology* **1985,** *164*, 1324-1331.

131.   Dharmadi, Y.; Murarka, A.; Gonzalez, R., Anaerobic fermentation of glycerol by *Escherichia coli*: a new platform for metabolic engineering. *Biotechnology and bioengineering* **2006,** *94*, 821-829.

132.   Pinske, C.; McDowall, J. S.; Sargent, F.; Sawers, R. G., Analysis of hydrogenase 1 levels reveals an intimate link between carbon and hydrogen metabolism in *Escherichia coli* K-12. *Microbiology* **2012,** *158*, 856-868.

133.   Jacobi, A.; Rossmann, R.; Böck, A., The hyp operon gene products are required for the maturation of catalytically active hydrogenase isoenzymes in *Escherichia coli. Archives of microbiology* **1992,** *158*, 444-451.

134.   Maier, T.; Binder, U.; Böck, A., Analysis of the hydA locus of *Escherichia coli*: two genes (hydN and hypF) involved in formate and hydrogen metabolism. *Archives of Microbiology* **1996,** *165*, 333-341.

135.   Hopper, S.; Babst, M.; Schlensog, V.; Fischer, H. M.; Hennecke, H.; Böck, A., Regulated expression in vitro of genes coding for formate hydrogenlyase components of *Escherichia coli. Journal of Biological Chemistry* **1994,** *269*, 19597-19604.

136.   Messenger, S. L.; Green, J., FNR-mediated regulation of hyp expression in *Escherichia coli. FEMS microbiology letters* **2003,** *228*, 81-86.

137.   Partridge, J. D.; Bodenmiller, D. M.; Humphrys, M. S.; Spiro, S., NsrR targets in the *Escherichia coli* genome: new insights into DNA sequence requirements for

binding and a role for NsrR in the regulation of motility. *Molecular Microbiology* **2009,** *73*, 680–694.

138.   Gardner, P. R.; Gardner, A. M.; Martin, L. A.; Salzman, A. L., Nitric oxide dioxygenase: An enzymic function for flavohemoglobin. *Proceedings of the National Academy of Sciences* **1998,** *95*, 10378-10383.

139.   Lutz, S.; Jacobi, A.; Schlensog, V.; Böhm, R.; Sawers, G.; Böck, A., Molecular characterization of an operon (hyp) necessary for the activity of the three hydrogenase isoenzymes in *Escherichia coli. Molecular microbiology* **1991,** *5*, 123-135.

140.   Lacasse, M. J.; Zamble, D. B., [NiFe]-Hydrogenase Maturation. *Biochemistry* **2016,** *55* (12), 1689-701.

141.   Paschos, A.; Bauer, A.; Zimmermann, A.; Zehelein, E.; Bock, A., HypF, a carbamoyl phosphate-converting enzyme involved in [NiFe] hydrogenase maturation. *J Biol Chem* **2002,** *277* (51), 49945-51.

142.   Petkun, S.; Shi, R.; Li, Y.; Asinas, A.; Munger, C.; Zhang, L.; Waclawek, M.; Soboh, B.; Sawers, R. G.; Cygler, M., Structure of hydrogenase maturation protein HypF with reaction intermediates shows two active sites. *Structure (London, England: 1993)* **2011,** *19*, 1773-1783.

143.   Shomura, Y.; Higuchi, Y., Structural basis for the reaction mechanism of S-carbamoylation of HypE by HypF in the maturation of [NiFe]-hydrogenases. *J Biol Chem* **2012,** *287* (34), 28409-19.

144.   Watanabe, S.; Matsumi, R.; Atomi, H.; Imanaka, T.; Miki, K., Crystal structures of the HypCD complex and the HypCDE ternary complex: transient intermediate complexes during [NiFe] hydrogenase maturation. *Structure (London, England: 1993)* **2012,** *20*, 2124-2137.

145.   Stripp, S. T.; Soboh, B.; Lindenstrauss, U.; Braussemann, M.; Herzberg, M.; Nies, D. H.; Sawers, R. G.; Heberle, J., HypD Is the Scaffold Protein for Fe-(CN)$_2$CO Cofactor Assembly in [NiFe]-Hydrogenase Maturation. *Biochemistry* **2013,** *52*, 3289-3296.

146.   Soboh, B.; Stripp, S. T.; Bielak, C.; Lindenstrauß, U.; Braussemann, M.; Javaid, M.; Hallensleben, M.; Granich, C.; Herzberg, M.; Heberle, J.; Sawers, R. G., The [NiFe]-hydrogenase accessory chaperones HypC and HybG of *Escherichia coli* are iron- and carbon dioxide-binding proteins. *FEBS Letters* **2013,** *587*, 2512-2516.

147.   Blokesch, M.; Böck, A., Maturation of [NiFe]-hydrogenases in *Escherichia coli*: The HypC Cycle. *Journal of Molecular Biology* **2002,** *324* (2), 287-296.

148.   Drapal, N.; Bock, A., Interaction of the hydrogenase accessory protein HypC with HycE, the large subunit of *Escherichia coli* hydrogenase 3 during enzyme maturation. *Biochemistry* **1998,** *37*, 2941-2948.

149.   Magalon, A.; Bock, A., Analysis of the HypC-hycE complex, a key intermediate in the assembly of the metal center of the *Escherichia coli* hydrogenase 3. *The Journal of biological chemistry* **2000,** *275*, 21114-21120.

150.   Rowe, J. L.; Starnes, G. L.; Chivers, P. T., Complex transcriptional control links NikABCDE-dependent nickel transport with hydrogenase expression in *Escherichia coli. J Bacteriol* **2005,** *187* (18), 6317-23.

151.   Maier, T.; Lottspeich, F.; Böck, A., GTP Hydrolysis by HypB is Essential for Nickel Insertion into Hydrogenases of *Escherichia Coli. European Journal of Biochemistry* **1995,** *230*, 133–138.

152.   Olson, J. W.; Mehta, N. S.; Maier, R. J., Requirement of nickel metabolism proteins HypA and HypB for full activity of both hydrogenase and urease in *Helicobacter pylori. Molecular Microbiology* **2001,** *39*, 176–182.

153.   Pinske, C.; Sargent, F.; Sawers, R. G., SlyD-dependent nickel delivery limits maturation of [NiFe]-hydrogenases in late-stationary phase *Escherichia coli* cells. *Metallomics* **2015,** *7* (4), 683-90.

154.   Leach, M. R.; Zhang, J. W.; Zamble, D. B., The role of complex formation between the *Escherichia coli* hydrogenase accessory factors HypB and SlyD. *The Journal of biological chemistry* **2007,** *282*, 16177-16186.

155.   Blokesch, M.; Rohrmoser, M.; Rode, S.; Böck, A., HybF, a Zinc-Containing Protein Involved in NiFe Hydrogenase Maturation. *Journal of Bacteriology* **2004,** *186* (9), 2603-2611.

156.   Hube, M.; Blokesch, M.; Böck, A., Network of Hydrogenase Maturation in *Escherichia coli*: Role of Accessory Proteins HypA and HybF. *Journal of Bacteriology* **2002,** *184* (14), 3879-3885.

157.   Pinske, C.; Sawers, R. G., Delivery of iron-sulfur clusters to the hydrogen-oxidizing [NiFe]-hydrogenases in *Escherichia coli* requires the A-type carrier proteins ErpA and IscA. *PLoS One* **2012,** *7* (2), e31755.

158.   Vinella, D.; Brochier-Armanet, C.; Loiseau, L.; Talla, E.; Barras, F., Iron-sulfur (Fe/S) protein biogenesis: phylogenomic and genetic studies of A-type carriers. *PLoS genetics* **2009,** *5*, e1000497.

159.   Bowman, L.; Balbach, J.; Walton, J.; Sargent, F.; Parkin, A., Biosynthesis of *Salmonella enterica* [NiFe]-hydrogenase-5: probing the roles of system-specific accessory proteins. *JBIC Journal of Biological Inorganic Chemistry* **2016**, 1-9.

160.   Fritsche, E.; Paschos, A.; Beisel, H. G.; Böck, A.; Huber, R., Crystal structure of the hydrogenase maturating endopeptidase HYBD from *Escherichia coli. Journal of molecular biology* **1999,** *288*, 989-998.

161.   Magalon, A.; Böck, A., Dissection of the maturation reactions of the [NiFe] hydrogenase 3 from *Escherichia coli* taking place after nickel incorporation. *FEBS Letters* **2000,** *473*, 254-258.

162.   Binder, U.; Maier, T.; Böck, A., Nickel incorporation into hydrogenase 3 from *Escherichia coli* requires the precursor form of the large subunit. *Archives of Microbiology* **1996,** *165*, 69-72.

163.   Berks, B. C., A common export pathway for proteins binding complex redox cofactors? *Molecular microbiology* **1996,** *22*, 393-404.

164.   Berks, B. C.; Sargent, F.; Palmer, T., The Tat protein export pathway. *Molecular Microbiology* **2000,** *35*, 260–274.

165.   Yahr, T. L.; Wickner, W. T., Functional reconstitution of bacterial Tat translocation in vitro. *The EMBO journal* **2001,** *20*, 2472-2479.

166.   Rodrigue, A.; Chanal, A.; Beck, K.; Müller, M.; Wu, L. F., Co-translocation of a periplasmic enzyme complex by a hitchhiker mechanism through the bacterial tat pathway. *The Journal of biological chemistry* **1999,** *274*, 13223-13228.

167.   Dubini, A.; Sargent, F., Assembly of Tat-dependent [NiFe] hydrogenases: identification of precursor-binding accessory proteins. *FEBS letters* **2003,** *549*, 141-146.

168.   Menon, N. K.; Robbins, J.; Peck, H. D., Jr; Chatelus, C. Y.; Choi, E. S.; Przybyla, A. E., Cloning and sequencing of a putative *Escherichia coli* [NiFe] hydrogenase-1 operon containing six open reading frames. *Journal of bacteriology* **1990,** *172*, 1969-1977.

169.   McKinlay, J. B.; Harwood, C. S., Photobiological production of hydrogen gas as a biofuel. *Current Opinion in Biotechnology* **2010,** *21* (3), 244-251.

170.   Volbeda, A.; Fontecilla-Camps, J. C., Structural bases for the catalytic mechanism of Ni-containing carbon monoxide dehydrogenases. *Dalton Transactions* **2005,** (21), 3443-3450.

171.   Solomon, E. I.; Sundaram, U. M.; Machonkin, T. E., Multicopper Oxidases and Oxygenases. *Chemical Reviews* **1996,** *96* (7), 2563-2606.

172.   Pita, M.; Gutierrez-Sanchez, C.; Olea, D.; Velez, M.; Garcia-Diego, C.; Shleev, S.; Fernandez, V. M.; De Lacey, A. L., High Redox Potential Cathode Based on Laccase Covalently Attached to Gold Electrode. *The Journal of Physical Chemistry C* **2011,** *115* (27), 13420-13428.

173.   Volkov, A. G., The electrochemical mechanism of photosystem II functioning in chloroplasts. *Journal of Electroanalytical Chemistry and Interfacial Electrochemistry* **1986,** *205* (1), 245-257.

174.   Kung, Y.; Doukov, T. I.; Seravalli, J.; Ragsdale, S. W.; Drennan, C. L., Crystallographic Snapshots of Cyanide- and Water-Bound C-Clusters from Bifunctional Carbon Monoxide Dehydrogenase/Acetyl-CoA Synthase. *Biochemistry* **2009,** *48* (31), 7432-7440.

175.   Serrano-Posada, H.; Centeno-Leija, S.; Rojas-Trejo, S. P.; Rodriguez-Almazan, C.; Stojanoff, V.; Rudino-Pinera, E., X-ray-induced catalytic active-site reduction of a multicopper oxidase: structural insights into the proton-relay mechanism and O_2-reduction states. *Acta Crystallographica Section D* **2015,** *71* (12), 2396-2411.

176.   Schindelin, H.; Kisker, C.; Schlessman, J. L.; Howard, J. B.; Rees, D. C., Structure of ADP.AIF4-stabilized nitrogenase complex and its implications for signal transduction. *Nature* **1997,** *387* (6631), 370-376.

177.   STIEFEL, E. I.; GEORGE, G. N., Ferredoxins, Hydrogenases, and Nitrogenases: Metal-Sulfide Proteins. In *Bioinorganic Chemistry*, Bertini, I.; Gray, H. B.; Lippard, S. J.; Valentine, J. S., Eds. University Science Books: Mill Valley, CA, 1994; pp 365-453.

178.   Suga, M.; Akita, F.; Hirata, K.; Ueno, G.; Murakami, H.; Nakajima, Y.; Shimizu, T.; Yamashita, K.; Yamamoto, M.; Ago, H.; Shen, J.-R., Native structure of photosystem II at 1.95 A resolution viewed by femtosecond X-ray pulses. *Nature* **2015,** *517* (7532), 99-103.

179.   Horak, K. T.; VanderVelde, D. G.; Agapie, T., Tuning of Metal Complex Electronics and Reactivity by Remote Lewis Acid Binding to π-Coordinated Pyridine Diphosphine Ligands. *Organometallics* **2015,** *34* (19), 4753-4765.

180. Burgess, B. K.; Lowe, D. J., Mechanism of Molybdenum Nitrogenase. *Chemical Reviews* **1996,** *96* (7), 2983-3012.

181. Megiatto, J. D.; Antoniuk-Pablant, A.; Sherman, B. D.; Kodis, G.; Gervaldo, M.; Moore, T. A.; Moore, A. L.; Gust, D., Mimicking the electron transfer chain in photosystem II with a molecular triad thermodynamically capable of water oxidation. *Proceedings of the National Academy of Sciences* **2012,** *109* (39), 15578-15583.

182. Shleev, S.; Christenson, A.; Serezhenkov, V.; Burbaev, D.; Yaropolov, A.; Gorton, L.; Ruzgas, T., Electrochemical redox transformations of T1 and T2 copper sites in native *Trametes hirsuta* laccase at gold electrode. *Biochemical Journal* **2005,** *385* (3), 745-754.

183. Schultz, F. A.; Gheller, S. F.; Burgess, B. K.; Lough, S.; Newton, W. E., Electrochemical characterization of the iron-molybdenum cofactor from *Azotobacter vinelandii* nitrogenase. *Journal of the American Chemical Society* **1985,** *107* (19), 5364-5368.

184. Wang, V. C.; Ragsdale, S. W.; Armstrong, F. A., Investigations of two bidirectional carbon monoxide dehydrogenases from *Carboxydothermus hydrogenoformans* by protein film electrochemistry. *Chembiochem* **2013,** *14* (14), 1845-51.

185. Wang, V. C. C.; Islam, S. T. A.; Can, M.; Ragsdale, S. W.; Armstrong, F. A., Investigations by Protein Film Electrochemistry of Alternative Reactions of Nickel-Containing Carbon Monoxide Dehydrogenase. *The Journal of Physical Chemistry B* **2015,** *119* (43), 13690-13697.

186. Yehezkeli, O.; Tel-Vered, R.; Wasserman, J.; Trifonov, A.; Michaeli, D.; Nechushtai, R.; Willner, I., Integrated photosystem II-based photo-bioelectrochemical cells. *Nat Commun* **2012,** *3*, 742.

187. Lamle, S. E.; Vincent, K. A.; Halliwell, L. M.; Albracht, S. P. J.; Armstrong, F. A., Hydrogenase on an electrode: a remarkable heterogeneous catalyst. *Dalton Transactions* **2003**, 4152-4157.

188. Blanford, C. F.; Armstrong, F. A., The pyrolytic graphite surface as an enzyme substrate: microscopic and spectroscopic studies. *Journal of Solid State Electrochemistry* **2006,** *10* (10), 826-832.

189.   Léger, C.; Bertrand, P., Direct Electrochemistry of Redox Enzymes as a Tool for Mechanistic Studies. *Chemical Reviews* **2008,** *108*, 2379-2438.

190.   Fernandez, V. M.; Hatchikian, E. C.; Patil, D. S.; Cammack, R., ESR-detectable nickel and iron-sulphur centres in relation to the reversible activation of *Desulfovibrio gigas* hydrogenase. *Biochimica et Biophysica Acta (BBA) - General Subjects* **1986,** *883*, 145-154.

191.   Abou Hamdan, A.; Dementin, S.; Liebgott, P.-P.; Gutierrez-Sanz, O.; Richaud, P.; De Lacey, A. L.; Rousset, M.; Bertrand, P.; Cournac, L.; Léger, C., Understanding and Tuning the Catalytic Bias of Hydrogenase. *Journal of the American Chemical Society* **2012,** *134*, 8368-8371.

192.   Hexter, S. V.; Esterle, T. F.; Armstrong, F. A., A unified model for surface electrocatalysis based on observations with enzymes. *Physical Chemistry Chemical Physics* **2014,** *16*, 11822-11833.

193.   Hexter, S. V.; Grey, F.; Happe, T.; Climent, V.; Armstrong, F. A., Electrocatalytic mechanism of reversible hydrogen cycling by enzymes and distinctions between the major classes of hydrogenases. *Proceedings of the National Academy of Sciences of the United States of America* **2012,** *109*, 11516-11521.

194.   Vincent, K. A.; Parkin, A.; Lenz, O.; Albracht, S. P. J.; Fontecilla-Camps, J. C.; Cammack, R.; Friedrich, B.; Armstrong, F. A., Electrochemical Definitions of O_2 Sensitivity and Oxidative Inactivation in Hydrogenases. *Journal of the American Chemical Society* **2005,** *127*, 18179-18189.

195.   Jones, A. K.; Lamle, S. E.; Pershad, H. R.; Vincent, K. A.; Albracht, S. P. J.; Armstrong, F. A., Enzyme Electrokinetics: Electrochemical Studies of the Anaerobic Interconversions between Active and Inactive States of *Allochromatium vinosum* [NiFe]-hydrogenase. *Journal of the American Chemical Society* **2003,** *125*, 8505-8514.

196.   Fourmond, V.; Infossi, P.; Giudici-Orticoni, M.-T.; Bertrand, P.; Léger, C., "Two-Step" Chronoamperometric Method for Studying the Anaerobic Inactivation of an Oxygen Tolerant NiFe Hydrogenase. *Journal of the American Chemical Society* **2010,** *132*, 4848-4857.

197. Fernández, V. M.; Aguirre, R.; Hatchikian, E. C., Reductive activation and redox properties of hydrogenase from *Desulfovibrio gigas*. *Biochimica et Biophysica Acta (BBA) - Protein Structure and Molecular Enzymology* **1984,** *790* (1), 1-7.

198. Hamdan, A. A.; Liebgott, P.-P.; Fourmond, V.; Gutiérrez-Sanz, O.; Lacey, A. L. D.; Infossi, P.; Rousset, M.; Dementin, S.; Léger, C., Relation between anaerobic inactivation and oxygen tolerance in a large series of NiFe hydrogenase mutants. *Proceedings of the National Academy of Sciences* **2012,** *109*, 19916-19921.

199. Radu, V.; Frielingsdorf, S.; Evans, S. D.; Lenz, O.; Jeuken, L. J. C., Enhanced Oxygen-Tolerance of the Full Heterotrimeric Membrane-Bound [NiFe]-Hydrogenase of *Ralstonia eutropha*. *Journal of the American Chemical Society* **2014,** *136*, 8512-8515.

200. Page, C. C.; Moser, C. C.; Chen, X.; Dutton, P. L., Natural engineering principles of electron tunnelling in biological oxidation–reduction. *Nature* **1999,** *402*, 47-52.

201. Frielingsdorf, S.; Schubert, T.; Pohlmann, A.; Lenz, O.; Friedrich, B., A Trimeric Supercomplex of the Oxygen-Tolerant Membrane-Bound [NiFe]-Hydrogenase from *Ralstonia eutropha* H16. *Biochemistry* **2011,** *50*, 10836-10843.

202. Radu, V.; Frielingsdorf, S.; Lenz, O.; Jeuken, L. J., Reactivation from the Ni-B state in [NiFe] hydrogenase of *Ralstonia eutropha* is controlled by reduction of the superoxidised proximal cluster. *Chem Commun (Camb)* **2016,** *52* (12), 2632-5.

203. Hulanicki, A.; Głąb, S., Analytical Chemistry Division Commission on Analytical Reactions and Reagents+. In *Redox Indicators. Characteristics and Applications*, Pergamon: 1978; p 465.

204. Pandelia, M.-E.; Fourmond, V.; Tron-Infossi, P.; Lojou, E.; Bertrand, P.; Léger, C.; Giudici-Orticoni, M.-T.; Lubitz, W., Membrane-Bound Hydrogenase I from the Hyperthermophilic Bacterium *Aquifex aeolicus*: Enzyme Activation, Redox Intermediates and Oxygen Tolerance. *Journal of the American Chemical Society* **2010,** *132*, 6991-7004.

205. Michaelis, L.; Eagle, H., Some Redox Indicators. *The Journal of biological chemistry* **1930,** *87*, 713-727.

206. Cracknell, J. A.; Wait, A. F.; Lenz, O.; Friedrich, B.; Armstrong, F. A., A kinetic and thermodynamic understanding of O_2 tolerance in [NiFe]-hydrogenases. *Proceedings of the National Academy of Sciences* **2009,** *106*, 20681-20686.

207.   Lenz, O.; Ludwig, M.; Schubert, T.; Bürstel, I.; Ganskow, S.; Goris, T.; Schwarze, A.; Friedrich, B., H2 Conversion in the Presence of O$_2$ as Performed by the Membrane-Bound [NiFe]-Hydrogenase of *Ralstonia eutropha*. *ChemPhysChem* **2010,** *11*, 1107-1119.

208.   Saggu, M.; Zebger, I.; Ludwig, M.; Lenz, O.; Friedrich, B.; Hildebrandt, P.; Lendzian, F., Spectroscopic Insights into the Oxygen-tolerant Membrane-associated [NiFe] Hydrogenase of *Ralstonia eutropha* H16. *Journal of Biological Chemistry* **2009,** *284*, 16264-16276.

209.   Goris, T.; Wait, A. F.; Saggu, M.; Fritsch, J.; Heidary, N.; Stein, M.; Zebger, I.; Lendzian, F.; Armstrong, F. A.; Friedrich, B.; Lenz, O., A unique iron-sulfur cluster is crucial for oxygen tolerance of a [NiFe]-hydrogenase. *Nature Chemical Biology* **2011,** *7*, 310-318.

210.   Dance, I., What is the trigger mechanism for the reversal of electron flow in oxygen-tolerant [NiFe] hydrogenases? *Chem. Sci.* **2015,** *6* (2), 1433-1443.

211.   Forzi, L.; Sawers, R. G., Maturation of [NiFe]-hydrogenases in *Escherichia coli*. *BioMetals* **2007,** *20*, 565-578.

212.   Pinske, C.; Sawers, R. G., Delivery of Iron-Sulfur Clusters to the Hydrogen-Oxidizing [NiFe]-Hydrogenases in *Escherichia coli* Requires the A-Type Carrier Proteins ErpA and IscA. *PLoS ONE* **2012,** *7*, e31755.

213.   Vincent, K. A.; Cracknell, J. A.; Lenz, O.; Zebger, I.; Friedrich, B.; Armstrong, F. A., Electrocatalytic hydrogen oxidation by an enzyme at high carbon monoxide or oxygen levels. *Proceedings of the National Academy of Sciences of the United States of America* **2005,** *102* (47), 16951-16954.

214.   Hamilton, C. M.; Aldea, M.; Washburn, B. K.; Babitzke, P.; Kushner, S. R., New method for generating deletions and gene replacements in *Escherichia coli*. *Journal of Bacteriology* **1989,** *171*, 4617-4622.

215.   Heermann, R.; Zeppenfeld, T.; Jung, K., Simple generation of site-directed point mutations in the *Escherichia coli* chromosome using Red®/ET® Recombination. *Microbial Cell Factories* **2008,** *7*, 14.

216.   Wang, J.; Sarov, M.; Rientjes, J.; Hu, J.; Hollak, H.; Kranz, H.; Xie, Y.; Stewart, A. F.; Zhang, Y., An improved recombineering approach by adding RecA to λ Red recombination. *Molecular Biotechnology* **2006,** *32* (1), 43-53.

217.	Zhang, Y.; Buchholz, F.; Muyrers, J. P. P.; Stewart, A. F., A new logic for DNA engineering using recombination in *Escherichia coli*. *Nat Genet* **1998,** *20* (2), 123-128.

218.	Datsenko, K. A.; Wanner, B. L., One-step inactivation of chromosomal genes in *Escherichia coli* K-12 using PCR products. *Proceedings of the National Academy of Sciences* **2000,** *97*, 6640-6645.

219.	Hayashi, K.; Morooka, N.; Yamamoto, Y.; Fujita, K.; Isono, K.; Choi, S.; Ohtsubo, E.; Baba, T.; Wanner, B. L.; Mori, H.; Horiuchi, T., Highly accurate genome sequences of *Escherichia coli* K‑12 strains MG1655 and W3110. *Molecular Systems Biology* **2006,** *2*, 2006.0007.

220.	Casadaban, M. J.; Cohen, S. N., Analysis of gene control signals by DNA fusion and cloning in *Escherichia coli*. *Journal of Molecular Biology* **1980,** *138* (2), 179-207.

221.	Hanahan, D., Techniques for transformation of E. coli. In *DNA cloning: a practical approach*, Glover, D. M., Ed. IRL Press: Oxford, United Kingdom, 1985; Vol. 1, pp 109-135.

222.	Wulff, P.; Day, C. C.; Sargent, F.; Armstrong, F. A., How oxygen reacts with oxygen-tolerant respiratory [NiFe]-hydrogenases. *Proceedings of the National Academy of Sciences* **2014,** *111*, 6606-6611.

223.	Worth, C. L.; Preissner, R.; Blundell, T. L., SDM: a server for predicting effects of mutations on protein stability and malfunction. *Nucleic Acids Res* **2011,** *39* (Web Server issue), W215-22.

224.	Wright, J. J.; Salvadori, E.; Bridges, H. R.; Hirst, J.; Roessler, M. M., Small-volume potentiometric titrations: EPR investigations of Fe-S cluster N_2 in mitochondrial complex I. *Journal of Inorganic Biochemistry* **2016**.

225.	Armstrong, F. A.; Evans, R. M.; Hexter, S. V.; Murphy, B. J.; Roessler, M. M.; Wulff, P., Guiding Principles of Hydrogenase Catalysis Instigated and Clarified by Protein Film Electrochemistry. *Acc Chem Res* **2016,** *49* (5), 884-92.

226.	Flanagan, L. A.; Wright, J. J.; Roessler, M. M.; Moir, J. W.; Parkin, A., Re-engineering a NiFe hydrogenase to increase the H_2 production bias while maintaining native levels of O_2 tolerance. *Chemical Communications* **2016,** *52* (58), 9133-6.

227. Roessler, M. M.; Evans, R. M.; Davies, R. A.; Harmer, J.; Armstrong, F. A., EPR Spectroscopic Studies of the Fe–S Clusters in the O_2-Tolerant [NiFe]-Hydrogenase Hyd-1 from *Escherichia coli* and Characterization of the Unique [4Fe–3S] Cluster by HYSCORE. *Journal of the American Chemical Society* **2012,** *134*, 15581-15594.

228. Murphy, B. J.; Hidalgo, R.; Roessler, M. M.; Evans, R. M.; Ash, P. A.; Myers, W. K.; Vincent, K. A.; Armstrong, F. A., Discovery of Dark pH-Dependent H+ Migration in a [NiFe]-Hydrogenase and Its Mechanistic Relevance: Mobilizing the Hydrido Ligand of the Ni-C Intermediate. *Journal of the American Chemical Society* **2015,** *137*, 8484-8489.

229. Khanna, N.; Lindblad, P., Cyanobacterial Hydrogenases and Hydrogen Metabolism Revisited: Recent Progress and Future Prospects. *International Journal of Molecular Sciences* **2015,** *16* (5), 10537-10561.

230. Pandelia, M.-E.; Nitschke, W.; Infossi, P.; Giudici-Orticoni, M.-T.; Bill, E.; Lubitz, W., Characterization of a unique [FeS] cluster in the electron transfer chain of the oxygen tolerant [NiFe] hydrogenase from *Aquifex aeolicus*. *Proceedings of the National Academy of Sciences* **2011,** *108*, 6097-6102.

231. Robichon, C.; Luo, J.; Causey, T. B.; Benner, J. S.; Samuelson, J. C., Engineering Escherichia coli BL21(DE3) Derivative Strains To Minimize *E. coli* Protein Contamination after Purification by Immobilized Metal Affinity Chromatography. *Applied and Environmental Microbiology* **2011,** *77* (13), 4634-4646.

232. Hansen, A. L.; Kay, L. E., Measurement of histidine pK_a values and tautomer populations in invisible protein states. *Proc Natl Acad Sci U S A* **2014,** *111* (17), E1705-12.

233. Edgcomb, S. P.; Murphy, K. P., Variability in the pK_a of histidine side-chains correlates with burial within proteins. *Proteins* **2002,** *49* (1), 1-6.

234. Stojek, Z., The Electrical Double Layer and Its Structure. In *Electroanalytical Methods*, 1 ed.; Scholz, F., Ed. Springer-Verlag Berlin Heidelberg: 2002; pp 3-4.

235. Parsons, R., The electrical double layer: recent experimental and theoretical developments. *Chemical Reviews* **1990,** *90* (5), 813-826.

236. Rousset, M.; Montet, Y.; Guigliarelli, B.; Forget, N.; Asso, M.; Bertrand, P.; Fontecilla-Camps, J. C.; Hatchikian, E. C., [3Fe-4S] to [4Fe-4S] cluster conversion in *Desulfovibrio fructosovorans* [NiFe] hydrogenase by site-directed mutagenesis.

Proceedings of the National Academy of Sciences of the United States of America **1998,** *95*, 11625-11630.

237.   Wiedenbeck, J.; Cohan, F. M., Origins of bacterial diversity through horizontal genetic transfer and adaptation to new ecological niches. *FEMS Microbiology Reviews* **2011,** *35* (5), 957.

238.   Laurinavichene, T. V.; Tsygankov, A. A., H_2 consumption by *Escherichia coli* coupled via hydrogenase 1 or hydrogenase 2 to different terminal electron acceptors. *FEMS Microbiology Letters* **2001,** *202*, 121–124.

239.   Trchounian, K.; Sanchez-Torres, V.; Wood, T. K.; Trchounian, A., *Escherichia coli* hydrogenase activity and H_2 production under glycerol fermentation at a low pH. *International Journal of Hydrogen Energy* **2011,** *36* (7), 4323-4331.

240.   Murphy, B. J.; Sargent, F.; Armstrong, F. A., Transforming an oxygen-tolerant [NiFe] uptake hydrogenase into a proficient, reversible hydrogen producer. *Energy & Environmental Science* **2014,** *7*, 1426.

241.   Menon, N. K.; Chatelus, C. Y.; Dervartanian, M.; Wendt, J. C.; Shanmugam, K. T.; Peck, H. D., Jr; Przybyla, A. E., Cloning, sequencing, and mutational analysis of the hyb operon encoding *Escherichia coli* hydrogenase 2. *Journal of bacteriology* **1994,** *176*, 4416-4423.

242.   Lamichhane-Khadka, R.; Kwiatkowski, A.; Maier, R. J., The Hyb Hydrogenase Permits Hydrogen-Dependent Respiratory Growth of *Salmonella enterica* Serovar Typhimurium. *mBio* **2010,** *1*.

243.   Kim, J. Y.; Jo, B. H.; Cha, H. J., Production of biohydrogen by recombinant expression of [NiFe]-hydrogenase 1 in *Escherichia coli*. *Microbial Cell Factories* **2010,** *9*, 54.

244.   Harwood, C. R.; Cutting, S. M., Chemically defined growth media and supplements. In *Molecular biological methods for Bacillus*, Harwood, C. R.; Cutting, S. M., Eds. Wiley: Chichester, United Kingdom, 1990; p 548.

245.   Studier, F. W., Protein production by auto-induction in high-density shaking cultures. *Protein Expr Purif* **2005,** *41*, 207-234.

246.   Böck, A.; King, P. W.; Blokesch, M.; Posewitz, M. C., Maturation of Hydrogenases. In *Advances in Microbial Physiology*, Poole, R. K., Ed. Academic Press: 2006; Vol. Volume 51, pp 1-225.

247.   Pinske, C.; Jaroschinsky, M.; Linek, S.; Kelly, C. L.; Sargent, F.; Sawers, R. G., Physiology and bioenergetics of [NiFe]-hydrogenase 2-catalyzed H_2-consuming and H_2-producing reactions in *Escherichia coli. J Bacteriol* **2015,** *197* (2), 296-306.

248.   Bren, A.; Hart, Y.; Dekel, E.; Koster, D.; Alon, U., The last generation of bacterial growth in limiting nutrient. *BMC Systems Biology* **2013,** *7* (1), 1-9.

249.   Pinske, C.; McDowall, J. S.; Sargent, F.; Sawers, R. G., Analysis of hydrogenase 1 levels reveals an intimate link between carbon and hydrogen metabolism in *Escherichia coli* K-12. *Microbiology (Reading, England)* **2012,** *158*, 856-868.

250.   Laurinavichene, T. V.; Zorin, N. A.; Tsygankov, A. A., Effect of redox potential on activity of hydrogenase 1 and hydrogenase 2 in *Escherichia coli. Arch Microbiol* **2002,** *178* (6), 437-42.

251.   Linley, E.; Denyer, S. P.; McDonnell, G.; Simons, C.; Maillard, J.-Y., Use of hydrogen peroxide as a biocide: new consideration of its mechanisms of biocidal action. *Journal of Antimicrobial Chemotherapy* **2012,** *67* (7), 1589-1596.

252.   Peng, S.; Stephan, R.; Hummerjohann, J.; Tasara, T., Evaluation of three reference genes of *Escherichia coli* for mRNA expression level normalization in view of salt and organic acid stress exposure in food. *FEMS Microbiology Letters* **2014,** *355* (1), 78-82.

253.   Zhou, K.; Zhou, L.; Lim, Q. E.; Zou, R.; Stephanopoulos, G.; Too, H.-P., Novel reference genes for quantifying transcriptional responses of *Escherichia coli* to protein overexpression by quantitative PCR. *BMC Molecular Biology* **2011,** *12* (1), 1-9.

254.   Berman, H. M.; Westbrook, J.; Feng, Z.; Gilliland, G.; Bhat, T. N.; Weissig, H.; Shindyalov, I. N.; Bourne, P. E., The Protein Data Bank. *Nucleic Acids Research* **2000,** *28*, 235-242.

255.   Schrodinger, LLC, The PyMOL Molecular Graphics System, Version 1.8. 2015.

256.   Neidhardt, F. C.; Ingraham, J. L.; Schaechter, M., *Physiology of the bacterial cell. A molecular approach.* Sinauer associates: Sunderland, MA, 1990; p 507.

257.   Bard, A. J.; Faulkner, L. R., *Electrochemistry Methods: Fundementals and Applications.* 2 ed.; Wiley: 2001.

258.   Sander, R., Compilation of Henry's law constants (version 4.0) for water as solvent. *Atmospheric Chemistry and Physics* **2015,** *15* (8), 4399-4981.